

This electronic thesis or dissertation has been downloaded from the King's Research Portal at <https://kclpure.kcl.ac.uk/portal/>

## Cellular Mechanisms of Morphogenesis in Palate Development

Brock, Lara

*Awarding institution:*  
King's College London

The copyright of this thesis rests with the author and no quotation from it or information derived from it may be published without proper acknowledgement.

### END USER LICENCE AGREEMENT



Unless another licence is stated on the immediately following page this work is licensed

under a Creative Commons Attribution-NonCommercial-NoDerivatives 4.0 International

licence. <https://creativecommons.org/licenses/by-nc-nd/4.0/>

You are free to copy, distribute and transmit the work

Under the following conditions:

- Attribution: You must attribute the work in the manner specified by the author (but not in any way that suggests that they endorse you or your use of the work).
- Non Commercial: You may not use this work for commercial purposes.
- No Derivative Works - You may not alter, transform, or build upon this work.

Any of these conditions can be waived if you receive permission from the author. Your fair dealings and other rights are in no way affected by the above.

### Take down policy

If you believe that this document breaches copyright please contact [librarypure@kcl.ac.uk](mailto:librarypure@kcl.ac.uk) providing details, and we will remove access to the work immediately and investigate your claim.

This electronic theses or dissertation has been downloaded from the King's Research Portal at <https://kclpure.kcl.ac.uk/portal/>

**Title:** Cellular Mechanisms of Morphogenesis in Palate Development

**Author:** Lara Brock

The copyright of this thesis rests with the author and no quotation from it or information derived from it may be published without proper acknowledgement.

#### END USER LICENSE AGREEMENT



This work is licensed under a Creative Commons Attribution-NonCommercial-NoDerivs 3.0 Unported License. <http://creativecommons.org/licenses/by-nc-nd/3.0/>

You are free to:

- Share: to copy, distribute and transmit the work

Under the following conditions:

- Attribution: You must attribute the work in the manner specified by the author (but not in any way that suggests that they endorse you or your use of the work).
- Non Commercial: You may not use this work for commercial purposes.
- No Derivative Works - You may not alter, transform, or build upon this work.

Any of these conditions can be waived if you receive permission from the author. Your fair dealings and other rights are in no way affected by the above.

#### Take down policy

If you believe that this document breaches copyright please contact [librarypure@kcl.ac.uk](mailto:librarypure@kcl.ac.uk) providing details, and we will remove access to the work immediately and investigate your claim.

# **Cellular Mechanisms of Morphogenesis in Palate Development**

A thesis submitted to King's College London for the degree of  
Doctor of Philosophy

Lara Brock

2013

Craniofacial Development and Stem Cell Biology Department  
King's College London

## **Declaration**

No part of the work referred to in the present thesis has been submitted in support of an application for another degree or qualification of this or any other university or institute of learning.

## Abstract

Mechanisms that result in directional tissue growth include cell proliferation, orientated cell division, an increase in cell size, a change in the cell density and cell death. These were investigated in the development of the mouse palatal shelves between stages E11.5 – E15.5. The aim was to develop and apply image processing tools to automatically analyse images of fixed specimens to reveal cellular behaviours that can be applied to understand directional growth and diagnosing the mechanism of its failure in mutant tissue in the palate and more generally. Techniques included immunohistochemistry after frozen or paraffin sectioning and imaging on the confocal microscope. Analysis of images was done using programs such as ImageJ, Volocity and R.

This analysis was carried out on CD-1 wild-type mice to provide a thorough understanding of the mechanisms of cellular morphogenesis throughout normal palate development. It was then performed on mutant *Tbx-1*, *Msx-1* and *Wnt1-Cre;ERK2<sup>fl/fl</sup>* mice all of which have a cleft palate phenotype to demonstrate how a better understanding of the links between genetic mutations, tissue phenotypes and cellular disruption can be gained.

## Acknowledgements

I would like to thank my supervisors Prof. Jeremy Green and Prof. Martyn Cobourne for giving me the opportunity to work in their lab and for their support throughout my PhD.

Special thanks goes to Andrew Economou who has been in the lab with me throughout my time in the Tower and offered me invaluable intellectual and technical support. Many thanks go to Ashley Young for her practical support at the beginning of my project and her friendship throughout.

I could not of done this without the support of Angela Gates and her unrivalled knowledge of the CFD and PhD process. I have greatly appreciated the help and support from my co-workers and friends in the lab, including Tree, Kieran, Leena and many others who have come and gone over the years. I would also like to thank the rest of the CFD and BSU staff who have helped in numerous ways during the past four years.

I would not have got as much out of this experience if it had not been for the overwhelming support from my family, friends and Vesta RC. I am particularly grateful for my Dad's proof reading skills. I am proud to say the rowers of Putney know more about the palate than they ever thought they would and have helped me to achieve more in a boat than I ever thought I would.

## Contents Page

<b>Cellular Mechanisms of Morphogenesis in Palate Development .....</b>	<b>1</b>
<b>Declaration .....</b>	<b>2</b>
<b>Abstract.....</b>	<b>3</b>
<b>Acknowledgements .....</b>	<b>4</b>
<b>Contents Page .....</b>	<b>5</b>
<b>List of Figures.....</b>	<b>12</b>
<b>List of Tables .....</b>	<b>17</b>
<b>Abbreviations.....</b>	<b>18</b>
<b>1.0 Introduction.....</b>	<b>21</b>
<b>1.1. Cleft lip and palate and lower facial birth defects.....</b>	<b>21</b>
<b>1.2 Normal development of the palate.....</b>	<b>22</b>
1.2.1 Summary of early face development .....	23
1.2.2 Formation of the primary palate.....	23
1.2.3 Secondary palate development .....	24
1.2.3.1 Palatal shelf outgrowth .....	24
1.2.3.2 Rugae .....	26
1.2.3.3 Palatal shelf elevation .....	27
1.2.3.4 Palatal Shelf Fusion .....	32
<b>1.3 Primary and secondary palates in different species .....</b>	<b>33</b>
<b>1.4 Cellular processes that cause directional growth .....</b>	<b>34</b>
1.4.1 Localised cell division.....	36
1.4.2 Polarised cells and orientated cell behaviours.....	36
1.4.3 Orientated cell division .....	37
1.4.4 Cell spacing .....	38
1.4.4.1 Cell Shape .....	38
1.4.4.2 Apoptosis .....	39
<b>1.5 Aims of this study.....</b>	<b>40</b>
<b>2.0 Materials and methods .....</b>	<b>41</b>
<b>2.1 Solutions .....</b>	<b>41</b>
2.1.1 10X Phosphate Buffered Saline (PBS) (pH 7.5) .....	41
2.1.2 PBT (TritonX) .....	41

2.1.3 PBT (Tween).....	41
2.1.4 Paraformaldehyde (PFA) (4%) .....	41
2.1.5 Dent's fixative.....	41
2.1.6 Mowiol.....	41
2.1.7 Bromodeoxyuridine (BrdU) .....	42
2.1.8 Iododeoxyuridine (IddU) .....	42
2.1.9 Sodium Citrate (pH 6).....	42
2.1.10 Polymerase Chain Reaction (PCR) digestion high molecular weight (HMW) Buffer (for digesting Tbx-1).....	42
2.1.11 0.5M Tris-HCl (pH 8.0) .....	43
2.1.12 1M NaCl .....	43
2.1.13 10% SDS .....	43
2.1.14 EDTA pH 8.0 .....	43
<b>2.2 Genotyping Protocol.....</b>	<b>43</b>
2.2.1 <i>Tbx-1</i> Primers.....	43
2.2.2 <i>Tbx-1</i> PCR master mix .....	43
2.2.3 <i>Tbx-1</i> PCR conditions .....	44
2.2.4 <i>Msx-1</i> Primers .....	44
2.2.5 <i>Msx-1</i> PCR master mix .....	44
2.2.6 <i>Msx-1</i> PCR conditions.....	44
<b>2.3 Mice.....</b>	<b>44</b>
2.3.1 Wild type CD-1 .....	45
2.3.2 <i>Tbx-1</i> <sup>-/-</sup> mouse line .....	45
2.3.3 mT/mG mouse line .....	45
2.3.4 <i>Msx-1</i> <sup>-/-</sup> mouse line .....	45
2.3.5 Embryo collection.....	46
2.3.6 Embryo fixation .....	46
2.3.7 Embryo processing .....	46
2.3.7.1 Paraffin embedding .....	46
2.3.7.2 Gelatin embedding .....	46
<b>2.4 Sectioning .....</b>	<b>47</b>
2.4.1 Microtome sectioning .....	47
2.4.2 Cryosectioning .....	47
<b>2.5 Immunohistochemistry.....</b>	<b>47</b>
2.5.1 IddU/BrdU/DAPI fluorescent immunohistochemistry.....	47
2.5.2 Gamma-tubulin, phosphohistone-H3 and DAPI immunohistochemistry .....	48
2.5.3 Golgi apparatus and DAPI immunohistochemistry.....	49



2.5.4 Fibronectin antibody .....	49
2.5.5 BrdU immunohistochemistry for brightfield imaging .....	50
<b>2.6 Image acquisition.....</b>	<b>50</b>
2.6.1 Fluorescent images.....	50
2.6.2 Brightfield images.....	51
<b>2.7 Image processing .....</b>	<b>51</b>
2.7.1 Calculating relative amounts of proliferation .....	51
2.7.2 Creating Heat Maps in R .....	52
<b>2.8 Combining the heat maps .....</b>	<b>54</b>
<b>2.9 Measuring the palate's proportions.....</b>	<b>54</b>
<b>2.10 Measuring angles in Volocity.....</b>	<b>54</b>
2.10.1 Measuring the Orientation of Cell Division .....	55
2.10.2 Measuring the orientation of the Golgi apparatus .....	56
2.10.3 Creating radar plots.....	57
<b>3.0 Developing a cell nuclei and proliferation identification protocol.....</b>	<b>58</b>
<b>3.1 Current cell counting methods .....</b>	<b>58</b>
<b>3.2 How the protocol was developed.....</b>	<b>58</b>
3.2.1 Brightfield image analysis.....	59
3.2.1.1 Identifying all cells in a brightfield image.....	59
3.2.1.2 Identifying proliferating cells in brightfield images .....	59
3.2.1.3 Discussion on identifying cells from brightfield images .....	63
<b>3.2.2 Fluorescent image analysis .....</b>	<b>64</b>
3.3.1 Identifying cell nuclei in fluorescent images.....	65
3.3.2 Identifying proliferating cells in fluorescent images.....	67
3.3.3 Extracting data from Volocity.....	68
<b>3.4 Discussion.....</b>	<b>68</b>
<b>4.0 Localised cell proliferation.....</b>	<b>70</b>
<b>4.1 Introduction to Localised Cell Proliferation .....</b>	<b>70</b>
4.1.2 Cell proliferation in the palate .....	70
4.1.3 Proliferation in the limb.....	73
<b>4.2 Localised cell proliferation: Methods .....</b>	<b>74</b>
<b>4.3 Localised cell proliferation: Results.....</b>	<b>74</b>
4.3.1 Wild-type palate development .....	74
4.3.2 Localised cell proliferation overview during palate development.....	76
4.3.3 Regional changes in localised cell proliferation .....	78
4.3.3.1 Localised cell proliferation along the anterioposterior axis.....	78

4.3.3.2 Proliferation in the maxillary process prior to palatal shelf outgrowth, E9.5- E10.5 .....	79
4.3.3.3 Proliferation during the initial outgrowth, E11.5-E13.5 .....	81
4.3.3.4 Proliferation after elevation, E14.0-E15.5 .....	84
4.3.3.5 Localised cell proliferation and the epithelium .....	89
<b>4.4 Localised cell proliferation: Discussion.....</b>	<b>90</b>
4.4.1 Localised cell proliferation methods discussion .....	90
4.4.2 Localised cell proliferation in the palate .....	93
<b>5.0 Polarised cells and orientated cell behaviours.....</b>	<b>97</b>
<b>5.1 Introduction to the Golgi apparatus and polarised cell behaviours .....</b>	<b>97</b>
5.1.1 Cell migration .....	97
5.1.2 Neural crest cell migration .....	101
5.1.3 Cell migration within the palate.....	102
5.1.4 The Golgi apparatus and cell migration .....	104
5.1.4.1 Structure and function of the Golgi apparatus.....	104
5.1.4.2 Migrating mesenchymal cells and the Golgi.....	104
5.1.4.3 Uniform Golgi positioning in limb bud development .....	105
5.1.4.4 Golgi positioning, directed secretion and wound healing .....	105
<b>5.2 Polarised cells and orientated cell behaviours: Methods .....</b>	<b>107</b>
<b>5.3 Polarised cells and orientated cell behaviours: Results .....</b>	<b>108</b>
5.3.1 Orientation of the Golgi during the initial outgrowth .....	108
5.3.1 Orientation of the Golgi after elevation .....	114
<b>5.4 Polarised cells and orientated cell behaviours: Discussion.....</b>	<b>117</b>
5.4.1 Golgi orientation assay discussion .....	117
5.4.2 Polarised cells during palate development discussion .....	118
<b>6.0 Orientated Cell Division.....</b>	<b>120</b>
<b>6.1 Introduction to orientated cell division .....</b>	<b>120</b>
6.1.1 Possible cues behind orientated cell divisions .....	121
6.1.2 Cortical cues .....	121
6.1.3 Cell shape .....	122
6.1.4 Cell-cell and cell-ECM adhesions .....	122
6.1.5 Extracellular signalling pathways involved: PCP pathway .....	123
6.1.6 Orientated cell divisions during gastrulation .....	124
6.1.7 Mouse and chick limb development.....	125
<b>6.2 Orientated cell division methods .....</b>	<b>127</b>
<b>6.3 Orientated cell division: Results.....</b>	<b>127</b>

6.3.1 Early wild-type palatal outgrowth .....	127
6.3.1.1 Orientated cell divisions during initial palatal outgrowth, E11.5.....	127
6.3.1.2 Orientated cell divisions during palatal outgrowth, E12.5.....	128
6.3.1.2 Orientated cell divisions prior to elevation, E13.5 .....	128
6.3.1.3 Orientated cell divisions post-elevation, E14.5 .....	132
<b>6.4 Orientated cell division: Discussion.....</b>	<b>133</b>
6.4.1 Orientated cell divisions assay discussion.....	133
6.4.2 Orientated cell divisions in palate development.....	134
<b>7.0 Internuclear Spacing .....</b>	<b>136</b>
<b>7.1 Introduction to internuclear spacing, cell spacing and cell shape.....</b>	<b>136</b>
7.1.1 Cell density changes in the palate .....	136
7.1.2 Cell density changes that cause cleft palate .....	137
7.1.3 Density-dependent growth in the developing chick limb and face.....	137
7.1.4 Investigating cell density in a hamster's palate .....	140
7.1.5 Cell shape and morphogenesis .....	140
7.1.5.1 Changes in cell shape during palate development .....	142
7.1.6 Extracellular matrix composition and the palate.....	142
<b>7.2 Internuclear Spacing: Methods.....</b>	<b>145</b>
<b>7.3 Internuclear Spacing: Results.....</b>	<b>145</b>
7.3.1 Changes in cell density in the maxillary process (E9.5-E10.5).....	145
7.3.2 Changes in cell density during the initial palatal outgrowth (E11.5-E13.5).....	145
7.3.3 Changes in cell density during post-elevational growth (E14.0-E15.5) .....	150
7.3.4 Cell spacing changes along the oronasal axis.....	154
<b>7.4 Internuclear spacing: Discussion .....</b>	<b>156</b>
7.4.1 Method used to investigate cell density .....	156
7.4.2 Cell spacing during palate development.....	157
<b>8.0 Palate Development in the <i>Tbx-1</i> Knockout Mouse.....</b>	<b>160</b>
<b>8.1 <i>Tbx-1</i><sup>-/-</sup> Introduction .....</b>	<b>160</b>
8.1.1 <i>Tbx-1</i> <sup>-/-</sup> phenotype .....	160
8.1.2 <i>Tbx-1</i> in development.....	161
8.1.2.1 <i>Tbx-1</i> in the palate.....	161
8.1.2.2 <i>Tbx-1</i> craniofacial defects derived from the pharyngeal arches .....	163
8.1.2.3 <i>Tbx-1</i> and heart development.....	163
8.1.2.4 <i>Tbx-1</i> in thyroid and parathyroid development.....	164
8.1.3 <i>Tbx-1</i> Expression Pattern and signaling pathway .....	165
<b>8.2 <i>Tbx-1</i><sup>-/-</sup> palate development: Methods .....</b>	<b>168</b>

<b>8.3 <i>Tbx-1</i><sup>-/-</sup> palate development: Results</b> .....	<b>168</b>
8.3.1 <i>Tbx-1</i> <sup>-/-</sup> phenotype .....	169
8.3.2 Localised cell proliferation in the <i>Tbx-1</i> <sup>-/-</sup> mutant.....	172
8.3.2.1 Overview of localised cell proliferation during <i>Tbx-1</i> <sup>-/-</sup> palate development .	172
8.3.2.2 Regionalised changes in cell proliferation along the AP axis of the <i>Tbx-1</i> <sup>-/-</sup> palate .....	172
8.3.2.3 Regionalised changes in cell proliferation shown in the heat maps of the <i>Tbx-1</i> <sup>-/-</sup> palate.....	174
8.3.3 Golgi positioning in the <i>Tbx-1</i> <sup>-/-</sup> mutant .....	181
8.3.3.1 Golgi positioning during the initial outgrowth, E11.5-E12.5.....	181
8.3.3.2 Golgi positioning at the end of the outgrowth stage, E13.5.....	182
8.3.3.3 Golgi positioning after failed elevation in the <i>Tbx-1</i> <sup>-/-</sup> mutant palate, E14.5.	183
8.3.4 Orientated cell division in the <i>Tbx-1</i> <sup>-/-</sup> mutant.....	188
8.3.5 Internuclear spacing in the <i>Tbx-1</i> <sup>-/-</sup> mutant .....	192
<b>8.4 <i>Tbx-1</i><sup>-/-</sup> palate development: Discussion</b> .....	<b>199</b>
<b>9.0 <i>Msx-1</i><sup>-/-</sup> knockout mouse</b> .....	<b>203</b>
<b>9.1 Introduction to <i>MSX-1</i></b> .....	<b>203</b>
9.1.1 <i>Msx-1</i> <sup>-/-</sup> phenotype .....	203
9.1.2 <i>Msx-1</i> expression pattern .....	205
9.1.3 <i>Msx-1</i> pathway in palatal development.....	205
<b>9.2 <i>Msx-1</i><sup>-/-</sup> Methods</b> .....	<b>207</b>
<b>9.3 <i>Msx-1</i><sup>-/-</sup> Results</b> .....	<b>207</b>
9.3.1 <i>Msx-1</i> <sup>-/-</sup> phenotype .....	207
9.3.2 Localised cell proliferation in the <i>Msx-1</i> <sup>-/-</sup> palate .....	209
9.3.2.1 Localised cell proliferation overview .....	209
9.3.2.2 Proliferation along the AP axis in <i>Msx-1</i> <sup>-/-</sup> mice.....	211
9.3.2.3 Distribution of proliferation in the <i>Msx-1</i> <sup>-/-</sup> palate.....	211
9.3.3 Internuclear spacing in the <i>Msx-1</i> <sup>-/-</sup> palate .....	217
<b>9.4 <i>Msx-1</i><sup>-/-</sup> Discussion</b> .....	<b>222</b>
<b>10.0 <i>Wnt1-Cre;ERK2</i><sup>fl/fl</sup> Mutant Mouse</b> .....	<b>224</b>
<b>10.1 Introduction to <i>Wnt1-Cre;Erk2</i><sup>fl/fl</sup> phenotype</b> .....	<b>224</b>
<b>10.1.2 The <i>Erk2</i> pathway</b> .....	<b>226</b>
10.1.2.1 Upstream of <i>Erk2</i> .....	226
10.1.2.2 Downstream of <i>Erk2</i> .....	227
<b>10.1.3 <i>Erk2</i> is required for neural crest development</b> .....	<b>228</b>
<b>10.2 <i>Wnt1-Cre;Erk2</i><sup>fl/fl</sup> Materials and Methods</b> .....	<b>228</b>

<b>10.3 <i>Wnt1-Cre;Erk2<sup>fl/fl</sup></i> Results .....</b>	<b>229</b>
10.3.1 Palate development in the <i>Wnt1-Cre;Erk2<sup>fl/fl</sup></i> mouse .....	229
10.3.2 Localised cell proliferation in the <i>Wnt1-Cre;Erk2<sup>fl/fl</sup></i> palate.....	229
10.3.2.1 Quantity of proliferation .....	229
10.3.2.2 Distribution of proliferation.....	230
10.3.3 Internuclear spacing in the <i>Wnt1-Cre;Erk2<sup>fl/fl</sup></i> palate.....	232
<b>10.4 <i>Wnt1-Cre;Erk2<sup>fl/fl</sup></i> Discussion .....</b>	<b>235</b>
<b>11.0 General Discussion and Future Considerations.....</b>	<b>237</b>
<b>11.1 General discussion on palatogenesis .....</b>	<b>237</b>
11.1.1 Cellular behaviours contributing to initial palatal outgrowth.....	237
11.1.2 Palatal elevation.....	239
11.1.3 Post-elevational growth .....	242
11.1.4 Epithelial influence on the mesenchyme.....	243
11.1.5 Mouse models of cleft palate.....	243
<b>11.2 General discussion on assays and possible future improvements .....</b>	<b>246</b>
11.2.1 How to improve/develop these assays .....	246
11.2.1.1 Proliferation.....	246
11.2.1.2 Heat map analysis.....	246
11.2.1.3 Measuring orientation of the Golgi or spindles.....	247
11.2.2 Further investigations.....	247
11.2.3 Other assays that could be included.....	250
11.3 Summary of findings .....	252
<b>12.0 Appendix .....</b>	<b>253</b>
<b>12.1 <i>Pbx-1<sup>-/-</sup></i> mouse development.....</b>	<b>253</b>
<b>12.2 Mandible development in <i>Wnt1Cre-Tgfβr2<sup>fl/fl</sup></i> mice .....</b>	<b>255</b>
<b>12.3 Mouse probe experiment.....</b>	<b>257</b>
<b>12.4 The R macro .....</b>	<b>260</b>
<b>12.5 Investigating a double injection protocol.....</b>	<b>274</b>
<b>12.6 Tables of p-values from Watson U<sup>2</sup> statistical tests for Golgi and spindle, wild-type and <i>Tbx-1</i> orientation datasets .....</b>	<b>276</b>
<b>13.0 References .....</b>	<b>294</b>

## List of Figures

	Page
Figure 1.1 Structure of the palate and varieties of cleft palate	22
Figure 1.2 SEMs and frontal sections of the developing mouse head E9.5-E14.5	25
Figure 1.3 Stages of palatal development and possible elevation techniques	28
Figure 1.4 Cellular mechanisms of morphogenesis	35
Figure 2.1 Regions the heat maps were divided into for analysis	53
Figure 2.2 Diagram to show where length measurements were taken	55
Figure 2.3 How the orientation of the Golgi/spindles were	56
Figure 3.1 Method for counting the total number of cells in the ROI	60
Figure 3.2 Graphs showing manual and automated cell count totals	62
Figure 3.3 Automated protocol to identify cells in Volocity	66
Figure 4.1 Signaling pathway involving <i>sprouty2</i> controlling proliferation.	72
Figure 4.2 Investigation into proliferation rates in the developing limb bud	73
Figure 4.3 Images and dimensions of the mouse maxillary process and palate during development	75
Figure 4.4 Proliferation index results represented as graphs	77
Figure 4.5 Proliferation heat maps of sagittal E9.5 and E10.5 embryo heads	80
Figure 4.6 Proliferation heat maps of E11.5 palatal shelves	82
Figure 4.7 Proliferation heat maps of E12.5 palatal shelves	83
Figure 4.8 Proliferation heat maps of E13.5 palatal shelves	85
Figure 4.9 Proliferation heat maps of E14.0 palatal shelves	86
Figure 4.10 Proliferation heat maps of E14.5 palatal shelves	87
Figure 4.11 Proliferation heat maps of E15.5 palatal shelves	88
Figure 4.12 Proliferation heat maps in sagittal sections before and after elevation	90

Figure 5.1 Polarised cells and cellular mechanisms	100
Figure 5.2 Pathways of neural crest cells migration	101
Figure 5.3 <i>Wnt5a</i> acts as a chemoattractant in the palate and limb development	103
Figure 5.4 Examples of cell intercalation in development	107
Figure 5.5 Rose plots summarising Golgi angle in relation to the nuclear centre at E11.5	109
Figure 5.6 Rose plots summarising Golgi angle in relation to the nuclear centre at E12.5	110
Figure 5.7 Rose plots summarising Golgi angle in relation to the nuclear centre at E13.5	111
Figure 5.8 Rose plots summarising Golgi angle in relation to the nuclear centre along the AP axis at E12.5 and E13.5	112
Figure 5.9 Rose plots summarising Golgi angle in relation to the nuclear centre at E14.5	115
Figure 5.10 Rose plots summarising Golgi angle in relation to the nuclear centre along the AP axis at E14.5	116
Figure 6.1 Stages of mitosis and PCP signaling pathway	120
Figure 6.2 Orientated cell division during development	124
Figure 6.3 Orientated cell divisions in vertebrates	126
Figure 6.4 Rose plots summarising mitotic spindle angles at E11.5	128
Figure 6.5 Rose plots summarising mitotic spindle angles at E12.5	129
Figure 6.6 Rose plots summarising mitotic spindle angles at E13.5	130
Figure 6.7 Rose plots summarising mitotic spindle angles at E14.5	131
Figure 7.1 Changes in cell spacing around palate elevation	138
Figure 7.2 Cell spacing changes during limb development	139
Figure 7.3 Changes in cell shape change during development	141
Figure 7.4 Cell shape changes during palate development	143
Figure 7.5 Spacing heat maps of sagittal E9.5 and E10.5 embryo heads	146
Figure 7.6 Spacing heat maps of E11.5 palatal shelves	147
Figure 7.7 Spacing heat maps of E12.5 palatal shelves	148

Figure 7.8 Spacing heat maps of E13.5 palatal shelves	149
Figure 7.9 Spacing heat maps of E14.0 palatal shelves	151
Figure 7.10 Spacing heat maps of E14.5 palatal shelves	152
Figure 7.11 Spacing heat maps of E15.5 palatal shelves	153
Figure 7.12 Changes in cell density during post-elevational growth	154
Figure 7.13 Spacing heat maps in sagittal sections before and after elevation	155
Figure 8.1 <i>Tbx-1</i> <sup>-/-</sup> mutant mice and their defects	161
Figure 8.2 Expression pattern of <i>Tbx-1</i> during palate development	166
Figure 8.3 DAPI images of <i>Tbx-1</i> <sup>-/-</sup> mutant palate development	170
Figure 8.4 Wild-type and <i>Tbx-1</i> <sup>-/-</sup> height and width measurements	171
Figure 8.5 Proliferation index results represented as graphs	172
Figure 8.6 Proliferation heat maps of E11.5 wild-type and <i>Tbx-1</i> <sup>-/-</sup> palatal shelves	176
Figure 8.7 Proliferation heat maps of E12.5 wild-type and <i>Tbx-1</i> <sup>-/-</sup> palatal shelves	177
Figure 8.8 Proliferation heat maps of E13.5 wild-type and <i>Tbx-1</i> <sup>-/-</sup> palatal shelves	178
Figure 8.9 Proliferation heat maps of E14.5 wild-type and <i>Tbx-1</i> <sup>-/-</sup> palatal shelves	179
Figure 8.10 Proliferation heat maps of E15.5 wild-type and <i>Tbx-1</i> <sup>-/-</sup> palatal shelves	180
Figure 8.11 Rose plots summarising Golgi angle in relation to the nuclear centre at E11.5 for wild-type and <i>Tbx-1</i> <sup>-/-</sup> palatal shelves	184
Figure 8.12 Rose plots summarising Golgi angle in relation to the nuclear centre at E12.5 for wild-type and <i>Tbx-1</i> <sup>-/-</sup> palatal shelves	185
Figure 8.13 Rose plots summarising Golgi angle in relation to the nuclear centre at E13.5 for wild-type and <i>Tbx-1</i> <sup>-/-</sup> palatal shelves	186
Figure 8.14 Rose plots summarising Golgi angle in relation to the nuclear centre at E14.5 for wild-type and <i>Tbx-1</i> <sup>-/-</sup> palatal shelves	187



shelves	
Figure 8.15 Rose plots summarising the distribution of mitotic angles at E11.5 for wild-type and <i>Tbx-1</i> <sup>-/-</sup> palatal shelves	189
Figure 8.16 Rose plots summarising the distribution of mitotic angles at E12.5 for wild-type and <i>Tbx-1</i> <sup>-/-</sup> palatal shelves	190
Figure 8.17 Rose plots summarising the distribution of mitotic angles at E13.5 for wild-type and <i>Tbx-1</i> <sup>-/-</sup> palatal shelves	191
Figure 8.18 Rose plots summarising the distribution of mitotic angles at E14.5 for wild-type and <i>Tbx-1</i> <sup>-/-</sup> palatal shelves	192
Figure 8.19 Spacing heat maps of E11.5 wild-type and <i>Tbx-1</i> <sup>-/-</sup> palatal shelves	194
Figure 8.20 Spacing heat maps of E12.5 wild-type and <i>Tbx-1</i> <sup>-/-</sup> palatal shelves	195
Figure 8.21 Spacing heat maps of E13.5 wild-type and <i>Tbx-1</i> <sup>-/-</sup> palatal shelves	196
Figure 8.22 Spacing heat maps of E14.5 wild-type and <i>Tbx-1</i> <sup>-/-</sup> palatal shelves	197
Figure 8.23 Spacing heat maps of E15.5 wild-type and <i>Tbx-1</i> <sup>-/-</sup> palatal shelves	198
Figure 9.1 <i>Msx-1</i> <sup>-/-</sup> mutant mice phenotype	204
Figure 9.2 Wild-type and <i>Msx-1</i> <sup>-/-</sup> height and width measurements and DAPI images of <i>Msx-1</i> <sup>-/-</sup> palate development	208
Figure 9.3 Wild-type and <i>Msx-1</i> <sup>-/-</sup> proliferation index results	209
Figure 9.4 Wild-type and <i>Msx-1</i> <sup>-/-</sup> proliferation index results along the AP axis	210
Figure 9.5 Proliferation heat maps of E11.5 wild-type and <i>Msx-1</i> <sup>-/-</sup> palatal shelves	212
Figure 9.6 Proliferation heat maps of E12.5 wild-type and <i>Msx-1</i> <sup>-/-</sup> palatal shelves	214
Figure 9.7 Proliferation heat maps of E13.5 wild-type and <i>Msx-1</i> <sup>-/-</sup> palatal shelves	215
Figure 9.8 Proliferation heat maps of E14.5 wild-type and <i>Msx-1</i> <sup>-/-</sup> palatal shelves	216
Figure 9.9 Spacing heat maps of E11.5 wild-type and <i>Msx-1</i> <sup>-/-</sup> palatal shelves	218
Figure 9.10 Spacing heat maps of E12.5 wild-type and <i>Msx-1</i> <sup>-/-</sup> palatal shelves	219

palatal shelves	
Figure 9.11 Spacing heat maps of E13.5 wild-type and <i>Msx-1</i> <sup>-/-</sup> palatal shelves	220
Figure 9.12 Spacing heat maps of E14.5 wild-type and <i>Msx-1</i> <sup>-/-</sup> palatal shelves	221
Figure 10.1 <i>Wnt1-Cre;Erk2</i> <sup>fl/fl</sup> phenotype	225
Figure 10.2 Wild-type and <i>Wnt1-Cre;Erk2</i> <sup>fl/fl</sup> height and width measurements	230
Figure 10.3 Wild-type and <i>Wnt1-Cre;Erk2</i> <sup>fl/fl</sup> proliferation index results	231
Figure 10.4 Proliferation heat maps of E13.5 and E14.5 wild-type and <i>Wnt1-Cre;Erk2</i> <sup>fl/fl</sup> palatal shelves	233
Figure 10.5 Spacing heat maps of E13.5 and E14.5 wild-type and <i>Wnt1-Cre;Erk2</i> <sup>fl/fl</sup> palatal shelves	234
Figure 12.1 <i>Pbx-1</i> <sup>-/-</sup> ; <i>Pbx-2</i> <sup>+/-</sup> ; <i>Crect</i> <sup>Cre</sup> and wild-type proliferation and internuclear spacing heat maps	254
Figure 12.2 Heat maps showing the proliferation and internuclear spacing in wild-type and <i>Wnt1Cre-Tgfβr2</i> <sup>fl/fl</sup> palatal outgrowths and mandibles at E11.5	256
Figure 12.3 Images and heat maps from preliminary experiments when elevation was induced to investigate changes in Internuclear spacing	259
Figure 12.4 Creating the heat maps	261
Figure 12.5 Graph to show the cycle time	275

## List of Tables

	<b>Page</b>
Table 5.1 Table of major embryonic migratory events	99
Table 12.1 Table of proliferation labelling index and cell cycle times for different injection protocols	274
Table 12.2 Table of p-values from statistical tests on the wild-type Golgi orientation data	277
Table 12.3 Table of p-values from statistical tests on the wild-type spindle orientation data	282
Table 12.4 Table of p-values from statistical tests on the <i>Tbx-1</i> wild-type and mutant Golgi orientation data	286
Table 12.5 Table of p-values from statistical tests on the <i>Tbx-1</i> wild-type and mutant spindle orientation data	291

## Abbreviations

3D	Three-dimensional
5-FU	5-fluorouracil
6-MP	6-mercaptopurine
AER	Apical ectodermal ridge
AP	Anteroposterior
Barx-1	BARX homeobox 1
bHAND	Basic helix-loop-helix
BMP	Bone morphogenic protein
bp	Base pairs
BrdU	Bromodeoxyuridine
C57BL/6	C57 black 6
Cadh2	Cadherin-2
cAMP	Cyclic adenosine monophosphate
CLP	Cleft lip and/or palate
CP	Cleft palate
CREB	cAMP response element-binding protein
CRKL	Crk-Like Protein
DAB	3,3'-Diaminobenzidine
DAPI	4',6-diamidino-2-phenylindole
df	Dental follicle
DGS	DiGeorge syndrome
Dlx	Distal-less homeobox 5
DMSO	Dimethylsulphoxide
DNA	Deoxyribonucleic acid
dp	Dental pulp
ECM	Extracellular matrix
EGF	Epidermal growth factor
Egfp	Enhanced green fluorescent protein
Elk1	Ets1-like
EMT	Epithelial-mesenchyme transition
Erk	Extracellular signalling-regulating kinase
Fgf	Fibroblast growth factor
FgfR2	Fibroblast growth factor receptor 2
Fig	Figure
Fox	Forkhead box
Fzd	Frizzled

GAG	Glycosaminoglycans
GM130	Golgi matrix protein
Golgi	Golgi apparatus
GPCR	G-protein coupled receptor
GRB2	Growth factor receptor bound protein-2
Gsk	Glycogen synthase kinase
GTP	Guanosine triphosphate
HMW	Heavy molecular weight
IddU	Iododeoxyuridine
ITCN	Image-based tool for counting nuclei
Jag2	Jagged2
K14-Cre	Keratin-14-Cre
$\lambda$	Lambdoidal junction
LAS-AF	Leica Application Suite Advanced Fluorescence
LIF	Leica Image Files
M	Molar
MAPK	Mitogen-activated protein kinase
Mdb	Mandible
MEE	Medial edge epithelium
Mek	Map kinase or Erk Kinase
MES	Medial edge seam
mG	Membrane-targeted green fluorescent protein
MKK	MARK kinase kinase
Mkp	MAPK phosphatase
MSK	Mitogen- and stress-activated protein kinases
Msx	MSX homeobox gene
mT	Membrane-targeted tandem dimer Tomato
MTOC	Microtubule organising centre
MTRF	Myocardin-related transcription factor
Myf5	Myogenic factor 5
MyoD	Myogenic differentiation 1
NBrdU	Total number of BrdU cells
NCC	Neural crest cells
NCFCS	Neuro-cardio-facial-cutaneous syndromes
NIddU	Total number of IddU cells
NIH	National Institute of Health
NS	Nasal septum
NT	Total number of cells
OC	Oral cavity
OCT	Optimal cutting temperature

OE	Oral epithelium
Osr2	Odd-skipped related 2
Pax	Paired box
PBS	Phosphate buffered saline
PBT (Triton-X)	PBS and TritonX
PBT (Tween)	PBS and Tween
Pbx	Pbx homeobox gene
PCNA	Proliferating cell nuclear antigen
PCP	Planar cell polarity
PCR	Polymerase chain reaction
PFA	Paraformaldehyde
PH-3	Phosphohistone-H3
PS	Palatal shelf
RGB	Red/green/blue
RNA	Ribonucleic acid
ROI	Region of interest
Ror2	Related orphan receptor
rpm	Revolutions per minute
rRNA	Ribosomal RNA
RSK	Ribosomal s6 kinase
RTK	Receptor tyrosine kinase
SEMs	Scanning electron micrographs
Shh	Sonic hedgehog
SHO2	Shadoo
SOS	Son of sevenless
Spry2	Sprouty2
SRF	Serum response factor
T	Tongue
TAC	Triamcinolone acetonide
Tbx	T-box transcription factor
TC	Cell cycle time
Tgf $\beta$	Transforming growth factor $\beta$
Ti	Interval time
tRNA	Transfer RNA
TUNEL	TdT-mediated biotin-dUTP nick-end labelling
VCFS	Velo-cardio-facial syndrome
VNO	Vomeronasal organ
Wnt11r	Wnt11 related
Zfhx	Zinc finger homeobox gene

# 1.0 Introduction

## 1.1. Cleft lip and palate and lower facial birth defects

Around one in seven hundred children are born with a cleft lip and palate (Castilla, 2001). It is the most prevalent craniofacial facial defect and is caused by a combination of genetic and environmental factors (Murray, 2002). Babies born with a cleft can have disfigurement and functional problems associated with feeding, speech and hearing as well as psychological problems in later life (Wehby and Cassell, 2010). The primary defect can be corrected with surgery starting from when the baby is just three months old but can still lead to increased morbidity and mortality rates (Christensen et al., 2004). Cleft lip and palate (CLP) occurs when there is a failure in the development of the facial prominences and involves clefting of the lip, or the lip and palate. However in around one in 2,000 births a cleft palate (CP) occurs alone where the lip is completely intact (Fig. 1.1). Both CLP and CP can be syndromic and occur along with other symptoms (e.g. heart defects in DiGeorge Syndrome (Takahashi et al., 1999)), but in the majority of cases, around 70% (Stanier and Moore, 2004), they are non-syndromic and occur without any other major defects or disabilities. Many human genetic mutations have been shown to result in a cleft palate (Murray, 2002), but there is little understanding of the cellular basis of the defects. Genetically modified mice have been created to model human cases of cleft palate and are widely used by craniofacial development researchers.

The principal rationale behind the work described in this thesis is that by studying the normal development of the early craniofacial region, through a systematic study of the mechanisms controlling morphogenesis, greater understanding of how genetic mutations that lead to cellular disruption can be gained. Further knowledge can contribute to the development of novel therapies, or even prevention, such as tissue engineering involving stem cells (Zuk, 2008).

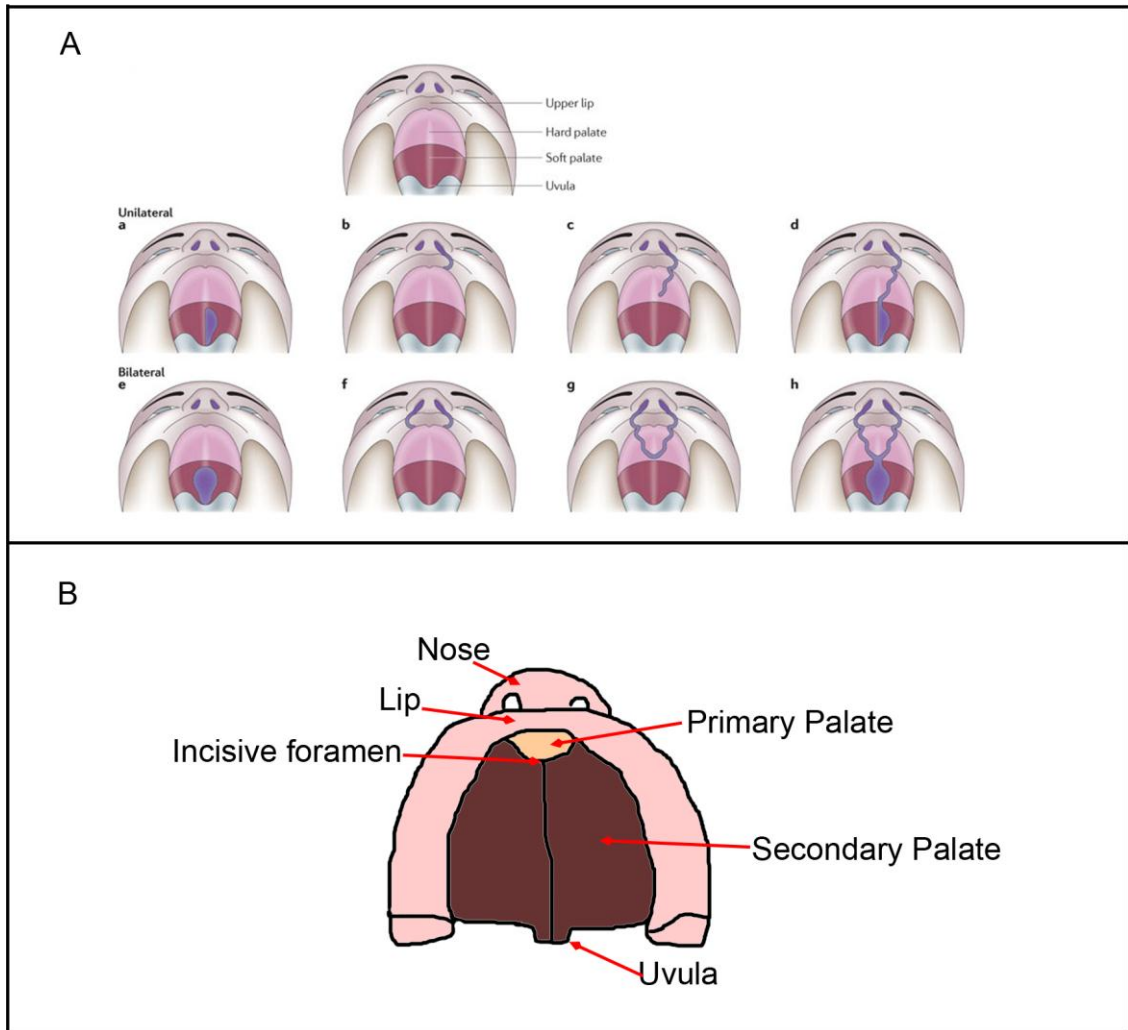


**Figure 1.1 Structure of the palate and varieties of cleft palate.** A) Diagrams demonstrating the varieties of cleft lip palate a) Unilateral cleft of the soft palate b) unilateral cleft lip c) unilateral cleft lip and hard palate d) Unilateral cleft lip, hard and soft palate e) bilateral cleft soft palate f) bilateral cleft lip g) bilateral cleft lip and hard palate h) bilateral cleft lip, hard and soft palate B) Structure of the complete palate viewed from below with the mandible removed. Adapted from Dixon et al., 2011.

## 1.2 Normal development of the palate

The palate is the tissue that eventually separates the oral and nasal cavities and is made up of the primary and secondary palate. The primary palate develops from the frontonasal process, prior to the secondary palate, but at the same time as the lip. It is separated from the lip by the vestibular lamina, which forms the cavity between the jaw and teeth and the cheek and lips. The secondary palate extends posteriorly from the incisive foramen and primary palate (Fig. 1.1B). Its anterior two-thirds are known as the hard palate and contain the palatine bone whilst the posterior third is known as the



soft palate and is muscular. This study has focused on the development of the secondary palate in the common mouse, *mus musculus*.

### **1.2.1 Summary of early face development**

The face develops from five processes, the frontonasal process, the paired maxillary and the paired mandibular processes (Fig. 1.3) beginning at around the fourth week in human embryogenesis, E9.0 in a mouse embryo. The development of these processes is driven by neural crest cell migration and proliferation. Neural crest cells (NCC) migrate from the pharyngeal arches (Johnston, 1966). In humans there are six pharyngeal arches. The first pharyngeal arch forms the mid- and lower face (Szabo-Rogers et al., 2010). Pharyngeal arches have a core of two mesenchymal cell populations, one derived from the neural crest and the other from cranial mesoderm (Grenier et al., 2009), situated between an outer ectoderm and inner endoderm layer. The extent to which neural crest populations contribute to each facial primordia varies (McGonnell et al., 1998). For example, in a mouse the mesencephalic crest and crest cells from the lateral prosencephalic neural fold migrate and contribute to the mesenchyme of the frontonasal process, but the crest cells from the anterior neural ridge of the prosencephalon do not contribute to it (Osumiyamashita et al., 1994). The neural crest derived mesenchyme generally gives rise to the facial skeleton whereas the muscles originate from the mesoderm-derived cells.

### **1.2.2 Formation of the primary palate**

The frontonasal and the paired maxillary processes arise from the first pharyngeal arch at E9.5. The nasal placodes form from a thickening of the surface ectoderm on the frontonasal processes at around E10.0. The frontonasal process continues to grow around the placodes forming nasal pits and the thickenings are now recognised as the medial and lateral nasal processes (Liu et al., 2008). By E10.5 the nasal pits have become slits due to the continued growth of the maxillary process and the ventrolateral growth of the medial nasal process. The medial and lateral nasal processes begin to fuse, starting at the posterior point and the maxillary process continues to grow forcing the medial nasal process mediofrontally. The maxillary and medial nasal processes begin to fuse as growth continues. The junction where the maxillary process, the medial nasal process and the lateral nasal process fuse is

known as the lambdoidal junction ( $\lambda$ ) (Ferretti et al., 2011). This fusion results in the nasal pits becoming the nose chambers and nasal ducts forming the base and the central portion of the nose.

By E12.5 the upper lip philtrum and the primary palate are formed by the midline meeting of the maxillary processes followed by disintegration of the epithelia at the contact surface and the fusing of the mesenchyme populations. If these fail to fuse cleft lip can occur and this can lead to cleft palate (Dibiase, 2010).

### **1.2.3 Secondary palate development**

The secondary palate is derived from the maxillary process and initially appears as two vertical outgrowths from the base of the maxillary process at around E11.5 in mouse or four weeks in a human embryo. During normal development these outgrowths continue to grow vertically downwards, parallel to the tongue until around E14.0 in the mouse or eight weeks in human (Diewert, 1985). By this stage the mandibular process has elongated and the tongue has dropped and the palatal shelves elevate into a horizontal position above the tongue. By E14.5 the shelves have met beneath the nasal septum and are separating the nasal and oral cavities; the epithelium then disintegrates and there is confluence of the mesenchyme by E16.5. Then the palatal shelves also fuse with the primary palate at the anterior border and the nasal septum above. The mesenchyme of the secondary palate differentiates into the maxillary and palatine bones of the hard palate (Vieira, 2008). The most posterior region of the palatal shelves becomes the muscular soft palate.

#### **1.2.3.1 Palatal shelf outgrowth**

The paired palatal outgrowths appear as bulges of mesenchyme with a thin epithelial layer along the ventral side above the primitive oral cavity at E11.5. As they develop they form characteristic shapes that vary along the anteroposterior axis. The anterior palate can be seen at E13.5 as a corner of the maxillary process which stretches out into a flat projection (finger-like in frontal section) pointing diagonally towards the far corner of the tongue and the tip is about level with the base of the tongue (Fig. 1.2D''-F'' & Fig. 1.3A-C). In the mid-palate, where the developing molar can be seen, the

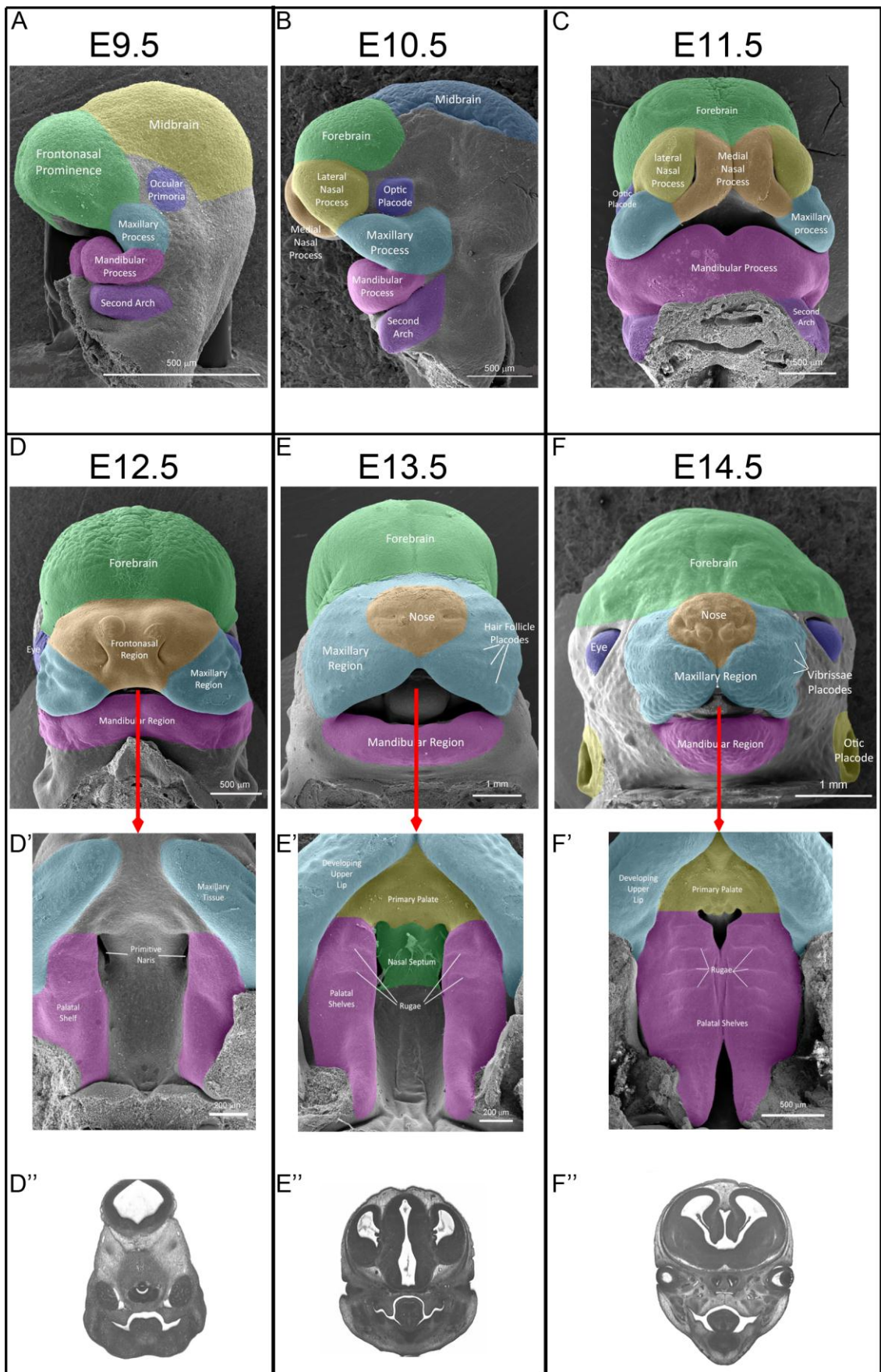


**Figure 1.2 SEMs and frontal sections of the developing mouse head E9.5-E14.5** A) Sagittal view of E9.5 mouse embryo B) Sagittal view of E10.5 mouse embryo C) Frontal view of E11.5 mouse embryo D) Frontal SEM of an E12.5 mouse embryo D') The top of the oral cavity viewed from below with the mandible and tongue removed at E12.5 D'') Frontal section of an E12.5 mouse embryo head E) Frontal SEM of an E13.5 mouse embryo E') The top of the oral cavity viewed from below at E13.5. The palatal shelves are still growing vertically E'') Frontal section of an E13.5 mouse embryo head F) Frontal SEM of an E14.5 mouse embryo F') The top of the oral cavity viewed from below at E14.5 when the palate is horizontal and touching in the mid-palate F'') Frontal section of an E14.5 mouse embryo head. Scale shown by scale bar in panels SEMs from [facebase.org](http://facebase.org) and frontal sections from [embryoimaging.org](http://embryoimaging.org)

palatal shelf is wider, in the mediolateral axis, and thickenings of the epithelium, known as rugae, become noticeable. The posterior palate has a more rounded distal end and grows truly vertically alongside the tongue.

Observations have been made on the mesenchymal cells at E13.5 (Brinkley and Bookstein, 1986; Ferguson, 1977), where they are seen to become more dispersed, but very little is understood about earlier stages or the cellular mechanisms behind this initial outgrowth. It is presumed that a burst in proliferation is responsible for increased cell numbers and therefore the outgrowth (Burdett et al., 1988). Molecular studies, such as those on the ephrin-B1 mutant mouse (Bush and Soriano, 2010), reveal matching regions of decreased proliferation and stunted growth but whether the stunting is due only to reduced proliferation was not investigated.

### 1.2.3.2 Rugae

The surface of the palate is characterised by a series of ridges or rugae, which start as epithelial thickenings and develop into transverse ridges on the oral side of the hard palate (Fig. 1.4) that play a role in mastication. Mice have 8 rugae but their number and arrangement are species dependent (Pantalacci et al., 2008).

They begin to form soon after the palatal shelves appear (Peterkova et al., 1987). Their development can be described in five stages; first an epithelial thickening burrows into the mesenchyme (Pantalacci et al., 2008). Then the epithelium protrudes, while the mesenchyme condenses, and the cells rearrange as the ruga progresses from a primitive to a definitive ruga. A fibrous stroma forms and dorsal lateral vaults appear where the epithelium thins. Finally the epithelial cells keratinize.

The order in which rugae appear is marked by the expression of sonic hedgehog (*Shh*) (Pantalacci et al., 2008). Numbering the rugae 1 to 8 according to their eventual anterior-to-posterior position, ruga 8 is the first ruga to appear followed by ruga 2, ruga

3 and ruga 1. After this each ruga appears sequentially between ruga 3 and ruga 8. This process involves an anterior-posterior extension between ruga 2 and ruga 8 and each new ruga appears immediately posterior to the preceding ruga (Pantalacci et al., 2008; Welsh and O'Brien, 2009). These studies of rugal development suggest there is a growth zone anterior to ruga 8 in which new rugae appear but they only focus on the epithelium and do not explain the anisotropy of the growth or distinguish growth from proliferation (Economou et al., 2012).

### **1.2.3.3 Palatal shelf elevation**

A definitive mechanism for palatal shelf elevation has been widely sought and theorised over but never satisfactorily confirmed. There has been debate over whether the forces causing elevation are intrinsic to the palatal shelves or extrinsic and produced by another part of the developing craniofacial region.

The contribution of extrinsic forces to palatal elevation has been investigated and possible mechanisms include the descent of the tongue after the elongation of the mandible (Coleman, 1965), initiation of the embryo mouth opening reflex causing the tongue to lower (Humphrey, 1969), an increase in head height with no change in width (Sandham, 1985), the shelves being pushed up by the tongue (Walker, 1971) and the embryo's head lifting off its chest allowing the mandible and tongue to drop and causing the PS to rise (Sandham, 1986; Walker, 1971). Ferguson demonstrated through a series of simple embryological experiments (Ferguson, 1978) that the shelves are able to elevate through intrinsic forces alone and at a time prior to embryo reflexes. This was done by inserting a blunt probe into the embryo's oral cavity and manually lowering the mandible and observing the elevation of the palatal shelves. The mandible was then released, causing the palate to return to its natural vertical position. The closer to natural elevation this experiment was performed the more rapidly the shelves would elevate, and just prior to natural elevation, the shelves were able to remain in a horizontal position after the mandible was released. An experiment

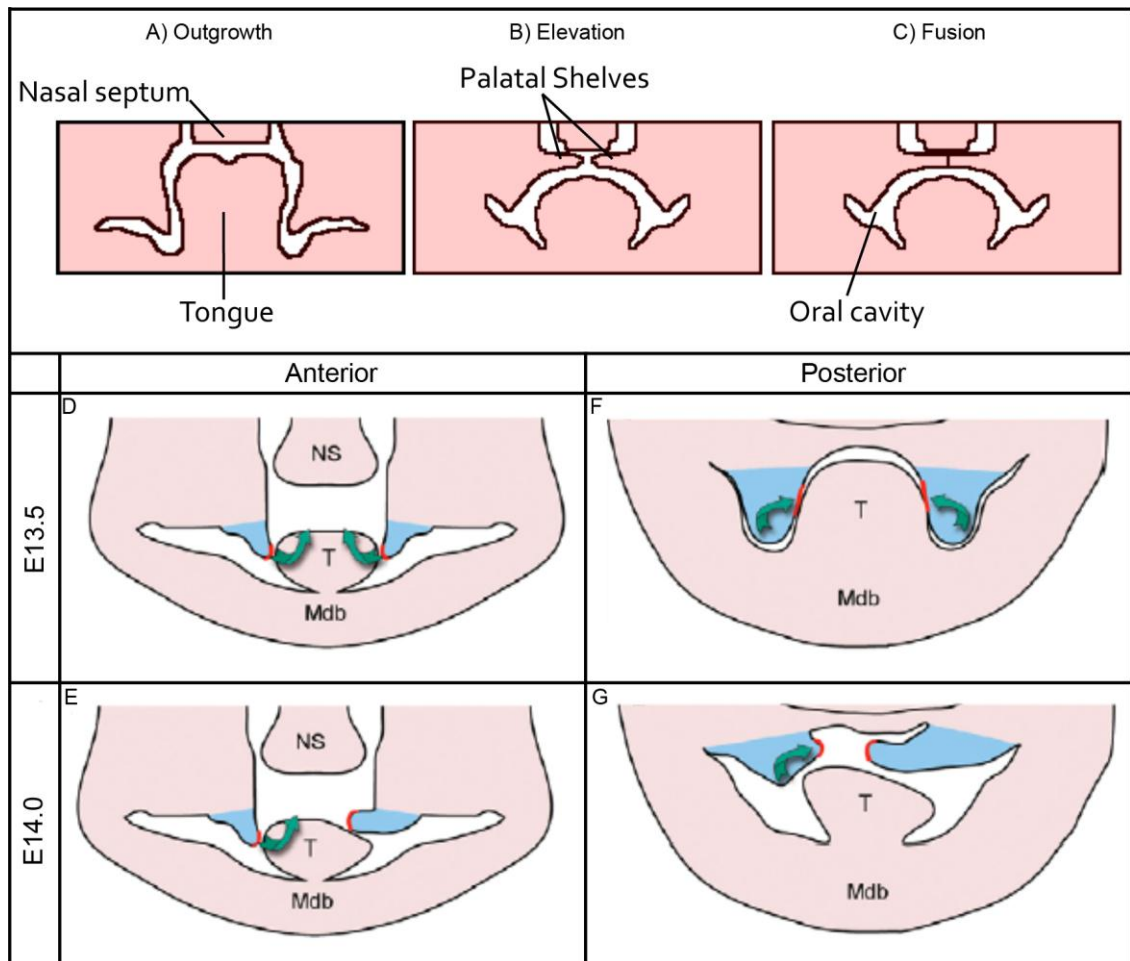


**Figure 1.3 Stages of palatal development and possible elevation techniques** A-C) Diagram of a frontal view of the oral cavity during A) the outgrowth phase of palate development B) Once the palatal shelves have elevated C) The palatal shelves grow towards the midline and one they touch fusion occurs D) Anterior palatal shelves at E13.5 prior to elevation E) Anterior palatal shelves, at E14.0, are thought to elevate by a “flip-up” mechanism. This may not occur at the same time F) Posterior palatal shelves at E13.5 G) Posterior palatal shelves, at E14.0, are thought to elevate by remodeling over the tongue. Palatal shelves are shaded blue. Green arrows mark palatal shelf movements during elevation. Red region marks where the cells that will form the MEE are. NS, nasal septum; T, tongue; Mdb, mandible. D-G adapted from Bush and Jiang, 2012.

was also done to mimic the mouth opening reflex but the tongue would only become withdrawn from the oral cavity once the mandible had been depressed enough to rip the tissue (Ferguson, 1978). To test if a change in pressure in the nasal cavity or a change in the angulation of the cranial base was contributing to palatal shelf elevation the skull, brain and nasal septum were dissected out, but the palate was still able to elevate when the tongue was depressed. It has often been observed that PS elevation is an asymmetrical process with one shelf being able to elevate before the other; this does not favour an extrinsic force, as the majority of those suggested would result in symmetrical PS elevation.

Throughout the last century of palatal research several theories on the intrinsic force causing palatal shelf elevation have evolved. One describes the palatal shelves elevating in a wave-like motion where the mesenchyme retracts back from the vertical position and flows horizontally out of the medial wall resulting in an elevated palate dorsal to the tongue (Walker and Fraser, 1956). Walker and Fraser also observed that this tissue remodelling began posteriorly and then moved anteriorly until the entire shelf has elevated, whereas work in the rat agreed with the mechanism, but claimed the movement commenced in the middle of the palate and extended in both directions (Coleman, 1965). This theory, wherever movement commences, agreed with previous work (Lazzaro, 1940; Peter, 1924; Walker and Fraser, 1956) in many respects, but it was one of the first to propose that the shelves could elevate regardless of the position of the tongue. A variation on this is where there is a complete retraction of the vertical palate and a regrowth out horizontally (Pons-Tortella, 1937; Walker and Fraser, 1956), but it has been shown that the transition is too rapid for it to be growth (Walker and Fraser, 1956). After observing that the shelves were still elevating whilst immersed in dehydrating 70% ethanol Walker and Fraser concluded that elastic fibres in the connective tissue must generate the intrinsic force not acid mucopolysaccharide (Lazzaro, 1940; Walker and Fraser, 1956).

Another common theory involves a “flip up” mechanism. This could be due to the contraction of the prospective nasal side and/or the expansion of the basal sulcus in a mechanism like a bimetallic strip. This “flip-up” mechanism is thought to be a consequence of a build-up of glycosaminoglycans (GAG), mainly hyaluronic acid (Larsson, 1962), secreted by the mesenchymal cells into the ECM. These secreted molecules are highly electrostatically charged and a single molecule can bind up to ten times its own weight in water. This means that a small change in concentration of GAG can result in a large change in the osmotic concentration and cell density. This leads to increased turgor pressure and rigidity within the palate, which might have facilitated elevation. Staining has shown that there is more hyaluronic acid in the anterior and on the prospective nasal side of the palate prior to shelf elevation (Brinkley and Morris-Wiman, 1987). Shelf elevation occurs when the intrinsic forces trying to flip up the palate overcome the extrinsic factors preventing it from elevating, such as the presence of the tongue acting as a solid barrier.

There have also been suggestions that the intrinsic force is due to the contraction of actomyosin or microfilaments in smooth muscle or other palatal mesenchyme cells (Babiarz et al., 1979). It was shown that the contractile proteins, actin and myosin,

were present in the palate (Lessard et al., 1974). Their presence does not mean they are active and this work was done prior to the development of antibodies such as anti-phospho-myosin, as an activity measure. The same group indentified three contractile regions of the palate where the changes in the mesenchymal cell shape, from elongated to rounded, during elevation are thought to create a direct elevational force (Babiarz et al., 1979).

Before molecular signalling pathways between epithelium and mesenchyme were discovered there was speculation over whether the epithelium plays a physical role in PS elevation. In an experiment in which about 40% of the epithelial cells were scraped off the future oral side (Bulleit and Zimmerman, 1985) the palatal shelves were prevented from elevating. When a wound was created twice the size of the scraped area the shelves still managed to elevate. It was not possible to predict what other damage or immune response the scraping might have caused and it would be impossible to reproduce exactly the same amount of damage when the experiment was repeated (Bulleit and Zimmerman, 1985).

The 1980s saw the beginning of the molecular era (Costantini and Lacy, 1981) and mouse models of cleft palate began to be generated. Genetic studies helped identify specific molecules involved in palatogenesis but did not answer questions like the one posed by this thesis. Cleft palate has been due to a failure of the PS to elevate in the case of the *fibroblast growth factor receptor 2 (Fgfr2)*, *sprouty2*, *Wnt5A*, *Frizzled*, *glycogen synthase kinase 3 $\beta$  (Gsk3 $\beta$ )* and GABA mutants (He et al., 2008; He et al., 2010; Jin et al., 2008; Matsumura et al., 2011; Snyder-Warwick and Perlyn, 2012; Oh et al., 2010; Yu et al., 2010). Work on the fibroblast growth factor and its receptors supports the “flip up” mechanism, because the *Fgfr2* mutant has been found to have increased proliferation on the future oral side of the shelf and decreased GAG content (Snyder-Warwick and Perlyn, 2012). This is also seen in the mutant of the transcription factor *odd-skipped related 2 (Osr2)* with less proliferation on the future nasal side of the palatal shelf at E13.5. This still has not increased understanding of the mechanism behind palatal elevation much further.

Support for the palate elevating by tissue remodelling comes from work on a *Zfhx1a* mouse mutant that has delayed PS elevation (Jin et al., 2008). The *Zfhx1a* gene encodes for a transcription regulator that may function by modulating the transforming growth factor beta (TGF $\beta$ ) pathway. They showed that the distal end of the vertical



palate does not become the medial edge of the horizontal palate. The cells destined to be the medial edge epithelium, which disappears when the palatal shelves fuse, are identifiable before the palatal shelves come into contact. The medial edge epithelial markers, MMP-13 and the expression pattern of Jagged2 (*Jag2*), were found on the medial side of the vertical shelf suggesting that the shelf reorientates by the horizontal outgrowth of the medial side of the vertical palatal shelf (Jin et al., 2010). Carbon labelling also supports this tissue remodelling mechanism (Chou et al., 2004). These experiments involved placing carbon particles at various sites on the palatal shelf and culturing the explants. The results showed tissue remodelling occurring, but only in the anterior and posterior palate, with the explanation that the mid-palate elevates by “rotation” and “medial elongation”.

Some clefts that form due to the failure of the shelves to elevate could occur because a cellular mechanism such as proliferation has been disrupted. In the negative regulator of Fgf signalling *Sprouty2* (Matsumura et al., 2011) there is an increase in proliferation in the anterior palatal shelf, or in mice with a mutation in the Wnt receptor frizzled there is a disruption in the polarisation of the cells (Yu et al., 2010). These disruptions mean that the palate does not reach the correct size or state needed for the elevation mechanism to occur.

The neurotransmitter  $\gamma$ -aminobutyric acid (GABA) is known to regulate cell migration, proliferation, survival and differentiation (Varju et al., 2001) as well as neuronal activities. In teratological experiments with GABA and its agonists it has been shown to cause cleft palate through failed PS elevation whereas GABA antagonists can stimulate elevation (Wee and Zimmerman, 1983). Therefore GABA is important in the process of palate development (Gritli-Linde, 2007). More recently it has been demonstrated that the effect of GABA is indirect by culturing palatal explants from mice with defects in the GABA signalling pathway, specifically *Gad1* and *Viaat* mutant mouse (Oh et al., 2010). These mice have a cleft palate when they develop *in vivo* but manage to develop normally in culture, showing the defect is not intrinsic to the palate. It was then shown that the GABA<sub>A</sub> agonist muscimol could rescue the cleft palate phenotype in both mutants (Oh et al., 2010). The conclusion was that GABA operates at the level of embryo movement and is not intrinsic to the palate. Therefore it is not one of the processes dealt with in this thesis.

#### 1.2.3.4 Palatal Shelf Fusion

During normal palatogenesis, after the PS have successfully elevated, they extend towards the midline where the two medial edges come into contact, forming a midline epithelial seam (MES). The medial edge epithelium (MEE) then disintegrates leaving a continuous mesenchymal tissue. This fusion occurs first in the mid-anterior region, slightly posterior to ruga 2 and then proceeds in both an anterior and posterior direction. The secondary palate goes on to fuse with the nasal septum above, and the primary palate at the anterior. There are three main theories for the mechanism behind MEE disappearance; cell death through apoptosis, epithelial-mesenchymal transformation (EMT) or migration of the epithelial cells to the oral or nasal epithelium. Although there has been debate as to which of these applies, they are, in fact, not mutually exclusive.

Cell migration of the MES was observed using an in vitro culture system (Carette and Ferguson, 1992) and using Dil to track cells and a confocal microscope to image the specimen. It has been proposed that apparent migration is a passive event as a result of cell cycle arrest in the epithelial cells that surround a still-growing mesenchyme (Cui et al., 2003), so the fixed number of epithelial cells are stretched over a larger volume making it appear as though they are migrating.

Evidence for cell death being involved in the disappearance of the MES has been gathered over many years. Examples include the presence of lysosomes and dense bodies in MES cells (Greene and Pratt, 1976), evidence of cell cycle and DNA arrest (Pratt and Martin, 1975), changes in lysosomal enzymes and the degradation of intracellular organelles (Ads et al., 1983; Hayward, 1969). TUNEL staining revealed that apoptosis begins in the MEE before the shelves make contact and occurs in the epithelial cells along the seam, in the oral and nasal epithelium, in the epithelial triangles at the corners of the fusing edge and in the mesenchyme as the macrophages phagocytose the dead cells (Martinez-Alvarez et al., 2000).

Further evidence for cell death has come from work on  $TGF-\beta_3$ . In the  $TGF-\beta_3$  mutant mice the shelves grow and elevate normally, but when they come into contact with each other nothing happens. Even when placed together in culture fusion does not occur unless  $TGF-\beta_3$  is added to the culture medium (Taya et al., 1999).  $TGF-\beta_3$  is expressed in the MEE prior to shelf elevation and  $TGF-\beta_3$  mutant mice have

decreased levels of apoptosis (Martinez-Alvarez et al., 1996) supporting the theory that the MES disintegration involves programmed cell death.

Theories involving EMT came first from morphological observations and cell tracking studies using lipophilic molecules, such as carboxyfluorescein (Griffith and Hay, 1992) but the results remain unconvincing. The number of mesenchymal cells labelled is so low they could simply be an artefact or due to diffusion of the dye or they could be macrophages that have phagocytised apoptotic epithelial cells. EMT was proposed after MEE were infected with a replication-defective help-free retroviral vector, CXL, carrying the *Escherichia coli lacZ* gene. The PS were cultured and fusion occurred and  $\beta$ -galactosidase activity was detected, located in clusters of stellate shaped cells surrounded by similarly shaped mesenchyme with no evidence of apoptotic activity. More recently in vivo analysis using a Cre/loxP technology has enabled more precise cell tracking of the MES cells. Both a *Shh* and a *Keratin-14-Cre (K14-Cre)* Rosa reporter mice were used. The epithelial cells were tracked into islands of epithelial cells as the seam disintegrates, but as these disappeared so did any sign of the staining, proving that EMT does not occur (Vaziri Sani et al., 2005). One study concluded that all three mechanisms, i.e. cell death, cell migration and EMT were occurring (Martinez-Alvarez et al., 2000) to cause the MES to disappear.

### **1.3 Primary and secondary palates in different species**

The palatal shelves in vertebrates develop from bilateral outgrowths of the maxillary processes from the first pharyngeal arch. Reptiles do not have a secondary palate except the crocodylians where the palate develops horizontally and fuses in the midline (Ferguson, 1988). In birds the palatal shelves also grow horizontally, but they never fuse, creating a physiological cleft palate (Shah et al., 1987). In mammals, including the camel (Konsowa, 2009), rodents, baboons (Bollert and Hendrick.Ag, 1971) and humans (Luke, 1976) the bilateral outgrowths develop vertically down the sides of the tongue and then elevate into a horizontal position above the tongue and fuse.

Mouse palatogenesis resembles human palatogenesis, the major difference between the two is the time scale of events. Mouse palatogenesis, from initial outgrowth to fusion takes around six days whereas in humans these processes take around six weeks. Mouse mutant models of human cleft palates have shown that the molecular mechanisms are conserved between the two species. Through studying wild type mice

we can discover the cellular mechanisms behind facial morphogenesis and eventually compare these to mice carrying genetic mutations affecting the craniofacial region. Cellular mechanisms are more than gene expression and morphogen secretion. Analysis is being done using molecular expression patterns, but the field lacks a thorough study mapping growth patterns and looking into the cell behaviours behind them.

#### **1.4 Cellular processes that cause directional growth**

Setting aside issues of palatal fusion, this thesis focuses on the two prior processes, namely palatal shelf outgrowth and elevation. Both of these involve growth in the literal sense – tissues or parts of tissues getting bigger. Importantly, palate outgrowth and elevation involve directional growth.

Growth is used to describe many processes involved in morphogenesis but it only begins to describe the range of cellular mechanisms that could be involved. Development of an embryo from a single cell to a complex organism involves a lot more than it just getting bigger. Often studies go no further than to look at a single proliferation marker in a sprinkling of examples when studying growth, after presuming that proliferation must be the main or only contributing mechanism. Cell proliferation cannot be solely responsible for the variety and complexity of organisms that exist. Major factors in growth are the directionality of the growth and the mechanisms behind the forces driving it.

Directional growth can be caused by directional behaviours, such as orientated cell division, or by non-directional behaviours occurring in certain regions, (e.g. localized cell proliferation). Mechanisms that can contribute to directional growth include proliferation, apoptosis and changes in cell shape and size (Fig. 1.4). The amount each of these mechanisms contributes to morphogenesis will vary from tissue to tissue, for example in the limb it has been demonstrated that cell proliferation cannot contribute solely to outgrowth and explain the change in limb bud shape (Boehm et al., 2010) and other contributing mechanisms have since been identified. The palate is another system, comparable to the limb, which initially develops from a simple outgrowth. A lot of work, both new and old and from a range of labs has looked into how proliferation changes during the development of the palate.

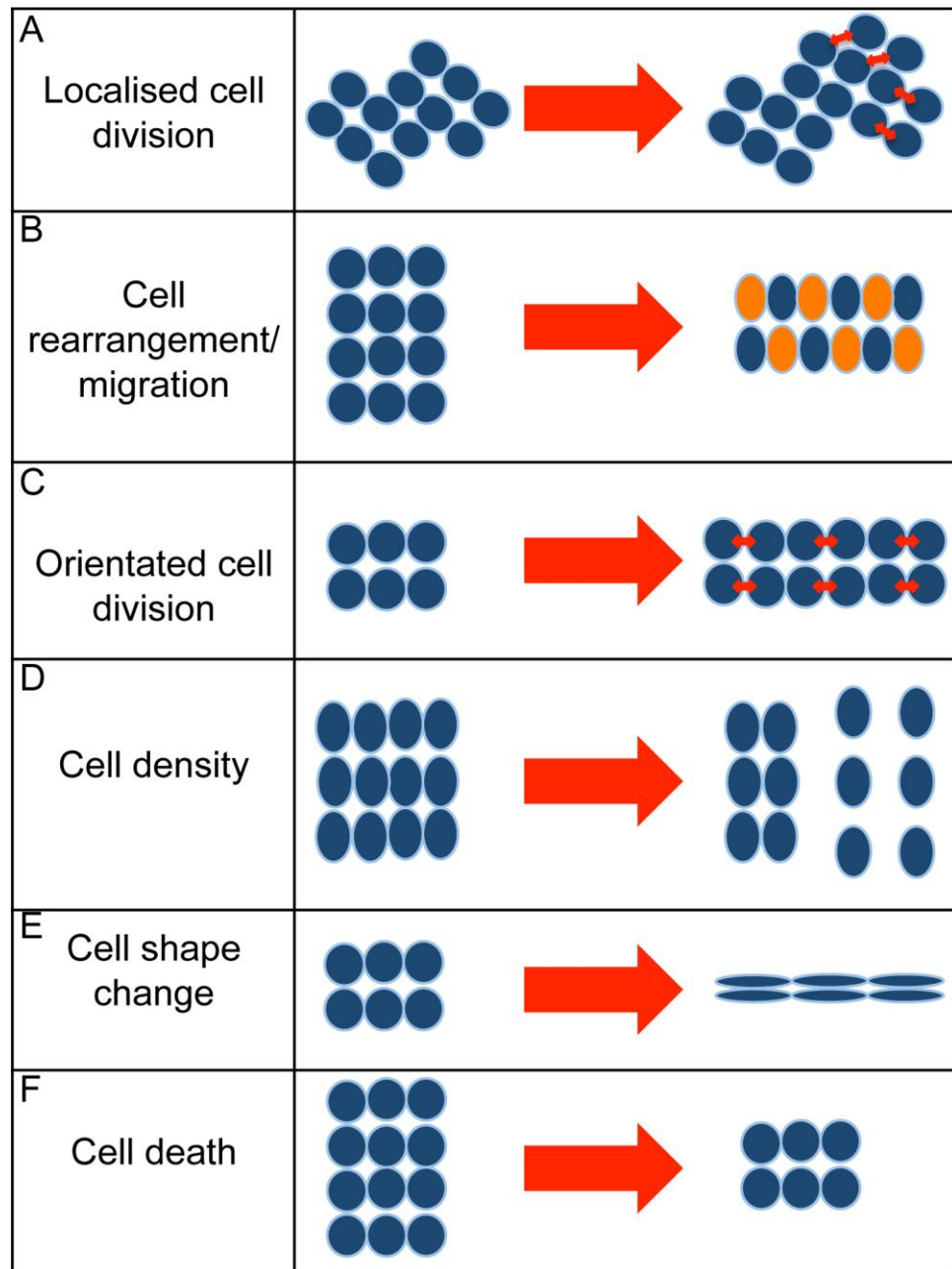


**Figure 1.4 Cellular mechanisms of morphogenesis** A) Localised cell division B) Cell rearrangement/migration C) Orientated cell division D) Cell density E) Cell shape change F) Cell death. Blue/orange circles represent cells showing the potential impact of each cellular mechanism on a uniform sheet of cells.

The growth of the facial prominences is likely to be caused by more than just localized cell proliferation; to create a specific organ of the correct size, shape and orientation other mechanisms such as orientated cell division, cell shape change and cell rearrangement/migration may also play a role in the development of the tissue. A range of cellular mechanisms that are potentially contributing to morphogenesis of the palate will be briefly described here and looked at more thoroughly in the following chapters.

#### **1.4.1 Localised cell division**

It appears easy to understand how cell proliferation leads to growth (Fig. 1.4A), the cell undergoes mitosis and two daughter cells are formed. More cells generally take up more space therefore the tissue grows, but this is not the case in early frog development when the cells are dividing but the embryo remains the same overall size. For growth to happen the cells have to increase in size and there must be a homeostatic mechanism controlling and limiting the size of the cells. Cell division resets the size of the daughter cells requiring the homeostatic mechanism to drive their growth again leading to growth of the tissue (Kafri et al., 2013).

It is a process that is apparently easy to quantify, with many markers available to highlight which stage of the cell cycle a certain cell is in and therefore whether it is cycling. They range from Ki67 which will mark all active stages of the cell cycle to bromodeoxyuridine (BrdU) which marks cells in the S phase of the cell cycle, cells undergoing DNA synthesis, during exposure to BrdU.

Cell division can contribute to directional growth simply by regional control of proliferation so it only occurs in certain parts of the tissue or at different rates across the tissue. A simple change in expression pattern or levels of the modulating factors could easily disrupt this sort of regional behavioural pattern, resulting in a cleft palate.

#### **1.4.2 Polarised cells and orientated cell behaviours**

Polarised cell behaviours are a vital part of early craniofacial development; one of the first mechanisms to occur is the migration of the neural crest cells from the pharyngeal arches into the facial prominences. Cell migration and other polarised cell behaviours could also be occurring on a smaller scale, potentially within the palatal shelf

analogously to what has been demonstrated in the developing limb bud. Elongation in particular could involve cell rearrangement including two types of intercalation (Keller, 2006) - radial (the primary mechanism of epiboly, the spreading of ectoderm over the outside of an early vertebrate embryo) and planar (mediolateral planar intercalation is central to convergent extension, the elongation of the primary body axis during gastrulation) (Fig. 1.4B). These can allow a tissue to elongate without the addition of new cells or any change in volume.

It is possible to use the Golgi apparatus as a marker of cell polarisation because this organelle is known to align with the apical side of the cell in a polarised epithelium and with the leading edge of a migrating cell. If cells lose their correct and possibly coordinated polarity it could lead to the incorrect development of the palate and cause a cleft to form.

### **1.4.3 Orientated cell division**

When a cell undergoes proliferation two identical daughter cells are formed from the parent cell. This process starts with the cell entering prophase when the chromosomes condense, the nuclear membrane disintegrates and the centrioles move towards opposite ends of the cell. Next is metaphase when microtubules attach the centrioles to the centrosomes and align the chromosomes along the centre of the cell, the metaphase plate. At this stage the mitotic spindles are potentially still highly mobile. Time-lapse confocal microscopy has shown that spindles in the neuroepithelium of the rat cerebral cortex rotate within the plane of the epithelium until anaphase begins (Minc & Piel, 2012; Adams, 1996). It is during anaphase that the identical chromatids separate and migrate towards the centrioles at either end of the cell. At which point the cell enters telophase, new nuclear membranes are formed and cytokinesis begins resulting in two new cells. The orientation of the cleavage therefore depends on the position of the centrioles and the spindles formed with them. If all the cells form new daughter cells in the same orientation then the tissue will grow in that direction (Fig 1.4C).

The dividing of a cell into its two daughter cells could be producing a force that contributes to the growth of the tissue. If the angles of division are distributed uniformly or randomly the growth is isotropic whereas if there is a bias in one direction then the growth could be anisotropic. Alternatively the orientation of the cell division

could be dictated by the overall growth of the tissue elongating the cell, creating a long axis along which it is favourable for the spindle to align. Disruption of orientated cell division in the palate could, for example cause the tissue to expand isotropically and so fail to grow anisotropically at the outgrowth stage.

#### **1.4.4 Cell spacing**

Cells that are more spaced out will take up a larger volume resulting in a larger tissue and if the same number of cells were tightly packed together then the overall tissue will be smaller (Fig 1.4D). There are several possible mechanisms behind changes in cell spacing, the cells themselves could be changing shape, the amount of the extracellular matrix could be changing or cell death or proliferation might be occurring. To investigate changes in spacing within the tissue the distance between the centroid of each nucleus was used. This nuclear spacing measure will blend two possible underlying mechanisms, cell shape change and changes in the amount of ECM. Once any changes have been identified, using the nuclear spacing measure, the mechanism behind the change can be investigated further.

Changes in cell spacing could disrupt palatogenesis, potentially forming a cleft palate. For example if the cells do not condense when it is required signals that rely on cell-cell contact could be lost. Tendon formation in the limb is disrupted after the loss of cadherin-11 leading to cell separation and changes in cell shape (Richardson et al., 2007). Alternatively if the cells adhere to one another too closely when the mesenchyme is required to flow, as suggested by some theories of palate elevation (see section 1.2.3.3 and (Walker and Fraser, 1956)), then this process might fail. Cell density and growth have also been linked in chick wing development when the “density dependent control of cell divisions” hypothesis was formed (Summerbell and Wolpert, 1972). If a clear pattern is found in the cell density during palate development it could be critical that this is maintained to prevent formation of a cleft palate.

##### **1.4.4.1 Cell Shape**

Changes in cell shape can remodel the tissue and contribute to elongation. This mechanism could be caused by the cell's intrinsic forces and remodelling of the cytoskeleton, or by external forces acting upon the cell and forcing it into a different shape (Fig 1.4E). Throughout development the importance and influence that the



shape of a cell can have has been demonstrated, such as in *Drosophila* germband extension (Lecuit and Lenne, 2007), during closure of the neural tube in vertebrates (Suzuki et al., 2012), in deciding cell fates (McBeath et al., 2004), and during plant growth (Zhang et al., 2011). Changes in cell shape can be involved in bending epithelial sheets. For example apical constriction involves myosin driving the contraction of actin filaments around the apical end of the cell (Martin et al., 2009). This results in the cell's cytoplasm and organelles being forced towards the basal end of the cell causing basal widening and the cells end up wedge shaped. This has been studied in different organisms for example chick neurulation (Schoenwolf et al., 1988) and *Xenopus* gastrulation (Lee and Harland, 2007) but most extensively in *Drosophila* in the processes of ventral furrow formation (Lecuit, 2010; Sawyer et al., 2010).

Different cell shapes have been observed in different regions of the palate and their shapes change throughout the process of elevation (Babiarz et al., 1979). For this analysis the palate was split into three along its AP axis and changes from rounded to elongated and back again to round cells were seen in both of the anterior two-thirds. If these shape changes are vital to the elevation process then any disruption could prevent elevation occurring and cause a cleft palate.

#### **1.4.4.2 Apoptosis**

Programmed cell death, or apoptosis (Fig 1.4F), occurs when cells die due to their own action and it is another mechanism that contributes to morphogenesis during development. Apoptosis is an intrinsic suicide mechanism, during which the cell membrane is carefully maintained so that the cell's contents do not cause an immune response but the fragments it breaks up into can be neatly phagocytosed by macrophages.

Killing off specific cells can help mould tissues or fuse them by breaking down boundaries. Otherwise too many of one type of cell might be present. It is also possible that towards the end of development of an organ the cells required for its growth and morphogenesis are different from those that form the final organ and so the developing cells are killed off. Apoptosis could be used on a small scale to do the final sculpting of an organ or on a larger scale to remove entire structures, for example in the uterus in male mammals or the tail of a tadpole. Digit formation requires

apoptosis, clearly demonstrated by adding the apoptosis inhibitor caspase to a chick embryo resulting in webbed feet (Huang and Hales, 2002; Hurlle et al., 1996).

There is evidence of apoptosis being involved in the fusion stage of palate development (see section 1.2.3.4) and a cleft palate can result simply by one process in this final stage of palate development not working correctly. However, only miniscule levels of apoptosis have been found in the wild-type mesenchyme at earlier stages (Goudy et al., 2010; Rice et al., 2004), and this mechanism will not be considered further in this thesis.

## **1.5 Aims of this study**

The objective of this study was to investigate the links between genetic mutations and the resulting cleft palate phenotypes at the level of cellular behaviour. To this end, there were four specific aims:

To develop, adapt and apply a set of established and new techniques for labelling and imaging cells

To analyse those images to extract quantitative measures of underlying cellular phenotypes specifically on sectioned material

To create a cell phenotype dataset for the normal development of the palatal mesenchyme

To compare normal and various cleft palate phenotypes at the cell phenotype level

## **2.0 Materials and methods**

### **2.1 Solutions**

All solutions were made up with deionized water.

#### **2.1.1 10X Phosphate Buffered Saline (PBS) (pH 7.5)**

80mM Na<sub>2</sub>HPO<sub>4</sub>

20mM NaH<sub>2</sub>PO<sub>4</sub>·2(H<sub>2</sub>O)

100mM NaCl

Made with nuclease-free H<sub>2</sub>O. pH adjusted and autoclaved

#### **2.1.2 PBT (TritonX)**

1 litre PBS

2 ml TritonX

#### **2.1.3 PBT (Tween)**

1 litre PBS

2 ml Tween

#### **2.1.4 Paraformaldehyde (PFA) (4%)**

40g PFA in 1 litre of warm 1xPBS

Loosely seal with lid and let stir on hotplate at 60°C all day.

#### **2.1.5 Dent's fixative**

80% CH<sub>3</sub>OH

20% Dimethylsulphoxide (DMSO)

#### **2.1.6 Mowiol**

2.4g Mowiol 4-88 (Polyvinylalcohol 4-88)

6.0g Glycerol

Mix well

Add 6.0ml H<sub>2</sub>O while still mixing

Leave at room temperature for 2 hours

Add 12ml 0.2M Tris-HCl (pH 8.5)

Incubate at 50°C for 10 minutes and mix further. Incubate at 50°C overnight until dissolved. Centrifuge at 5000g (or 4100rpm) for 15minutes. Collect and store supernatant at -20°C.

### **2.1.7 Bromodeoxyuridine (BrdU)**

Make up a 10mg/ml stock solution

Add 0.01mg BrdU powder to 1ml PBS

### **2.1.8 Iododeoxyuridine (IddU)**

Make up a 10mg/ml stock solution

Add 0.01mg IddU powder to 1ml PBS

### **2.1.9 Sodium Citrate (pH 6)**

28g tri-sodium citrate

~850ml H<sub>2</sub>O

Adjust to pH6.0 using citric acid.

Fill up to 1 litre with H<sub>2</sub>O.

Autoclave.

### **2.1.10 Polymerase Chain Reaction (PCR) digestion high molecular weight (HMW) Buffer (for digesting Tbx-1)**

10mM Tris-HCl (pH 8.0)

4ml 0.5M Tris-HCl

150mM NaCl

30ml 1M NaCl

10mM Ethylene Diamine Tetra Acetic Acid (EDTA)-NaOH (pH 8.0)

4ml 0.5M EDTA

0.1% Sodium Dodecyl Sulphate (SDS)

2ml 10% SDS

Make up to 200ml with H<sub>2</sub>O

### **2.1.11 0.5M Tris-HCl (pH 8.0)**

30.28g Tris

~450ml H<sub>2</sub>O

Adjust to pH8.0 with HCl

Fill up to 500ml with H<sub>2</sub>O

Autoclave

### **2.1.12 1M NaCl**

11.60g NaCl

Fill up to 200ml with H<sub>2</sub>O

Autoclave

### **2.1.13 10% SDS**

10g SDS

Fill up to 100ml with H<sub>2</sub>O

### **2.1.14 EDTA pH 8.0**

29.22g EDTA

~170ml dH<sub>2</sub>O

Adjust to pH8.0 with NaOH

Fill up to 200ml with H<sub>2</sub>O

Autoclave

## **2.2 Genotyping Protocol**

### **2.2.1 *Tbx-1* Primers**

The genotype of the *Tbx-1* mice was determined using PCR analysis with three *Tbx-1* specific primers. The primer's sequences were: TAR2R- 5' TCG ACT AGA GCT TGC GGA AC; Wt F3- 5' AGT CTG GGG ACT CTG GAA GG; Wt R3- 5' AAG GCA GAT CCT GCT ACA CC.

### **2.2.2 *Tbx-1* PCR master mix**

0.5µl dNTPs

0.5µl F3  
0.5µl R3  
0.5µl TAR2R  
0.5µl taq  
2.5µl MgCl<sub>2</sub>  
2.5µl 5x PCR Digestion Buffer  
16.5µl H<sub>2</sub>O  
1µl DNA

### **2.2.3 *Tbx-1* PCR conditions**

95°C 15 minutes, (95°C 30 seconds, 65°C 20 seconds, 72°C 30 seconds) x 33 cycles, 72°C 10 minutes 4°C hold. The results were run on a 2% agarose gel. Two bands were generated after PCR reaction a 200 base pair (bp) wild-type and a 150bp mutant.

### **2.2.4 *Msx-1* Primers**

The genotype of the *MSX-1* mice was determined using PCR analysis with three *MSX-1* specific primers. The primer's sequences were: *MSX1* -3' TGC AGG ACC GCC AAG AGG AAA AGA GAG GCC; *MSX1* -5' TTC TCC AGC TCG CTC AGC CTC ACC; *LacZ* -3' GGCAAA GCG CCA TTC GCC ATT CAG GC.

### **2.2.5 *Msx-1* PCR master mix**

5.125µl H<sub>2</sub>O  
0.625µl 3 in 1 primer mix  
6.25µl KAPPA2G robust ready mix (KAPA Biosystems)  
1µl DNA

### **2.2.6 *Msx-1* PCR conditions**

95°C 1-3 minutes, (95°C 15 seconds, 60°C 15 seconds, 72°C 15 seconds) x 35 cycles, 72°C 10 minutes 4°C hold. The results were run on a 1% agarose gel. One band was generated after PCR reaction a 300 base pair (bp) wild-type or a 200bp mutant.

## **2.3 Mice**

### **2.3.1 Wild type CD-1**

The CD-1 mouse strain was used for all wild-type (WT) mice experiments. The mice were housed in the Biological Services Unit, New Hunts House, Guy's Campus, King's College London, UK. BSU technicians carried out maintenance of CD-1 mice, timed matings and plug checking.

### **2.3.2 *Tbx-1*<sup>-/-</sup> mouse line**

The *Tbx-1* mouse strain was provided by Professor Peter Scambler, Institute of Child Health, UCL, (Papangeli and Scambler, 2013). Four mice were provided carrying a *Tbx-1* null allele in a C57BL/6 genetic background. The colony was maintained by breeding heterozygous *Tbx-1* males with wild-type C57BL/6 females. *Tbx-1* null embryos were generated by mating heterozygous *Tbx-1* males with heterozygous *Tbx-1* females.

### **2.3.3 mT/mG mouse line**

The Gt(ROSA)26Sor<sup>tm4(ACTB-tdTomato,-EGFP)</sup>Luo/J mouse strain (referred to henceforth as the mT/mG strain) was purchased from the Jackson Laboratory, stock number 007576. The mice have loxP sites either side of a membrane targeted tdTomato (mT) cassette and all cells express red fluorescent protein. The mT cassette is deleted when the mouse is bred with a Cre recombinase expressing mouse and the targeted tissues will express membrane-targeted EGFP (mG) and appear green. The colony was maintained by breeding homozygous x homozygous mice. The embryos were kept in the dark as much as possible throughout processing and staining by wrapping their container with foil or placing a box over them while on the laboratory bench.

### **2.3.4 *Msx-1*<sup>-/-</sup> mouse line**

The colony was maintained by breeding heterozygous *Msx-1* males with wild-type CD-1 females. *Msx-1* null embryos were generated by mating heterozygous *Msx-1* males with heterozygous *Msx-1* females.

### **2.3.5 Embryo collection**

The day that the vaginal plug was discovered was counted as embryological day 0.5 (E0.5). Once the desired embryological day was reached the mother was sacrificed by CO<sub>2</sub> asphyxia and cervical dislocation and the embryos were immediately dissected out and placed in PBS on ice.

### **2.3.6 Embryo fixation**

Embryos were removed from the uterus, in PBS, using fine-tipped forceps under a dissecting microscope. The heads were dissected off and fixed in 4% PFA overnight at 4°C.

### **2.3.7 Embryo processing**

#### **2.3.7.1 Paraffin embedding**

Embryos were washed for 2x1 hour in PBS. Then dehydrated through an ethanol series, 30%, 50%, 70%, 85%, 95%, 100% for 1 hour in each on a rocker at room temperature. Embryos were placed in histoclear for 2 x 1 hour at room temperature and then in a 50:50 histoclear:paraffin mixture and kept in a 63°C oven for 1 hour. Then 5 x 1 hour paraffin changes in the 63°C oven. Next they were embedded in the desired orientation in a metal mould and left on an ice block to cool. They were stored in boxes at room temperature.

#### **2.3.7.2 Gelatin embedding**

Embryos were washed at room temperature 2 x 1 hour in PBS. They were then placed in 15% sucrose/PBS until they sunk to the bottom of the jar. They were removed from the sucrose and place in a 50:50 mix of 30% sucrose and 15% gelatin (type B) and left at 37°C until sunk or overnight. The specimens were embedded in fresh sucrose:gelatin mix on ice and then transferred to -80°C to freeze and stored.



## **2.4 Sectioning**

### **2.4.1 Microtome sectioning**

Paraffin wax embedded samples for sectioning were firstly trimmed using a razor blade and then sectioned on a microtome (Leica RM2295) at 8µm thick using disposable microtome blades (Leica). Serial sections were mounted on to slides (Superfrost Plus, VWR) using a 42°C deionised H<sub>2</sub>O filled waterbath and floating the wax ribbons on to the slides. Slides were placed on to a hot block to be dried overnight at 42°C.

### **2.4.2 Cryosectioning**

Samples embedded for cryosectioning were removed from the -80°C freezer and placed in the -25°C freezer for 1 hour. A chuck was placed in the -80°C freezer for the same length of time. The block, with the sample embedded in it, was stuck on to the top of a chuck using an optimal cutting temperature (OCT) compound and this was immediately placed in the -20°C freezer for at least 1 hour. The chuck with the block attached was placed in the cryostat and trimmed using a razor blade. 30µm thick sections were cut and immediately placed on to slides (Superfrost Plus, VWR) and stored in the -20°C freezer until staining.

## **2.5 Immunohistochemistry**

### **2.5.1 IddU/BrdU/DAPI fluorescent immunohistochemistry**

BrdU, a thymidine analogue, is used in an immunohistochemical technique to visualise proliferating cells as it marks the S phase in the mitotic cycle. The BrdU injected intraperitoneally into a pregnant female mouse is incorporated into newly synthesized DNA throughout the maternal and embryonic body in place of thymidine as the cells replicate. Cells which have BrdU incorporated were detected using an antibody against BrdU and visualised using a fluorescent secondary antibody. IddU is another thymidine analogue also used to identify proliferating cells. By using monoclonal antibodies BrdU and IddU were identified.

DAPI (4',6-diamidino-2-phenylindole) is capable of passing through cell membranes and has a very strong affinity with DNA and was used to mark the nuclear position in all cells.

Mouse embryos were labelled with IddU via intraperitoneal injection into pregnant females (50 mg/100 g body wt) 2.5 hours prior to sacrifice.

The heads were removed, fixed with PFA and embedded in wax. 8 µm thick frontal wax sections were stained for BrdU incorporation by dewaxing with xylene (2 x 15 minutes), rehydrated (100%, 90%, 70%, 50% EtOH, 5 mins each), and washed PBS (2 x 5 mins) and then in 0.2% TritonX in PBS (PBT) 5 min. Antigen retrieval was performed by microwaving at full power for 4 x 5 minutes in 10mM sodium citrate (pH 6), topped up with RNase-free H<sub>2</sub>O between microwaving (Panasonic Inverter Microwave Oven, model NN-SD997S) and then cooled on ice for 10 minutes. The sections were placed in blocking solution (10% goat serum in PBT) for 1 hour at room temperature. Primary antibody (Anti-BrdU Pure, BD Biosciences) was diluted (1:200) in blocking solution and the slides were incubated overnight at 4°C. The primary antibody was washed off in PBT (3 x 10 minutes). The sections were blocked again with 10% goat serum in PBT for 2 hours at room temperature. Secondary antibody (polyclonal goat anti-mouse immunoglobulins/biotinylated, DAKO) was diluted (1:200) in block and incubated for one hour at room temperature. The slides were washed in PBT for 10 minutes before being incubated with DAPI (1:1000) for 10 minutes. Finally they were washed for 4 x 15 minutes in PBS and coverslipped using Mowiol.

### **2.5.2 Gamma-tubulin, phosphohistone-H3 and DAPI immunohistochemistry**

The gamma-tubulin antibody allows the centromeres to be visualized and by measuring the angle of a line drawn between them the orientation of mitosis to be calculated. All cells stain with anti-gamma tubulin antibodies, so to make it clearer which cells are undergoing mitosis a phosphohistone-H3 antibody is used which highlights cells in the S-phase of the cell cycle.

The embryos were embedded for cryosectioning in sucrose/gelatin and were cut frontally in 30 µm sections and immediately placed on Superfrost Plus slides. For staining the slides were placed in 2 x 10 minute PBS washes and then in pre-cold (-20°C) methanol for 20 minutes. Before another 10 minute PBS wash. Samples were

blocked using a 10% goat serum/3% BSA/PBT (0.1% TritonX) solution for 1 hour at room temperature and then they were placed in primary antibody, 1:500 dilution anti-gamma-tubulin and 1:300 dilution anti-phosphohistone-H3 in blocking solution overnight at 4°C. The primary antibody was washed off through 3 x 10 minutes in PBT (0.1% Tween). The sections were blocked again for 1 hour at room temperature and then secondary antibodies were added (1:200 Alexa-fluor 635-goat-anti-rabbit antibody and 1:300 Alexa-fluor 488-goat-anti-mouse antibody) for 1 hour at room temperature. The slides were washed in PBT for 10 minutes before being incubated with DAPI (1:1000) for 10 minutes. Finally they were washed for 4 x 15 minutes in PBS and coverslipped using Mowiol.

### **2.5.3 Golgi apparatus and DAPI immunohistochemistry**

The embryos were embedded for cryosectioning in sucrose/gelatin and were cut frontally in 30 µm sections and immediately placed on Superfrost Plus slides. For staining the slides were placed in PBS for 2 x 10 minute washes. Samples were blocked using a 10% goat serum/3% BSA/PBT (0.1% TritonX) solution for 1 hour at room temperature and then they were placed in primary antibody (1:500 rabbit-anti-Giantin antibody; Abcam), in blocking solution overnight at 4°C. The primary antibody was washed off through 3x10 minutes in PBT (0.1% Tween). The sections were blocked again for an hour at room temperature and then secondary antibodies were added (1:300 Alexa-fluor 488-goat-anti-rabbit antibody) for 1 hour at room temperature. The slides were washed in PBT for 10 minutes before being incubated with DAPI (1:1000) for 10 minutes. Finally they were washed for 4 x 15 minutes in PBS and coverslipped using Mowiol.

### **2.5.4 Fibronectin antibody**

When the immunohistochemical protocol described in 2.5.3 was carried out on the *Tbx-1*<sup>-/-</sup> mouse line there was no endogenous membrane fluorescence. Therefore a monoclonal mouse-anti-fibronectin primary antibody (Thermo Scientific, FBN11) and the secondary antibody 1:200 Alexa-fluor 568-goat-anti-mouse were also included. Fibronectin is found in the ECM and helped to identify which stained Golgi belong to which nuclei.

### **2.5.5 BrdU immunohistochemistry for brightfield imaging**

Mouse embryos aged E13.5 and E14.5 were labelled with BrdU via intraperitoneal injection into pregnant females (20 mg/100 g body wt) 2 hours prior to sacrifice. The heads were removed, fixed with paraformaldehyde and embedded in wax. 8 µm thick frontal wax sections were stained for BrdU incorporation by dewaxing with xylene (2 x 10 minutes), rehydrated (100%, 100%, 95%, 90%, 70% EtOH, 5 mins each), and washed PBS (2 x 5 mins). To block the endogenous peroxidases the slides were immersed in 3% H<sub>2</sub>O<sub>2</sub> and 10% Methanol in PBS, for 15 minutes, then washed in 0.2% TritonX in PBS (PBT) 5 min. Antigen retrieval was performed by microwaving at full power for 4 x 5 minutes in 10mM sodium citrate (pH 6), topped up with RNase free H<sub>2</sub>O between microwaving and then cooled on ice for 10 minutes. The sections were blocked with 10% goat serum and 0.2% gelatin in PBT for 1 hour at room temperature. Primary antibody (Anti-BrdU Pure, BD Biosciences) was diluted (1:100) in block and the slides were incubated overnight at 4°C. The primary antibody was washed off in PBT (3 x 10 minutes). Secondary antibody (polyclonal goat anti-mouse immunoglobulins/biotinylated, DAKO) was diluted (1:100) in block and incubated for 1 hour at room temperature. The slides were washed in PBT (3 x 10 minutes) before being incubated with streptavidin-peroxidase (Invitrogen) diluted 50:50 in blocking solution for 10 minutes at room temperature. Next the slides were washed in PBT (10 minutes) followed by PBS (3 x 5 minutes) and the cells were visualised using DAB kit (Vector Laboratories). To counter-stain the tissue it was immersed in haematoxylin for 30 seconds and then placed under running tap water for three minutes. Finally the slides were washed in PBS then distilled water for 30 seconds each, dehydrated (30%, 50%, 70%, 90%, 95% and 100% EtOH 3 minutes each) and coverslipped with DPX.

## **2.6 Image acquisition**

### **2.6.1 Fluorescent images**

Images were taken on a TCS SP5 Leica confocal microscope with a HCX PL APO CS N.A. 1.25 X40 oil immersion objective using the Leica Application Suite Advanced Fluorescence (LAS-AF) program. This instrument was equipped with a XY-motorised stage and images were stitched together using the LAS-AF software. Single-plane images were taken for the IddU/BrdU/DAPI staining as this was sufficient to detect all

the nuclei in the section. Z-stacks were taken of the Giantin and gamma-tubulin staining. Optical sections were taken at 0.17µm, half the size of the system's optimized intervals. All images were taken at a 1024 x 1024 pixel resolution and 4 frame averages.

## **2.6.2 Brightfield images**

Brightfield images were taken on a Zeiss Axioskop upright microscope with Axioacam HR camera at 10x magnification using Axiovision version 4.8.

## **2.7 Image processing**

Leica Image Files (LIF) were taken directly from the confocal microscope and opened in Volocity (PerkinElmer). Once a .LIF was imported into Volocity the noise was removed from every channel in every image using an inbuilt fine filter.

A protocol was developed to identify cells in each of the channels (see chapter 3) and to record the co-ordinates of the centroid of each cell in a table. The columns of interest in this table, which can be extracted as a tab delimited table, were Name, ID, Item Name, Centroid X, Centroid Y, Centroid X (µm), Centroid Y (µm). From this every object was identified from the co-ordinates of its centroid and which image it originated from.

### **2.7.1 Calculating relative amounts of proliferation**

The amount of proliferation was calculated for just the palatal outgrowth region (the proximal boundary is shown by the red dotted line in Fig. 2.2). The original images were cropped to the ROI in Volocity and the cell identification protocol was run (described in chapter 3). The table of image data generated by Volocity can be opened in Microsoft Excel and subtotals of the total number of cells and the total number of proliferating cells calculated for each image. This allows the relative amount of proliferation to be calculated:

$$\text{Relative Proliferation (\%)} = \frac{\text{Total number of proliferating cells (BrdU/IddU labelled)}}{\text{Total number of cells (DAPI labelled)}} \times 100$$

Error bars on graphs show one standard deviation; this was calculated using Microsoft Excel. T-tests were carried out in Microsoft Excel with a p value  $p < 0.05$  considered statistically significant.

### **2.7.2 Creating Heat Maps in R**

For measuring nuclear spacing and displaying the data graphically, the R Package (Team, 2012) was used. R is an open source software package for data manipulation, graphical representation and statistical analysis. Andrew Economou (Green Lab, KCL) wrote macros in R that generated heat maps of the palate showing variations in either cell spacing or cell proliferation. These heat maps were based on the image data, mainly the cell co-ordinates, which was extracted by Volocity. Details of the macros are in the Appendix of this thesis.

The colour scale of the heat maps can be altered. For the palate data a cell spacing scale of 3  $\mu\text{m}$  to 18  $\mu\text{m}$  was used, this was selected because the entire range of colours was being used over the different stages and it had fewest blanks left by regions that are off the scale.

The heat maps were averaged over different numbers of neighbours creating a smoothed average effect. The spacing heat maps were averaged over one set of neighbours. To calculate the local proliferation index two sets of neighbours were used.

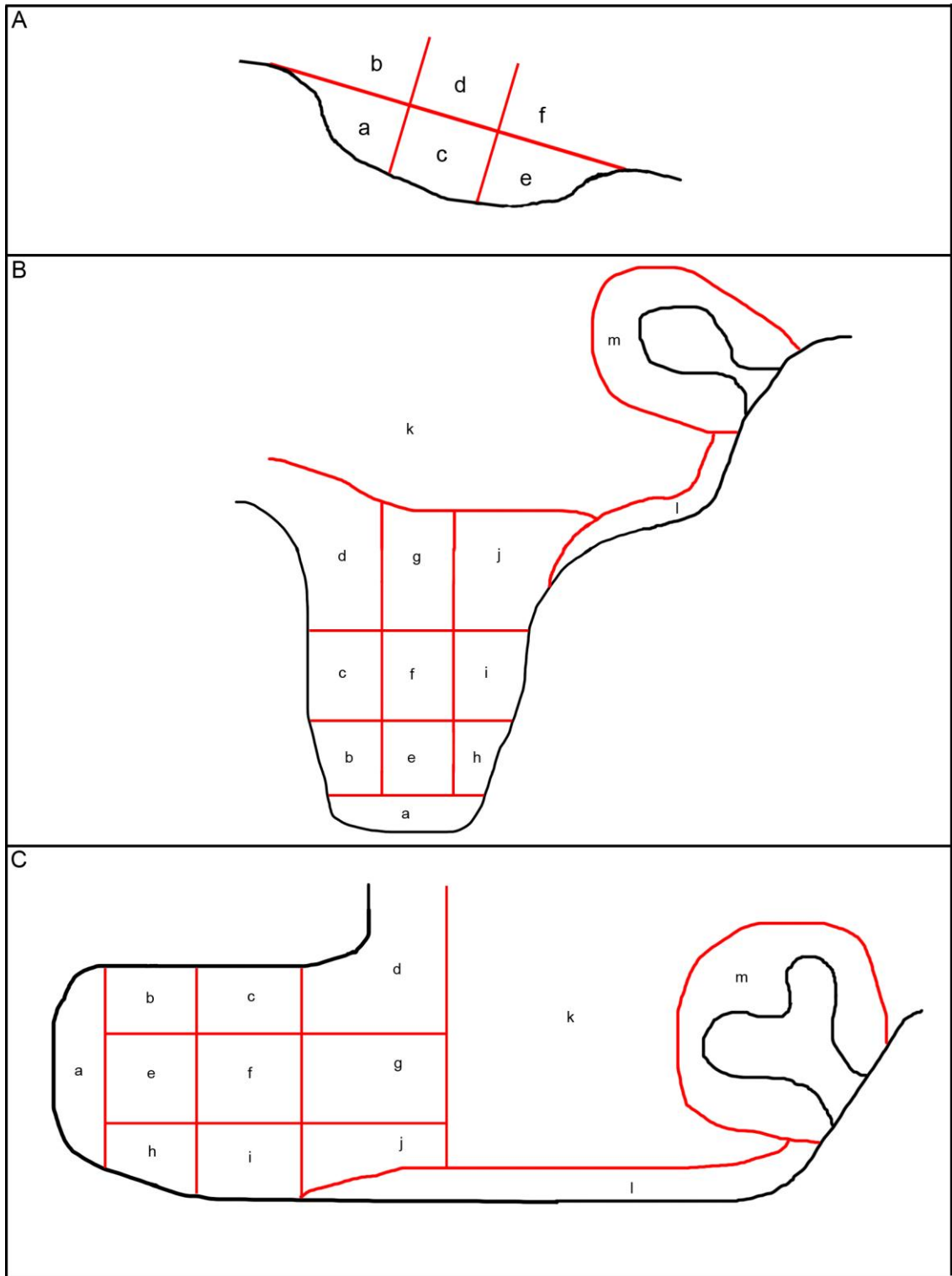


**Figure 2.1 Regions the heat maps were divided into for analysis** A) The small outgrowth at E11.5 was divided along the mediolateral axis and the mesenchyme directly distal to it was also measured B) The regions the palatal outgrowth was divided into if it had not elevated (E12.5, E13.5 and unelevated mutants) C) The regions an elevated palate was divided into.

## **2.8 Combining the heat maps**

Andrew Economou's R macro (see appendix) is also able to produce heat maps that summarise data from several sections using the commands "rotate", "translate", "combine" for spacing heat maps and "combine2" for proliferation heat maps. Once the images were registered by manual trial and error an average heat map was created from the data from all the heat maps.

## **2.9 Measuring the palate's proportions**

The .LIF file contains enough information about the images taken and the objective used for measurements to be taken using the line tool (Fig. 2.2). Several lines can be drawn at once and the information collated in a single table and exported to Microsoft Excel where graphs were created and T-tests carried out.

The height of the palatal outgrowth was considered to be the distance between the distal edge in the centre of the palatal outgrowth and a line drawn between the two shoulders of the palatal outgrowth prior to elevation (Fig. 2.2, white arrow marks the height and the red dotted line marks the proximal boundary) or post elevation a line was drawn perpendicular to the oral edge to the nasal shoulder (Fig. 2.2B, white arrow marks the height and the red dotted line marks the proximal boundary). The width of the palatal outgrowth was measured as the distance between the (prospective) oral and (prospective) nasal sides, a quarter of the height back from the distal tip and at an angle that was perpendicular to the line drawn to measure the height (Fig 2.2, white arrow).

## **2.10 Measuring angles in Volocity**

Once the .LIF were imported into Volocity the noise was removed and the image was then cropped into different sections for analysis. Cropping the z-stacks in the XY-plane gave the computer smaller image files to be process. Orientations were measured as follows:



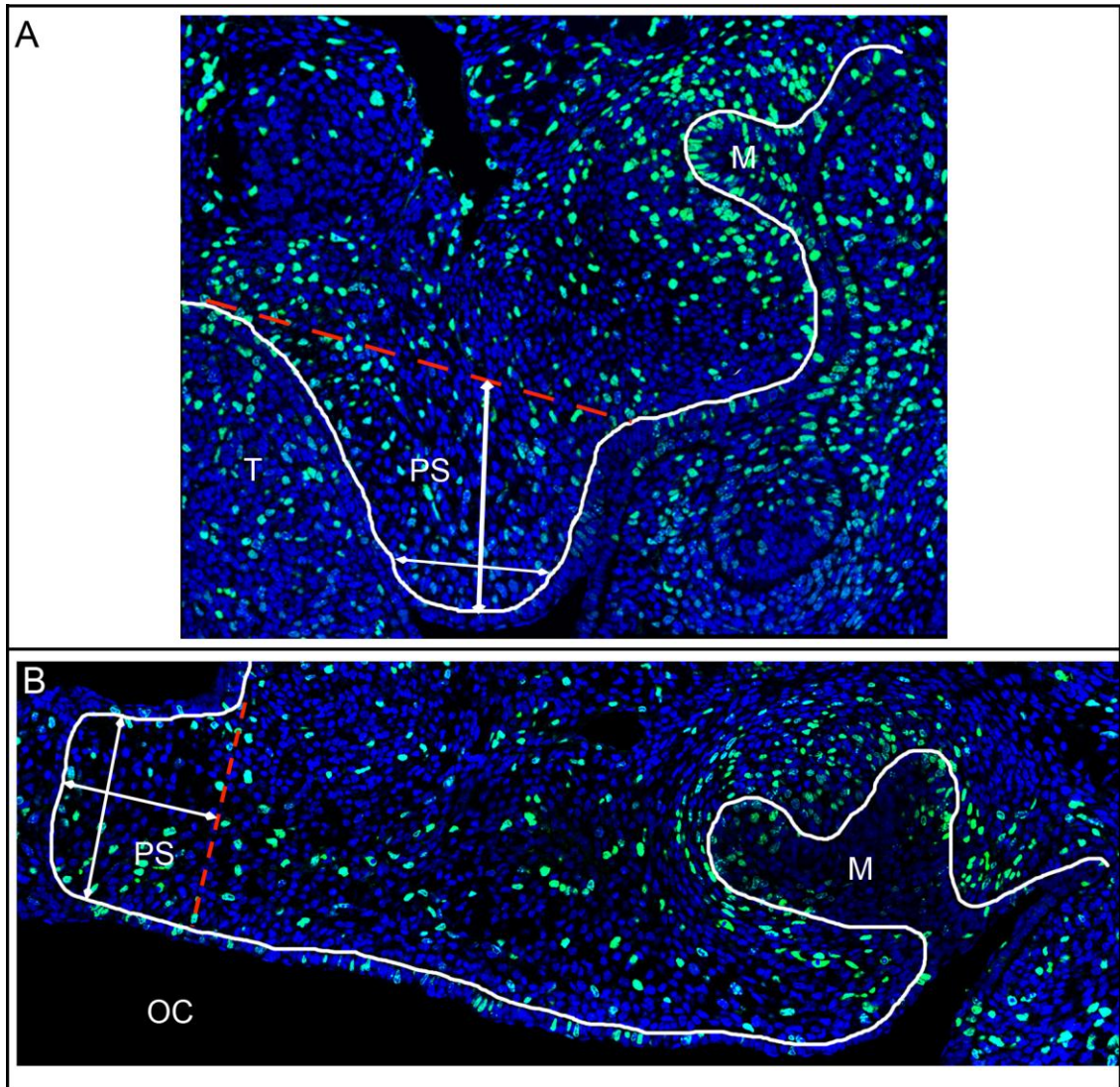


**Figure 2.2 Diagram to show where length measurements were taken** A) Before elevation the height was considered to be the length of a line drawn from the centre of the distal tip to the proximal boundary of the palatal outgrowth marked by the red dotted line. The width was taken at a distance of about one quarter of the height back from the distal tip B) After elevation the proximal boundary was between the nasal shoulder and the oral epithium, marked by the red dotted line. To measure the height a line was drawn between the proximal boundary and the medial edge. The width was measured the same distance back from the medial edge as before elevation. M, molar tooth bud; OC, oral cavity; PS, palatal shelf; T, tongue.

### 2.10.1 Measuring the Orientation of Cell Division

Gamma-tubulin staining allows the centrioles to be visualised. The DAPI and the mT/mG fluorescent membrane allowed individual cells to be identified and the PH-3 staining meant that proliferating cells were quickly located.

A Z-stack of the 30  $\mu\text{m}$  thick section was taken every 120  $\mu\text{m}$  along the anterioposterior axis. Volocity allows the user to scroll through the Z-stack and mark

the location of the centre of one centromere, highlighted by the gamma-tubulin antibody, and then to continue to scrolling through the stack to find and mark the centre of the cell's other centromere (Fig. 2.3A, C-D). Once each of these was selected the angle between them was recorded in a table, along with other measurements such as the co-ordinates of the centromeres and name of the original image. This table was exported into Microsoft Excel for further analysis.

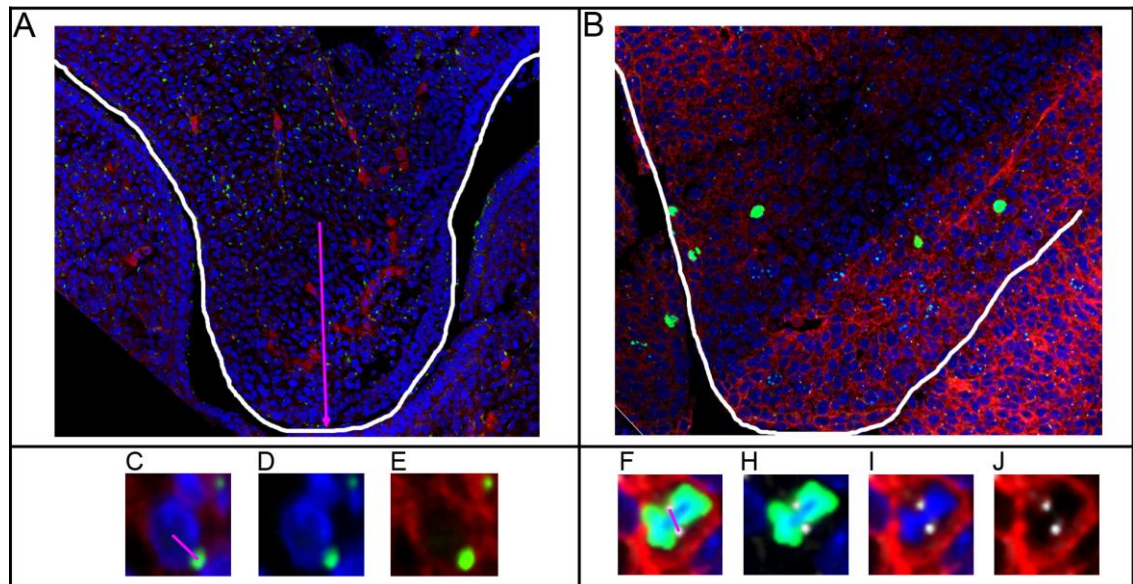


**Figure 2.3 How the orientation of the Golgi/spindles were measured** A) A single slice of the z-stack from the mT/mG mice stained for DAPI and Giantin. The Golgi were measured relative to the distal edge of the palate. Therefore the angle of the distal edge in each image was measured B) A single slice from the z-stack of an mT/mG mouse stained for PH-3, DAPI and gamma-tubulin C) The centre of the nuclear DAPI stain was identified and the angle between this and the centre of the Golgi stain was measured (purple line) D) Image of just DAPI and Giantin stain E) Image of the mT/mG membrane and Giantin stain. Using a combination of the three stains allowed each Golgi and its nucleus to be identified manually F) Purple line represents the angle between the middle points of the two centroids of the proliferating cell H) Image showing just the DAPI, PH-3 and gamma-tubulin stain I) Image of just the DAPI, mT/mG membranes and gamma-tubulin stain J) Image of just the mT/mG membranes and the gamma-tubulin stain.

### 2.10.2 Measuring the orientation of the Golgi apparatus

The image was treated exactly as described in section 2.10, but the line was drawn from the centre of the Giantin stain for the Golgi apparatus and the centre of the nucleus of the corresponding cell (Fig. 2.3B, E-G). The mT/mG mouse line was also used for these images so the cell membrane was also visible to help identify which Golgi stain belongs to which cell.

### 2.10.3 Creating radar plots

The data tables were extracted from Volocity and opened in Microsoft Excel. In Excel the angles were pooled into 30-degree groups and the square root of the frequency in each group was used to create rose diagrams. This meant the area of each segment in a rose plot represented the frequency. Often the length of each segment is used to show the frequency, but this can be misleading because it emphasizes a small difference simply due to the way the data is displayed.

The mean angle and statistical significance of the results were calculated in R using the free package "CircStats" (Agostinelli, 2009). The non-parametric Watson's  $U^2$  test was used to test the dataset against both a circular uniform distribution and a von Mises distribution (also known as a circular Normal distribution) (Bergin, 1991; Concha and Adams, 1998; Mardia, 1975). The null hypothesis being tested was that "the two distributions are not significantly different from each other". A p value  $p < 0.05$  was considered statistically significant. Also in the CircStats package is a Watson's two-sample test of homogeneity, this allowed any two distributions of angles to be compared statistically. This was used to see if the distribution varied significantly between pairs of different experimental datasets (rather than between experimental and uniform or experimental and von Mises Normal).

## **3.0 Developing a cell nuclei and proliferation identification protocol**

### **3.1 Current cell counting methods**

The established method of calculating the amount of proliferation occurring in a tissue is to perform an immunohistochemical stain, take images of the histological sections and to count the number of cells that are proliferating in a particular region by hand. When there are significant numbers of specimens to analyse, this is slow, laborious and open to human error, such as cells being missed. Time constraints may also limit the area over which proliferation is measured on one image and the number of images or specimens that are included in the study.

The aim of this project was to capture cellular behaviours more comprehensively than previously reported in the literature, and therefore large areas of tissue and large numbers of images were to be analysed, an automated protocol to identify individual cells in images was needed. By developing automated cell identification, counting and analysis techniques a much larger amount of data was analysed quickly and without user bias. It produced a standard method that can be used across the field and applied to other systems, making data more collaborative. Previous methods for counting BrdU cells did not include a total cell count (Soames et al., 1994) or used a different staining protocol (Deng et al., 2009) and software that is not readily available.

This project involved extracting data from a large number of images to build up a detailed picture of the cellular mechanisms occurring in the palate throughout development. Therefore it was of particular benefit to have an automated system and so one was developed.

### **3.2 How the protocol was developed**

BrdU was detected with secondary antibodies that were visualised using 3,3'-Diaminobenzidine (DAB) staining or by being fluorescently tagged and viewed under a

UV light. In DAB staining a visible brown stain was produced after a secondary antibody conjugated to a peroxidase enzyme bound and oxidised the DAB.

The long-term aims of this research group include mapping the cellular processes that contribute to the development of the entire face, not just the palate. Sections stained with DAB do not fade and can be easily stored at room temperature. Therefore they could be stained and stored ready to image the desired ROI. Initial investigations were carried out on sections visualised using DAB and counterstained with haematoxylin. ImageJ (<http://rsb.info.nih.gov/ij/>) was used to analyse the images. This is a freely available and easy to use image-processing program.

### **3.2.1 Brightfield image analysis**

#### **3.2.1.1 Identifying all cells in a brightfield image**

Total nuclear count was based on the haematoxylin stain, including cells that were also BrdU-positively stained. The image was cropped to the ROI and turned into an 8-bit greyscale image, as required by the ImageJ plugins used for the subsequent counting. The contrast was enhanced using the 'auto' function in the brightness and contrast window. The total number of cells was obtained using the Image-based Tool for Counting Nuclei (ITCN) plugin (Byun, 2008) in ImageJ. This requires an estimation of the diameter of a cell, the minimum distance between two cells, a threshold level and to select the box 'detect dark peaks' as the plugin otherwise counts bright regions, but the haematoxylin stained nuclei are dark. For the counting cell the variables were set to: dark peak detection: on, inter-nuclear distance estimate: 14  $\mu\text{m}$ , minimum: 7  $\mu\text{m}$  and threshold: zero. This produced a count that was tested and found to be accurate to within  $\pm 3\%$  of the manual count (Fig. 3.1A & 3.2A).

#### **3.2.1.2 Identifying proliferating cells in brightfield images**

To count only the BrdU positive nuclei the computer has to be able to pick out the darkly stained nuclei. Setting a threshold and programming the computer to count the number of regions or cells that are above this threshold did this.

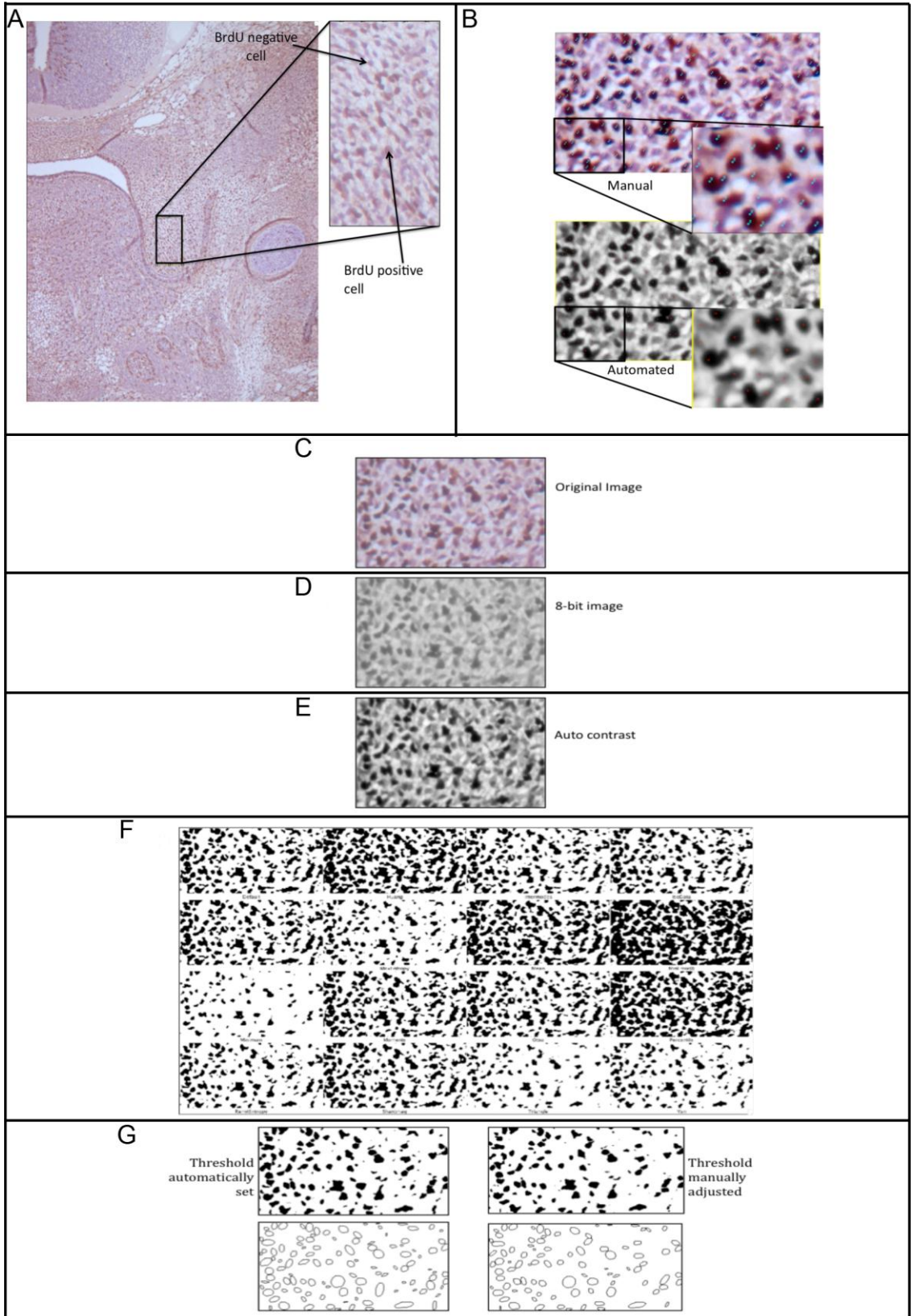


**Figure 3.1 Method for counting the total number of cells in the ROI** A) Frontal section E13.5 embryo showing the ROI from the centre of the palatal shelf with a positive and negative BrdU cell picked out B) ROI after the manual and the automated total cell count C-H) Steps for counting the BrdU positive cells C) The same ROI as for the total cell count D) ImageJ turns it into a monochrome image E) The contrast is automatically adjusted to enhance the dark positively stained cells F) There are many different algorithms already available in ImageJ to adjust the threshold; max entropy and minimum appeared to be the most accurate when compared to the original image G) After using the max entropy algorithm to set the threshold level the image is converted to binary and the watershed tool is used to separate nuclei that are overlapping. The particle counter then counts the cells, leaving a masked image of what has been counted. There are many different ways to set a threshold in ImageJ; most of the methods compute an ideal separation of the background from the foreground based on the image histogram using a variety of Information Theory principles to find the ideal cutoff. The ideal can be different depending on the nature of the image and the features that the user wants to segment. ImageJ allows all of its automatic threshold algorithms to be tested at once so that the best can be chosen by trial-and-error. Following conversion to 8-bit images and auto contrast enhancement (Fig. 3.1C); the differently thresholded images were compared to a copy of the original. The results (Fig. 3.1C) showed that two methods 'max entropy' and 'minimum' were close enough to the count of nuclei made by eye to warrant further verification.

Using the minimum algorithm (Prewitt and Mendelso.MI, 1966) to set the threshold resulted in no cells being counted in some sections while counts in other sections were hugely overestimated (Fig. 3.2B). Using the max entropy algorithm (Kapur et al., 1985) consistently underestimated the threshold level therefore over-estimating the number of BrdU positive cells but was the better of the two tested methods (Fig. 3.2B).

It is possible for the contrast between the BrdU positive stained cells and other cells to vary, even on the same slide and this is where most of the different methods failed to separate the positive and negative nuclei. Three different methods were tried to see if through pre-processing the image it allowed the automatic thresholding to be more accurate.

The first method tried used the fact that BrdU and the counterstain are different colours by extracting a single colour channel in ImageJ and then ran the threshold on this new image. Neither the BrdU nor haemotoxylin stains are single colours therefore

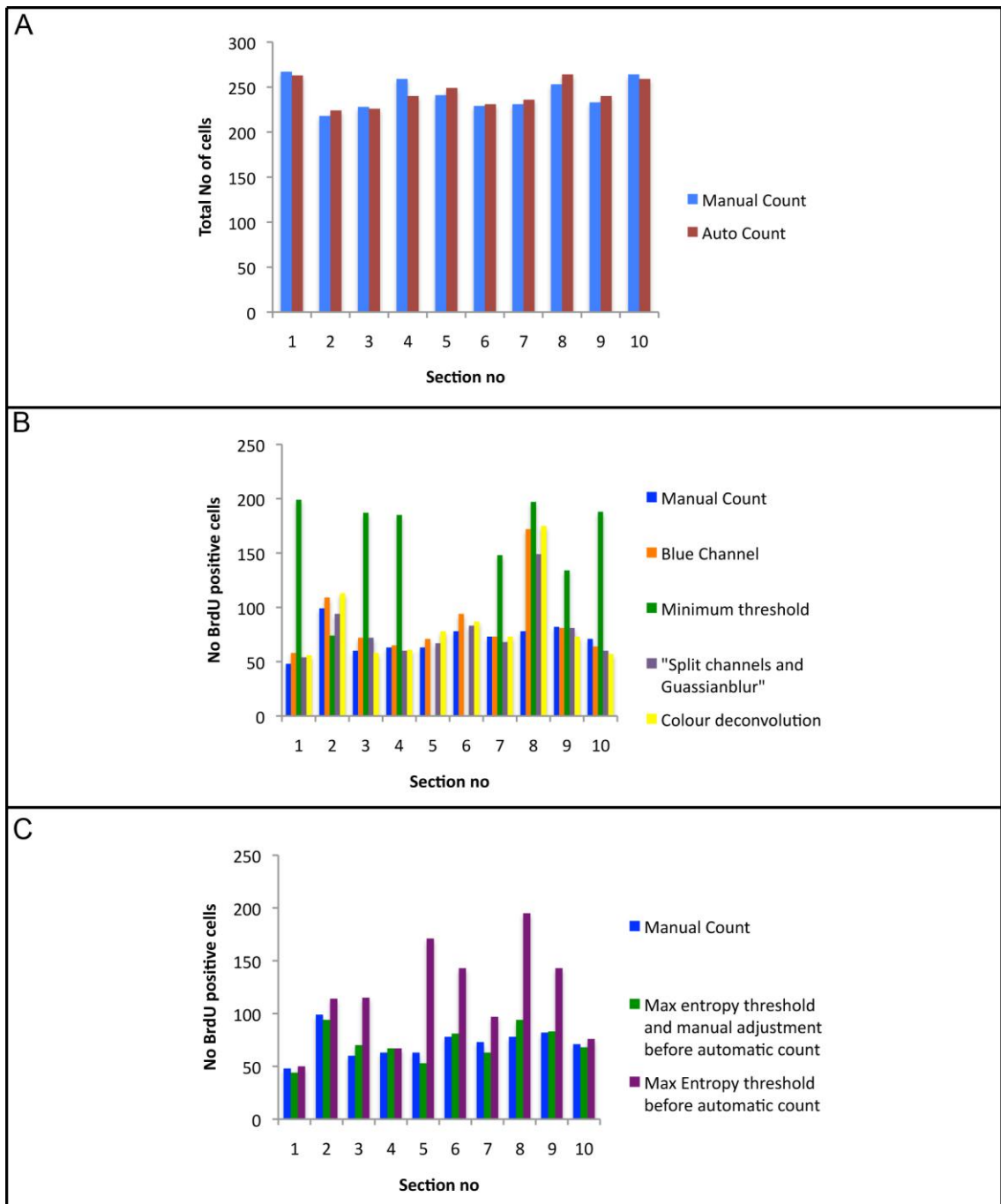


**Figure 3.2 Graphs showing manual and automated cell count totals** A) The automated total cell count using the ITCN plugin was within 3% of the manual count B) Other methods involved preprocessing the image and using a different threshold algorithm but none of these were as accurate as the method described in figure 3.1 B) Manually adjusting the threshold subsequent to using the max entropy algorithm to set the threshold level produced the most accurate count.

they appear in multiple colour channels. This meant they overlapped so when a single channel was extracted there were still remnants of both stains. Extracting the blue channel removed most haemotoxylin stained cells while leaving the BrdU stained cells to be identified. This method was very accurate until the BrdU staining was weak



compared to the counterstain and then it would hugely over estimate the count (Fig. 3.2B, section 8). Therefore another, more robust, method was sought.

Blurring the image using ImageJ's inbuilt Gaussian filter, with the radius set to 1, could have improved the separation and made boundaries smoother because it gets rid of noise in the image. Rather than simply separating colour channels as above, a more sophisticated colour deconvolution method (Landini, 2004) was tested. This produced one image of blue nuclei and one of brown nuclei. Neither of these methods improved the result of using the max entropy algorithm to automatically set the threshold (Fig. 3.2B).

After the threshold level was set, but before the counts were done, the image was converted to binary and the watershed segmentation tool was used to automatically cut apart cells that were touching (Fig. 3.1C). The total number of BrdU positive cells was counted using the particle analysis tool. This required particle size and circularity measurements; the formulae for circularity is  $4\pi(\text{area}/\text{perimeter}^2)$ .

It was not possible to get a satisfactorily accurate count by an entirely automated method due to the variable contrast of staining. It was, however, possible to apply a preprocessing step consisting of manual adjustment to the threshold level, using a copy of the original image next to the monochrome image as a guide. The threshold level (displayed as an adjustable slider on the screen) was decreased until only the BrdU positive cells were in the image (Fig. 3.1C). These methods were validated using ten adjacent sections and this showed the computer-assisted counts had a high degree of accuracy (Fig. 3.2B & C), with a percentage difference between the manual and semi-automated methods of less than 9.58%.

### **3.2.1.3 Discussion on identifying cells from brightfield images**

A macro was set up within ImageJ to count the total number of cells using the steps described in 3.2.1.1 above with a single "click" enabling an image containing hundreds of cells to be counted in less than 1 minute. By changing only a few variables, such as the inter-nuclear distance this method could be applied to other tissue types.

A huge advantage of doing chromogenic staining for brightfield imaging (rather than immunostaining – see below) was that the staining of the specimens was highly stable

and the sections could be stored long term. It was possible to stain the entire head and then image the regions of interest as and when they were required rather than having to start again using more embryos and taking more time to process and stain them.

The amount by which the threshold has to be manually altered varied between sections, because it depended on how much difference there was in the staining between the background and the positively stained cells. This varied from section to section even after changes were made, such as increasing the amount of solution added to each slide and using parafilm coverslips to prevent the slides drying.

It was much quicker to have the computer count the number of BrdU positive cells as well as being unbiased. Any experimenter having to do the task on a large dataset would get tired and make mistakes. Using this method allowed a large amount of data to be processed quickly, because apart from decreasing the threshold, the rest of the process could be done by simply running a macro, and it was easy to learn how to decrease the threshold by the correct amount by comparing the original and thresholded images. With more practice it became a quick and simple task. Using this method each image was analysed in under a minute.

This protocol still required the analyst to remain at the computer, load in each image and do the manual adjustment. Ideally the process would be completely automated, including being able to go through an entire dataset at once without needing individual images loaded. Therefore a different approach was sought.

### **3.2.2 Fluorescent image analysis**

Staining against the incorporated BrdU with a fluorescent secondary antibody is a well-established method and promises fewer steps, less variability and higher contrast than chromogenic enzyme-coupled methods. The higher contrast in particular in principle would allow the computer to more easily separate the foreground from the background. Additionally by using fluorescently tagged antibodies to stain the sections, other fluorescent stains could be used on the same sections. For example IddU and BrdU potentially allowing the cell cycle time to be calculated (Boehm et al., 2010). The fluorescently stained sections were imaged on the confocal microscope. This had a motorised stage connected and software that automatically stitched

together the image at the end of the scan. This allowed a larger region to be captured in the image using a 40x objective not the 10x used in the brightfield study.

Fluorescent images were taken using a DAPI stain to see the cell nucleus in one channel and a fluorescently tagged anti-IddU antibody was used to see the proliferating cells in a different channel (Fig 3.3C).

The ITCN plugin and the nuclear counter designed to identify stained cell nuclei in ImageJ were both tested, but produced counts with a percentage error of  $\pm 7.05\%$ . Rather than re-optimize the counting method in ImageJ it was decided to test the commercial program Volocity.

Volocity identifies the individual cells using information from the image, such as threshold values for the pixels and the average cell size. It allows a measurement protocol to be built up using a variety of tools to identify cells. As the protocol was altered the output was up-dated and the results shown, not just in a table, but also as coloured regions. Each region was randomly assigned a colour and represented the area Volocity thought was an individual nucleus (Fig. 3.3D & E). This made the protocol easier to develop, because it was clear whether cells were being amalgamated or missed. The steps involved in using and optimising Volocity for this project are outlined as follows:

### **3.3.1 Identifying cell nuclei in fluorescent images**

The first task was to identify the best range of intensities to pick out in the blue cell nuclei channel. Volocity could use a variety of techniques to identify fluorescent objects such as by percentage intensity, intensity, standard deviation of the intensity, hue/saturation/intensity (HSI) or red/green/blue (RGB) colour information. The DAPI was a single colour so the HIS and RGB techniques were not appropriate. This meant the intensity value of the pixels was tested as a means of setting the threshold to identify the cell nuclei. There was very little noise in the DAPI channel. Therefore the

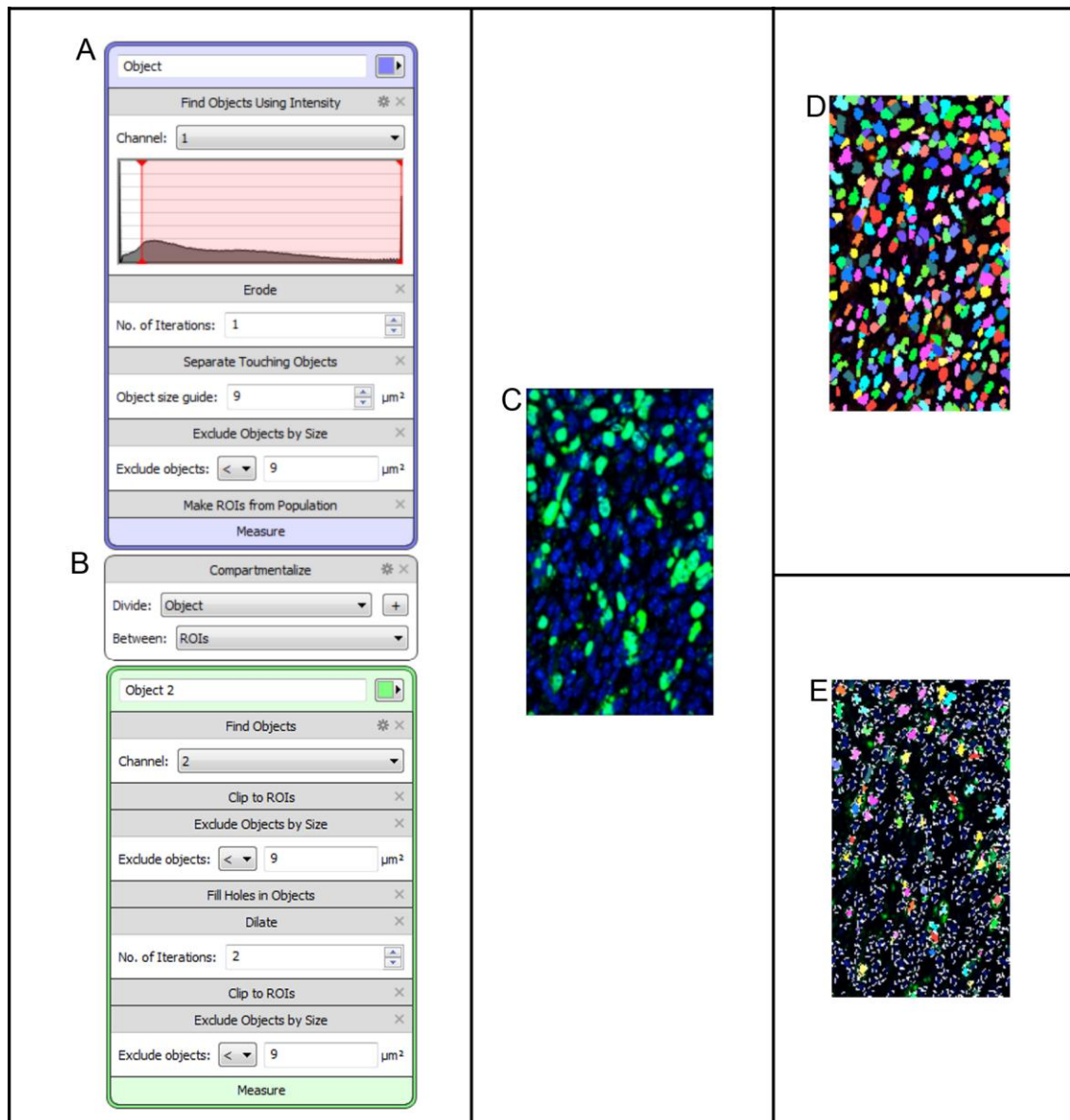


**Figure 3.3 Automated protocol to identify cells in Velocity** A) Velocity protocol to identify cells using an intensity threshold as described in the text. The blue box shows how the DAPI DAPI cells were identified. B) These were then made segmented to identify any cells that are IddU positive using the second channel as shown in the green box C) Sample of a image with both the DAPI (blue) and IddU (green) cells D) Every cell identified from the DAPI stain becomes an object and is represented with a randomly assigned colour E) From the segmented image the IddU-positive cells are identified and represented by randomly assigned colours.

vast majority of the intensity values could be included. An automatic threshold was set for pixel intensity in the blue channel of between 20-255 to separate the signal from the background (Fig. 3.3A).

The general problem with the protocol was that because the cells in some regions were so tightly packed the computer was struggling to identify individual nuclei. This was overcome by the objects identified by the threshold being filtered using the “erode” processing tool, this helped separate closely packed nuclei by shrinking each

object by a single pixel (Fig. 3.3A). An average radius of a nucleus was calculated from the images and this was used in the 'separate touching objects' tool to again help identify individual nuclei in tightly packed tissue. The computer measured the distance of each pixel from the edge of the object and examined the distribution of the pixel to decide if a one pixel thick row of pixels should be removed to create two objects. Finally to help get rid of any noise, objects less than the average radius were excluded from the count by the "exclude objects by size tool".

This final protocol was settled on after many variations were tried, to test different threshold ranges, and verified against ten sections containing between 100-200 cells that were firstly counted by hand (Fig. 3.3D). This final protocol was accurate to within  $\pm 4\%$  and saved a substantial amount of time.

### **3.3.2 Identifying proliferating cells in fluorescent images**

IddU- or BrdU-positive cells were identified among the imaged objects identified by the segmentation described above. Specifically, to identify the nuclei that were IddU or BrdU positive an intensity threshold was used in the 488 channel or the 568 channel respectively. A variety of intensity ranges were tested and the most accurate results were from an intensity range between 10-255 (Fig. 3.3B). This is a very large range but an inbuilt tool called a "local contrast adjustment" was also applied as part of this threshold. This compared pixel intensities within a set radius and used a local background intensity to select objects, rather than using the same value for the entire image. This helped prevent positive cells being missed, because sometimes one side of the image appeared brighter than the other. Once Volocity had identified objects, those below a minimum size (usually speckly noise) were discarded, again helping to reduce false positives. Volocity could identify objects with holes in, and this happened because the proliferation staining was often not continuous but consisted of large bright spots across the nucleus. The appearance of the stain within each nucleus varied because it depended on the exact stage in the cell cycle was in at the endpoint of the experiment. To prevent two objects being counted where there should only be one, firstly any holes were filled in using the "fill holes in objects" tool, which filled in any holes that were entirely surrounded by pixel already considered to be an object (Fig 3.3B). To join any objects within the same nucleus the "dilate" tool was applied that enlarged objects by a set number of iterations. Once two objects touched they became a single object. The objects were then clipped back to the ROI as the dilation

might have made them exceed the borders of the nuclei. Volocity then excluded any small objects one final time; this got rid of any odd pixels left when the objects were clipped back to the ROI.

This final cell identification protocol was validated against 10 sections containing between 100-200 cells. The cells were counted by hand and then tested in Volocity. This protocol was accurate to within  $\pm 6\%$  of manual counts.

### **3.3.3 Extracting data from Volocity**

The two protocols, described in 3.2.1 and 3.3.2 above, can be combined to run as a single process (Fig. 3.3A & B). Once Volocity had identified each object it created a table with a range of data for each object. All the cell nuclei were classed as “object 1” and all the positive IddU cells were classed as “object 2” allowing the information to either be extracted together or separately. The columns of interest, which could be extracted as a tab delimited table, were Name, ID, Item Name, Centroid X, Centroid Y, Centroid X ( $\mu\text{m}$ ), Centroid Y ( $\mu\text{m}$ ). From this, every object could be identified from the co-ordinates of its centroid and the image it originated from.

## **3.4 Discussion**

The cell identification protocol developed here allowed data on thousands of cells to be gathered automatically with an accuracy of  $\pm 4\%$  for the total nuclei count and  $\pm 6\%$  for the proliferating cell count. . Although counts in the test images that were manually counted were very carefully checked and re-checked, it must be remembered that in general manual counts may not always be 100% accurate as cells in the field may be missed or double-counted. The automated method developed here therefore compares well with manual methods.

There was very little difference in the accuracy of the protocols to identify the nuclei of every single cell between brightfield and fluorescent images. Fluorescent imaging benefited from the accuracy of the DAPI identification process by creating a ROI from the identified cell nuclei. However, while the brightfield method required a manual check or adjustment to the thresholding, the protocol followed to identify the fluorescent cells was completely automated. It could handle a large dataset at once

and recorded the co-ordinates of the nuclear centroids and the name of the image they had come from. This information allowed further automated analysis to be done (see chapter 2.7).

The immunohistochemistry involving DAB visualization and counterstaining involved more consumables and had extra steps compared to the technique using fluorescent antibodies. This made it more expensive and time consuming. Also fluorescent imaging is safer than DAB staining, which has been linked to bladder cancer; although extra precautions could be taken to reduce the risks if the DAB method was being used.

On large confocal datasets the Velocity protocol could take hours to run, but it could be left to complete overnight. It was possible to run other programs at the same time, but required a lot of the computer's processing power.

The methods developed as described in this chapter could be scaled up. For example, research groups studying different structures could collaborate by acquiring a single set of images that cover the regions of interest to both groups, by utilising a motorised microscope stage so that they can be quickly analysed. This requires fewer mice, or species of interest, to be used and saves both groups time.

Ideally in the future an ImageJ cell identification macro, ideally based on the Velocity measurements protocol described here, will be created. It would be preferable to have the cell identification technique in ImageJ because it is free to download, making it more widely available. It is also possible to get ImageJ to open a series of images saved in the same folder. Therefore the process can be automated for entire datasets using this program.

## **4.0 Localised cell proliferation**

### **4.1 Introduction to Localised Cell Proliferation**

#### **4.1.2 Cell proliferation in the palate**

The role of localized cell proliferation has been investigated in the developing palate of various species, but generally at low resolution (i.e. with very limited sampling). Studies have focused on the process of palate elevation, not initial outgrowth or growth towards the midline after elevation. A study into vertical palatal shelf development in hamsters claimed to have demonstrated that disrupting proliferation by inhibiting DNA synthesis stunted the initial outgrowth of the palate (Burdett et al., 1988). This work used a treatment with 6-mercaptopurine (6-MP) that inhibits DNA synthesis by preventing the synthesis of purine nucleotides, adenine and guanine, but it did not take into account other processes that the 6-MP could have been interfering with, such as spindle orientation, cell shape or cell rearrangement.

Further work in the hamster, this time using histone-3 mRNA in situ hybridisation (Shah et al., 1994), implied that relative proliferation peaks early in development and then decreases steadily. In addition, proliferation was distributed randomly over the palatal shelves with different areas fluctuating in no clear order. Labelling cultured quail palates with <sup>3</sup>H-thymidine showed that quail also displays a peak in relative proliferation during early palate development (Hehn et al., 1995). Frontal sections of the palate were divided into four quarters and this analysis indicated that the location of the peak proliferation varied randomly.

A gradient of proliferation during the development of the secondary palate was demonstrated in the rat embryo; the highest relative proliferation was shown to be at the 'tip' (i.e. prospective medial edge) of the outgrowing palate and when divided into thirds along the anterioposterior axis the anterior third had the highest relative proliferation (Nanda and Romeo, 1975). The study focused on the time around palatal shelf elevation and the highest levels were found just before elevation and then a steady decrease was observed as the palates fused. After elevation the region of



highest proliferation varied, and overall the palatal shelf had similar levels of proliferation.

Relative proliferation has been shown to be higher in the epithelium on the future oral side compared to the prospective nasal side at E13.5 (Luke, 1989), from counts of <sup>3</sup>H-thymidine labeled cells. This differential proliferation might contribute to palatal shelf elevation, but another reason the prospective oral side would have higher proliferation is because the rugae form there. When measuring proliferation in the epithelium the rugae must be taken into account, because proliferation has been shown to vary not just between rugal and interrugal tissue, but a “rugal growth zone” has also been identified where the new rugae appear. Relative proliferation is higher in developing rugae and drops off within the rugae as they mature whereas it remains higher in the interrugal regions (Pantalacci et al., 2008; Welsh and O'Brien, 2009). It has been noted that the mesenchyme immediately below the rugae is condensed, but the exact mechanism by which this occurs has not been reported. The epithelium thins as the palate outgrows further, suggesting that the mesenchyme below is driving the growth and stretching the epithelium (Luke, 1989) although differential thinning between mid- and anterior-palate (Economou et al., 2013) suggest that this is not the whole story.

Sasaki et al., (2004) studied the CL/Fr mouse mutant, a strain in which 15-40% spontaneously develop a cleft. They compared proliferation in CL/Fr mice with a cleft to littermates that did not develop a cleft and to wild-type, C57Bl/6, mice of the same strain. They found that proliferation in the palatal mesenchyme was highest in the wild-type, followed by the CL/Fr without a cleft and the CL/Fr with a cleft had the lowest proliferation (Sasaki et al., 2004). They therefore assumed the cleft was due to the level of proliferation, although no other cell behaviours were investigated. The expression of *Pax-9*, a transcription factor thought to increase cell proliferation, was also assessed in these mice. In the control strain and the CL/Fr without a cleft *Pax-9* was found to be in the MEE at E13.5 and E14.5 and was down-regulated by E15.5 when the shelves are fusing (Hamachi et al., 2003). This down-regulation did not occur in the CL/Fr mice with a cleft linking the expression of *Pax-9* to the process of palatal fusion.

The modulation of proliferation in organogenesis, such as the limb, has been linked to the interplay between *Tbx-3* and *Bmp-4*, which are co-expressed in the palatal mesenchyme at E13.5. *Bmp-4* caused up-regulation of *Tbx-3* and *Tbx-3* causes down-regulation of *Bmp-4*. Over-expression, by electroporation, of either gene caused an

increase in proliferation in the palate, shown in a PCNA assay (Lee et al., 2007). The addition of the *Bmp-4* inhibitor NOGGIN, via beads in a culture system, results in a decrease in proliferation (Lee et al., 2007). The *Tbx-3* knockout mouse does not have a cleft palate therefore interplay between these two genes might be involved in the fine-tuning of proliferation around the time of palate elevation and fusion but they are not in the main pathway driving proliferation in the palate.

The *Sprouty2* (*Spry2*) knockout mouse has increased proliferation in the palate and a cleft palate. The *sprouty* genes are involved in Fgf signal modulation and *Spry2* acts as an Fgf inhibitor (Matsumura et al., 2011). Disruption of *Spry2* leads to excess cell proliferation in the palatal shelves (Fig. 4.1). The shelves of the mutant failed to elevate in the anterior and mid-regions of the palate and the posterior palate displayed an abnormal shape, which changed after E14.5 but did not manage to elevate. When placed together in culture the mutant shelves fused correctly (Matsumura et al., 2011). Expression of other factors in the Fgf signaling pathway also show disorganised expression patterns and higher levels of gene expression in the palate of this cleft palate model, such as *Shh*, *Msx-1* and *Barx-1* (Welsh et al., 2007). The role of *Spry2* is dosage dependent (Welsh et al., 2007) and this demonstrates that signaling thresholds in palate development are very important.

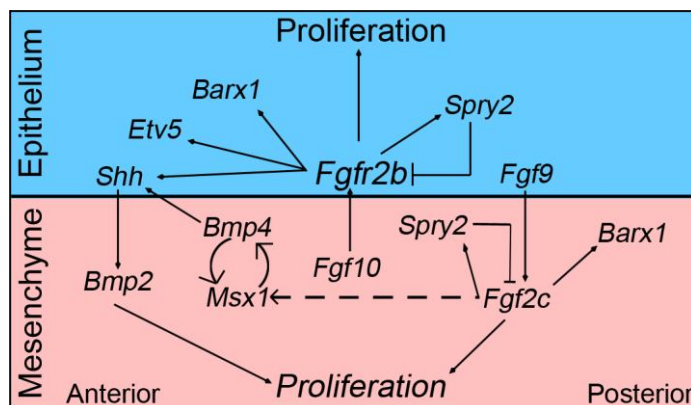


**Figure 4.1 Signaling pathway involving *sprouty2* controlling proliferation.** The molecular control of proliferation is thought to involve factors in both the epithelium and the mesenchyme. Adapted from Welsh et al., 2007.

Proliferation, in several species, peaks in early development but an exact location of this peak, if there is one, has not been clarified. A conclusive time series of proliferation throughout palate development in the mouse is missing from the literature. Genetically modified mice with a cleft palate phenotype have demonstrated that proliferation is disrupted in models of cleft palate. This does not explain whether the

CP is a consequence of the abnormal proliferation or another mechanism is causing the CP and the change in proliferation level.

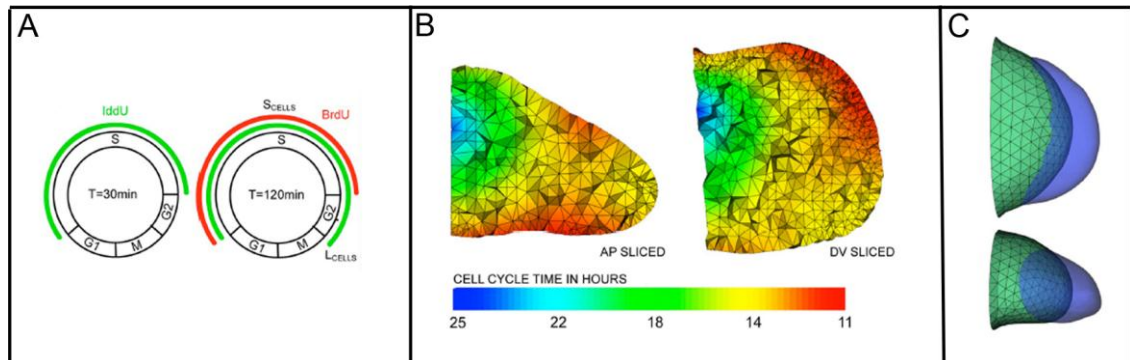


**Figure 4.2 Investigation into proliferation rates in the developing limb bud** A) Protocol for timings and theory behind the double injection protocol to calculate cell cycle time B) Heat maps of cell cycle times in the outgrowing limb bud C) Model showing growth that would occur if proliferation was the only contributing mechanism (green) and actual growth that occurs in the limb bud over this time period (blue) showing that proliferation cannot be the only cellular mechanism of morphogenesis contributing to limb outgrowth. Adapted from Boehm et al., 2010.

#### 4.1.3 Proliferation in the limb

Detailed analysis has been carried out of the role of proliferation in limb bud morphogenesis and the timing and the gross shape of the limb bud are similar enough to that of the palate to warrant detailed comparison. Models of limb development have been based on “growth-based morphogenesis” for years, where local cell proliferation is isotropic but there is a non-uniform proliferation gradient driving the overall directional tissue growth (Lu et al., 2006; Morishita and Iwasa, 2008). In “growth-based morphogenesis” elongation was accounted for by an Fgf gradient diffusing out from the apical ectodermal ridge (AER) and controlling the level of local cell proliferation. This system allowed large deformations and meant as the tissue developed the proliferating region would change (Lu et al., 2006; Verheyden et al., 2005). This “growth-based morphogenesis” theory was tested by a detailed study (Boehm et al., 2010) into the rates of localized cell division to see if they were enough to account for the growth of the developing limb bud over a six-hour period. The length of the cell cycle in the developing limb bud was calculated using a pulse-chase protocol of IddU and BrdU injections (Fig. 4.2A) into pregnant female mice. Proliferation index data were used as the input to create a computational model where the only variable contributing to growth was this rate of localized cell proliferation. They discovered that the amount of growth from six hours of proliferation was not

enough to account for the amount of growth that actually occurs (Fig. 4.2) and demonstrated that other directional cell behaviours occur in the same tissue and these could also be contributing to the outgrowth of the limb bud (Boehm et al., 2010).

## **4.2 Localised cell proliferation: Methods**

Sample collection, staining and imaging were performed as described in sections 2.3-2.6 and the image processing is described in sections 2.7-2.8. The localised IddU index for the palatal mesenchyme was calculated for at least three embryos at each stage using wild-type CD-1 mice. Some proliferation studies (Boehm et al., 2010; Martynoga et al., 2005) are now being extended to look at cell cycle times rather than just relative proliferation. For example to investigate the contribution of proliferation in limb development (Boehm et al., 2010) a double IddU/BrdU injection protocol was used but the calculation assumes that the entire population of cells are proliferating and this was found not to be the case in the palate therefore the IddU index was extracted instead. For further details see the Appendix.

## **4.3 Localised cell proliferation: Results**

### **4.3.1 Wild-type palate development**

Before theories can be formed on the mechanisms contributing to palatogenesis an understanding of how its shape and dimensions change during development is required. Sagittal images of the maxillary process at E9.5 and E10.5 and frontal images of the palate from E11.5 to E15.5 are provided in figure 4.3A-G and the changes in height and width of the palate during development (as described in section 2.9, Fig. 2.2) are described below (Fig. 4.3H-J).

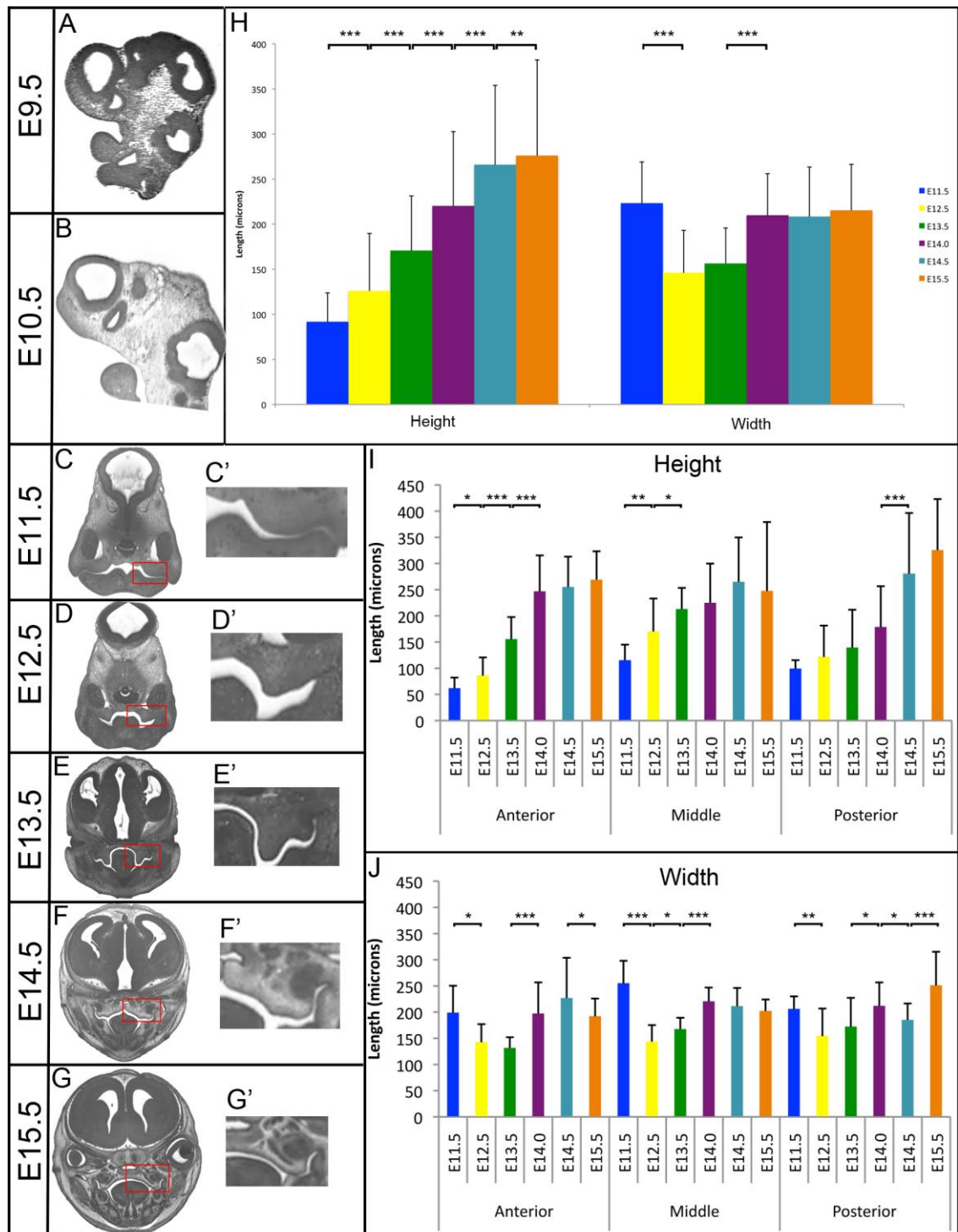


**Figure 4.3 Images and dimensions of the mouse maxillary process and palate during development** A) E9.5 sagittal image B) E10.5 sagittal image C) E11.5 frontal image D) E12.5 frontal image E) E13.5 frontal image F) E14.5 frontal image G) E15.5 frontal image. Palate outlined by a red box and blown up in C'-G'. Images in A-G adapted from [www.embryoimaging.org](http://www.embryoimaging.org) H) Average changes in the height and width of the palate I) Average changes in height along the AP axis from E11.5-E15.5 J) Average changes in the width of the palate along the AP axis from E11.5-E15.5. Error bars display 1 standard deviation. Results of t-tests are shown \* $p < 0.05$  \*\* $p < 0.01$  \*\*\* $p < 0.001$ .

When the palate initially appeared at E11.5 (Fig. 4.3C') it was over twice as wide as it was long (Fig. 4.3H). The length of the palate got significantly longer at every time

point taken. The difference in length between before and after elevation was twice that at any other stage (Fig. 4.3H). In contrast the width decreased significantly in the first twenty-four hours, so that at E12.5 the palate was displaying its characteristic “U” shape (Fig. 4.3D’). There was only a very small increase in the width as the palate continued to grow down the side of the tongue at E13.5 (Fig. 4.3E’). There was then a sudden and significant increase in width after the palate had elevated. The overall width then remained fairly constant (Fig. 4.3H).

The change in height and width was not exactly the same along the AP axis (Fig. 4.3I & J). The anterior palate increased in height significantly until immediately after elevation (Fig. 4.3I). Then a small increase was seen between E14.5 and E15.5, as the palatal shelves grew towards the midline (Fig. 4.3F’ & G’). The mid-palate increased in height significantly between E11.5 and E13.5 (Fig. 4.3I). There was only a small increase as the palate elevated and another as it grew towards the midline at E14.5. The posterior palate did increase in height before elevation but the increments were not considered statistically significant. There was only a significant increase in the height between E14.0 and E14.5 in the posterior palate (Fig. 4.3I).

The changes in the width of the palate were more consistent along the AP axis. There was always a significant decrease between E11.5 and E12.5 (Fig. 4.3J). The anterior palate then continued to decrease in width slightly until there was a significant increase between E13.5 and E14.0 (Fig. 4.3J). The mid-palate started to widen again after E12.5 and continued to do so until E14.0 (Fig. 4.3J). The posterior palate also increased its width between E12.5 and E14.0, but it then significantly decreased by E14.5 (Fig. 4.3J). The posterior palate significantly increased its width between E14.5 and E15.5 whereas the anterior and mid-palate saw a decrease.

#### **4.3.2 Localised cell proliferation overview during palate development**

Measurements of relative cell proliferation using IddU incorporation as described above show that there is an overall decrease across the whole palate mesenchyme during the period of development studied. The highest proliferation measured was that in the maxillary process at E9.5 and E10.5 (Fig. 4.4A) prior to palate development. There was no significant difference in the amount of proliferation at these stages but

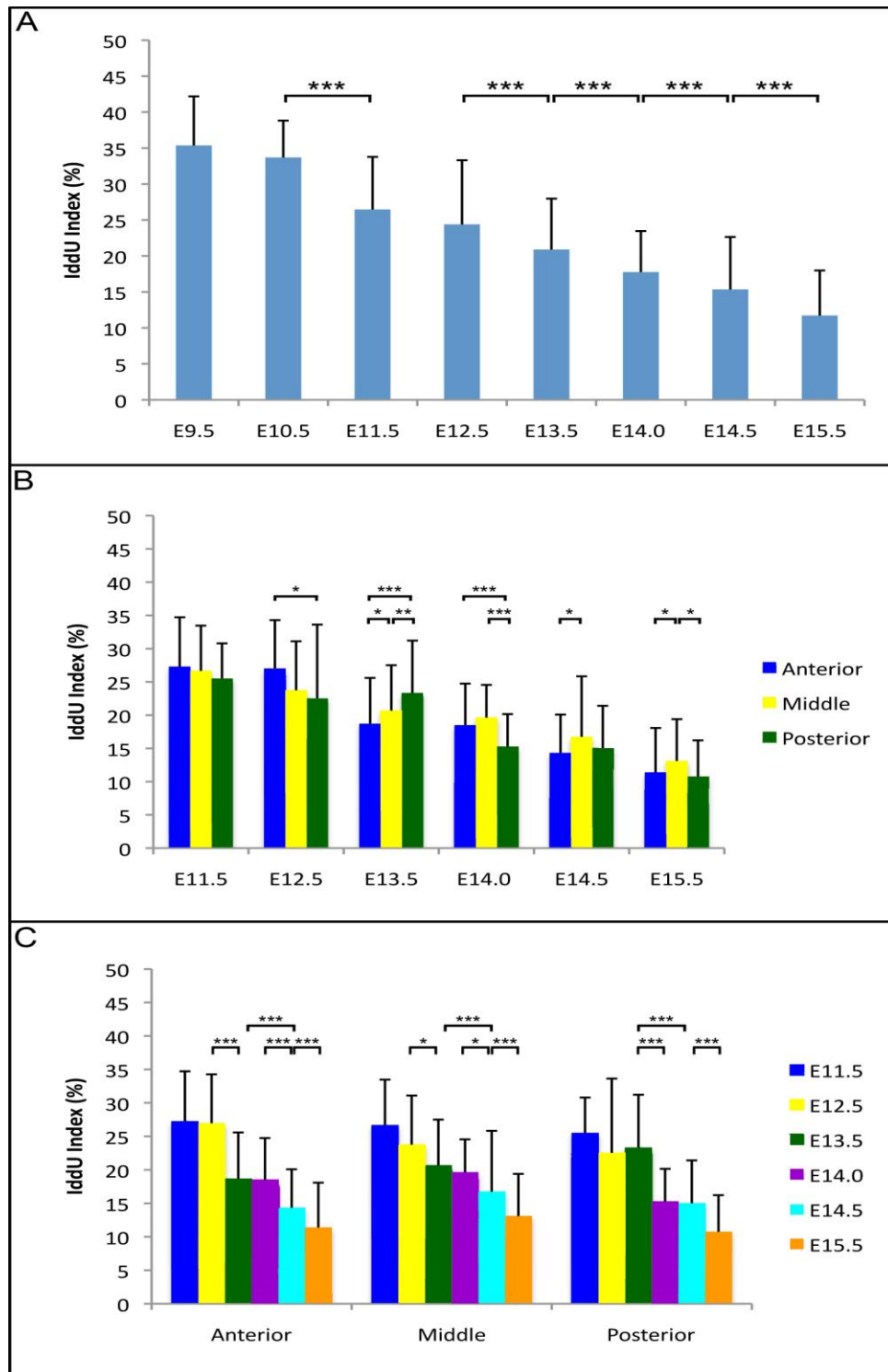


**Figure 4.4 Proliferation index results represented as graphs** A) Overall IddU index in the maxillary process (E9.5-E10.5) and the palatal outgrowth (E11.5 – E15.5) B) Average IddU index along the AP axis of the palatal shelves comparing changes within the palate at each developmental stage, E11.5 – E15.5 C) Average IddU index along the AP axis comparing changes over time in each region, E11.5 – E15.5. Error bars display 1 standard deviation. Results of t-tests are shown \* $p < 0.05$  \*\* $p < 0.01$  \*\*\* $p < 0.001$

the level of proliferation in the initial outgrowth of the palate when it is first seen at E11.5 is significantly lower (Fig. 4.4A) by around 10%. A similar level of proliferation is maintained throughout the initial 24 hours of the outgrowth period but between E12.5 and E13.5 there is another significant drop in the amount of proliferation to an IddU index of 20% as the outgrowth stage comes to an end. The amount of proliferation drops by the same amount over the next 24 hours, during which the palatal shelves have also elevated. At stage E14.0, just after the shelves have elevated but before they have touched in the midline the proliferation is half way between its E13.5 and E14.5 values, so this decrease in proliferation seems to be a steady drop off rather than a sudden stop. There is a final significant drop in proliferation down to an IddU index of just 11% between E14.5 and E15.5 (Fig. 4.4A) by the end of which time the palatal shelves have fused.

### **4.3.3 Regional changes in localised cell proliferation**

Overall the amount of proliferation decreases as the palate develops but this does not occur as a uniform decrease across the palate. By splitting the palate into thirds along its anteroposterior axis or by looking at heat maps of sections throughout the embryo distinct differences in proliferation are evident as follows:

#### **4.3.3.1 Localised cell proliferation along the anterioposterior axis**

The amount of proliferation in the anterior palate does not change between E11.5 and E12.5 (Fig. 4.4C) but by E13.5 there is a drop of nearly 10%. Proliferation remains at this level for the next 12 hours before dropping significantly again by E14.5. There is another significant drop in proliferation by E15.5 in the anterior palate (Fig. 4.4C). Proliferation in the middle third of the palate closely matches the pattern seen in the overall level of proliferation with a steady significant decrease every 24 hours (Fig 4.4C). The posterior palate does show a decrease in proliferation between E11.5 and E12.5. There is not a significant change between E12.5 and E13.5 in the posterior, if anything the data shows a very minor increase but more samples are required before this can be confirmed (Fig 4.4C). Proliferation has fallen significantly by E14.0 in the posterior palate and the same level of proliferation was recorded at E14.5. There is a final significant drop in proliferation by E15.5 (Fig 4.4C).



The amount of proliferation along the AP axis does not vary at E11.5 whereas by E12.5 proliferation in the posterior palate is significantly lower than in the anterior third (Fig 4.4B). By E13.5 this pattern has reversed and proliferation is lowest in the anterior palate and significantly higher in both the middle and posterior thirds (Fig. 4.4B). By E14.0 proliferation in the posterior palate is once again significantly lower than proliferation in the anterior third (Fig. 4.4B), but proliferation in the anterior and mid-palate have not changed significantly since before palatal elevation. Once the palatal shelves have elevated the highest proliferation is constantly in the middle third of the palate (Fig. 4.4B), and despite both decreasing by E14.5, proliferation in the anterior palate is significantly lower than in the middle third. At E14.5 and E15.5 proliferation in the anterior and posterior thirds of the palate do not vary significantly from each other (Fig. 4.4B), but by the later stage, both are significantly lower than in the middle third.

Thus, based on regional analysis, there are two clear patterns of cell proliferation:

- 1) A steady overall decline in apparent proliferation rate, which is transiently faster around the time of elevation and
- 2) Proliferation rates appear different in anterior, middle and posterior shelf regions, consistent with different timings and processes of elevation.

#### **4.3.3.2 Proliferation in the maxillary process prior to palatal shelf outgrowth, E9.5-E10.5**

To try and relate the regional proliferation trends to actual morphology, the IddU index was mapped onto the tissue using the mapping method described in Chapter 2. The highest levels of proliferation (red regions in Fig. 4.5) can be seen in the maxillary process at E9.5 and E10.5 (Fig. 1.2A & B shows SEMs of the embryo with the maxillary process labelled). These sagittal sections show that at these stages a large proportion of the embryo is proliferating. The cooler colours show where the lowest regions of proliferation are occurring at this point in time and the greyed regions puts into context the tissue that was not imaged.

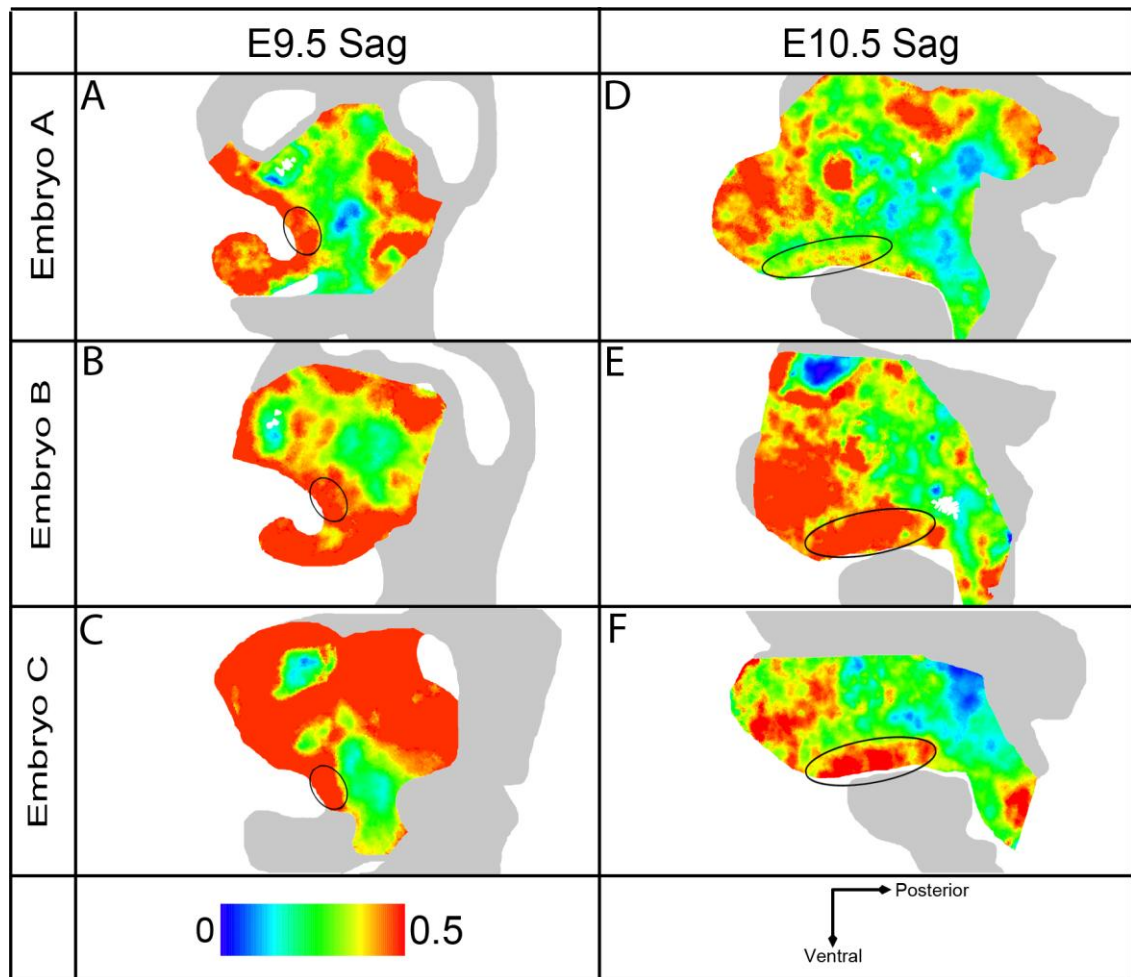


**Figure 4.5 Proliferation heat maps of sagittal E9.5 and E10.5 embryo heads** A-C) Heat maps showing IddU labelling index across a sagittal section at E9.5. Each heat map is an average of three individual sections and each of A-C is from a different embryo, from at least two different litters D-F) Heat maps showing IddU labelling index across a sagittal section at E10.5. Each heat map is an average of three individual sections and each of D-F is from a different embryo, from at least two different litters. The approximate location of the maxillary process is circled on each heat map. The grey region on the heat maps represents the rest of the embryo away from the ROI, which was not included in the heat map. The first and most striking impression of the proliferation heat maps is that they are quite variable between embryos. These sagittal heat maps are from a similar position along mediolateral axis. The embryos were staged using the plug date and limb development but it is likely that the exact time scale for development will vary between embryos, even in the same litter. Therefore the variations seen can be due to general natural variation and variations due to the exact stage of develop each individual embryo is at. Focussing on the location of initial maxillary outgrowth (circled in Fig. 4.4A-C) the level of proliferation appears to be fairly consistent and high at E9.5. By E10.5 the level of proliferation can already seen to be dropping off, mainly in embryo A, followed by embryo C and then embryo B (Fig. 4.4D-F).

#### **4.3.3.3 Proliferation during the initial outgrowth, E11.5-E13.5**

As mentioned above, true palatal outgrowth begins from the ventral face of the maxillary process at around E11.5. In the small outgrowth seen at E11.5 there is not a significant difference between the anterior and posterior palate. The difference between the proliferation level in the maxillary process compared to the initial outgrowth of the palate is clearly seen in the proliferation heat maps (which in Fig. 4.5 and 4.6 use the same colour scale). Proliferation often appears to be happening in small populations of cells, appearing as “hotspots” (arrows in Fig. 4.6) on the maps and the majority of these appear to be in the maxillary tissue adjacent to the palatal outgrowth. The patches of cooler colours could be a population of cells that are either not proliferative or all in a very similar stage of the cell cycle that did not pass through the S-phase while exposed to the IddU.

By E12.5, although the overall amount of proliferation has not dropped significantly compared to E11.5 (as mentioned above), the posterior third of the palate is now significantly lower than the anterior third (Fig. 4.4B; 4.7I-K), which remains at the same level as it was at E11.5. The heat maps show that proliferation is not uniform across the mediolateral axis (Fig. 4.7). Although the labelling map is quite noisy, there are some discernable trends. There is higher proliferation on the prospective oral side (appears dorsal at the anterior of an E12.5 palate) of the palate in the anterior of the palate at E12.5 (Fig. 4.7A-C, bracketed region). In the mid-palate at E12.5 proliferation varies more around the edge of the mesenchyme compared to the middle, demonstrated by the constant green region on the heat maps (Fig. 4.7D-E, bracketed region). In embryos G and H the mid-palate shows a subtle trend similar to that seen in the anterior, with higher proliferation on the prospective oral side (lateral in panels 4.7D and E). Embryo I does not match this pattern as clearly and because of the shape of the palate it appears to be slightly younger than the other two (it has a wider curved corner not a distinctive U shaped outline). However embryo I's heat maps have a greater area of cooler colours and this would be expected if the embryo was

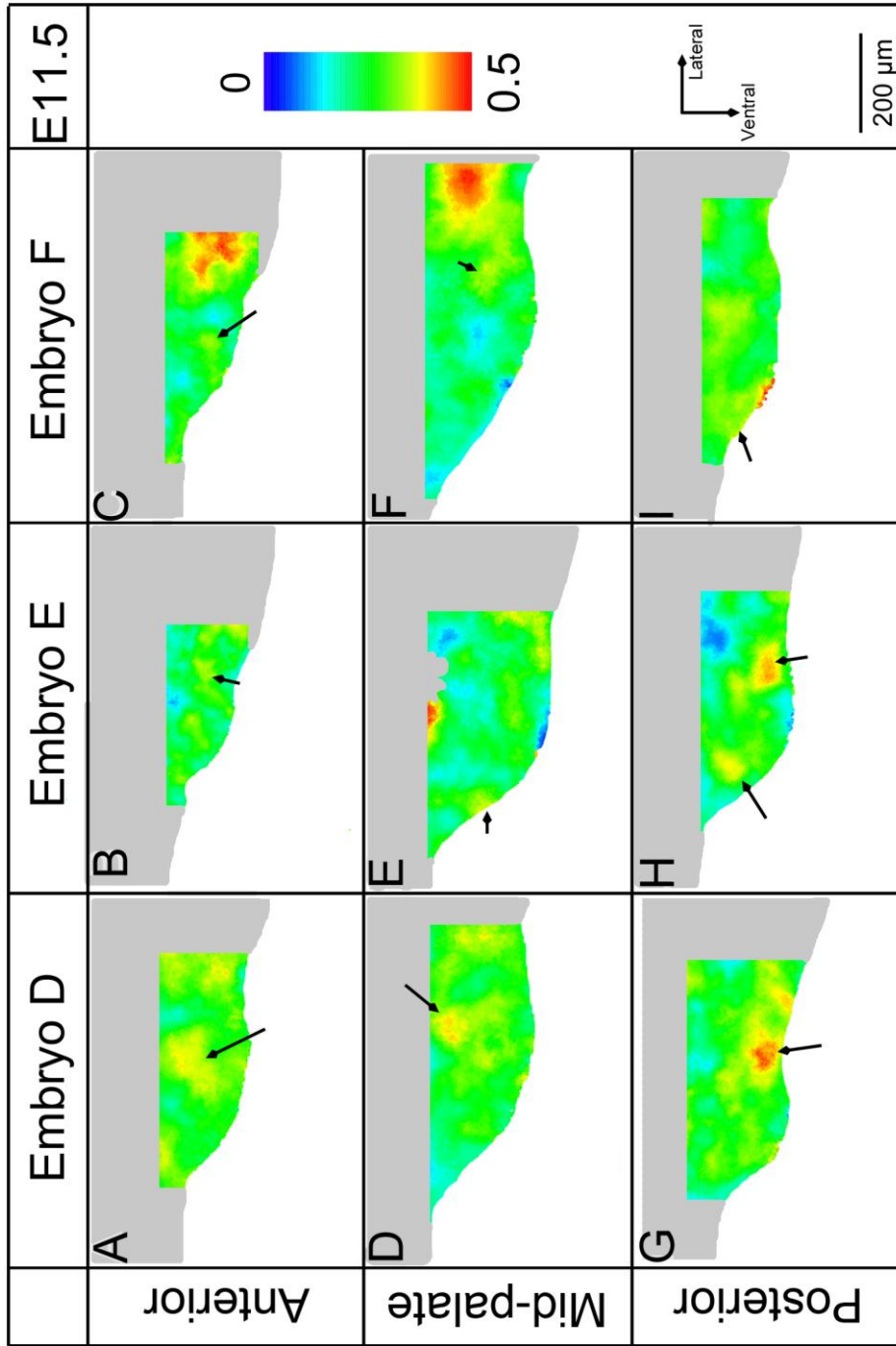


**Figure 4.6 Proliferation heat maps of E11.5 palatal shelves (A-C)** Heat maps of the anterior third of the palate (D-F) Heat maps of the middle third of the palate (G-I) Heat maps of the posterior third of the palate. Each heat map is an average of three individual sections and A, D and G; B, E and H and C, F and I are each from a different embryo, from at least two different litters. Black arrows highlight regions of higher proliferation; the majority is located in the maxillary process. The grey region on the heat maps represents the rest of the embryo away from the ROI, which was not included in the heat map. Scale bars represent 200  $\mu$ m.



older. The level of proliferation might always be lower in this embryo, it could be the runt of the litter, although this does not seem to be the case in the anterior palate; ideally more samples would have been analysed to help explain this.

In the posterior palate there is no consistent pattern within the sections and embryo I is again most different from the other two analysed (Fig. 4.7G-I). The palate now has higher amounts of proliferation than maxillary mesenchymal tissue it extends out of (Fig. 4.7).

The developing molar falls in the middle third of palate and the mesenchyme around the developing tooth bud condenses to form the dental papilla. This mesenchyme also maintains a higher level of proliferation than the mesenchyme adjacent to it (Fig. 4.9). The developing tooth bud and developing blood vessels are two structures that occur very close to the palatal outgrowth and often appear as regions of higher proliferation on the heat maps, shown as hot red and yellow colours (not shown for this stage, see figure below).

At E13.5 in the anterior and mid-palate a new pattern to the proliferation can be seen. There is lower proliferation on prospective oral side and higher proliferation on the prospective nasal side (Fig. 4.8, regions of low proliferation in brackets), the reverse of the difference seen at E12.5. Proliferation is relatively higher towards the distal tip of the outgrowth, most visible in the posterior palate at E13.5, where the larger regions of cool colours are located closer to the proximal end of outgrowth (Fig. 4.8G-I, black arrows). Generally there is more proliferation around the edge of the palatal outgrowth compared to the central mesenchyme as it grows at E12.5 and E13.5 (Fig. 4.7 & 4.8).

#### **4.3.3.4 Proliferation after elevation, E14.0-E15.5**

The E14.0 heat maps show ever-decreasing proliferation (Fig. 4.9); there is quite a lot of variation in the distribution of proliferation, particularly in the anterior two-thirds but there are two more constant regions of proliferation that stand out at E14.0. All the heat maps of the anterior and middle thirds show a constant green region towards their medial edge, somewhat on the ventral side (Fig. 4.9A-F, arrows). There are hints of other apparent consistencies, such as a region of slightly higher proliferation around the nasal shoulder in the anterior two-thirds of the palate at E14.0 the mesenchyme (red circles in Fig. 4.9B-C & E-F; unfortunately this region was not included in heat

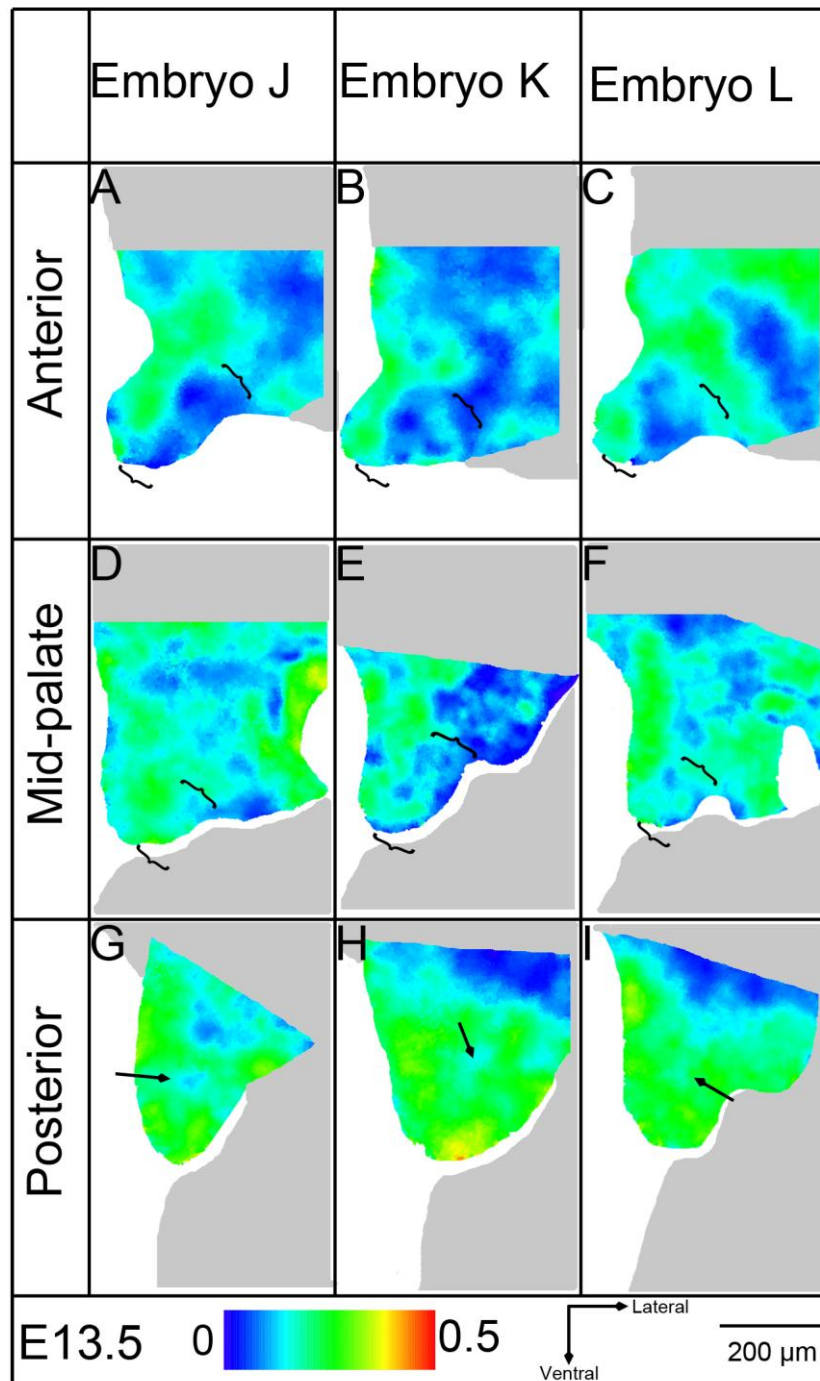


**Figure 4.8 Proliferation heat maps of E13.5 palatal shelves** A-C) Heat maps of the anterior third of the palate. Regions of low proliferation, the prospective oral side, marked with brackets D-F) Heat maps of the middle third of the palate. Regions of low proliferation, the prospective oral side, marked with brackets G-I) Heat maps of the posterior third of the palate. Spots of lower proliferation are marked with black arrows. These are found away from the tip of the palate D) Summary diagram of the posterior palatal shelf. Each heat map is an average of three individual sections and A, D and G; B, E and H and C, F and I are each from a different embryo, from at least two different litters. Scale bars represent 200  $\mu\text{m}$ . The grey region on the heat maps represents the rest of the embryo away from the ROI, which was not included in the heat map.

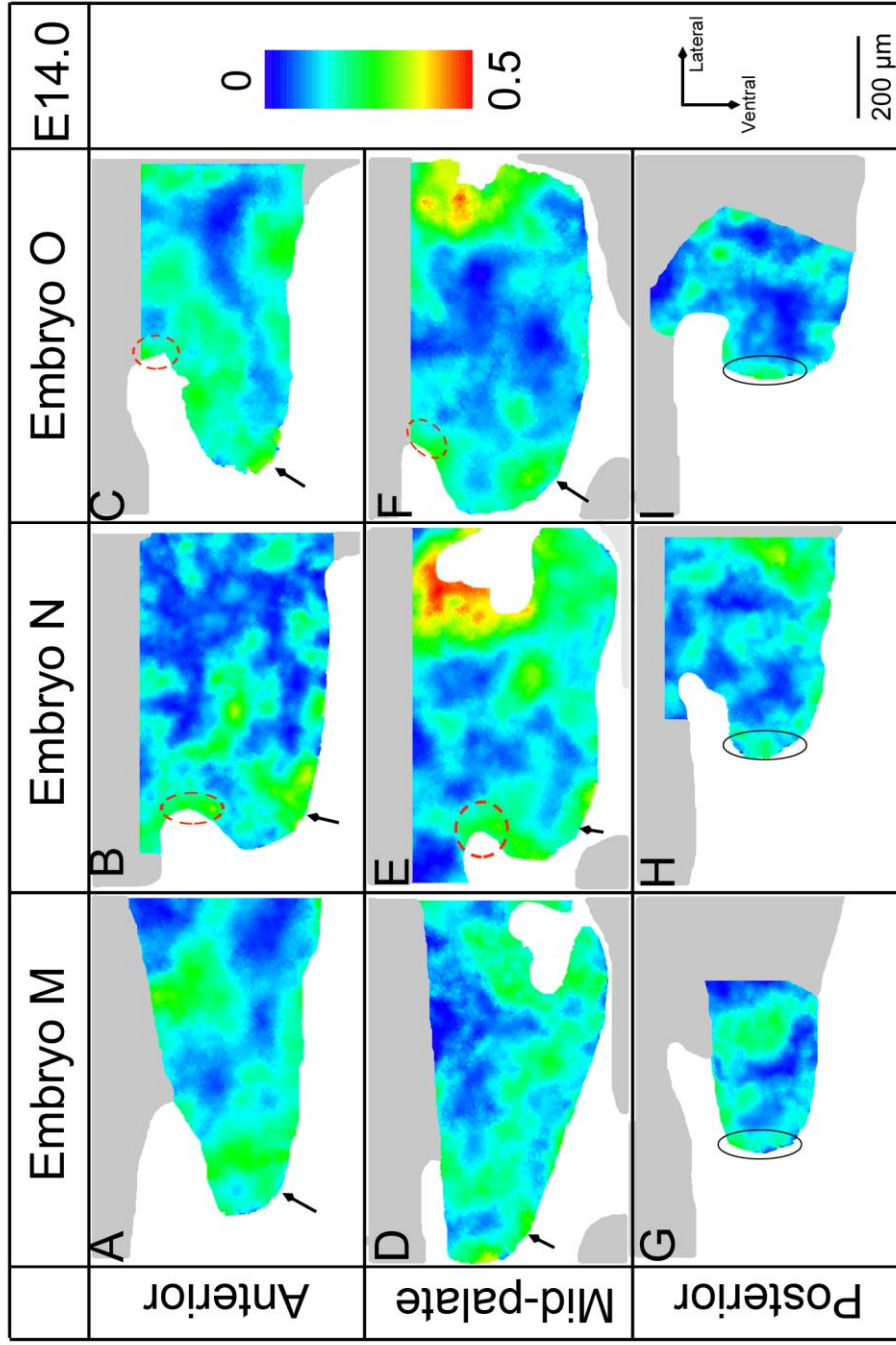


**Figure 4.9 Proliferation heat maps of E14.0 palatal shelves A-C)** Heat maps of the anterior third of the palate. Black arrows point to a region that displays a constant green colour between samples. Red circles highlight the nasal shoulder region D-F) Heat maps of the middle third of the palate. Black arrows point to a region that displays a constant green colour between samples. Red circles highlight the nasal shoulder region G-I) Heat maps of the posterior third of the palate. The highest level of proliferation is found at the distal tip region indicated by black circles. Each heat map is an average of three individual sections and A, D and G; B, E and H and C, F and I are each from a different embryo, from at least two different litters. Scale bars represent 200  $\mu\text{m}$ . The grey region on the heat maps represents the rest of the embryo away from the ROI, which was not included in the heat map.



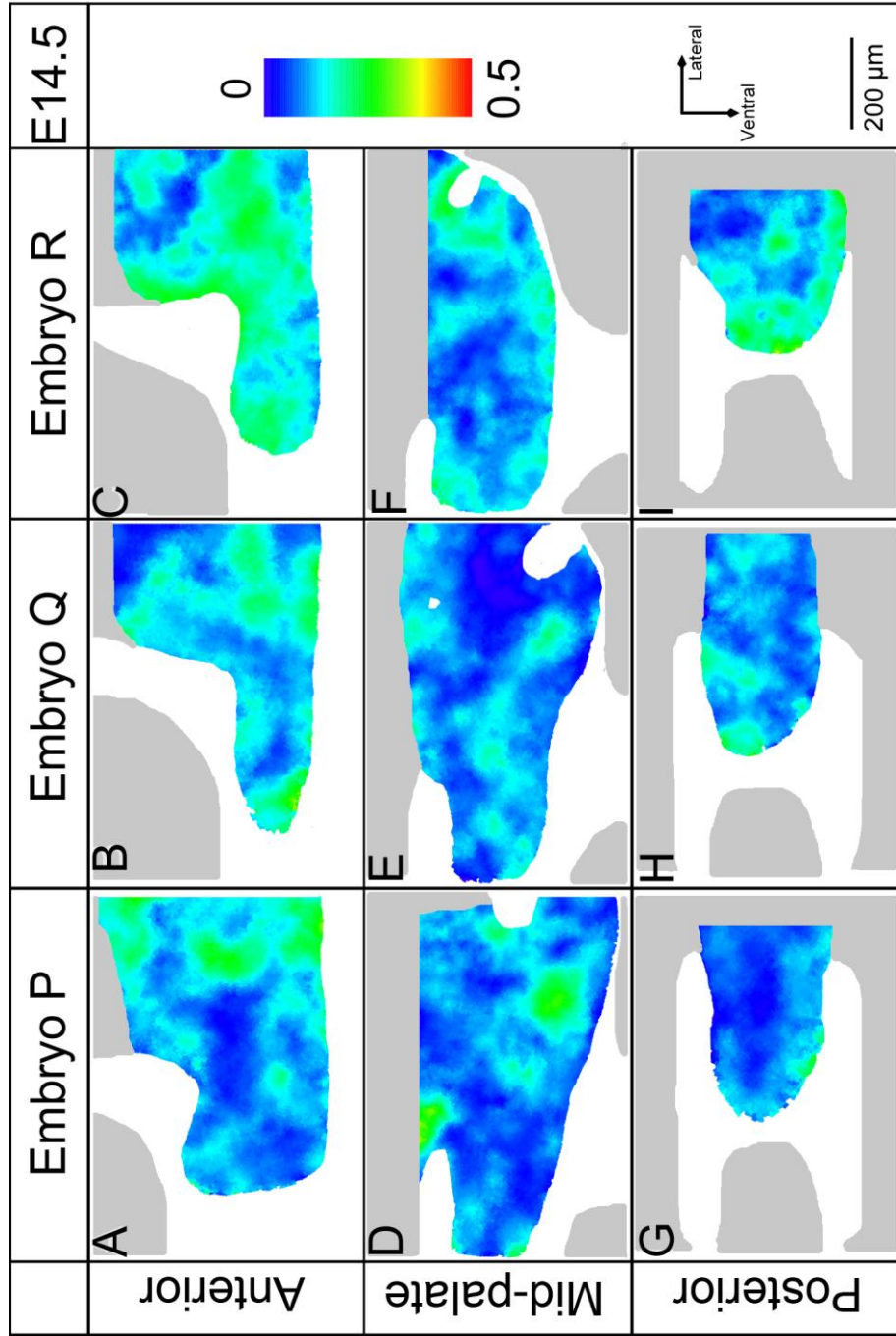


**Figure 4.10 Proliferation heat maps of E14.5 palatal shelves** A-C) Heat maps of the anterior third of the palate D-F) Heat maps of the middle third of the palate G-I) Heat maps of the posterior third of the palate. Each heat map is an average of three individual sections and A, D and G; B, E and H and C, F and I are each from a different embryo, from at least two different litters. Scale bars represent 200  $\mu$ m. The grey region on the heat maps represents the rest of the embryo away from the ROI, which was not included in the heat map.

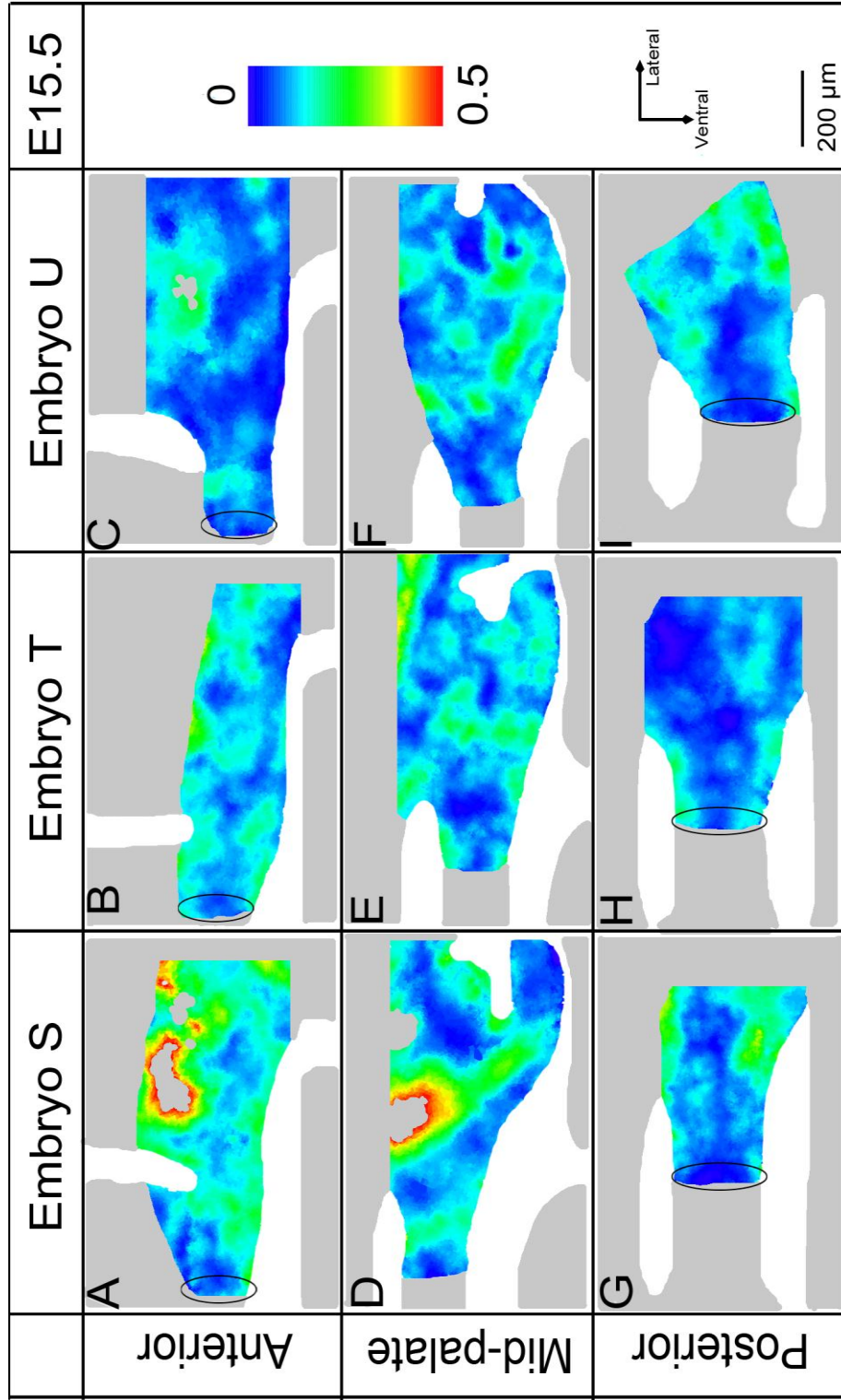


**Figure 4.11 Proliferation heat maps of E15.5 palatal shelves** A-C) Heat maps of the anterior third of the palate D-F) Heat maps of the middle third of the palate G-I) Heat maps of the posterior third of the palate. Each heat map is an average of three individual sections and A, D and G; B, E and H and C, F and I are each from a different embryo, from at least two different litters. Scale bars represent 200 µm. The grey region on the heat maps represents the rest of the embryo away from the ROI, which was not included in the heat map.

maps from embryo M). In contrast at E14.5 proliferation in this region has dropped off and it no longer stands out from the rest of the mesenchyme (Fig. 4.10). However, extreme caution should be taken to avoid the human tendency to see pattern in random shapes (see Discussion). Equally tentatively in the posterior third, proliferation increases toward the medial tip of the outgrowth (Fig. 4.9G-I, black circles).

By E14.5 the overall level of proliferation has dropped significantly, shown by the cool colours of the heat maps (Fig. 4.10), and it no longer stands out from the maxillary mesenchyme. At this stage the proliferation distribution seems to be highly variable and possibly random, yet this is at a time when the palate should be growing towards the midline (Fig. 4.10).

By E15.5 the anterior palate has reached the midline and the fusion process is nearly complete. Proliferation at the core of the medial edge of the anterior and posterior thirds is very low (Fig. 4.11, black circles) and this corresponds to where the two palatal shelves are fusing with each other in the midline and the nasal septum on their dorsal side. Blood vessels can be clearly seen forming as the patches of hot colours in the E15.5 heat maps (Fig. 4.11A & D) and the mesenchyme adjacent to the palatal outgrowth appears to have regions of higher proliferation compared to the palate again.

#### **4.3.3.5 Localised cell proliferation and the epithelium**

One potential source of variability within the mesenchyme was the formation of rugae at intervals in the oral-side epithelium. To investigate this, maps of proliferation at E13.5 and E14.5 in sagittal section were made. The rugae do not appear to have a massive impact on the mesenchyme below at E13.5 or E14.5 as shown in the sagittal sections (Fig. 4.12, white arrows indicate rugae). There is not a distinctive stripy pattern in the mesenchymal proliferation like that seen in the epithelium (Economou et al., 2013).

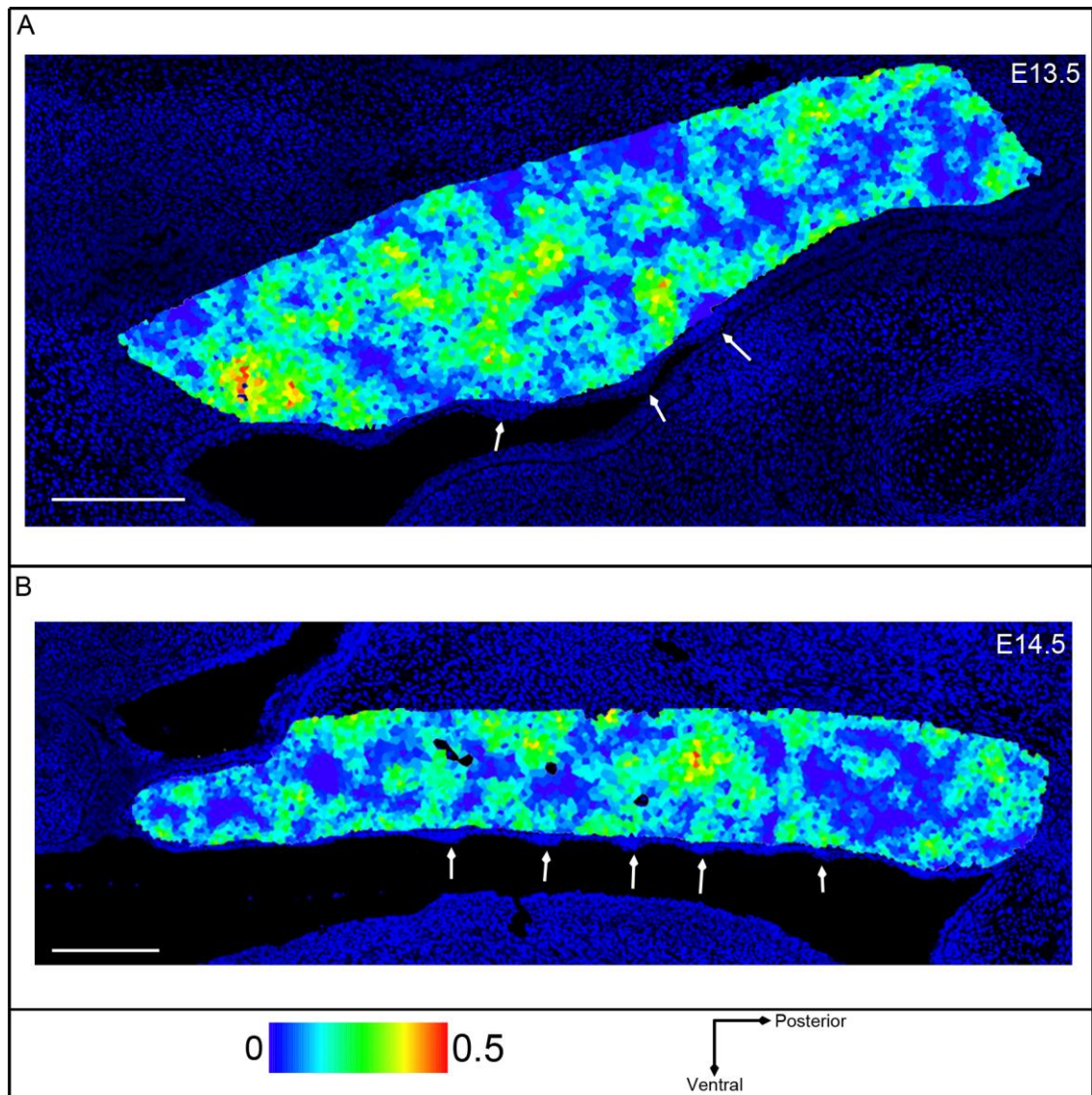


**Figure 4.12 Proliferation heat maps in sagittal sections before and after elevation** A) E13.5 proliferation heat map placed on top of a DAPI image of the embryo with the rugae present B) E14.5 heat maps and DAPI image. White arrows are pointing at the rugal thickenings. Scale bar represents 200  $\mu\text{m}$ .

#### 4.4 Localised cell proliferation: Discussion

##### 4.4.1 Localised cell proliferation methods discussion

This work has used an IddU index to compare relative amounts of proliferation across a tissue. Cells going through DNA synthesis while exposed to the IddU were labeled, and this method does not mark as many cells as an antibody like KI67 (present during  $G_1$ , S,  $G_2$  and mitosis), but includes more than PH-3 (present during the S-phase only). As the levels of proliferation starts high and drops off continually, it is best to use a

marker that has a dynamic range of labelling to cover real variations within the tissue. The injection method of using IddU is well established and easily reproducible by other labs and in other organs. All markers of the cell cycle (Ki67, PH-3, mitotic spindles etc) are indirect measures of proliferation because of the potential variability of the total length and proportion of the phase marked by each marker within the cell cycle (Muskhelishvili et al., 2003). Ideally further information could be gained from using a double labelling technique and calculating the cell cycle time. The calculations to work out the cell cycle times rely on several assumptions, such as cells are part of an asynchronous population, in a steady state growth phase and there are no non-proliferating cells to consider (Martynoga et al., 2005; Nowakowski et al., 1989). The developing palate only fulfilled these assumptions at E11.5. When the cell cycle time was calculated with the datasets from older stages the results were coming out at several hundreds of hours (see Appendix). The basis of this anomalous result could perhaps be some degree of synchrony among the cells, but otherwise remains unclear, despite many technical controls to ensure that all antibodies were working. Nonetheless, a single labelling index can be calculated and this still allows the relative levels of proliferation across development to be estimated.

A confocal microscope was used to take these images, which is worthwhile because it is effective at rejecting out-of-focus light and it removes noise from bleed-through fluorescence that a regular fluorescent microscope captures. The resulting high-resolution images with a large contrast between the positively stained cells and the black background make it easier for the computer to identify the different objects in the different channels, compared to a brightfield microscope or a regular fluorescent microscope. Also use of an XY-motorized stage meant the entire region of interest (ROI) could be imaged in one go and the Leica LAS-AF program is able to stitch the images together straight away, saving time and errors if it has to be done manually.

The maps shown were based on images taken of every other 8  $\mu\text{m}$  section, to build a detailed picture of wild-type palate development. There was a compromise between completeness and logistical feasibility. The wild-type analysis of the palate, a relatively small organ, still displayed significant differences along its AP axis, demonstrating that it is worthwhile maintaining a high resolution in the other assays performed. One caveat is that if each embryo had been more sparsely sampled the time could have been used to include more embryos overall.

The heat maps show the varying levels of proliferation across the tissue clearly in ways that an average in a graph might hide. The user can easily vary the scale of the heat maps and the computer can produce heat maps of an entire dataset without each individual image having to be treated separately. However, as is evident from the data in this chapter, proliferation is highly variable both within and between embryos in apparently the same tissue. This could be due to individual embryos developing at slightly different rates and so the developmental timescale is not completely accurate. E0 is the same for every embryo but the further from this time point they are the more evident variation between embryos might be.

To extract general patterns as well as to capture the variability, multiple samples have been shown and both individual and combined heat maps were presented. A more “high-tech” approach would have been to find a method for spatially registering larger numbers of maps. Spatial registration is a non-trivial exercise, both theoretically and logistically (Bagci and Bai, 2008; Bao et al., 2007; Crum et al., 2004; Guest and Baldock, 1995). Some averaging of adjacent sections was done within a single embryo, because these images only required a rigid registration, translations and rotations, to align them. This is very time consuming as it is done manually by trial and error. Only up to five heat maps were averaged at once because the variation in the shape and size of the palate became too great. The processing time significantly increased the larger and more numerous the sections included were. Any areas where the images did not overlap were left blank in the final summary heat map so it did not matter if the total area imaged varied in size. It has not yet been possible to average heat maps from different embryos because of the need for non-rigid registration. Averaging was attempted by manually aligning heat maps in ImageJ (or Adobe Photoshop) and then the images were made into a stack and a Z-projection produced using average pixel intensity. This was done using greyscale images, but it has not been possible to reassign the correct colour scale to the heat map projection. If more time had been available, not only would more specimens have been analysed at a higher temporal resolution but this more systematic and high-resolution approach to image registration and data averaging would have been taken.

This assay allows proliferation to be measured and displayed in a precise and clear way that can easily be reproduced by other groups and comparisons made between stages and phenotypes. Combining an established immunohistochemical method with a new automated image analysis technique sets a new standard for a high resolution investigation of proliferation that can be applied to numerous tissues and used to

asses new mutant phenotypes. There has already been interest from other groups in these methods, to look more closely at regions where they think they have seen unusual patterns in proliferation distribution and regions where they think the distribution of proliferation varies between mutants and wild-type (See chapter 10 and appendix). This analytical method has already been used in a National Institute of Health (NIH) grant proposal, establishing an official collaboration between Prof. Jeremy Green (KCL) and Prof. Yang Chai (University of Southern California).

#### **4.4.2 Localised cell proliferation in the palate**

Prior to the initiation of palate development proliferation is at a much higher level than ever seen in the palate. Therefore it is likely that proliferation is playing a significant role in the outgrowth of the facial processes and contributing to initial tissue elongation. The palatal outgrowth is tiny in comparison to the rest of the maxillary process and therefore the level of proliferation does not need to be as high to contribute to its outgrowth, explaining the significant drop in proliferation between the maxillary process at E10.5 and the palatal outgrowth at E11.5. Alternatively the difference could signify that proliferation plays less of a role in the outgrowth of the palate than other cellular behaviours.

During the first 48 hours of outgrowth a high level of proliferation is maintained but already by E12.5 the level is significantly different along the AP axis. Proliferation varies on a very local scale throughout development and this can be clearly seen by the apparent noise on the heat maps. The heat maps show small populations of cells have a similar level of proliferation, but rarely does this expand across a significantly large region of the palatal shelf. Even when proliferation is very low, after elevation, there is still a range of cool colours presented. One-way to find out which trends are important and which are just noise would be to study a larger number of samples.

The level of proliferation in the palate steadily decreases as development continues. This confirms previous but less complete studies in the hamster, quail, and rat (Hehn et al., 1995; Nanda and Romeo, 1975; Shah et al., 1994). Studies of other species have sometimes recorded variations in proliferation across the palate. For instance the rat palate appears to have a peak at its distal edge (Nanda and Romeo, 1975). The rate at which the level of proliferation dropped off, in a mouse palate, varied along the AP axis. There could be a relationship between the drop in proliferation and the

timing of palatal shelf elevation because this process is thought to be asynchronous along the AP axis.

Proliferation across the prospective oronasal axis clearly varies at E13.5, particularly in the anterior two-thirds. Since differential oronasal extension is a likely correlate of elevation and E13.5 is immediately prior to the palate elevating, these differences could be contributing to the process of elevation. The anterior palate in particular is thought to flip-up and the uneven proliferation seen at E13.5 could be contributing to this movement. However, one would expect that if this is the case that the higher proliferation rate would be on the prospective oral side, whose contour has to lengthen more than the prospective nasal side upon flip-up as an incontrovertible matter of geometry. This study shows exactly the opposite proliferation differential, which tends to argue against proliferation being a major driver of flip-up.

It has been suggested that the posterior palate elevates by more of a remodelling mechanism (Bush and Jiang, 2012) than a flip-up type movement. The posterior palate is the only region to show a rise in proliferation during palate development and this is seen at E13.5. It is possible that if other studies were sampling too sparsely and biased the posterior palate at this heavily studied stage then they might think that overall proliferation peaks prior to elevation instead of the small increase in just the posterior region recorded here. Alternatively it could be easily missed completely.

An increase in proliferation towards the tip of the palate is seen in the rat prior to elevation (Nanda and Romeo, 1975). As mentioned above, in the anterior two-thirds the difference in proliferation that stands out is along the prospective oronasal axis. This axis was not looked at by Nanda and Romeo. In the posterior palate the relatively higher levels of proliferation favour the distal end of the outgrowth, and when information is included from all the images and summarised there does appear to be a peak towards the distal end. This proliferation could be driving either the outgrowth of the palate or contributing to the remodelling mechanism that might be the cause of elevation in the posterior palate. The increase in proliferation in the posterior, with a slight focus at the distal end, could be putting pressure on the cells in the more proximal outgrowth and contributing to their remodelling. Experiments using a regional proliferation inhibitor (e.g. a culture system with the inhibitor soaked on to a bead) would help show which regions of proliferation are vital for elevation.



At E14.0 the region at the most proximal end of the outgrowth on the nasal side, the nasal shoulder, maintains a higher and more consistent level of proliferation than the rest of the palate. By E14.5 proliferation in this nasal shoulder region has declined and it matches the rest of the palate. The restriction of this small region of elevated proliferation to the anterior two-thirds of the palate could mean it is involved in the “flip-up” elevation process. The actions of the cells occupying this region during elevation result in the tissue forming a much sharper bend. The change in shape might have triggered the proliferation or the proliferative cells could be producing a force that contributes to the tissue bending. The nasal shoulder is one of the few consistent anatomical regions along the AP axis. Therefore this region could also be involved in initiating or conducting the process of elevation along the AP axis.

After the palatal shelves elevate they need to grow towards the midline allowing them to touch the opposing shelf and then fuse to form a complete secondary palate. Except it is also at this time point that a significant drop in proliferation is seen; the drop in overall proliferation between E13.5 and E14.5 is nearly double that recorded for the other 24-hour time points. The anterior and posterior regions have to grow further than the mid-palate to reach the midline, but proliferation remains lower in these regions and continues to fall as the palate begins to fuse. Therefore proliferation may not play a significant role in this part of palate morphogenesis.

The head is continually growing so a certain level of proliferation is required within the palate to allow it to keep up with the relative increase in size of the tissues around it. This required level of proliferation could be very similar to the level seen at E15.5 in the palate because at this stage the palatal shelves have fused and the palate simply needs to expand as the head grows around it. As with the other stages of palatal development it is possible that other cellular mechanisms are also contributing towards this growth.

Overall, from E12.5 through to E14.5 the amount of proliferation in the palate appears to fluctuate more in the mesenchyme nearest an epithelial boundary compared to the mesenchyme in the centre of the palate. This could be due to the signals controlling the level of proliferation coming from the epithelium. Consequently the outer mesenchyme is exposed to the signal first and for longer, whereas the more central mesenchyme only receives the longer lasting, potentially housekeeping signals that maintain proliferation. Signals controlling small fluctuations may not diffuse far into the mesenchyme and cause a significant response. It is not just proliferation in the

mesenchyme that varies throughout development. In the epithelium there are fluctuations as new rugae form along the prospective oral side and the prospective nasal side has consistently lower levels of proliferation (Luke, 1989) and a thinning epithelium. The growth of the mesenchyme is potentially causing the thinning of the epithelium on the prospective nasal side as it extends beneath it, but there is no clear link between proliferation as new rugae form and that of the mesenchyme.

Localised cell proliferation summary:

- 1) There was a clear decrease in proliferation as palate development progressed and the biggest drop in the amount of proliferation was correlated with the timing of elevation.
- 2) The heat maps showed oronasal differences but how these are linked to morphogenesis is unclear.
- 3) There are other more subtle trends but these are weak relative to the high level of variability between the heat maps.

## **5.0 Polarised cells and orientated cell behaviours**

### **5.1 Introduction to the Golgi apparatus and polarised cell behaviours**

Many mechanisms that could be contributing to palate development require the cells to be polarised. If this polarisation is uniform across a set of cells it could drive morphogenesis in a particular direction. In this project the Golgi apparatus was used as an indicator of cell polarisation (further details below). The Golgi apparatus is well established as an indicator of the direction of cell migration and/or of polarised secretion, both of which could be relevant in the palate. By measuring the position of the Golgi relative to the nuclei it was not possible to say that the cells were migrating, but a coherent distribution indicated some sort of coherent, polarised behaviour occurring.

For the palate to form, NCC must migrate from the posterior to the anterior side of the embryo and then form an outgrowth, which elongated ventrally. The cells could have stopped moving as soon as they reached the maxillary processes or soon after they entered the palatal outgrowth, but it is possible that directed cell movements also contributed to the continued directional growth of the palate. If these processes did not occur in the correct direction, at the correct speed or correct time the co-ordinated development of the palate would have been upset and it is likely to have resulted in a cleft palate.

#### **5.1.1 Cell migration**

Cell migration has been shown to take place, at least to some extent in palate development (see below) and it is therefore appropriate to outline some basics regarding cell migration during development and specifically leading up to palate development. Cell migration is a very important mechanism in embryogenesis and its major functions are conserved in evolution from single to multi-cellular organisms. In very early embryology migration of epithelial sheets is a lot more common, but there are cases of migration involving the redistribution of undifferentiated mesodermal cells. Later on in development migration is more commonly local rearrangements of differentiated cells into mature systems and networks.

Extensive work has been done on both the extracellular signalling pathways, which potentially organise the mechanism across an entire region of tissue, and the intracellular pathways, which contribute to an individual cells response (Kurosaka and Kashina, 2008). Major migratory events during embryogenesis are summarised in Table 5.1 from the review by Kurosaka and Kashina, 2008. Timescales for migratory events ranged from 12 to 120 hours and the development of the palate covered here lasted for 96 hours. Cells, for example the vagal or cardiac neural crest (Table 5.1) have been shown to be able to migrate millimetres, a lot further than would be required within the palate. The embryo is constantly growing as migration takes place so the migrating cells have to travel at relatively high speeds, which was estimated in Table 5.1, but there are different theories about whether the migration happens in short fast bursts or as a constant more steady migration (Druckebrod and Epstein, 2005, 2007; Kulesa et al., 2000).

For cell migration to occur the cell needs to polarise to define its leading edge from its rear edge (Ridley et al., 2003). The polarity of a migratory cell is initiated by many different growth factors and extracellular matrix proteins and these will often act on the rear of the cell rather than what will become the leading edge (Yam et al., 2007). This will cause an intracellular response and the rearrangement of microtubules and organelles. The first sign that a cell is migrating is protrusions of membrane from the leading edge as lamellipodia (branched dendritic network) and filopodia (long parallel bundles). These are both caused by actin microfilaments pushing the plasma membrane, an “actin treadmill” is set up where depolymerisation occurs at the rear end and polymerisation happens at the leading edge (Machacek and Danuser, 2006). The front protrusions of a migrating cell are rich in membrane-bound receptors and polarity protein complexes (Fig. 5.1). These are involved in actin polymerisation, integrin endo/exocytosis and maintaining the polarity of the cell.

For the cell to migrate forwards the actin filament in the extended protrusion attaches to the surrounding matrix via transmembrane proteins, integrins. Once the integrin binds it changes conformation and that leads to the initiation of signalling cascades that eventually cause the formation of focal adhesions and actin stress fibres. Myosin II is then involved in creating the forces to propel the cell forward (Beningo et al., 2001). As the cell moves the focal adhesions disassemble and release the extracellular matrix at that point (Vallotton et al., 2004; Webb et al., 2002).

Major types of embryonic migratory events (Adapted from Kurosaka & Kashina, 2008)									
Cell Types	Embryonic Events	Stages	Duration (hrs)	Origin	Destination	Maximum range	Distance (µm)	Speed (µm/hr)	
Epiblast cells	Gastrulation	E6.5	~24hrs	Primitive streak	Mesoderm	Neighboring cell layers	1	<0.04 µm/hr	
Primordial germ cells	General embryo patterning and organogenesis	E7.5-E12	96	Base of the allantois	Genital ridge	Within the tail region	1500	15 µm/hr	
Cranial neural crest		E8-E9	24	Mid-diencephalon to somite 5	Forebrain, craniofacial mesenchyme	Neck to front head	1000	40 µm/hr	
Vagal neural crest		E9-E14.5	120	Somites 1-5	Neurons in the gut	Neck to end of gut	10000	85 µm/hr	
			120	Somites 6-7	Neurons in the esophagus	Neck to stomach	3000	25 µm/hr	
Trunk neural crest		E8.5-E10.5	48	Somite 5 to caudal tip of neural tube	Sensory and sympathetic neurons, adrenal gland, schwann cells, pigment cells	Back to front	1500	30 µm/hr	
Sacral neural crest		E10-E10.5	12	Caudal region to somite 24	Hindgut	Back to front	1000	85 µm/hr	
		E14.5-E15	12	Hindgut	Spread within hindgut	Within an organ	1000	85 µm/hr	
Cardiac neural crest	Heart development	E8.5-E13.5	120	Otic placode to the end of somite 3	Cardiac outflow tract, septae, parts of ventricular myocardium via pharyngeal arches	Neck to heart	4000	35 µm/hr	
Extraembryonic mesoderm, endothelial, smooth muscle	Vasculogenesis and angiogenesis	E7-postnatal		Extraembryonic tissues and primitive streak	Mature circulatory system	Circulatory system	NA	NA	
Nerve cells	Brain development	E14.5-adulthood		Brain and ganglia	Nerve endings in the brain and throughout the body	Up to adult body length	NA	NA	

Finally the cell has to retract its rear end to allow the cell to advance. As the cell moves forward and stretches, activating calcium channels, the focal adhesions at the rear of the cell release their hold on the extracellular matrix and undergo a myosin II driven contraction. This retraction helps to maintain the cell's polarity and aids the continuation of this migration cycle (Kurosaka and Kashina, 2008).

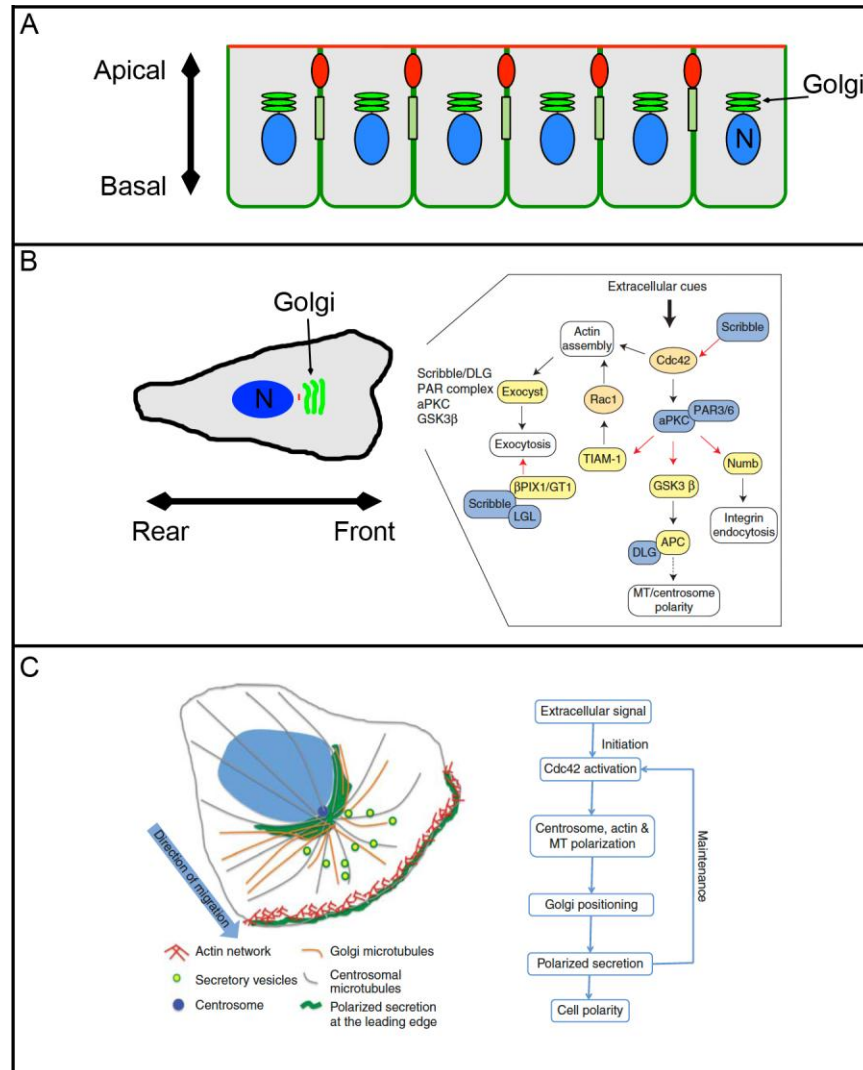


**Figure 5.1 Polarised cells and cellular mechanisms** A) Polarised epithelium the Golgi are all aligned on the apical side of the nucleus B) Polarised migrating mesenchymal cell with the Golgi between the nucleus and the front end of the cell. Potential signaling pathways setting up and maintaining the cells polarization C) Polarised mesenchymal cell resulting in cell organized cellular secretions and the events that could be setting up the polarisation. Blue arrow indicates the directions of migration. B and C adapted from Yadav & Linstedt, 2011. N, nucleus.

### 5.1.2 Neural crest cell migration

NCC are multipotent stem cells, which are derived through epithelial to mesenchyme transition shortly after neurulation. Firstly the NCC migrate and proliferate to produce the discrete swellings of the branchial arches. From here they migrate to a wide variety of locations and differentiate into the peripheral nervous system and various other structures. The maxillary process and palate are derived from the cranial neural crest cells; these originate from the first branchial arch (Fig. 5.2). Although they were first identified in the 1880s, it is only relatively recent techniques that have allowed the detailed mapping of migration of NCC in vivo in mouse (Chai et al., 2000).

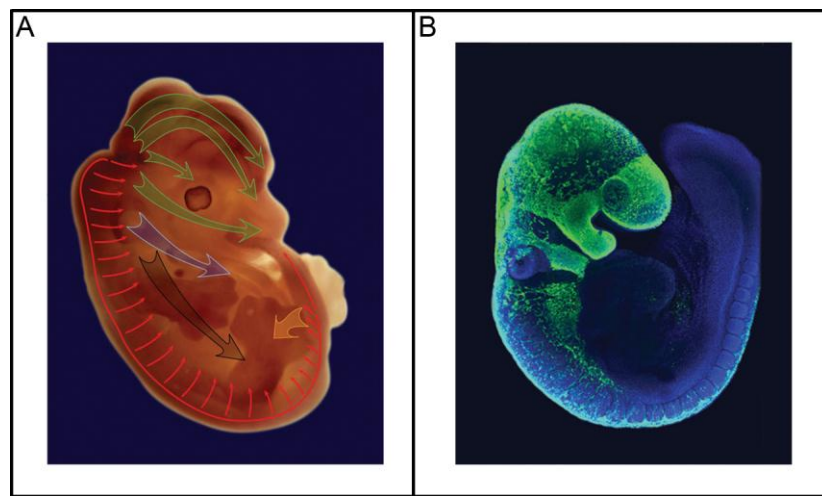


**Figure 5.2 Pathways of neural crest cells migration** A) NCCs migration from the somite region at the back of the embryo to a variety of different locations. Green arrows represents the route of the cranial neural crest cells; blue arrow, cardiac neural crest cells pathways; black arrow, vagal neural crest cells; orange arrow, sacral neural crest and thin red arrows trunk neural crest. Based on an E13.5 mouse embryo image, adapted from Kurosaka & Kashina, 2008 B) Cranial neural crest cells labeled with green fluorescent protein showing the extent of their migration. Adapted from Trainor & Barlow.

Studies have been done using Dil and antibodies, but a comprehensive cell lineage study was completed using a *Wnt1*/Cre reporter line of transgenic mice. *Wnt1* was only expressed during the development of the nervous system and encoded a short-range signal. Expression first appeared in the neural plate and became restricted to a region just anterior of the mid- and hindbrain isthmus by the time the neural tube had closed (McMahon et al., 1992). The *Wnt1*/Cre reporter line allowed NCC and their progeny to be fluorescently tagged and followed throughout development, even after the expression of *Wnt1* itself stopped.

Mutations in factors required for proper development of the NCC have been shown to result in a cleft palate. For example the transcription factor Sox9 is required for the formation of NCC (Spokony et al., 2002) and TGF- $\beta$  signalling plays a role in directing neural crest cells towards having non-neural fates. If TGF $\beta$  signalling was disrupted, specifically in the neural crest, then the embryo developed symptoms very characteristic of DiGeorge syndrome. This indicated that the correct migration and differentiation of NCC is required for the development of non-neural structures (Wurdak et al., 2005).

Another transcription factor Paired Box 3 (*Pax3*) is involved in early neural crest cell formation and aids migration by blocking differentiation signals from the local environment while the NCC begin to migrate. The expression of *Pax3* then stops as the NCC finish migrating and need to differentiate into their specific cell types. It acts through an inhibitor, *Sostdc1*, of bone morphogenic protein (Bmp) signalling (Wu et al., 2008). In normal development expression of *Pax3* persists only in the mesenchyme on the prospective nasal surface of the palate at E12.5 and E13.5. In the mutant where the level of *Pax3* has not been able to drop off expression persists throughout the entire mesenchyme of the palatal shelf and the shelves fail to elevate.

### 5.1.3 Cell migration within the palate

A graded expression of *Wnt5a* (Fig. 5.3C) and its receptor Ror2 has been demonstrated along the AP axis in the developing mouse palate (He et al., 2008). Migration of cells within the palate was demonstrated directly by live imaging of labelled cells and loss of *Wnt5a* activity halted this migration and resulted in a cleft palate (He et al., 2008). *Wnt5a* activates the non-canonical *Wnt* pathway, its targets include blocking the canonical *Wnt* pathway (seen in *Xenopus*, (Torres et al., 1996)) and regulating the planar cell polarity (PCP) pathway which is involved in convergent extension movement (Mlodzik, 2002).

The *Wnt5a*<sup>-/-</sup> mutant palate is short, rounded with a blunt end and lacks the ventrolateral indentation in the anterior whilst the posterior is shorter, broader and more wedged shaped (He et al., 2008). Elevation occurs, but a gap remains, so the palate never fuses in the anterior (although palatal shelves are capable of doing so when placed in close proximity in culture) and the posterior palate fails to elevate at all (Fig. 5.3A). The tongue does descend, giving the shelves the space to elevate;



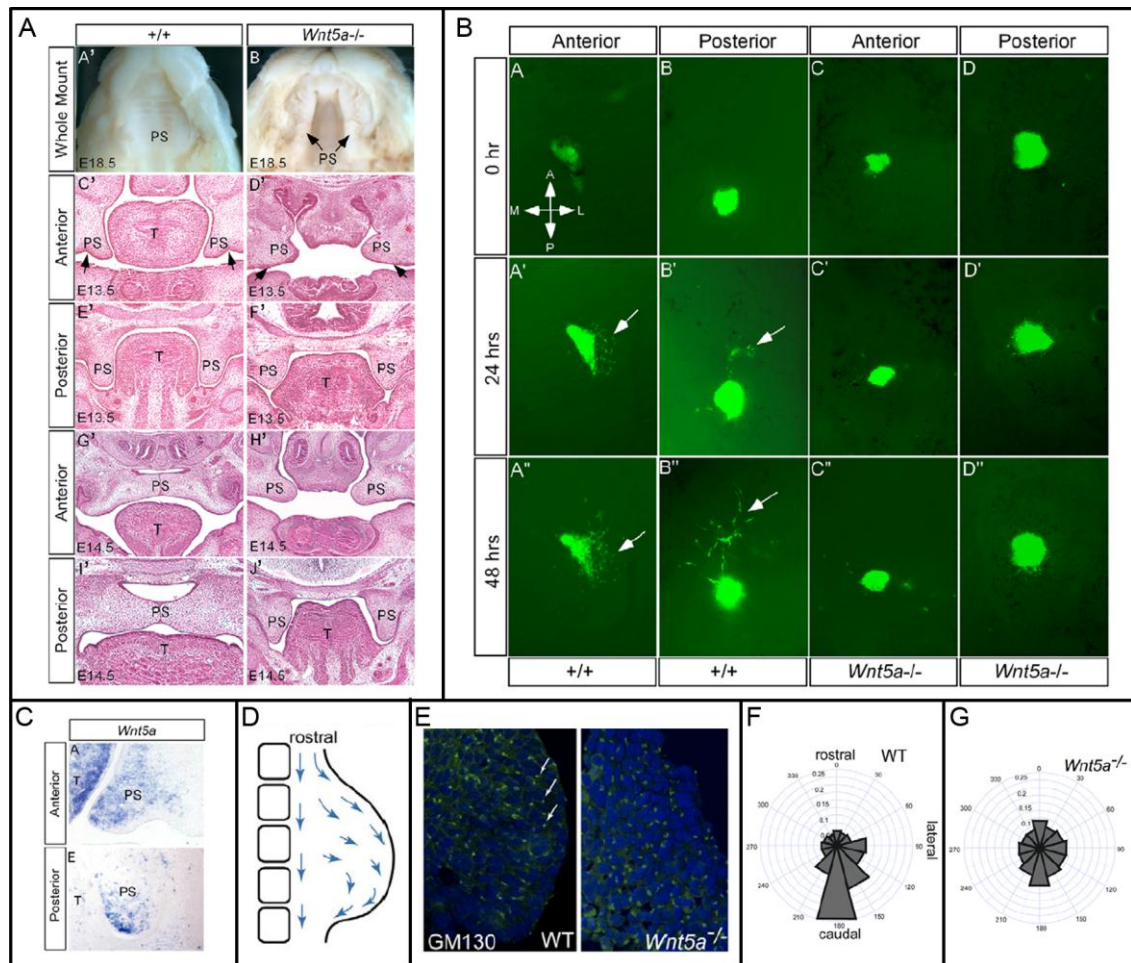


**Figure 5.3** *Wnt5a* acts as a chemoattractant in the palate and limb development A) Wild-type and *Wnt5A*<sup>-/-</sup> palate development A') View of the top of the mouth of with the mandible removed at E18.5 B') *Wnt5A*<sup>-/-</sup> palate at E18.5 has a cleft palate C'-D') anterior frontal sections of wild-type and *Wnt5A*<sup>-/-</sup> palates at E13.5 E'-F') posterior frontal sections of wild-type and *Wnt5A*<sup>-/-</sup> palates at E13.5 G'-H') anterior frontal sections of wild-type and *Wnt5A*<sup>-/-</sup> palates at E14.5 I'-J') posterior frontal sections of wild-type and *Wnt5A*<sup>-/-</sup> palates at E14.5 B) *Egfp* explants on a wild-type or *Wnt5A*<sup>-/-</sup> palate to demonstrate migrating cells. Adapted from He et al., 2005 C) Expression of *Wnt5A* in the anterior and posterior palate D) Migration of cells in limb development shown by looking at the orientation of the Golgi E) Orientation of the Golgi in wild-type and *Wnt5A*<sup>-/-</sup> limb bud F-G) Rose diagram of the orientation of the Golgi in the wild-type and *Wnt5A*<sup>-/-</sup> limb development. D-G adapted from Wyngaarden et al., 2010.

implying intrinsic mechanisms have been disrupted. When proliferation levels were measured, by counting BrdU-positive cells in boxed regions, they were found to be raised in the anterior palate but lower than normal in the posterior palate at E13.5 (He et al., 2008). The expression patterns of markers such as *Sox9* were different in the *Wnt5a* mutant palate, leading to investigations into migration patterns. Matching sections of *Actinβ-Egfp* mice were grafted on to different parts of E12.5 palatal shelves in culture and monitored. In 77% of grafts placed on the posterior palate *Egfp*-labelled cells were seen to have migrated towards the anterior of the palate (Fig. 5.3B). This directional behaviour could have been due to a chemoattractive gradient of *Wnt5a*, which had already been demonstrated in limb bud (Wyngaarden et al., 2010) and

pancreas development (Kim et al., 2005). When grafts were placed on the anterior palate cells were seen to migrate towards the prospective oral side of the shelf in 54% of cases. These directional behaviours were not observed in *Wnt5a* mutant palates, where migration appeared to be random or the cells did not move. By placing *Wnt5a* soaked beads on different parts of the tissue this lack of directional migration could be overcome and in wild-type mice cells were seen to migrate towards the bead.

*Wnt5a* is thought to be involved in inducing filopodia in migrating cells (Nishita et al., 2006). There are also other possible chemoattractants that show varied expression across the palate shelves. For example *Fgf10* is expressed in the anterolateral region (Alappat et al., 2005), which could be involved in the lateral migration. The total number of migrating cells in the palate might be small, but their impact on palate development could be magnified. Perhaps these migrating cells caused different genes to be expressed by the cells they migrated over and in turn impacted proliferation and other mechanisms of directional growth.

#### **5.1.4 The Golgi apparatus and cell migration**

The polarisation of cells in the palate for this study were assessed by measuring the position of the Golgi apparatus (Golgi) relative to the cell's nuclei. In polarised epithelial cells the Golgi lies on the anterior side of the nucleus (Nelson, 2009) and in migrating epithelial cells the Golgi is located on the side of the leading edge of the cell (Mellor, 2004).

##### **5.1.4.1 Structure and function of the Golgi apparatus**

The Golgi is found in eukaryotic cells and can be observed under a light microscope as a series of flattened sacks known as cisternae composed of plasma membrane and containing a large array of enzymes. Cytoplasmic vesicles fuse with the Golgi and allow its contents of post-translational proteins, lipids and polysaccharides to be modified and repackaged and then excreted ready for exocytosis or use elsewhere within the cell.

##### **5.1.4.2 Migrating mesenchymal cells and the Golgi**

For a cell to migrate it has to be polarised and work on these processes has often focused on the plasma membrane, but there is evidence of a link between the Golgi and the microtubule organising centre (MTOC) or centrosomes (Sutterlin and Colanzi, 2010) during interphase. The leading edge of a migrating cell extends protrusions out into the extracellular environment and to do this it needs constant supplies from the cell (Fig. 5.1C). The migrating cell sets up this asymmetric membrane traffic by reorganising its cytoskeleton and directing secretory traffic and recycling endosomes straight to the leading edge.

Preisinger et al. (2004) showed that the Golgi, specifically the Golgi matrix protein GM130, interacts with two key kinases, YSK1 and MST4, linking it to the MTOC and the establishment of polarisation in a cell. YSK1 and MST4 have opposing affects; YSK4 is involved in redirecting the Golgi towards the leading edge (Preisinger et al., 2004) and aids cell migration whereas MST4 activation inhibits cell migration without visible effects on the Golgi. If secretory traffic from the Golgi is blocked then the cell fails to migrate (Prigozhina and Waterman-Storer, 2004).

#### **5.1.4.3 Uniform Golgi positioning in limb bud development**

Work on limb bud development showed that the distribution of proliferation is not responsible for the elongation therefore directional cell behaviours were studied. Upon observation of an extensive and dynamic filopodia network the position of the Golgi in the early mouse limb bud was investigated and seen to show a distal bias (Boehm et al., 2010). Another group showed a caudal and lateral bias of the Golgi, showing that polarisation matched the direction of movement that had already been observed. When the same stage was looked at in a *Wnt5a* mutant this bias was not there (Fig. 5.3D-G), indicating that *Wnt5a* is involved in establishing cell polarisation (Wynngaarden et al., 2010).

#### **5.1.4.4 Golgi positioning, directed secretion and wound healing**

Golgi positioning can be an indication of polarised behaviours. This could be migration but it leads to directed secretions. To aid migration through the extracellular matrix cells secrete proteinases to break down other strong cell-cell and cell-adhesion bonds that are in its way, and activate other factors in the environment that will aid migration.

These are far from the only substances secreted from a cell into the extracellular matrix though.

A normal reaction to a scratch wound includes the Golgi being positioned towards the wound edge. Secretions are then directed towards this edge. The cells are polarised and migrate towards the wound edge to enable it to close and heal. All of these behaviours change after disruption of either of two golgin proteins, golgin-160 and GMAP210 (Yadav et al., 2009), involved in Golgi positioning through the recruitment of motor proteins and resulting in a dispersed Golgi apparatus. Secretions still occur but in random directions, the cells are no longer polarised and do not migrate towards the wound edge, inhibiting the healing process.

Changes and regional differences in extracellular matrix composition might be involved in setting up the intrinsic forces needed for a palate to elevate. These could be set up by directed secretion from the mesenchymal cells. If these secretions are disrupted, the elevation process could fail and consequently a cleft palate occurs.

### **5.1.5 Convergent extension**

To cause a tissue to elongate the cells do not always have to be migrating in the long axis of the tissue. Through a process known as convergent extension, the cells could be migrating perpendicularly to the axis of elongation and move in between the cells next to them, a mediolateral cell intercalation, forming a single longer, row of cells. The overall effect on the tissue is for it to become longer and narrower. To undergo this process forces need to be produced to intercalate the cells in one direction and then to elongate the tissue along a different axis. One way this is done is by the cell sending out protrusions and pulling itself along, as described above. These protrusions can be bipolar as seen in *Xenopus* gastrulation (Shih and Keller, 1992). Alternatively they have been shown to be monopolar in the *Xenopus* neural plate (Elul and Keller, 2000) and the nematode dorsal hypodermal cells where intercalation is driven by protrusions mainly occurring on the basal side (Williams-Masson et al., 1998).

Intercalation can occur in both epithelial and mesenchymal tissues and is controlled by several different pathways. Several systems that use cell intercalations to elongate require a signalling system along the axis of extension, such as *Drosophila* germ band

or hindgut (Fig. 5.4) (Lengyel and Iwaki, 2002; Myat, 2005). One of the main signalling pathways shown to be involved is the Wnt/PCP pathway (Roszko et al., 2009).

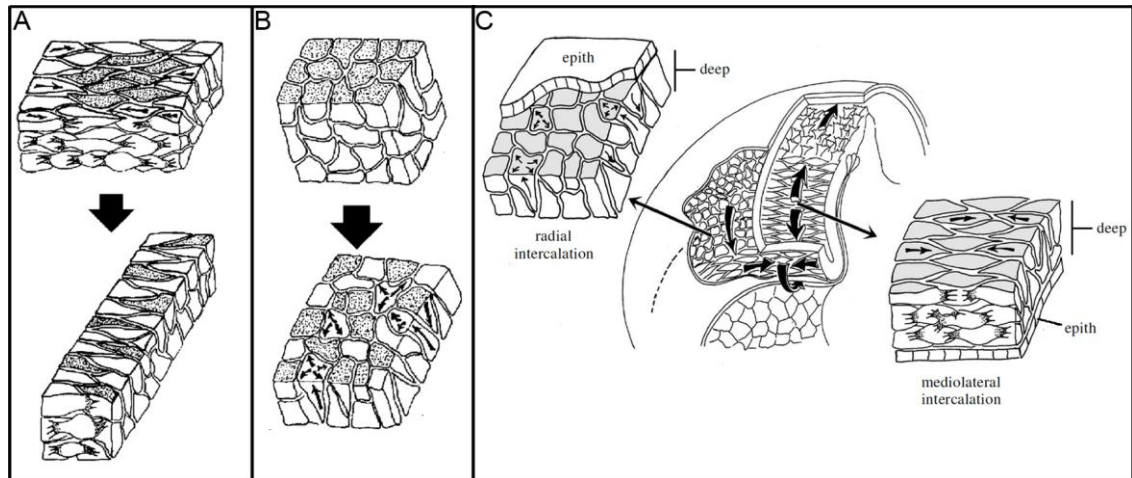


**Figure 5.4 Examples of cell intercalation during development** A) Mediolateral intercalation B) Radial intercalation C) Radial and mediolateral intercalation in *Xenopus* gastrulation. Adapted from Keller et al., 2000  
 “Mediolateral intercalation behaviours” (Shih and Keller, 1992) have been observed during *Xenopus* gastrulation (Fig. 5.4C). At early gastrula stages mesodermal cells in *Xenopus* were multipolar and extended protrusions in random directions. By mid-gastrula stage the cells were bipolar and extended protrusions towards neighbouring cells and used the traction to pull themselves between each other. These intercalations occurred radially first (Fig. 5.4B) and then mediolaterally (Fig. 5.4A). They also involved both the deep mesodermal cells and the mesodermal cells next to the organising epithelium (Keller et al., 2000; Shih and Keller, 1992). This was the main mechanism of cell motility responsible for the extension of the body axis in *Xenopus*. There are examples of convergent extension happening in epithelial sheets in *Drosophila* but these events can also be studied in a mesenchymal tissue by looking into *Drosophila* ovariole (Godt and Laski, 1995).

## 5.2 Polarised cells and orientated cell behaviours: Methods

An immunohistochemical stain was carried out, on frozen frontal sections of mT/mG mice with an n=3 per stage, against the Golgi along with a DAPI nuclear stain, as described in sections 2.3-2.5. Confocal z-stacks of the palatal region were taken at regular intervals (every 90  $\mu\text{m}$ ) along the AP axis. The orientation of the Golgi relative to the cell’s nucleus was measured, rose plots were created and Watson’s  $U^2$  test was performed to test for statistical significance (section 2.10 for further details). The full

results of the statistical tests for the Golgi orientation data are listed in table 12.2 (See Appendix) and a  $p < 0.05$  is considered statistically significant.

For this section different regions of the palate have been investigated as well as cells from the adjacent mesenchyme for comparisons. On the rose plots the  $180^\circ$  point represents the distal tip of the palate, where the plots are displayed on an outline of the palate they have been rotated so the  $180^\circ$  line matches distal point of the diagram. Initially the mesenchymal cells that made up the palatal outgrowth were split into thirds along both the proximodistal and prospective oronasal axis. No difference was found along the proximodistal axis behind the tip. Therefore these thirds were pooled and comparisons made across the prospective oronasal axis.

### **5.3 Polarised cells and orientated cell behaviours: Results**

The Golgi was used as an indication of the cell having polarised and having the potential to display polarised cell behaviours such as migration or directed secretion. If a majority of cells were showing the same directionality then it is possible that they were contributing to directional growth.

#### **5.3.1 Orientation of the Golgi during the initial outgrowth**

At E11.5 during the initial outgrowth of the palate from the base of the maxillary process the mesenchymal cells of the palatal outgrowth had an orientation that was statistically significantly different from a uniform distribution (Watson's  $U^2$  test,  $p < 0.01$ ; Fig. 5.5A). The maxillary mesenchyme adjacent to the palatal outgrowth also had a distribution that varied significantly from a uniform one, but both were also significantly different from a von Mises distribution. They appeared to have a similar bias to each other, which was in the direction the palate was elongating. The palatal outgrowth was very short and broad at E11.5 and the wide spread of the orientations in a distal direction, between  $90^\circ$  and  $270^\circ$ , seen on the rose plots matched this shape (Fig. 5.5).

The distribution in the palatal outgrowth as a whole remained statistically significantly different from a uniform distribution at E12.5, although the bias did not look as strong overall compared to E11.5 (Fig. 5.5 versus 5.6A). It was also significantly different

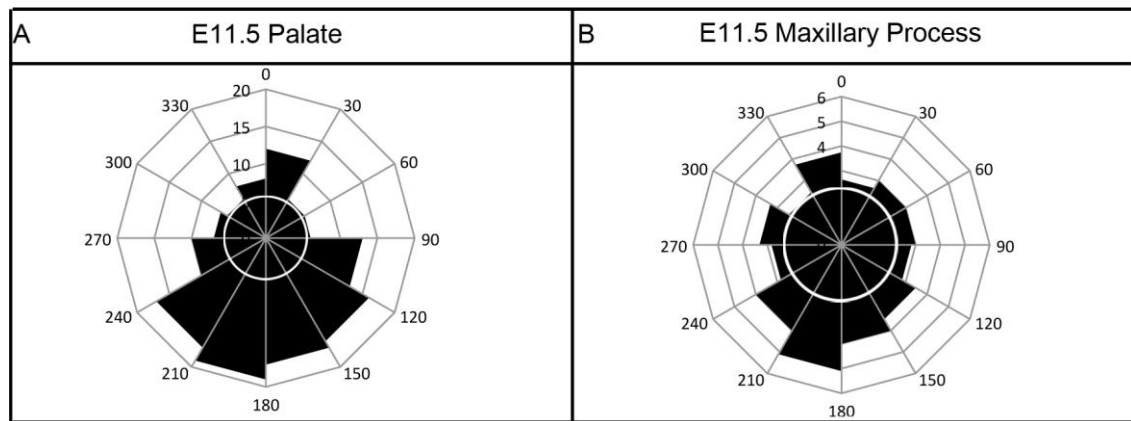


**Figure 5.5 Rose plots summarising Golgi angle in relation to the nuclear centre at E11.5** A) Orientation of the Golgi in cells in the palatal outgrowth B) Orientation of the Golgi in cells in the maxillary process. The white circle represents a uniform distribution. The 180° point is towards the distal tip of the palate.

from the distribution seen at E11.5 in both the palate and the adjacent mesenchyme. If the cells in the distal tip of the palatal shelf were considered on their own they showed a distribution that was significantly different from a uniform distribution (Fig. 5.6G), where the majority of the Golgi were still directed between 90° and 270°. The tip region (Fig. 5.6G) was also significantly different from the cells in the rest of the palatal outgrowth and the mesenchyme adjacent to the palate (Fig. 5.6C).

At E12.5 the prospective nasal and middle thirds displayed distributions that were significantly different from a uniform distribution (Fig. 5.6D & E). For the middle third a von Mises distribution could also be rejected meaning the distribution could be random (Fig. 5.6E). A small majority of the Golgi in the prospective nasal thirds appeared to be distributed between 90° and 180°, pointing towards the prospective oral side and the distal tip. The cells around the nasal shoulder (Fig. 5.6B) had a distribution that allowed both a uniform and a von Mises distribution to be rejected at E12.5.

If the measurements from the entire palatal outgrowth were pooled together (for example regions D-G in fig. 5.6) and divided along the AP axis then all three thirds displayed a non-uniform distribution. The distribution in the posterior third could also be considered significantly different from a uniform one and was significantly different from the middle third (Fig. 5.6I & J). Along the entire length of the AP axis at E12.5 the majority of the spindles appeared to be directed in the direction in which the outgrowth was elongating, but still with a wide spread distribution between 90° and 270° (Fig. 5.6 H-I).

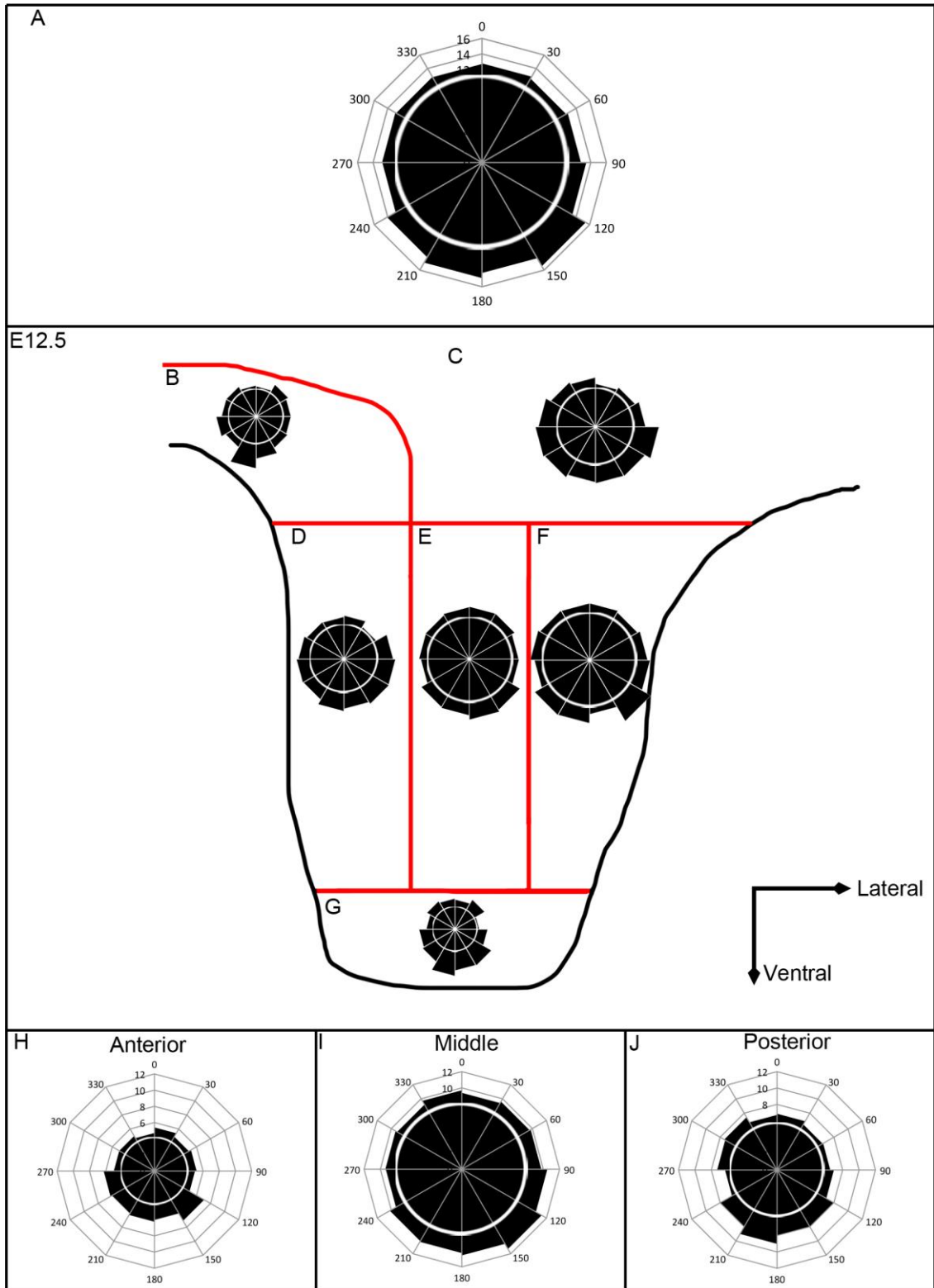


**Figure 5.6 Rose plots summarising Golgi angle in relation to the nuclear centre at E12.5** A) Orientation of the Golgi in cells in the palatal outgrowth B-G) Orientation of the Golgi in cells across different regions of the palate B) Shoulder region C) Mesenchyme adjacent to the palatal outgrowth D) Prospective nasal third E) Middle third F) Prospective oral third G) Tip H) Anterior I) Mid-palate J) Posterior. The white circle represents a uniform distribution. The 180° point is towards the distal tip of the palate.



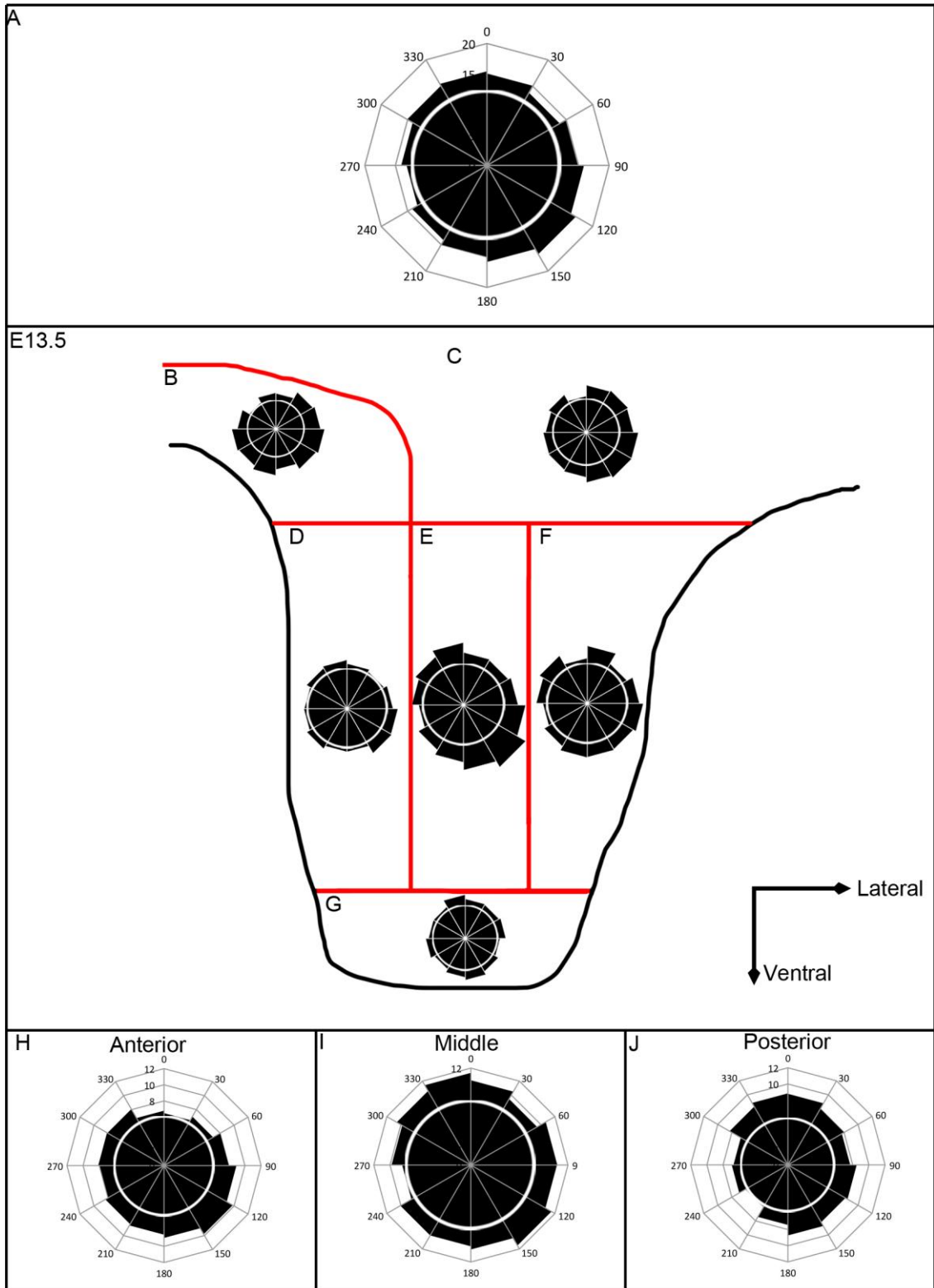


**Figure 5.7** Rose plots summarising Golgi angle in relation to the nuclear centre at **E13.5** A) Orientation of the Golgi in cells in the palatal outgrowth B-G) Orientation of the Golgi in cells across different regions of the palate B) Shoulder region C) Mesenchyme adjacent to the palatal outgrowth D) Prospective nasal third E) Middle third F) Prospective oral third G) Tip H) Anterior I) Mid-palate J) Posterior. The white circle represents a uniform distribution. The 180° point is towards the distal tip of the palate.

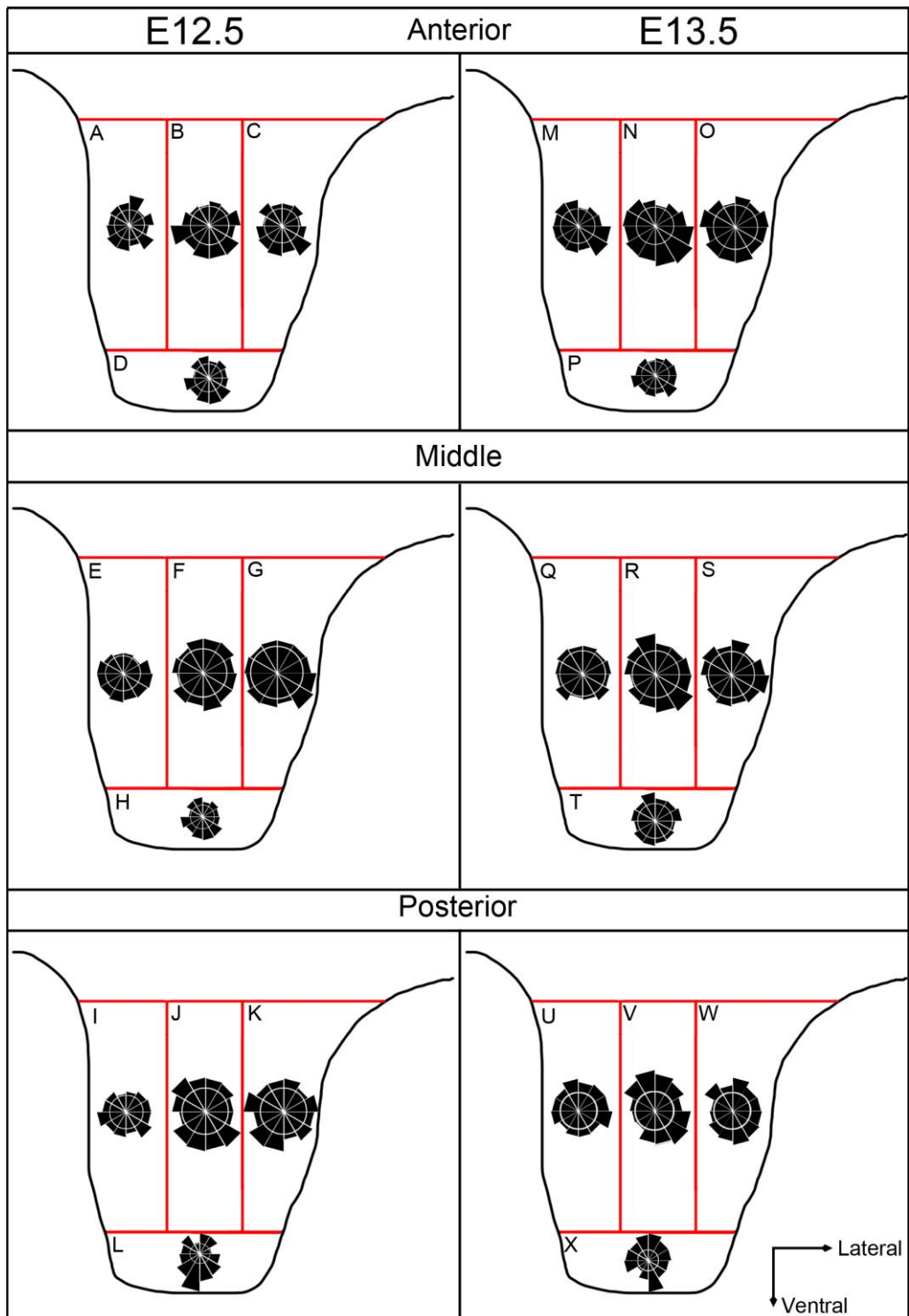


**Figure 5.8 Rose plots summarising Golgi angle in relation to the nuclear centre along the AP axis at E12.5 and E13.5** A-D) Orientation of the Golgi in cells in the E12.5 anterior palatal outgrowth A) Prospective nasal third B) Middle third C) Prospective oral third D) Tip E-H) Orientation of the Golgi in cells in the E12.5 mid-palatal outgrowth E) Prospective nasal third F) Middle third G) Prospective oral third H) Tip I-L) Orientation of the Golgi in cells in the E12.5 posterior palatal outgrowth I) Prospective nasal third J) Middle third K) Prospective oral third L) Tip M-P) Orientation of the Golgi in cells in the E13.5 anterior palatal outgrowth M) Prospective nasal third N) Middle third O) Prospective oral third P) Tip Q-T) Orientation of the Golgi in cells in the E13.5 mid-palatal outgrowth Q) Prospective nasal third R) Middle third S) Prospective oral third T) Tip U-X) Orientation of the Golgi in cells in the E13.5 posterior palatal outgrowth U) Prospective nasal third V) Middle third W) Prospective oral third X) Tip. The white circle represents a uniform distribution. The 180° point is towards the distal tip of the palate.

The palatal shelves were still elongating down either side of the tongue at E13.5, but the orientation of the Golgi had changed significantly in the palatal mesenchyme, and the distribution in the tip region was still significantly different from the maxillary cells adjacent to the palatal outgrowth (Fig. 5.7C & G). But the Golgi in the tip region now have a random distribution, which is significantly different from the tip region at E12.5 (Watson  $U^2$ ,  $p < 0.001$ ; Fig. 5.6G and 5.7G), although a uniform distribution could not be rejected for the tip region at E13.5.

The prospective nasal and oral thirds of the palatal outgrowth did not vary significantly from a uniform distribution at E13.5 (Fig. 5.7D & F). However, they were both significantly different from the middle third, where a uniform distribution could be rejected (Fig. 5.7E). In fact the middle third appeared to have more of a bimodal distribution with Golgi orientated both ventral-laterally and dorsal-medially. The prospective nasal third had changed its distribution significantly since E12.5 from weakly biased towards the distal edge to random. The apparent change seen in the middle third from distally biased to bipolar was not enough to be considered statistically significant ( $0.05 < p < 0.1$ ). The nasal shoulder region again had a distribution that differed from a uniform one, but was significantly different from its distribution at E12.5; it now appeared bimodal along a mediolateral axis (Fig. 4.7B).

The next stage of palate development was elevation. The anterior and posterior regions of the palate were thought to elevate via different processes and the orientation of the Golgi supported this idea. The anterior palate might be elevating by a flip-up mechanism whereas work on the posterior palate favours a remodelling mechanism of elevation. Overall, the posterior palate at E13.5 varied significantly from the anterior palate (Fig. 5.7H & J) and it also varied significantly from the posterior palate at E12.5 (Fig. 5.6J). At E12.5 in the posterior region and E13.5 in the anterior region the vast majority of the Golgi were distributed between  $90^\circ$  and  $330^\circ$  whereas in the posterior region at E13.5 the majority were in a dorsal and lateral orientation. To look at this pattern more closely the distribution of Golgi orientations along the AP axis between E12.5 and E13.5 were looked at in more detail (Fig. 5.8). The distribution of Golgi showed no significant difference in the anterior palate between the two stages (Fig. 5.8A-D versus M-P) or between the anterior and posterior palate at E12.5 (Fig. 5.8A-L). In contrast, both the tip region and the middle third of the posterior palate showed significant changes between E12.5 and E13.5 (Fig. 5.8I versus U & L versus X). The distribution of Golgi in the tip region changed most dramatically from a ventral to a dorsal direction, but the rose plots for the remainder of the posterior palate all

show a more dorsal bias at E13.5 (Fig. 5.8U-X). In regard to the remodelling theory of elevation one would potentially expected to see a medial bias to the rose plots in the posterior palate at E13.5. Although all have some Golgi orientated in a medial direction the majority have a more lateral tilt (Fig. 5.8U-X). At E13.5 there is also a significant difference in the Golgi distribution between the anterior and posterior in both the prospective nasal and the middle thirds of the palate (Fig. 5.8M versus U & N versus V). The rose plots for the middle third of the palate are significantly different from a uniform distribution in both the anterior and posterior thirds but the anterior has a ventral and medial bias compared to the dorsal and lateral bias in the posterior (Fig. 5.8N versus V).

### **5.3.1 Orientation of the Golgi after elevation**

After the palate had elevated the distribution of Golgi in the tip of the palate was uniform (Fig. 5.9B). At E14.5 the nasal, middle and oral thirds of the main part of the palatal shelf had a Golgi orientation distribution that was significantly different from a uniform one and significantly different from each other. The nasal side, which is significantly different from the prospective nasal side at E13.5, appeared to have a bimodal distribution along the mediolateral axis (Fig. 5.9C). In the middle third the majority of the Golgi were orientated between the cell's nuclei and the medial edge of the palate (Fig. 5.9E). In contrast along the oral edge the Golgi appeared to be orientated towards the oral cavity (Fig. 5.9G). This also varied from the distribution of the prospective oral third at E13.5.

The nasal shoulder region displayed a distribution that had changed significantly since E13.5, but could still be considered different from both a von Mises and a uniform distribution (Fig. 5.9D). It appeared to have a dorsomedial bias.

Along the AP axis none of the rose plots displayed a uniform distribution (Fig. 5.9H-J). Only the middle third showed a distribution that was significantly different from that region 24 hours earlier. This was also the only region of the palate that was definitely touching the other palatal shelf at this point. In this middle third the majority of the Golgi appeared to be orientated towards the medial edge (Fig. 5.9I). The anterior third had a very similar distribution of Golgi to the middle third (Fig. 5.9H), whereas the posterior palate had a significantly different distribution (Fig. 5.9J). To look at the differences along the AP axis in more detail these rose plots were broken up into

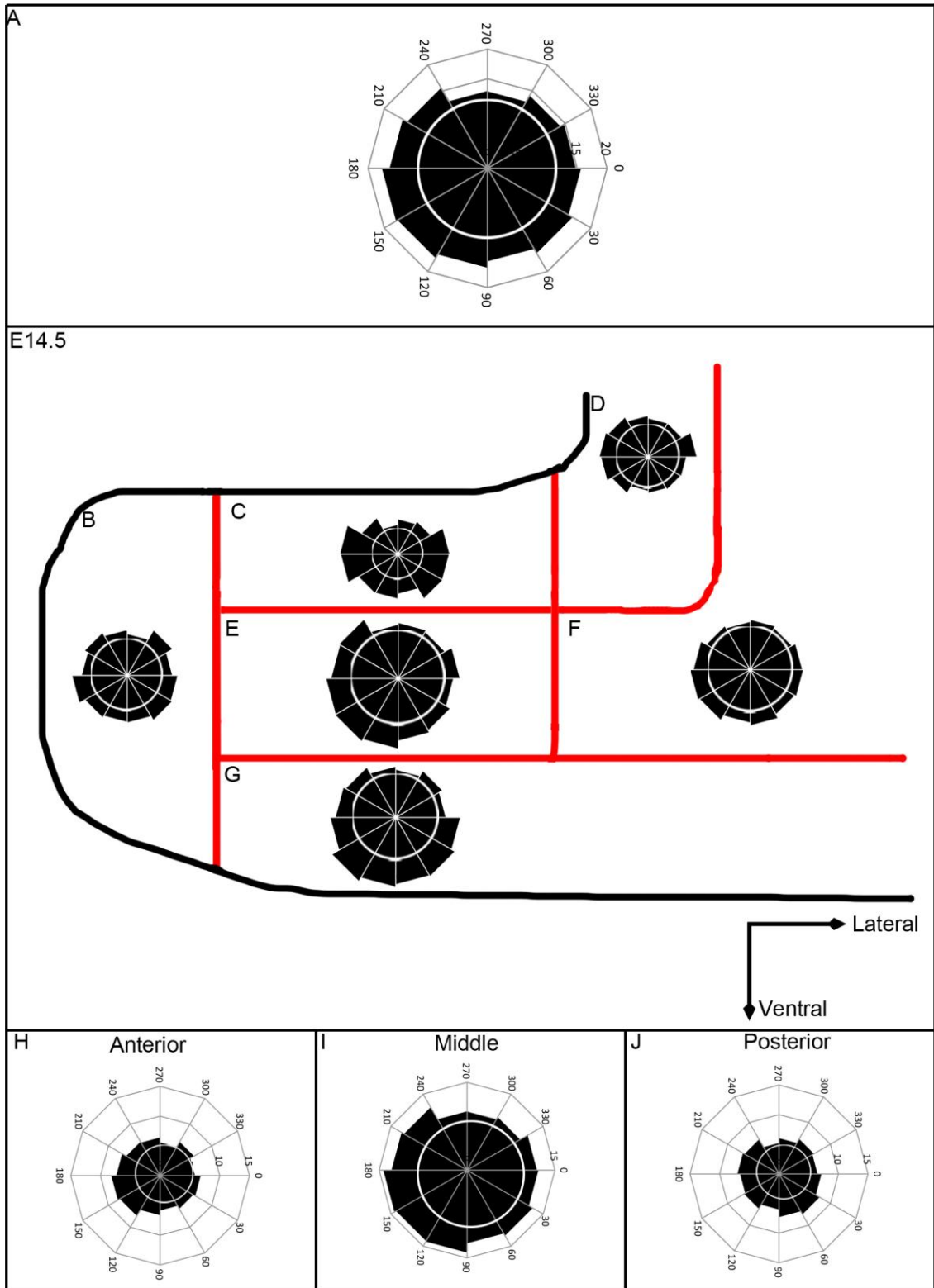


**Figure 5.9** Rose plots summarising Golgi angle in relation to the nuclear centre at **E14.5** A) Orientation of the Golgi in cells in the palatal outgrowth B-G) Orientation of the Golgi in cells different regions of the palate B) Tip C) Nasal third D) Nasal shoulder region E) Middle third F) mesenchyme adjacent to the palatal outgrowth G) Oral third H) Anterior I) Mid-palate J) Posterior. The white circle represents a uniform distribution. The 180° point is towards the distal tip of the palate.

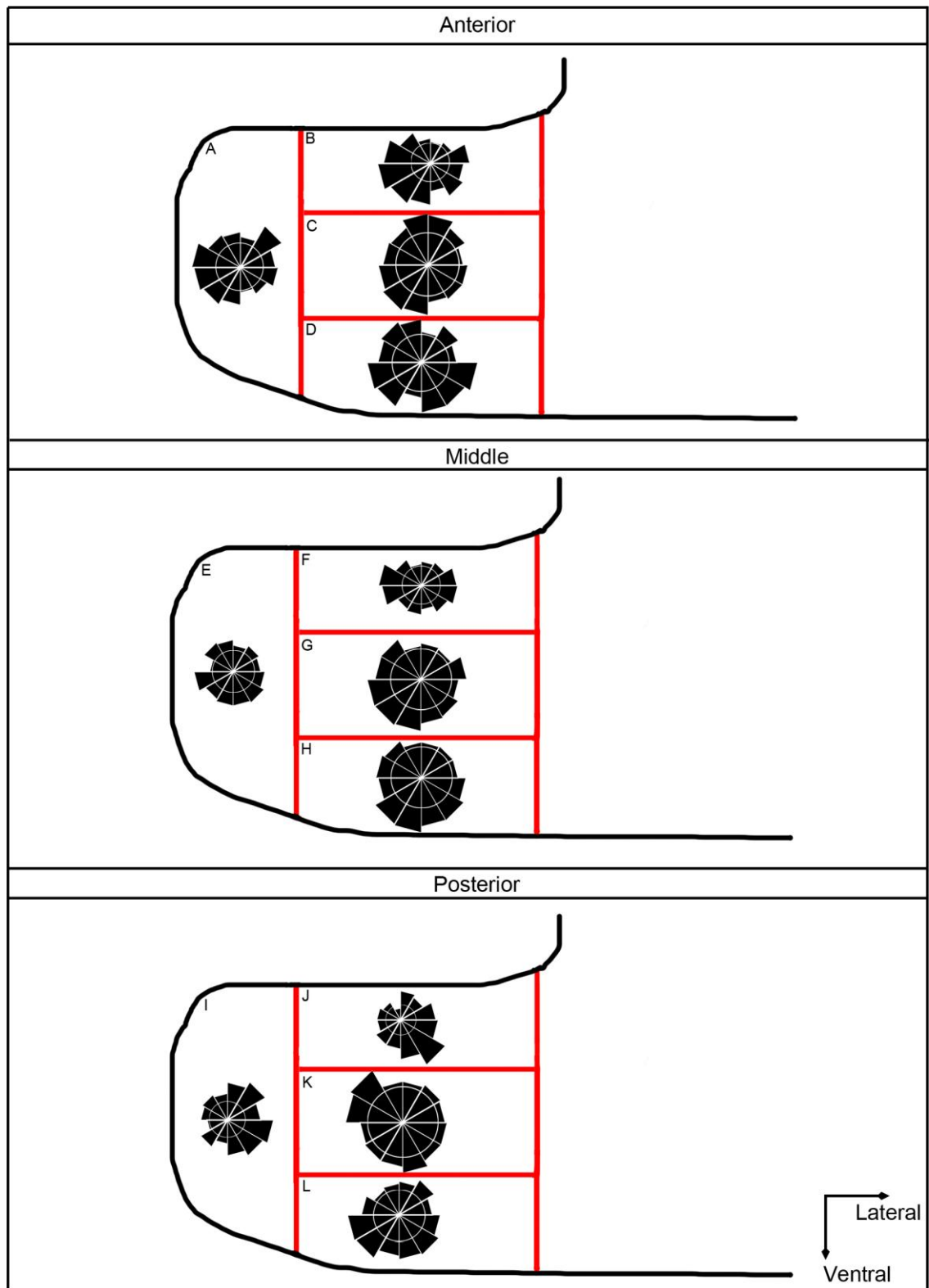


**Figure 5.10 Rose plots summarising Golgi angle in relation to the nuclear centre along the AP axis at E14.5** A-D) Orientation of the Golgi in cells different regions of the anterior E14.5 palate A) Tip B) Nasal third C) Middle D) Oral third E-F) Orientation of the Golgi in cells different regions of the E14.5 mid-palate E) Tip F) Nasal third G) Middle H) Oral third I-L) Orientation of the Golgi in cells different regions of the posterior E14.5 palate I) Tip J) Nasal third K) Middle L) Oral third. The white circle represents a uniform distribution. The 180° point is towards the distal tip of the palate.

different regions of the palate again (Fig. 5.10). The rose plots for the anterior palate, which was growing towards the midline, had a distinctive bias towards the medial edge. This was most clearly seen along the nasal side of the palate where the distribution of the Golgi is significantly different from a uniform distribution (Fig. 5.10B). In the mid-palate the nasal, middle and oral thirds all had Golgi distributions that varied significantly from a uniform distribution (Fig. 5.10F-H). The rose plot on the nasal side appeared to have a bilateral distribution, verified by it also varying significantly from a von Mises distribution. The middle third appeared to have a bias towards the medial edge whereas the distribution along the oral side had a ventral and medial bias (Fig. 5.10G & H). There was a random distribution of Golgi in the tip region in the mid-palate (Fig. 5.10E). The distributions of Golgi in the tip region and along the nasal side in the posterior third were significantly different from these regions in the anterior and mid-palate and significantly different from a uniform distribution (Fig. 5.10I & J). In the posterior third the rose plots of these two regions showed a lateral bias (Fig. 5.10I & J). The oral side of the posterior palate was significantly different from a uniform distribution. It showed a similar ventral bias to this region in the mid-palate (Fig. 5.10L).

## **5.4 Polarised cells and orientated cell behaviours: Discussion**

### **5.4.1 Golgi orientation assay discussion**

The images used in this assay took longer to capture because they were Z-stacks and not single images but the microscope could be left alone to complete the scan. For this study the measurement was made by hand by clicking on the centre of the nucleus and then the centre of its Golgi. In principle, the orientation of the Golgi with respect to the nucleus of each cell could have been measured by an automated or semi-automated image analysis approach. This would have required segmentation of each cell outline for unambiguous assignment of each Golgi to its nucleus as well as segmentation of the nucleus and the Golgi itself. In practice, the limiting factor was the membrane stain because in some regions there was too much noise and in others there were gaps in the fluorescence. Possibly the mT/mG mice could be crossed with a Wnt1/Cre reporter line. This would result in GFP labelling of all the NCC derived cell membranes in the palate. There was not time to breed the new mouse line, create and verify an automated technique for this project.

#### 5.4.2 Polarised cells during palate development discussion

The majority of the mesenchymal cells of the palate are derived from the migratory cranial NCC, which are migrating towards the distal tip of the maxillary process. The palatal shelf is at right angles to this. The mesenchymal cells in the maxillary process adjacent to the palate showed a directional bias towards the palatal outgrowth, which could be evidence of migration into the palate. The orientation of the Golgi in the palate, at E11.5, was also potentially indicating the direction in which these cells were migrating and this matches the direction of palatal shelf elongation. If this migration was occurring the directional growth of the palate at this stage could have been due to a combination of high levels of proliferation and the addition of cells from the maxillary process.

In the tip region of the outgrowth at E12.5 the orientation of the Golgi showed the cells were polarised in such a way as to make it possible for them to be contributing to the radial expansion of the outgrowth. That means as well as increasing in length it was increasing the width of the outgrowth, which is necessary, because the outgrowth got wider as it grew down the side of the tongue. This directional growth could still have been due to cell migration or cell rearrangements.

In the mid-palate at E13.5 the Golgi were distributed randomly, so there was no evidence of directed cell behaviours occurring, but in the anterior third there was a ventral bias. Therefore potentially the continued elongation of the palatal outgrowth here does involve directional cell behaviours. Overall during early palate development the orientation of the Golgi was in a ventral direction, towards the distal tip of the palate and the direction of overall tissue growth. If the cells are migrating through the ECM or past each other this might create a shear pattern, like water flowing through a pipe. The cells along each edge are hindered by friction from the relatively static epithelium whereas more central cells could move more freely.

It has been suggested that cells in the anterior palate migrate across to the prospective oral side with *Wnt5a* acting as a chemoattractant (He et al., 2008). The orientation of the Golgi recorded here offered some support to this idea. Cells at E12.5, particularly in the prospective nasal and the middle third of the palate had a slight bias towards the prospective oral side. Around 54% of cells were shown to migrate in this way (He et al., 2008) and 52% of cells from this investigation had a bias in the same direction at E12.5. At E13.5 55% of cells in the middle third displayed this bias. This movement could have been due to the different amounts of proliferation occurring on either side of the palate by this stage, causing a bulk movement of cells, not individually migrating cells, from a region of high proliferation to a region with lower proliferation. Alternatively this movement could have been starting to generate a force required to elevate the palate above the tongue. Maybe by building up potential energy on the lateral



side, which when released by the physical barrier imposed by the tongue being removed, the tissue can rebound causing the anterior palate to flip up.

The posterior palate, at E12.5, showed a distribution that had a ventral bias, similar to the tip of the overall outgrowth and could have been contributing to the elongation. In contrast just 24-hours later the equivalent posterior third had a dramatically different directional bias. The cells were now displaying direction behaviours back to the proximal end of the outgrowth and, slightly unexpectedly, towards the lateral side of the embryo. This directional behaviour could have been cell migration, and it could have been in preparation for elevation. The posterior palate is thought to elevate by a remodelling process, therefore polarised cell behaviours, such as cell migration, could be driving this initially by retracting into the proximal palate. Then there might be a second stage to the remodelling process where a stronger medial bias is seen to allow the palate to flow back over the tongue. To investigate this more fully a time course of stages between E13.5 and E14.5 would be useful as well as live cell imaging.

After elevation the cells just at the distal tip of the outgrowth displayed a uniform distribution. These cells were located directly behind the MEE that would shortly fuse with the opposing palatal shelf. These cells could have been lying quiescent until they received a signal informing them that the two palatal shelves had touched and palatal fusion could start to take place. Therefore they were possibly not involved in any directional behaviour helping the two palatal shelves grow towards the midline.

In contrast the cells in the rest of the palate, as well as the nasal shoulder region and the mesenchymal tissue adjacent to the palate, all had a bias towards the tip of the outgrowth and this could have been an indication that directional cell behaviours were driving growth towards the midline. Proliferation was very low in the palatal mesenchyme itself at this stage. Therefore the bias towards the midline seen in the adjacent mesenchyme, where proliferation is slightly higher, could have meant that cells were being recruited from further afield, migrating into the palate and contributing to directional growth. The cells in the nasal third seemed to have a bilateral distribution along the mediolateral axis and the cells in the oral side had a bias in a ventral direction as well as the medial one. Whether this was due to intermingled cells migrating in opposite directions or blending of two sub-regions of tissue each containing cells coherently migrating oppositely was not tested.

Orientated cell behaviours summary:

- 1) Overall the orientation of the Golgi was most often distally directed, i.e. in the direction of tissue growth.
- 2) The orientation of the Golgi in the posterior palate at E13.5 supports the remodelling theory of elevation.

## 6.0 Orientated Cell Division

### 6.1 Introduction to orientated cell division

Proliferation occurs throughout embryonic development contributing to overall growth, as the embryo gets bigger. Co-ordinated mitotic events can result in proliferation playing a significant role in shaping the embryo through directional growth.

The orientation of cell division relies on the orientation of the mitotic spindle, something that can be visualised and measured, allowing this mechanism to be monitored and quantified (Fig. 2.3F-J). The centrosomes of the cell align at opposite poles during prometaphase and align microtubule spindles across the cell. Although there is evidence of the metaphase spindles tumbling so that the orientation is not determined until anaphase (Adams, 1996). They then attach to the chromosomes via a kinetochore complex (Fig. 6.1A & B). The chromosomes are then pulled towards the two poles by controlled depolymerisation of the microtubules. Once this is complete cytokinesis can begin as the cell continues from anaphase to telophase.

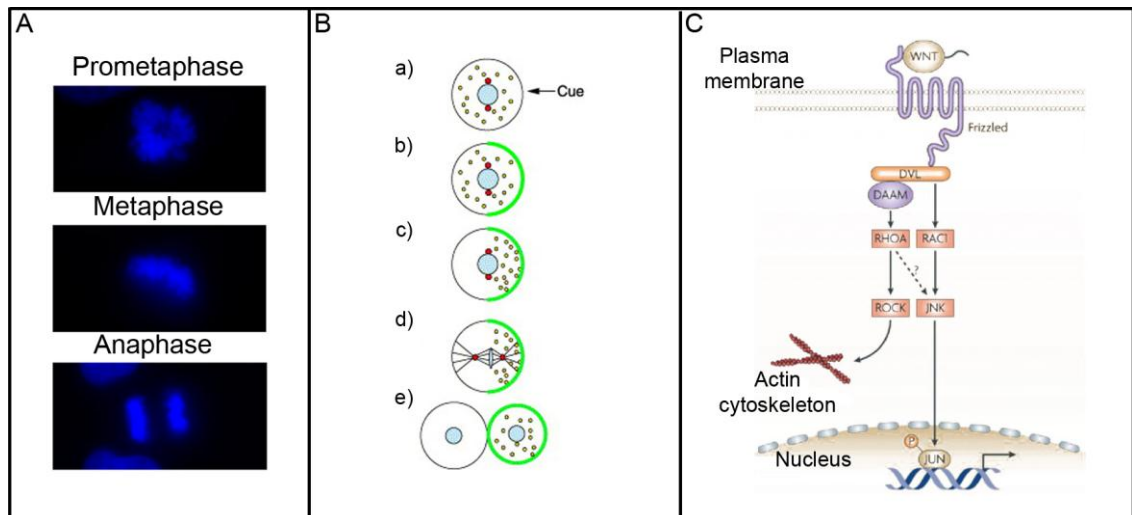


**Figure 6.1 Stages of mitosis and PCP signaling pathway** A) Characteristic DNA morphology by DAPI staining in different stages of mitosis. Adapted from Dellaire et al., 2005 B) General stages of polarization and orientated cell division a) Induction of polarity axis b) Response to polarity cue c) Asymmetric localization of proteins/RNA d) Mitotic spindle positioning e) Asymmetric cell division. Adapted from Ahringer, 2004 C) A simplified flow diagram of the noncanonical Wnt/PCP pathway. Adapted from Staal et al., 2008

For the orientation of the mitotic spindle to be specified the cells need to become

polarised. Firstly, signalling establishes asymmetry in the cell, and an identifiable polarity axis (Fig. 6.1B). It is thought that partition defective (PAR) proteins and microtubules play a role in setting up the polarity. To orientate the spindles themselves there is evidence for the motor protein, dynein, and the functionally linked dynactin being involved as the link between the microtubules and the cortex (Zheng et al., 2013). The link between dynein and the mitotic spindle is thought to be a heterotrimeric G protein (Ahringer, 2003).

This mechanism has been associated with directional growth in several different tissues (Castanon and Gonzalez-Gaitan, 2011). Some organs rely on isotropic orientation of cell divisions, so that divisions occur in all directions, such as in the developing sea urchin. Others depend on anisotropic orientation, where all the divisions occur with a directional bias.

A disruption in the orientation of cells divisions could in principle affect the directional growth of the entire palate and lead to a cleft. It is very important to know whether this process plays a role in the normal directional growth of the palate. This indicates the importance of including an assay to look at the orientation of cell division in studies of models of cleft palates.

### **6.1.1 Possible cues behind orientated cell divisions**

There is evidence that the orientation of cell division can be regulated by extrinsic signals and intrinsic cues (i.e. prior polarity of the cell). These interact with the microtubules causing them to re-orientate the spindles.

### **6.1.2 Cortical cues**

Cortical cues from other cells or the ECM are thought to play a larger role in spindle orientation than cell geometry. A change in the distribution of cues in the cells cortex can also contribute to the orientation of the spindle.

For example intrinsic cues are required in the *C. elegans* zygote during prophase, when the nucleus and centrosomes travel to the centre of the cell where they then orientate, and are dragged towards the posterior end of the cell (Gillies and

Cabernard, 2011). This specific orientation and control from intrinsic cues produces asymmetric divisions, which generate cell diversity.

### **6.1.3 Cell shape**

The first factor thought to be affecting the orientation of cell division was cell shape when in 1884 Oscar Hertwig demonstrated that cells divide along their long axis cited in Castanon and Gonzalez-Gaitan, 2011. This was demonstrated in *Xenopus* zygotes gently compressed between glass slides (Black and Vincent, 1988). It has been shown more recently, in cultured normal rat kidney cells, that the orientation of the spindles is parallel to the long axis of the cell, both spontaneously and, following mechanical manipulation of this axis (O'Connell and Wang, 2000). Microtubules were shown to be responsible for this latter change by disrupting the motor protein dynein, which inhibited the cell's ability to reposition its spindle.

### **6.1.4 Cell-cell and cell-ECM adhesions**

E-cadherin accumulates at cell-cell junctions and the position correlates with the location of the spindle within the cell. In zebrafish with an E-cadherin (*cadh2*) mutation the spindles do not orientate correctly and this results in defective neural tube morphogenesis (Zigman et al., 2011).

Cell culture systems have been used to explore the relationship between the extracellular matrix and the orientation of the mitotic spindles. HeLa cells were used because they become round during mitosis, meaning the cell has no long axis that is also thought to influence the mitotic spindle. The position that fibronectin in the ECM attached to the cell was shown to influence the orientation of cell division (They et al., 2005). This occurred by the ECM attaching to the cell during interphase and altering the location of actin at the membrane. This caused components within the cell to be rearranged and their new position was maintained through to mitosis, consequently altering the orientation of the spindles.

It is also possible for the cells to change from symmetric cell divisions to asymmetric ones. This happens in the epidermis at around E15.5 in mice. Cells that were dividing parallel to the basal layer switched their orientation by 90 degrees and started to divide perpendicularly to the basal layer. This caused cells to move into a deeper layer and it

changed their fate, seen through the expression of different markers from the proliferating cells (Lechler and Fuchs, 2005). Cells being able to change direction could be relevant at certain time points during palate development. For example when the migrating NCC heading towards the distal tip of the maxillary process are redirected through 90° into the palatal outgrowth or, if the posterior palate is elevating by a remodelling mechanism, then cells might switch from growth in the direction of elongation to growth in a proximal and medial direction. If one mechanism can change its direction then it could have a knock on affect on other direction behaviours.

### **6.1.5 Extracellular signalling pathways involved: PCP pathway**

Study of the mechanism behind orientated cell divisions led to work on the planar cell polarity (PCP) pathway (Simons and Mlodzik, 2008) (Fig. 6.1C) The non-canonical Wnt PCP pathway involves a Wnt ligand binding to a frizzled receptor on the cell's surface which then recruits Dishevelled (Dsh). This starts the PCP cascade that ends in actin modifications and alterations to the cell's cytoskeleton. This was first identified in *Drosophila* and *C. elegans* (Ahringer, 2003), but evidence of it being involved in vertebrates has been seen in zebrafish (Gong et al., 2004; Heisenberg et al., 2000; Wallingford et al., 2000). This was done by altering expression levels and applying different known antagonists of the PCP pathway. It resulted in random orientations of cell division (Castanon and Gonzalez-Gaitan, 2011). Dsh was one of the main targets of these experiments. Dsh is in the PCP pathway as well as the canonical Wnt/ $\beta$ -catenin pathway, but blocking the Wnt/ $\beta$ -catenin pathway did not affect the orientation of cell division. Inhibiting Wnt11 or Wnt5, both normally preferentially activating the PCP pathway, did affect the orientation of cell division in zebrafish gastrulation.

It is thought that external signals work with intrinsic cues to control the cell's polarity and the orientation of cell division, and the two can communicate in different ways. One way could be that the extrinsic signals cause the cell shape to change, and then the spindles align with the long axis of the cell. Alternatively the external signals could connect to an effector protein and interact with the spindles and centrosomes directly.

### 6.1.6 Orientated cell divisions during gastrulation

Gastrulation is the stage in development where the blastula changes into a multi-layered organism with defined axes and three definite germ layers are established, the ectoderm, mesoderm and endoderm (Fig. 6.2A). Gastrulation involves changes in cell shape, motility and adhesion. Other processes known to be involved include epiboly, invagination and convergent extension.

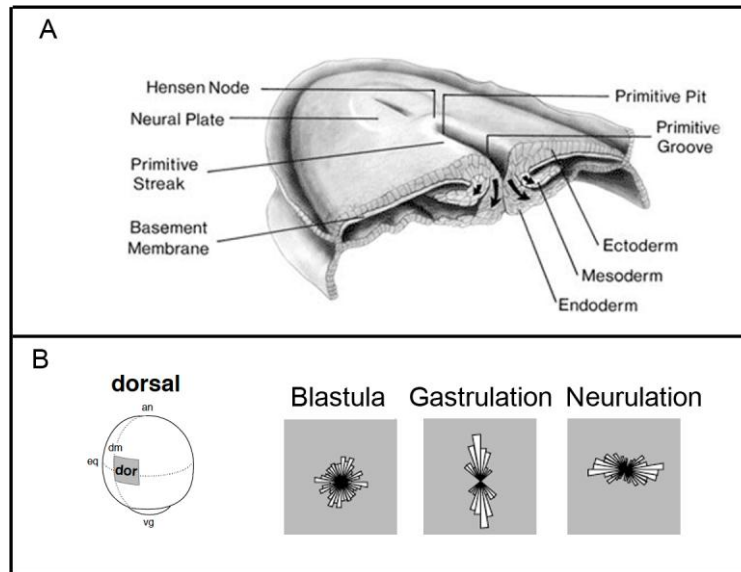


**Figure 6.2 Orientated cell division during development** A) Gastrulation in an amniote; epiblast cells migrate through the primitive streak to form three distinctive germ layers. Adapted from Dias & Partington, 2004 B) The orientation of cell division is random before gastrulation, it becomes aligned with the AP axis during gastrulation and the ML axis during neurulation at the level of the equator on the dorsal side of a zebrafish embryo. Adapted from Concha & Adams, 1998.

In birds and mammals the epiblast cells firstly form the primitive streak by converging at the midline. Then mesenchymal cells migrate anteriolaterally and start to differentiate into the different germ layers.

Studies of primitive streak formation in chick have shown that orientated cell divisions are involved by analysing the orientation of the DAPI plate during metaphase both along the primitive streak and elsewhere in the embryo. It was found that 50% of metaphase cells in the primitive streak were orientated perpendicularly to the anteroposterior axis and another 30% were within 45 degrees of this angle (Wei and Mikawa, 2000). In comparison metaphase plates were orientated randomly elsewhere in the embryo. This was only evident as the primitive streak extended anteriorly very early on; no bias in orientation was evident when the primitive streak was fully formed.

It has been extensively reported that orientated cell division plays a role in the early development of the zebrafish (Concha and Adams, 1998; Gong et al, 2004). During early gastrulation cells in the epiblast (Fig. 6.2B) are highly orientated and move in two distinctive directions, towards the vegetal pole by epiboly and towards the dorsal midline by lateral medial convergent movements. At this point cells can be seen to have a strong bias in their orientation of division along the anteroposterior axis. In contrast cells at the animal pole are still displaying random orientations. As gastrulation continues the primitive groove extends anteriorly and cells towards the animal pole also display an AP bias during cytokinesis. By the end of gastrulation 90% of divisions along the dorsal midline are occurring along the AP axis (Fig. 6.2B).

### **6.1.7 Mouse and chick limb development**

As previously mentioned, a study in the limb (Boehm et al., 2010) showed that contrary to the widely accepted theory of proximodistal growth being caused by a proliferation gradient, it is driven mainly by directional growth mechanisms, including orientated cell divisions. Two further studies came out around the same time showing that orientated cell divisions have a role throughout early development and limb bud elongation, and indicated that the Wnt/PCP pathway is involved (Gros et al., 2010; Wyngaarden et al., 2010).

The limb arises from the lateral plate mesoderm and its overlying ectoderm with a stereotypical shape; it is broader in the posterior region than at the anterior and very narrow in the dorsoventral axis. First it was shown that cells migrate from the rostral and lateral regions of the lateral plate mesoderm into the early limb bud, in both mouse and chick development (Wyngaarden et al., 2010) by following the linear displacement of Dil in culture. At this early stage in development, cells in the lateral plate mesoderm were dividing parallel to the embryo's rostrocaudal axis and the plane of the flank, whereas cells in the early limb bud divided perpendicularly to this axis (Wyngaarden et al., 2010). This pattern of elongation driven by orientated cell division in the limb bud along the proximodistal axis continued as the limb developed (Gros et al., 2010). It was suggested that this directional growth continued, because the division of one cell produced a force that influenced its neighbouring cells, increasing the likelihood that they divide in the same direction.

*Wnt5a* has been shown to be able to cause directional cell behaviours by interacting with the cytoskeleton in response to a chemical gradient (Witze et al., 2008). This was investigated by looking at the orientation of cell divisions in the developing limb bud of the *Wnt5a* mutant mouse. In the lateral plate mesoderm of the *Wnt5a* (Fig. 6.3) mutant the orientation of cell divisions lost their bias in the rostrocaudal axis (Wyngaarden et al., 2010). In the early mutant limb bud itself the orientation of cells divisions was a lot more disorganised than in the wild-type, but some elongation of the bud still occurs indicating that there is some redundancy to the role of *Wnt5a* in controlling orientated cell divisions. To investigate this further the orientation of cell division in the early chick limb bud was measured after c-Jun N-terminal kinase (JNK, acts downstream of *Wnt5a* in the Wnt/PCP pathway) activity was inhibited in a chick embryo explant. In this situation complete disorganisation of orientated cell divisions was found (Gros et al., 2010).

Fgfs act as a very important chemoattractant during limb development, controlling cell movement, but not the orientation of cell divisions. This was shown in chick limb development by using electroporation to target factors upstream of the Fgf/MAPK pathway. Changes were observed in the cell velocity and filopodia and lamellipodia, but not in the proximodistal orientation of cell division (Gros et al., 2010).

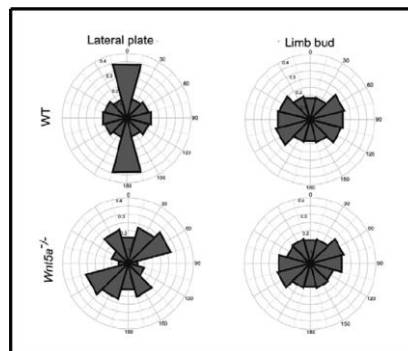


**Figure 6.3 Orientated cell divisions in the limb** In a developing mouse limb bud the lateral plate and the limb bud itself show orientated cell divisions and these are less apparent in the *Wnt5A*<sup>-/-</sup> mutant. Adapted from Wyngaarden et al., 2010.



## **6.2 Orientated cell division methods**

An immunohistochemical stain was used, on frozen frontal sections of mT/mG mice with an  $n=3$  per stage, against gamma-tubulin, PH-3 and DAPI, as described in sections 2.3-2.5. Confocal z-stacks of the palatal region were taken at regular intervals (every 90  $\mu\text{m}$ ) along the AP axis. The orientations of the centrosomes were measured in cells positive for PH3, rose plots were created and Watson's  $U^2$  test was performed to test for statistical significance (see section 2.10 for further details). The full results of the statistical tests for the spindle orientation data are listed in table 12.3 (see Appendix) and a  $p<0.05$  is considered statistically significant. For this section different regions of the palatal shelves have been investigated as well as cells from the adjacent mesenchyme for comparisons. In the rose plots the  $180^\circ$  point represents the distal tip of the palate, where the plots are displayed on an outline of the palate they have been rotated so the  $180^\circ$  line matches distal point of the diagram. These rose plots are showing mirror-image symmetry to reflect the symmetry of the spindles because this helps to reduce visual bias that would be produced from a  $180^\circ$  plot. Prior to performing the Watson's  $U^2$  test, which requires a distribution of angles spread over  $360^\circ$ , the value, in radians, of each angle was doubled.

## **6.3 Orientated cell division: Results**

To determine whether orientated cell divisions (OCD) could be a factor contributing to cleft palates the extent to which OCD occurs in normal palatal morphogenesis needs identifying. The number of mitotic events captured in the images was very low, due to the shortness of M-phase. Firstly to increase numbers spindles from all PH-3 positive cells were measured because anaphase spindles were too sparse.

### **6.3.1 Early wild-type palatal outgrowth**

#### **6.3.1.1 Orientated cell divisions during initial palatal outgrowth, E11.5**

There was no evidence of OCD occurring in the palatal mesenchyme at E11.5. The distribution of cell divisions in the palate did not significantly differ from that of the maxillary process' mesenchyme that it had grown out of (Fig. 6.4). It is not possible to reject the hypothesis that it did not come from a uniform distribution.

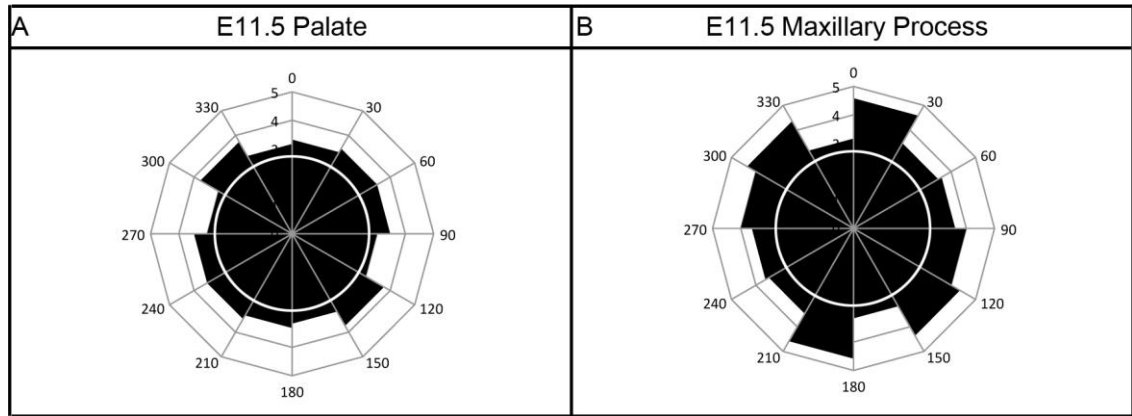


**Figure 6.4 Rose plots summarising mitotic spindle angles at E11.5** A) Distribution of mitotic spindle angles in the palatal outgrowth B) Distribution of mitotic spindle angles in cells in the maxillary process. The white circle represents a uniform distribution. The 180° point is towards the distal tip of the palate.

### 6.3.1.2 Orientated cell divisions during palatal outgrowth, E12.5

As the palate continued to grow vertically down either side of the tongue, the cells continued to show a random distribution of cell divisions across the entire palate. The divisions in every region of the palate examined did not vary significantly from a uniform distribution (Fig. 6.5). When the posterior third of the palatal mesenchyme was pooled together then this region was significantly different from a von Mises (circular normal) distribution. The rose plot for this region showed two peaks that were perpendicular to each other (Fig. 6.5J).

The rose plots showed a weak prospective oronasal bias in the prospective nasal, middle and prospective oral thirds of the palatal mesenchyme (Fig. 6.5D-F). In the tip region, 57% of the spindles were distributed between 120°-180° and 300°-360°, a proximodistal bias. There was a bias in the same direction in the mid-palate region (Fig. 6.5I), along the AP axis, whereas the rose plots for the anterior and posterior palate had the majority of spindles (60% and 52% respectively) orientated between 30-60° and 210-270° (Fig. 6.5H & J).

### 6.3.1.2 Orientated cell divisions prior to elevation, E13.5

At E13.5 neither of the palatal outgrowth or the maxillary mesenchyme showed a distribution that was significantly different from a uniform one. The rose plots showed

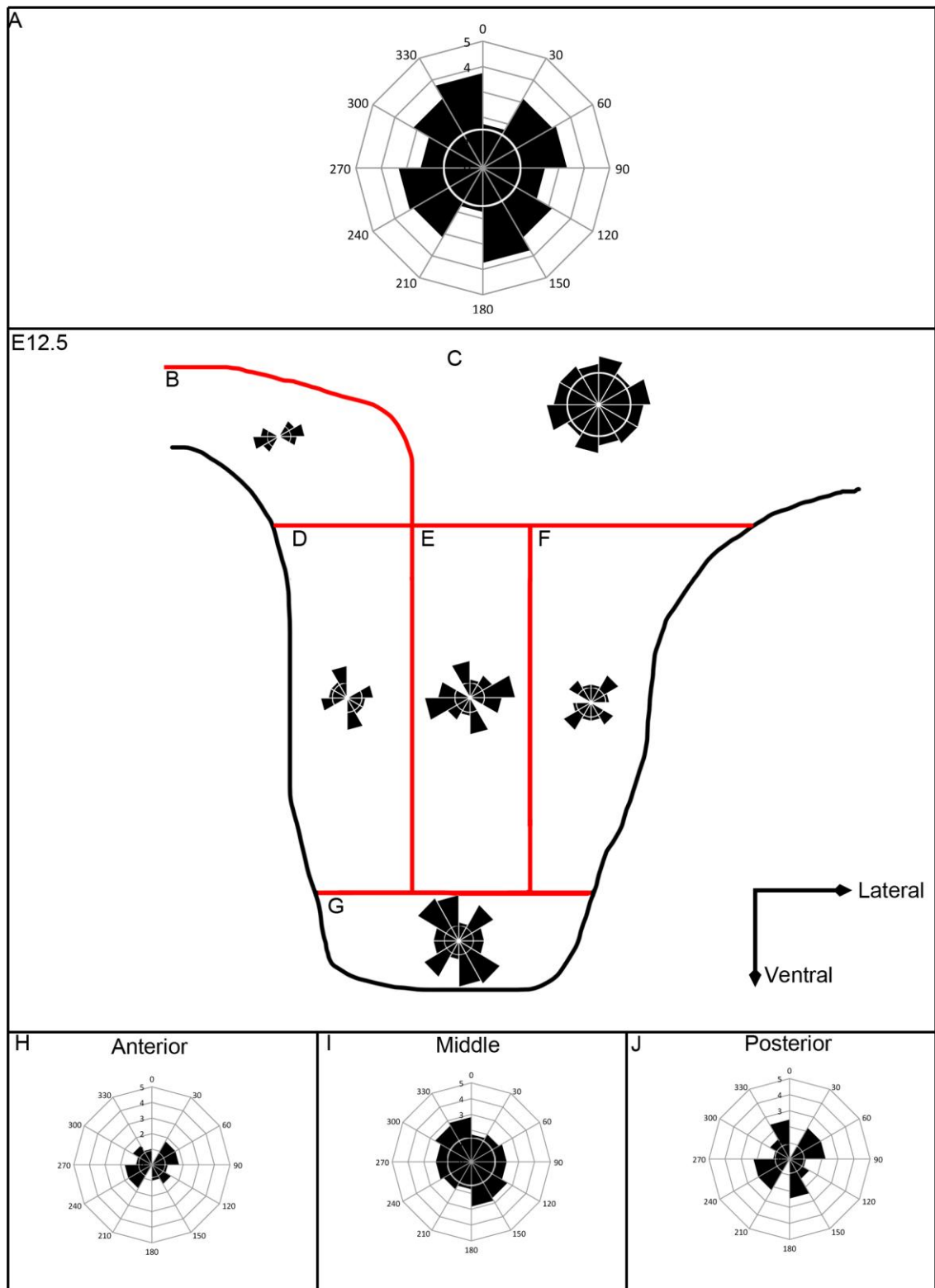


**Figure 6.5 Rose plots summarising mitotic spindle angles at E12.5** A) Distribution of mitotic spindle angles in the palatal outgrowth B-G) Distribution of mitotic spindle angles in cells across different regions of the palate B) Shoulder region C) Mesenchyme adjacent to the palatal outgrowth D) Prospective nasal third E) Middle third F) Prospective oral third G) Tip H) Anterior I) Mid-palate J) Posterior. The white circle represents a uniform distribution. The 180° point is towards the distal tip of the palate.

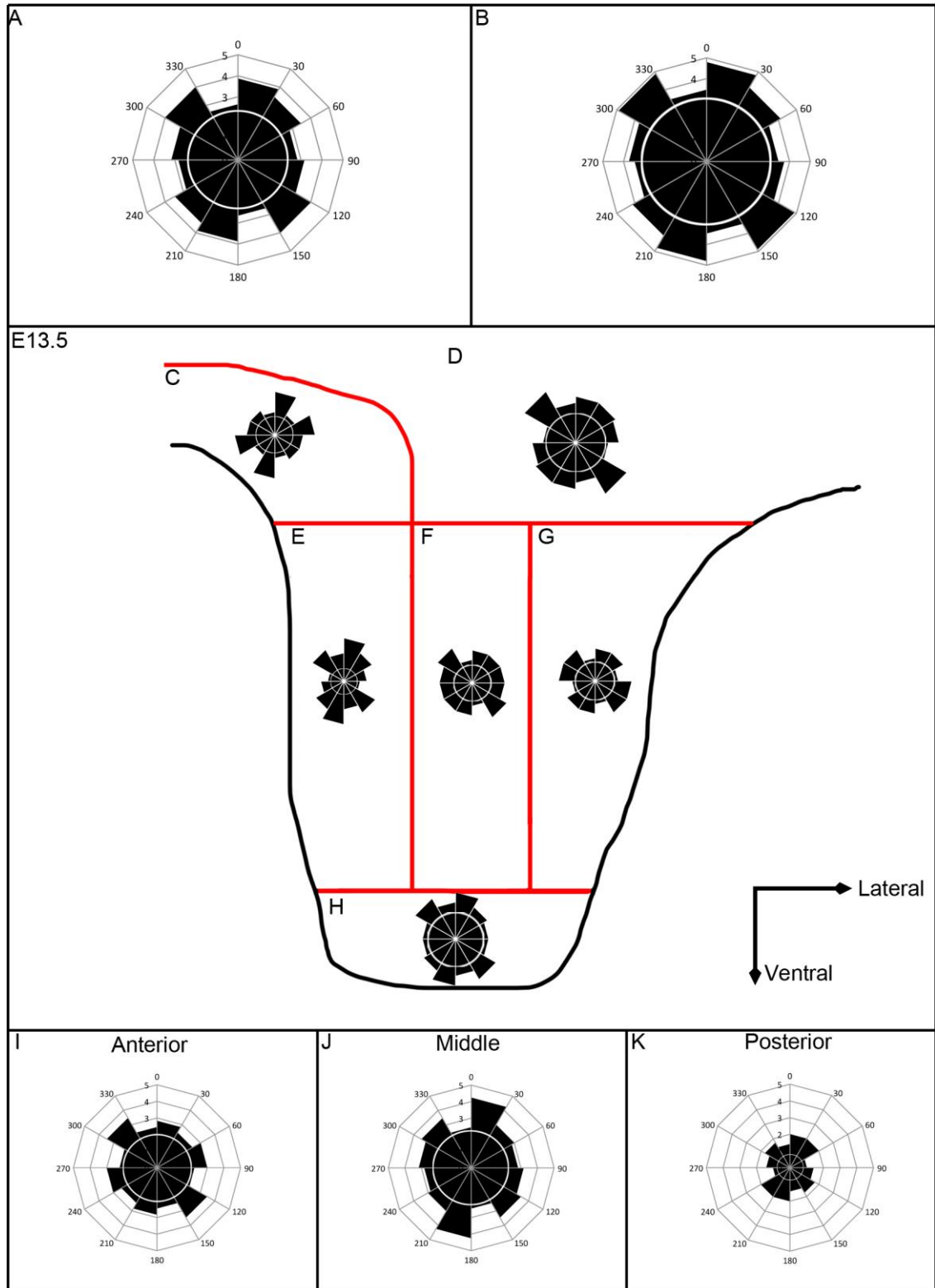


**Figure 6.6 Rose plots summarising mitotic spindle angles at E13.5** A) Distribution of mitotic spindle angles in the palatal outgrowth B-G) Distribution of mitotic spindle angles in cells across different regions of the palate B) Shoulder region C) Mesenchyme adjacent to the palatal outgrowth D) Prospective nasal third E) Middle third F) Prospective oral third G) Tip H) Anterior I) Mid-palate J) Posterior. The white circle represents a uniform distribution. The 180° point is towards the distal tip of the palate.

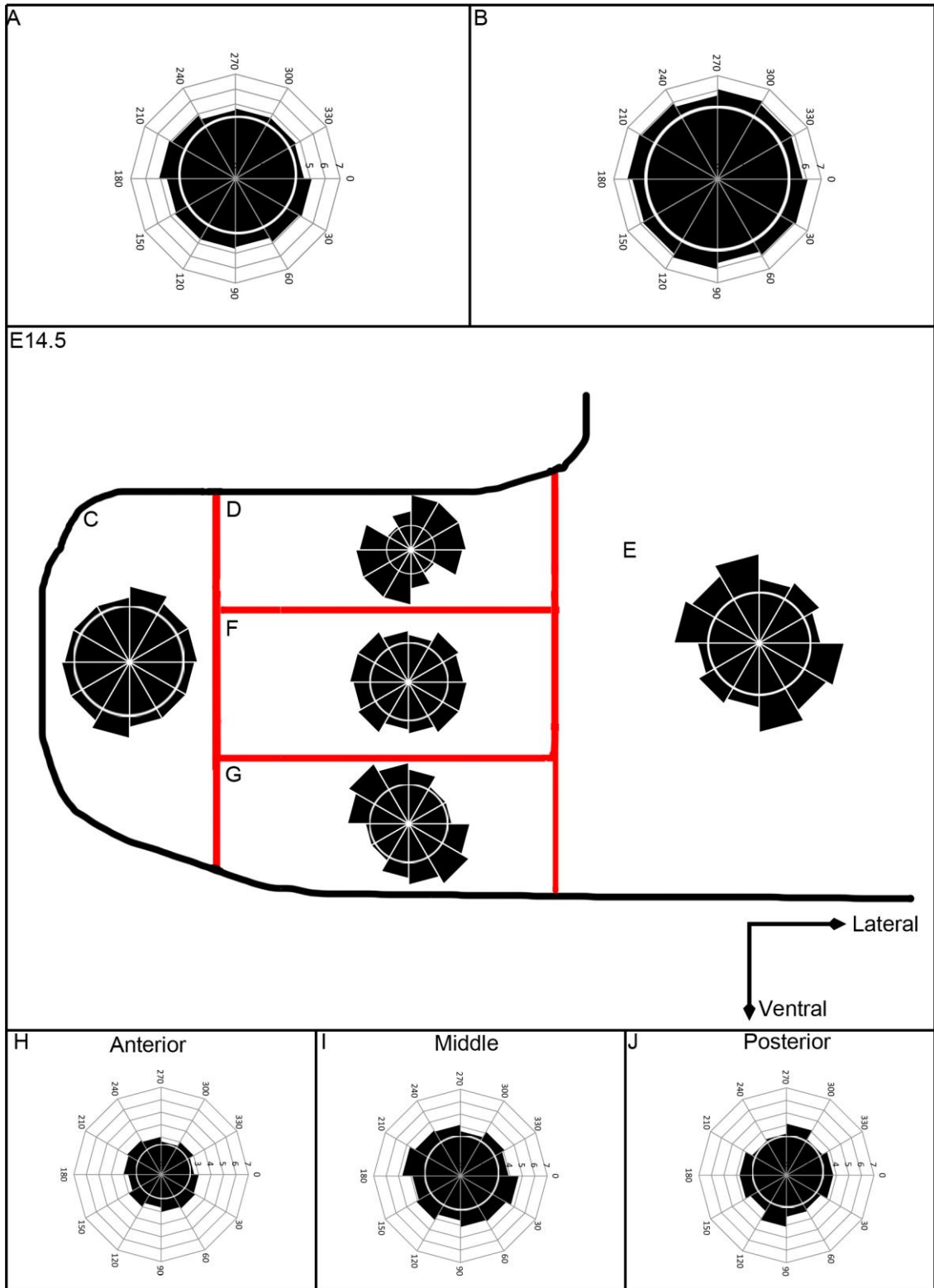


**Figure 6.7 Rose plots summarising mitotic spindle angles at E14.5** A) Distribution of spindles in the palatal outgrowth minus the tip region B) Distribution of mitotic spindle angles in the palatal outgrowth C-G) Distribution of mitotic spindle angles in cells different regions of the palate C) Tip D) Nasal third E) Mesenchyme adjacent to the palatal outgrowth F) Middle third G) Oral third H) Anterior I) Mid-palate J) Posterior. The white circle represents a uniform distribution. The 180° point is towards the distal tip of the palate. that overall in the palatal outgrowth more spindles were orientated along the dorsal

ventral axis (34%) compared to the mediolateral axis (25%) (Fig. 6.6B).

At E13.5 the palatal outgrowth showed differing distributions across its mediolateral axis. Along the prospective nasal side 45% of spindles were orientated along the proximodistal axis (Fig. 6.6G) with only 13% in the mediolateral axis and an average angle on the rose plot of 29° and 209°. The prospective oral side and the middle of the palate showed a bias that is ninety degrees different to the prospective nasal side (Fig. 6.6 E & F). In these regions the average angle was 120° and 300°, and 32% of spindles were orientated along the mediolateral axis and only 26% were orientated along the dorsoventral axis in total.

The distribution of mitotic angles in the tip region of the palate was not significantly different from the rest of the palate. The average angle in this region was 164° and 344°, a proximodistal direction. There were also no significant differences in the distributions along the palate's anteroposterior axis. The rose plots appeared to show that the distributions in the mid- and posterior palate were fairly similar (Fig. 6.6J & K).

### **6.3.1.3 Orientated cell divisions post-elevation, E14.5**

At E14.5 the palatal shelves were growing towards the midline and, particularly in the mid-palate, were touching the palatal shelf opposite, but the epithelial seam was still intact. A uniform distribution could not be rejected for the orientation of mitotic events within the palatal outgrowth at E14.5. Both the oral and nasal sides had a distribution that is largely orientated along the proximodistal axis, although with spindles tending to tilt in towards the medial edge as shown (Fig. 6.7D & G). The cells in the middle third, between these two regions, displayed a more uniform distribution (Fig. 6.7F).

At the tip of the palate at E14.5 the distribution appeared to be uniform and the rose plot indicated a slight oronasal excess (Fig. 6.7C). When the palatal outgrowth was taken as a whole there was no bias in the distribution but this was partly due to cells on the oral and nasal sides having perpendicular orientations and effectively "cancelling" each other out and producing a rose plot that looked uniform. This demonstrates that it is worthwhile breaking the palate up into different regions, because otherwise patterns might be missed. The anterior, mid- and posterior palate did not vary significantly from each other and their distribution did not differ from a

uniform distribution, but this again could be due to regions within the palate having perpendicular distributions (Fig. 6.7H-J).

## **6.4 Orientated cell division: Discussion**

### **6.4.1 Orientated cell divisions assay discussion**

Measuring the spindle angles was very time consuming and ideally in the future this method could be automated. The biggest hurdle to get over in the automating process is how the computer identifies which dots of tubulin stain go with which dot of DAPI, as discussed in Section 4.4.1. This would require a very strong membrane stain to ensure the computer could correctly threshold the membrane of each cell and then only consider the staining inside. It will take a long time for a computer to do this process as it has to handle a 3D volume, but it would not be hands on and could potentially be run over night.

It is particularly vital to remove as much background noise as possible from the images, particularly in the channel with the gamma tubulin stain because the computer would be trying to identify small spots of staining. In the proliferation analysis small spots could be removed as noise by the computer using a radius threshold. This would not be possible when trying to identify the tubulin stain, but higher quality confocal images take longer to acquire so sampling could become a very important method to save time and reduce confocal costs. This project identified many regional patterns in the development of the palate and if the sampling became too sparse these might be missed. Another method would be to use an anti-alpha tubulin antibody, which would stain a larger structure with a distinctive shape.

This analysis of OCD did not often vary from a uniform distribution or from distributions across the palate. This could have been because variations did not exist or because the number of spindles measured was not high enough. As the palate developed it increased in size, but the amount of proliferation decreased so the number of spindles present, judging by the PH-3 staining, was fairly constant. Therefore to get better data more mice need to be sampled or more images from each sample taken. Ideally measurements only want to be taken from cells in anaphase, because the orientation of the spindle can change, as the centrioles can tumble, between metaphase and

anaphase but this reduces the number of spindles per sample even more (Adams, 1996). It is also difficult to know the difference between having no trend because one does not exist and having no trend because the n number is not large enough.

#### **6.4.2 Orientated cell divisions in palate development**

The stages studied here only showed biases in cell division orientation that were weak or absent. This suggests that OCD did not play a major role in the elongation of the palate. It is also likely that the number of spindles measured was not high enough to show any subtle contribution.

Regardless of what this data showed spindle orientation could be a passive response to force, or independent regulators of cell shape rather than a driver of division orientation or directional growth. This is due to the tendency of a cell to divide along its long axis.

The distribution of spindle orientations during early palate development is possibly showing no apparent bias because the palate is growing and expanding at such a rate that the new cells are required everywhere. If there are other forces acting within the palate, causing it to both elongate and prepare for elevation, then there might not be a common long axis forming for the cells to divide along. Instead each cell would react to any forces that might be occurring in its immediate proximity.

The distribution with the strongest bias from this dataset occurred after palatal shelf elevation, when the level of proliferation has dropped significantly, in the mesenchyme on the nasal side of the palate. It is orientated along the proximodistal axis, with a slight medial tilt and there is a similar, but slightly weaker, bias on the oral side. The palate is elongating towards the midline at this stage but it is not possible to know whether this is a significant finding without more spindles being measured. Even then the bias could be a result of other behaviours influencing the orientation of the cell.

It has recently been shown that there is a *Wnt5a* gradient (Chen et al., 2008) in the palate and this might be contributing to cell migration patterns. Disruption of *Wnt5a* has been shown to disrupt the orientation of cell divisions in both the limb (Wyngaarden et al., 2010) and zebrafish gastrulation (Concha and Adams, 1998).



This means the signalling factors required for OCD to be contributing to growth via the PCP pathway are present, but there is no matching distribution in the OCD.

Overall the morphogenesis of the palate seems to rely on contributions from several different mechanisms but the orientation of cell divisions seems to have a very small role. It is still possible that a cleft palate might occur if something disrupted any control the palate has over the orientation of divisions.

## **7.0 Internuclear Spacing**

### **7.1 Introduction to internuclear spacing, cell spacing and cell shape**

To look at changes in cell density the internuclear distance was measured. When changes are seen in this it could be due to changes in the cell shape or size, alternatively it could be due to changes in the amount or composition of the ECM surrounding the mesenchymal cells. Possible roles these factors play during development are introduced below but although a connection between internuclear spacing and these behaviours is discussed it cannot be claimed.

#### **7.1.1 Cell density changes in the palate**

During development the distribution of the cells within the palate is not always uniform. Identifying spatial and temporal patterns in cell density could help uncover mechanisms behind morphogenesis. The cell could be using the packing information as a feedback signal, potentially to inform it whether to proliferate, realign with respect to other cells or to alter levels of extracellular matrix secretions. Cell density could directly contribute to elongation. If the cells spread out more then the tissue will take up more space. Changes in cell density could be involved in producing the intrinsic forces required for elevation.

Previous palatal studies have observed changes in cell density just prior to shelf elevation, but they did not focus on or quantify it (Ferguson, 1977; Sweney and Shapiro, 1970). That is except for one study in the 1980s, which created a short time series of changes in cell density around palatal shelf elevation (Brinkley and Bookstein, 1986). Smoothed spatial averaging was used to visualise trends across the palate and to make a mixture of in vivo and in vitro observations. Smoothed spatial averaging involved placing a grid on top of the image of the palate and counting the total number of cells in each  $600 \mu\text{m}^2$  box and using linear interpolations between adjacent box centres to create a contour map (Brinkley and Bookstein, 1986). The method tried to take into account every single cell, but the grid system struggled with the edges of the palate and different regions had to be weighted to try and overcome this. The algorithm used the notion of blurring to overcome sources of error and the

matrix relies on a “moderately centre-loaded” weighting field. The final display of grey dots (Fig. 7.1) can be tricky to decipher exact changes and the contour lines can be misleading as they were smoothed between the centre points of the boxes.

Brinkley and Bookstein focussed on changes around the elevation process and found that cell density did vary across the palate and in some places this was separate from a change in cell size or proliferation. Embryos were removed at different stages prior to elevation, some were fixed and measured straight away and others were suspended in culture for 6 or 12 hours. The initial or in vivo datasets are shown in figure 7.1. Prior to elevation, both in vivo and in vitro, Brinkley and Bookstein observed an increase in cell density towards the tip and prospective oral edge of the palate. They also found transient increases in cell density in the medial-nasal region post-elevation but overall cell density was lower post-elevation (Brinkley and Bookstein, 1986). The contour maps from their culture system vary from the in vivo time course. Some palates elevated earlier than expected, but as they had already removed the tongue, an extrinsic factor affecting elevation timing this is not surprising. It illustrates that caution is needed when interpreting cellular behaviours in a culture system.

### **7.1.2 Cell density changes that cause cleft palate**

There is a potential link between cell density and cell proliferation: rapid proliferation would be expected to increase local cell density. Changes in cell density are often attributed to changes in cell proliferation but the link between these two and morphogenesis is often unclear. An example in the palate is the effect of treatment of pregnant mice with triamcinolone acetonide (TAC). This drug inhibits RNA synthesis and proliferation, also decreases mesenchymal cell density and results in a cleft palate (Furukawa et al., 2004). It is difficult to tell whether the failure in elevation is due to not enough cells or the wrong density of cells. Given that palate elevation is sometimes attributed to increases in cell spacing (see below), the reduced cell density might be regarded as partly compensating for reduced cell number.

### **7.1.3 Density-dependent growth in the developing chick limb and face**

Work in the limb possibly indicated that changes in cell density could have a role in development by providing feedback as to when the next stage of development should

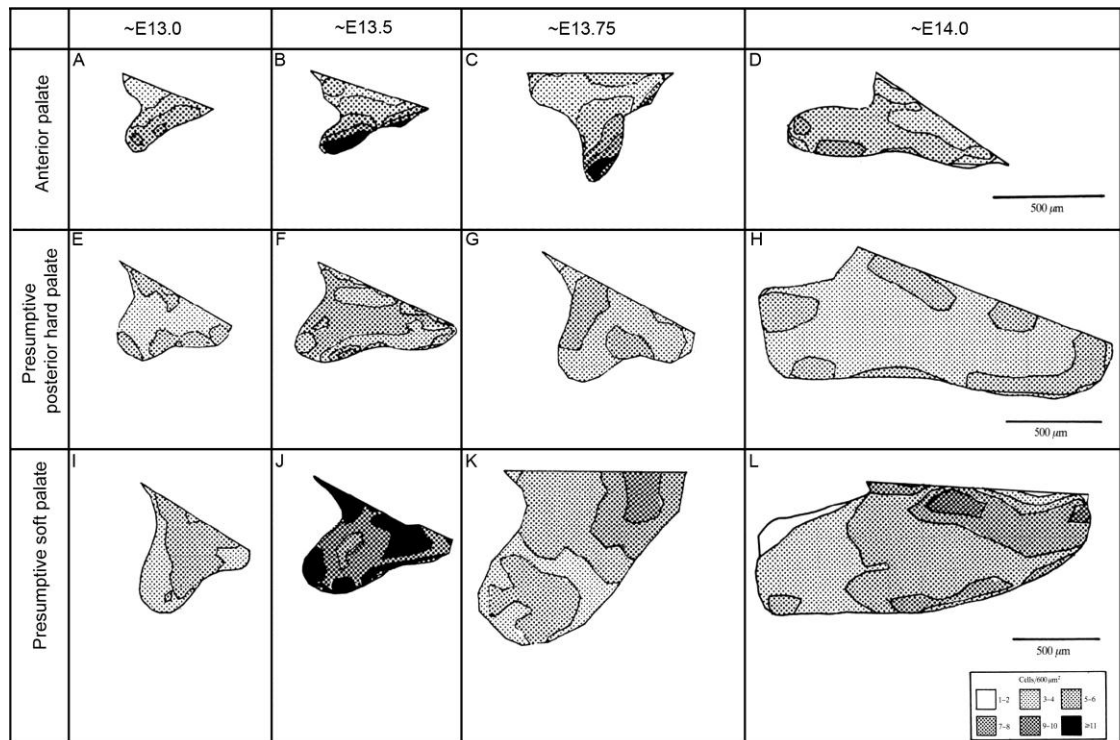


**Figure 7.1 Changes in cell spacing around palate elevation** A-D) Cell spacing in the anterior palate E-H) Cell spacing in the presumptive hard palate I-J) Cell spacing in the presumptive soft palate. Adapted from Brinkley & Bookstein, occur. The density-dependent control of cell division hypothesis (Dennis, 1977) was developed in the 1970s and states that a short-term increase in cell density will result in a decrease in cell proliferation (Summerbell and Wolpert, 1972). This correlation was investigated in the context of cell density being a possible regulator of early of limb bud outgrowth.

After removing the AER of the developing chick wing-bud a decrease in outgrowth and a loss of the distal parts was seen. Cells in the limb bud are normally more tightly packed at the proximal end, which steadily increases in cell density over time whereas the more distal end has lower density, which remains constant or becomes even less dense. In a wing-bud with its AER removed the proximal end behaved normally, but the distal end acted more like the proximal one and increased its cell density (Dennis, 1977; Galloway & Tabin, 2008); Galloway & Tabin, 2008). It has been suggested that this increase in density is due to the contractions around the wound-edge, causing the overall tissue size to decrease. The mitotic index fell at the distal end of the operated wing-bud; this change was first seen after the change in cell density. The ectoderm re-grows after 12 hours and by 24 hours the cell density returns to normal, after which the level of proliferation also returns to normal. The operated wing-bud will go on to develop into a normal adult limb with just the distal parts missing (Saunders, 1948).

This lag time in the effect on proliferation could be due to it being regulated by cell density or it could be due to changes in cell density happening to appear more quickly whilst unrelated changes in cell proliferation take longer to show.

A similar pattern of high density and low proliferation was shown along the limb's smaller dorsoventral axis (Fig. 7.2). It is thought unlikely that diffusible markers can control such a distinct difference over such a small distance, building the case for density-controlled proliferation. This density-dependent control identified in the limb led to investigations of other parts of the developing embryo looking for a similar mechanism.

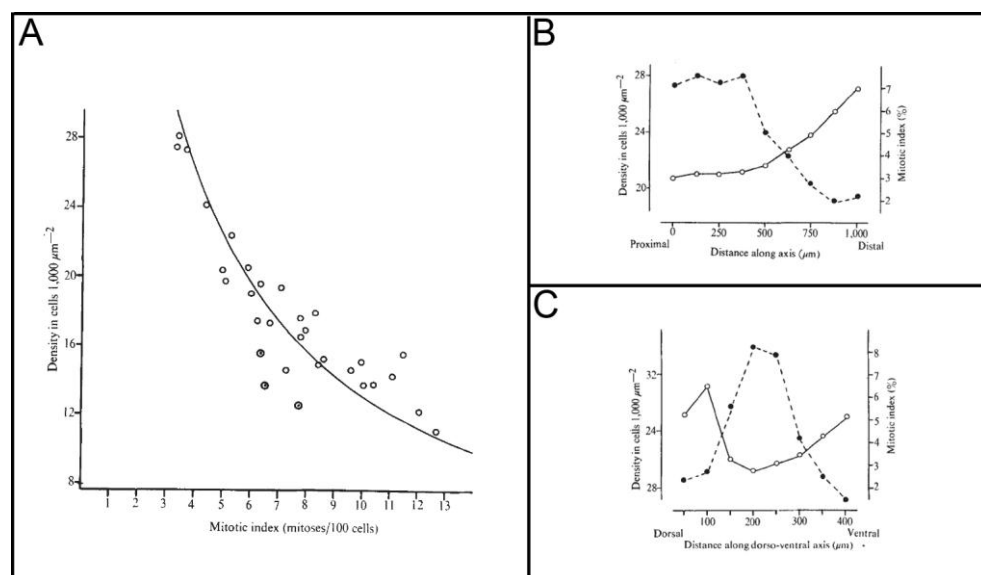


**Figure 7.2 Cell spacing changes during limb development** A) Relationship between cell density and mitotic index B) Differences in cell density along the proximodistal axis of the limb bud C) Differences in cell density along the dorsoventral axis of the limb. Adapted from Summerbell & Wolpert, 1972.

Cell density in relation to growth has also been examined in the chick face, specifically in the maxilla (Minkoff and Kuntz, 1978). The maxillary process in early chick facial development was found to have higher proliferation than the tissue around it and it declined at a slower rate throughout development. The maxillary process also had a fairly high cell density, which remained constant with only a slight increase over time, but not enough for density-dependent control of proliferation to explain the drop in proliferation over the course of chick facial development (Minkoff and Kuntz, 1978).

#### **7.1.4 Investigating cell density in a hamster's palate**

A correlation between cell density, cell proliferation and palate elevation was investigated in the hamster's palate. The aim was to see if a critical number of cells were required before elevation could occur or if a change in cell density had an impact on the level of proliferation (Shah et al., 1989). During the initial development both cell number and shelf area were increasing, but in the 24 hours leading up to elevation these remained constant. The study did not take into account any regional changes in cell density. It compared normal palatal shelves to those treated with 5-fluorouracil (5FU), which interferes with RNA and protein synthesis and damages the cells, rather than interfering with cell proliferation directly, resulting in a decrease in cell number. Elevation did not occur in the 5FU-treated palates until the cell density reached the level normally seen 24 hours before elevation. Although the 5FU treatment could also be affecting ECM formation, again demonstrating that caution is needed when interrupting cell density data. There was no evidence of a correlation between cell density and cell proliferation in this study (Shah et al., 1989).

#### **7.1.5 Cell shape and morphogenesis**

Although there is considerable extracellular matrix and thus cell-shape-independent spacing in palate mesenchyme, quite obviously cell shape (which for this discussion includes size) is a major contributor to tissue bulk and therefore tissue growth. In general, a cell's shape is a result of its composition and physical properties as well as internal and external forces acting upon the cell. Therefore changes could be a result of internal signalling or external interactions. Changes in cell shape under internal control are most likely to be a result of active reorganisation of the cell's cytoskeleton or changes in osmotic pressure; a previously explained example is the contraction of the rear end of the cell during migration. Whereas external influences on the cell's shape are normally due to adhesions with its environment, this could be between cells or between cells and the ECM. In cases where cell shape change contributes to overall morphogenesis the changes are co-ordinated across hundreds of cells so the system must be regulated with feedback mechanisms for both mechanical properties and protein translation (Paluch and Heisenberg, 2009).

This control needs to be on several levels, from influencing changes in adhesions between cells to how these changes affect the shape of a tissue and how the different

tissues interact to regulate morphogenesis across the entire embryo (Barone and Heisenberg, 2012). Different types and strengths of adhesions between cells in the zebrafish germband (Fig. 7.3A) are thought to control and maintain the different layers. Lots of tight adhesions, often through cadherins, will increase cortical tension and change the shape of the cell (Lecuit and Lenne, 2007) due to an actin and myosin network being created in the zone of contact. This can be seen across a sheet of cells such as an apical section of *Drosophila* (Fig. 7.3C), where most cells are hexagonal or pentagonal. As well as cortical tensions acting on individual cells, the entire tissue is affected by surface tension. Isolated cells are often spherical to minimise surface area but change shape when brought together (Fig. 7.3D).

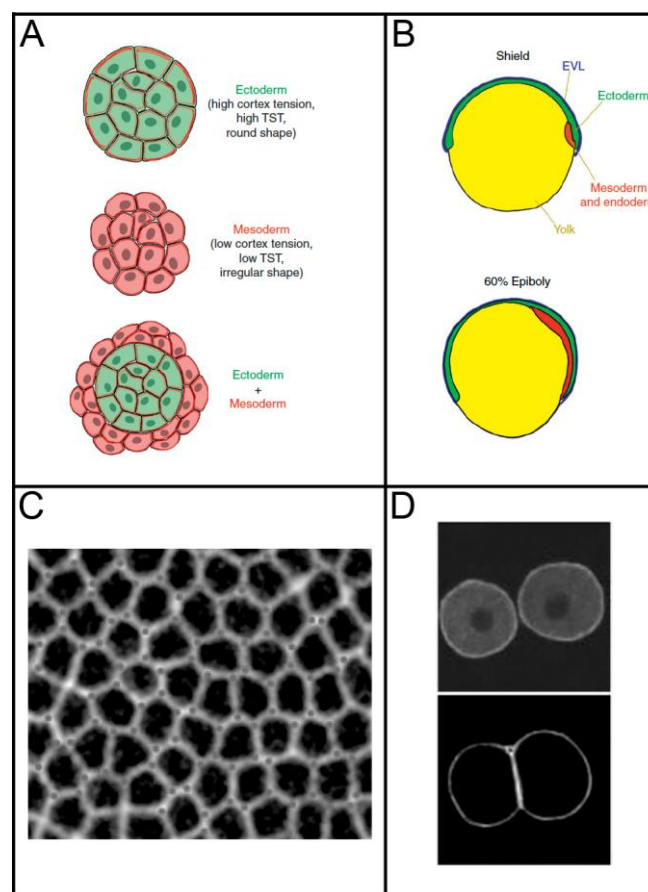


**Figure 7.3 Changes in cell shape change during development** A) Different types and strengths of adhesions help to maintain the different layers B) The formation of germ layers during gastrulation is controlled by the interactions between tissues with different cortical and adhesive properties. A & B adapted from Barone & Heisenberg, 2012 C) Cell-cell contact changes the shape of cells. Cells in an epithelium with a polygonal shape D) These mouse embryonic cells are spherical as single cells but have a different shape when adhered to each other. C & D adapted from Lecuit & Lenne, 2007.

Cell shape can be important in deciding cell fates, shown in human mesenchymal stem cells (McBeath et al., 2004): allowing or preventing cells to spread or not in cell culture resulted in switching cell fate between adipocytes or osteoblasts. Cell shape could also be involved in controlling which cells proliferate and which ones die, this could be occurring through tension dependent changes in the actin cytoskeleton (Huang and Ingber, 2000).


#### **7.1.5.1 Changes in cell shape during palate development**

Changes in cell shape have been observed during palate elevation in three different regions (Babiarz et al., 1979). The process of elevation was monitored by culturing embryo heads with the tongues removed and scoring the amount of elevation after 2 and 4 hours, between vertical, 45 degrees and horizontal (Babiarz et al., 1979). Along the prospective oral side of the tongue prior to elevation the cells were seen to be elongated perpendicular to the epithelium but after orientation to round up (Fig. 7.4). Other regions display the same shape before and after elevation, but during the process of elevation they assume different shapes. It was suggested that the forces created by the cells' changing shape contribute to the intrinsic forces required to elevate the palate however, it is not clear whether these in fact contribute to palate elevation or are instead a consequence of tissue movement. It is not clear how the analysis accounted for differing cell shapes along the anteroposterior axis and the changes were only seen in the mesenchymal cells underlying the epithelium not in the core of the palatal shelf. They could, for example, be a consequence of traction from movements occurring in the developing epithelium rather than force-generating behaviours within the mesenchyme. It is unclear how they accounted for all the cells in each region of interest or how they decided what the average cell shape was, as the images included in the paper look a lot more noisy than their diagrams show.

#### **7.1.6 Extracellular matrix composition and the palate**

The ECM is a fibrous mesh of mostly glycoproteins and proteoglycans, which is constantly synthesised and degraded during development, promoting sometimes rapid changes in the cellular microenvironment. The ECM is known to increase in volume and composition during palate development (Brinkley & Morris-Wiman, 1987) and this could have an impact on development in several different ways. It could be creating intrinsic forces or acting as a matrix over which cells can migrate. The ECM could be



		PALATE SHELF INDEX				
		Vertical 1	2	3	4	Horizontal 5
Anterior Palate	a. Oral side (Region 3)		N.D.			
	b. Tongue side opposite		N.D.			
	c. Tongue side bend (Pre-Region 2)		N.D.			
Mid-palate	a. Oral side (Region 3)		N.D.			
	b. Tongue side opposite		N.D.			
	c. Tongue side bend (Region 2)		N.D.			
Mid-posterior palate	a. Oral side (Post-Region 3)				N.D.	
	b. Tongue side opposite				N.D.	
	c. Tongue side bend (Region 2)				N.D.	

**Figure 7.4 Cell shape changes during palate development** Different regions of the palate display different cell shapes during palatal shelf elevation. Adapted from Babiarz et al., 1979.

controlling signalling to cells in different regions or preventing signalling via cell-cell contact. If any signalling pathways are influenced by the ECM then any cellular mechanism of morphogenesis could be affected by changes in the ECM (Daley and Yamada, 2013).

The ECM helps to stabilise developing branching structures, such as in the salivary and mammary glands as well as in the developing lungs. These are all branching structures and unless the ECM thickens in the cleft between the branches, no new branches will form and existing branches will regress. In contrast the ECM needs to be thinner at the tips of the branches to allow epithelial expansion (Grobstein and Cohen, 1965).

In the palate, there is a build-up of glycoproteins during development, particularly prior to elevation of the palate (see section 1.2.3.3). This is thought to produce the intrinsic force needed for the palate to elevate. It may also aid elevation indirectly by preventing strong adhesion between cells. TGF- $\beta$  and EGF can both stimulate the production of ECM production by palatal mesenchymal cells (D'Angelo and Greene, 1991; Foreman et al., 1991). Normally the ECM of the palate contains a mixture of collagen types I, III, IV, V, VI and IX, fibronectin, heparan, sulphate proteoglycan, laminin and tenascin (Dixon et al., 1993; Foreman et al., 1991).

To look for a contribution of ECM composition to palatal elevation the components of palatal ECM from mouse and chick were compared (Foreman et al., 1991). This is relevant to understanding elevation as the palatal shelves in birds develop horizontally and do not need to elevate. In fact the composition of the ECM between the two species was found to be very different. The ECM in chick was found to have lower protein content but higher GAG content than mouse, which increased over time in chick but decreased in mouse. In mouse the majority of the GAG content is hyaluronic acid and during development its level peaks just before elevation. In chick chondroitin-6-sulphate makes up the majority of the GAG and there is no peak in hyaluronic acid synthesis. The water content of palate tissue was very different between the species as well. In the mouse it peaked at E14.0, crucially at the same time as palatal shelf elevation, whereas in the chick it rose exponentially throughout development (Foreman et al., 1991). It has also been shown that collagens are important in palate development because inhibition of cross-links results in a cleft palate (Pratt and King, 1972).

There is the potential for the ECM to have many roles during embryonic and more specifically palate development. Its volume and composition have already been shown to change over time. Recent advances include even calculating its material textural properties in avian embryos (Loganathan et al., 2012). Analysis of the physical, mechanical and material properties of ECM will ultimately be essential for thorough understanding of its role in mechanisms of physical growth in general and palate elevation in particular.

## **7.2 Internuclear Spacing: Methods**

Sample collection, staining and imaging were performed as described in sections 2.3-2.6 and the image processing is described in sections 2.7-2.8. The cell density was calculated in R using the DAPI stain and at least three embryos from each stage were analysed. The results are displayed in heat maps where the hot colours highlight more densely packed regions and the cooler colours are more loosely packed ones.

## **7.3 Internuclear Spacing: Results**

### **7.3.1 Changes in cell density in the maxillary process (E9.5-E10.5)**

Observed in sagittal aspect, as the maxillary process developed at E9.5 and E10.5 the cell spacing remained at a constant uniform similar level to the immediately surrounding tissue (Fig. 7.5, circled regions). There were regions of tissue dorsal to the maxillary process where there were local increases in density, while regions towards the back of the head were in general less densely packed.

### **7.3.2 Changes in cell density during the initial palatal outgrowth (E11.5-E13.5)**

The initial palatal outgrowth began to appear at E11.5 and this had very similar packing to the maxillary process it was growing out of (Fig. 7.6). The E11.5 heat maps had more patches of yellow in the maxillary process itself than at E10.5 showing it had generally become more densely packed.

Despite considerable embryo-to-embryo variability, it is clear that by E12.5 the palatal outgrowth had more distinct characteristics in its AP axis with it appearing to have the most tightly packed cells in the anterior region, which is directed more horizontally towards the tongue than the middle and posterior palate (Fig. 7.7A-C). The cell density in the mid- and posterior palate has not varied greatly in the palatal outgrowth since E11.5.

At E13.5 the cell packing no longer appeared as uniform across the palatal outgrowth. The prospective nasal side of the palate was generally slightly less densely packed than the prospective oral side (Fig. 7.8). This was slightly more obvious in the anterior

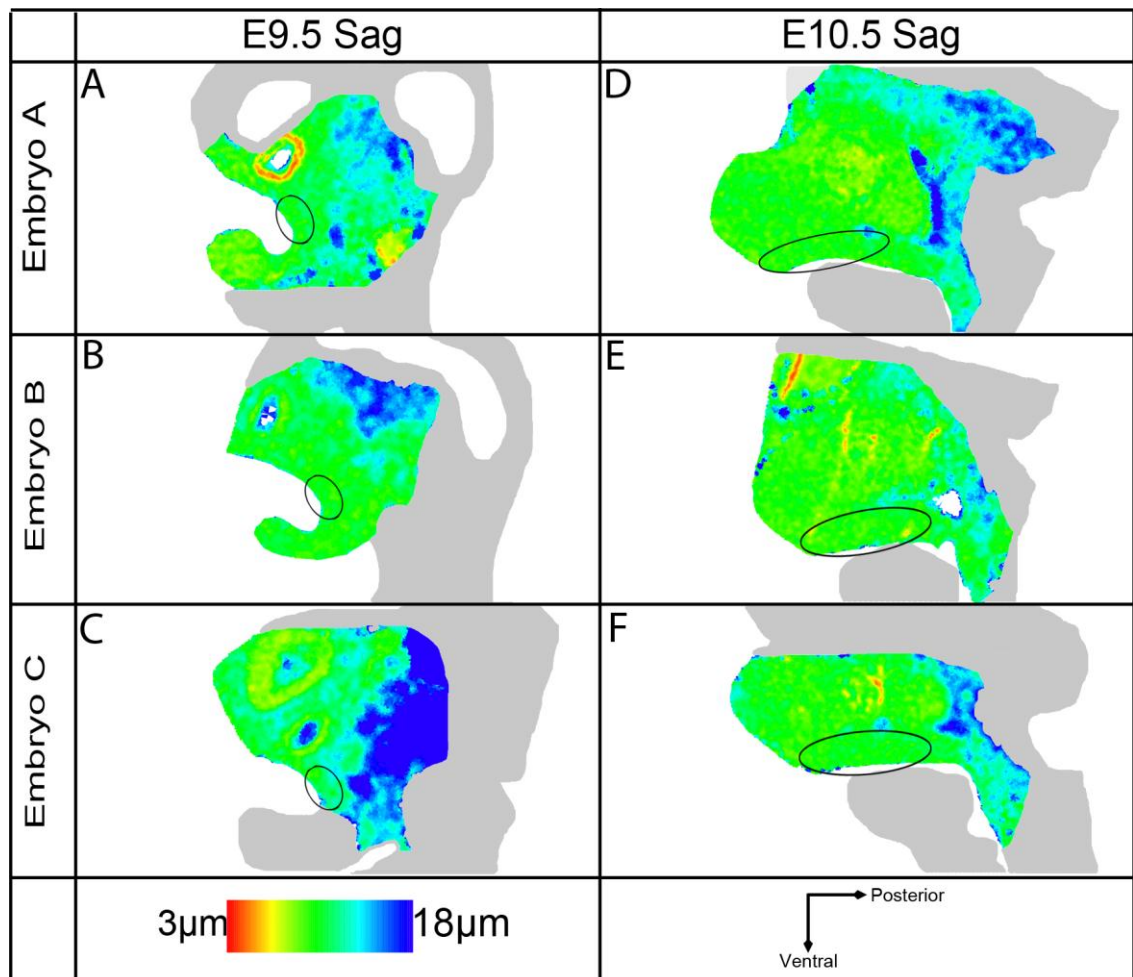


**Figure 7.5 Spacing heat maps of sagittal E9.5 and E10.5 embryo heads** A-C) Heat maps of sagittal sections at E9.5. Each heat map is an average of three individual sections and each of A-C is from a different embryo, from at least two different litters D-F) Heat maps of sagittal sections at E10.5. Each heat map is an average of three individual sections and each of D-F is from a different embryo, from at least two different litters. The approximate location of the maxillary process is circled on each heat map. The grey region on the heat maps represents the rest of the embryo away from the ROI, which was not included in the heat map.

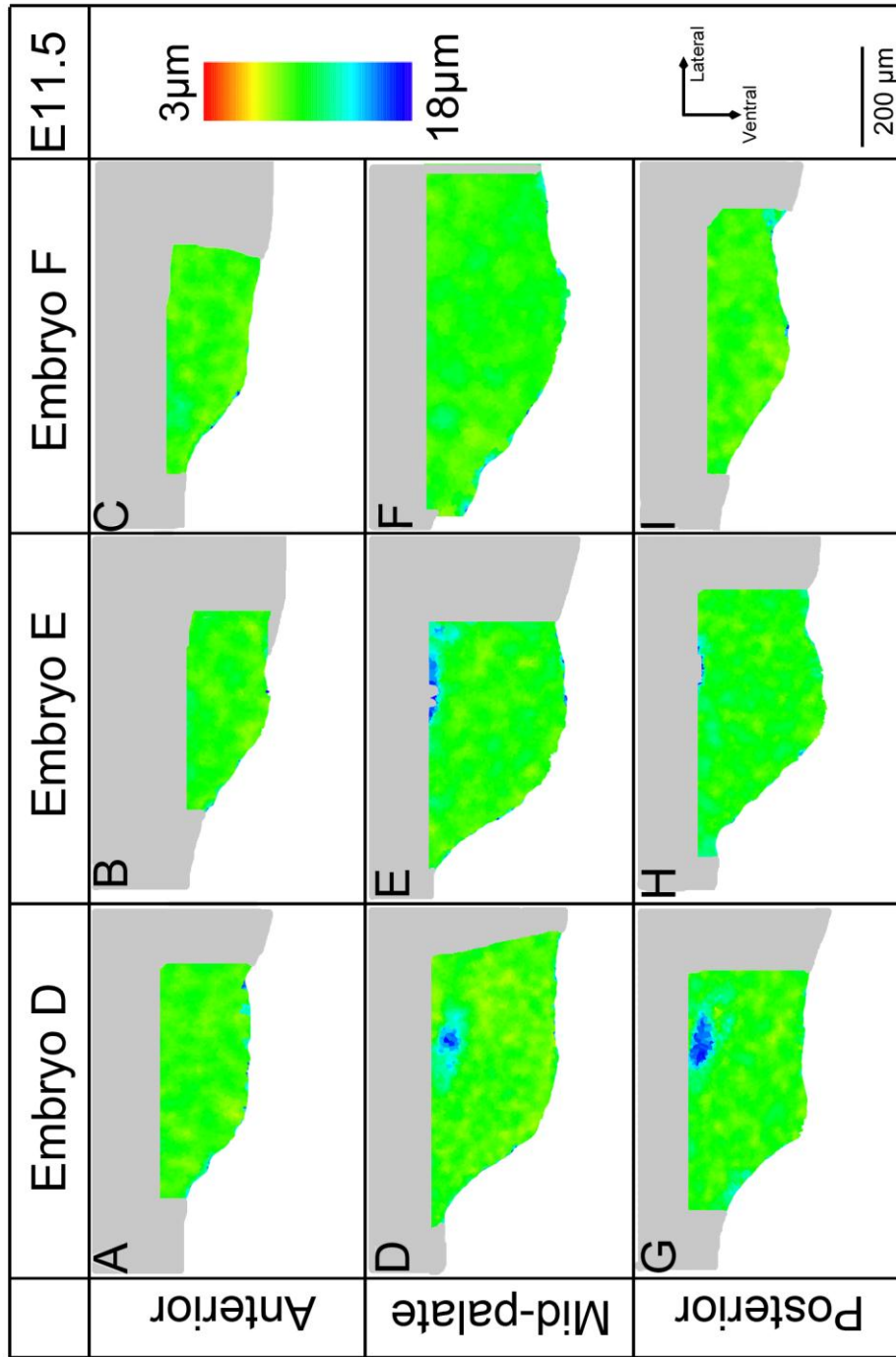


**Figure 7.6 Internuclear spacing heat maps of E11.5 palatal shelves** A-C) Heat maps of the anterior third of the palate D-F) Heat maps of the middle third of the palate G-I) Heat maps of the posterior third of the palate. Each heat map is an average of three individual sections and A, D and G; B, E and H and C, F and I are each from a different embryo, from at least two different litters. Scale bars represent 200  $\mu\text{m}$ . The grey region on the heat maps represents the rest of the embryo away from the ROI, which was not included in the heat map.

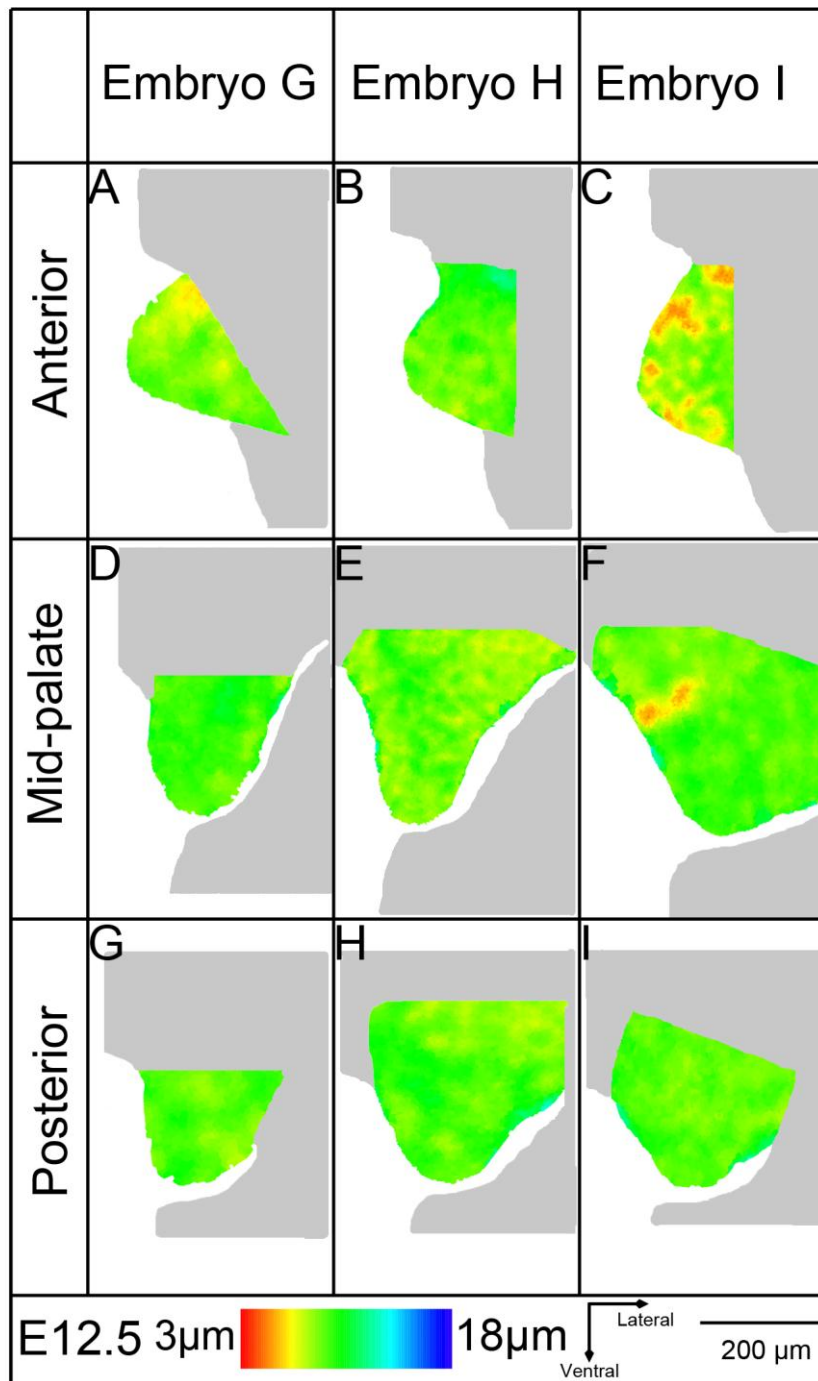


**Figure 7.7 Internuclear spacing heat maps of E12.5 palatal shelves** A-C) Heat maps of the anterior third of the palate D-F) Heat maps of the middle third of the palate G-I) Heat maps of the posterior third of the palate. Each heat map is an average of three individual sections and A, D and G; B, E and H and C, F and I are each from a different embryo, from at least two different litters. Scale bars represent 200  $\mu$ m. The grey region on the heat maps represents the rest of the embryo away from the ROI, which was not included in the heat map.

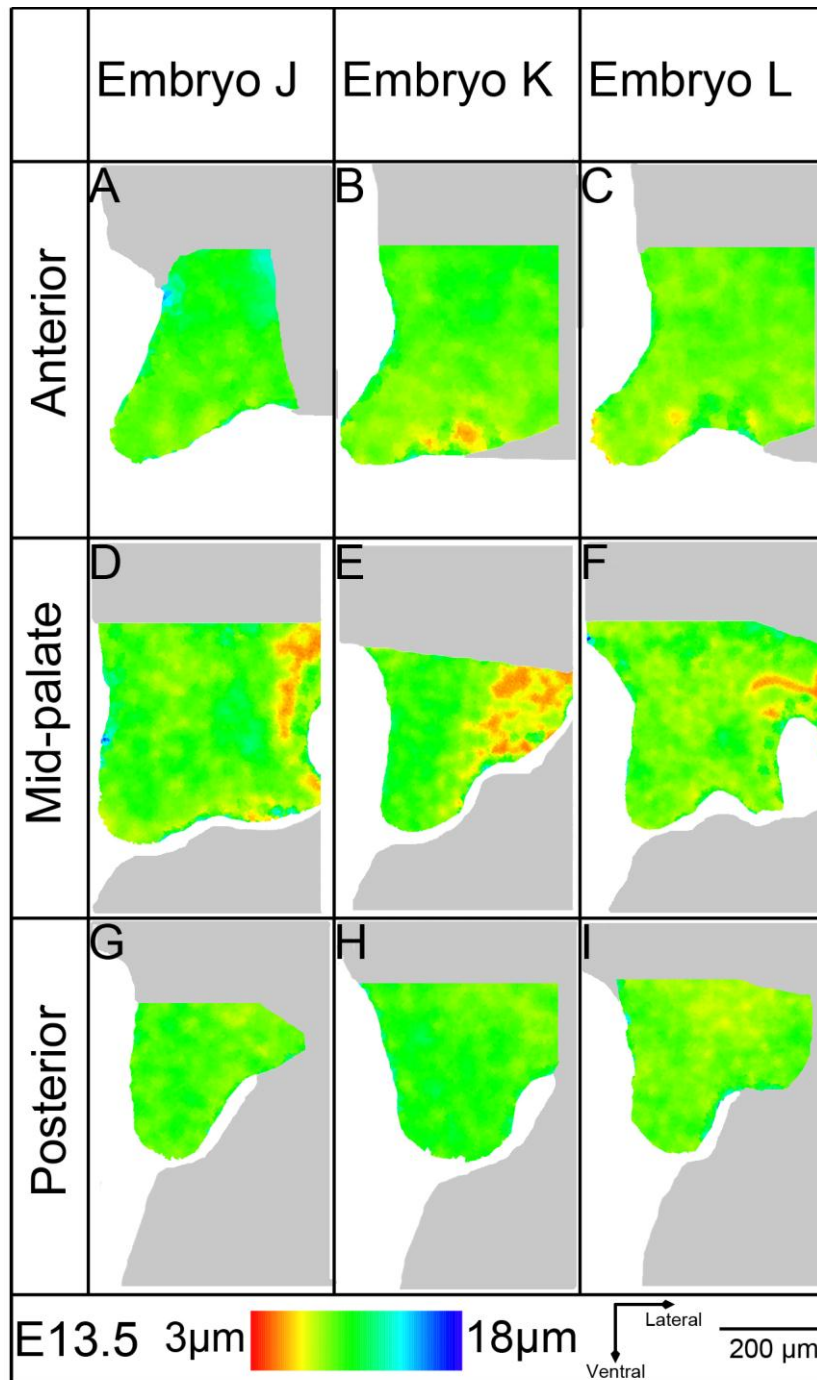


**Figure 7.8 Internuclear spacing heat maps of E13.5 palatal shelves** A-C) Heat maps of the anterior third of the palate. D-F) Heat maps of the middle third of the palate. G-I) Heat maps of the posterior third of the palate. Each heat map is an average of three individual sections and A, D and G; B, E and H and C, F and I are each from a different embryo, from at least two different litters. Scale bars represent 200  $\mu$ m. The grey region on the heat maps represents the rest of the embryo away from the ROI, which was not included in the heat map.

two thirds of the palate. The packing in the posterior third has not changed much since the previous time point. There were regions of more tightly packed cells more laterally, i.e. in the maxilla, towards the developing molar. The shoulder regions, where the proximal end of the palatal outgrowth meet the maxilla, do not show any dramatically varied packing to the rest of the palatal outgrowth.

The palate at E11.5 is fairly symmetrical, when looked at frontally, but by E13.5 the prospective nasal side of the outgrowth, in the mid-palate, has become much longer than the more densely packed prospective oral side.

### **7.3.3 Changes in cell density during post-elevational growth (E14.0-E15.5)**

After the palatal shelves have elevated they have to go through a second growth stage to reach the midline where they come into contact with each other and fuse. This process occurs first in the middle of the palate and then the shelves zip up along the anteroposterior axis. This small but vital movement is not coincident with a peak in proliferation but instead with an increase in cell spacing (Fig. 7.12). At E14.0, immediately after the shelves have elevated but before they are touching, the spacing in the middle third of the palate had increased compared to the anterior and posterior regions. This was conspicuous in a thick layer of mesenchyme running parallel to the oral surface of the palatal shelf (Fig. 7.9D-F, cyan and blue regions). The spacing continued to appear slightly more loosely packed in the mid-palate at E14.5 when the two shelves were touching but the epithelial seam was still completely intact (Fig. 7.10 & 7.12D-F). By E15.5 the shelves were touching along nearly the entire anteroposterior axis and there was evidence of fusion taking place where the epithelial seam had disintegrated, especially in the mid-palate region. The cell spacing at E15.5 had increased slightly in the mid-palate (Fig. 7.11D-F & 7.12H), where no more growth towards the mid-line was needed. In contrast, the spacing in the anterior region had decreased slightly and the shelves here were now touching and starting to fuse (Fig. 7.11A-C & 7.12G). These heat maps again highlight the variation between embryos, in terms of the relative levels of cell packing and the exact point in development that they were at. The posterior palate was also touching and fusing but the spacing has not decreased as much. Either it was a very rapid process that occurred in less than twenty-four hours or there was another process causing the posterior of the palatal shelves to reach the midline (Fig. 7.11G-I & 7.12F & I).



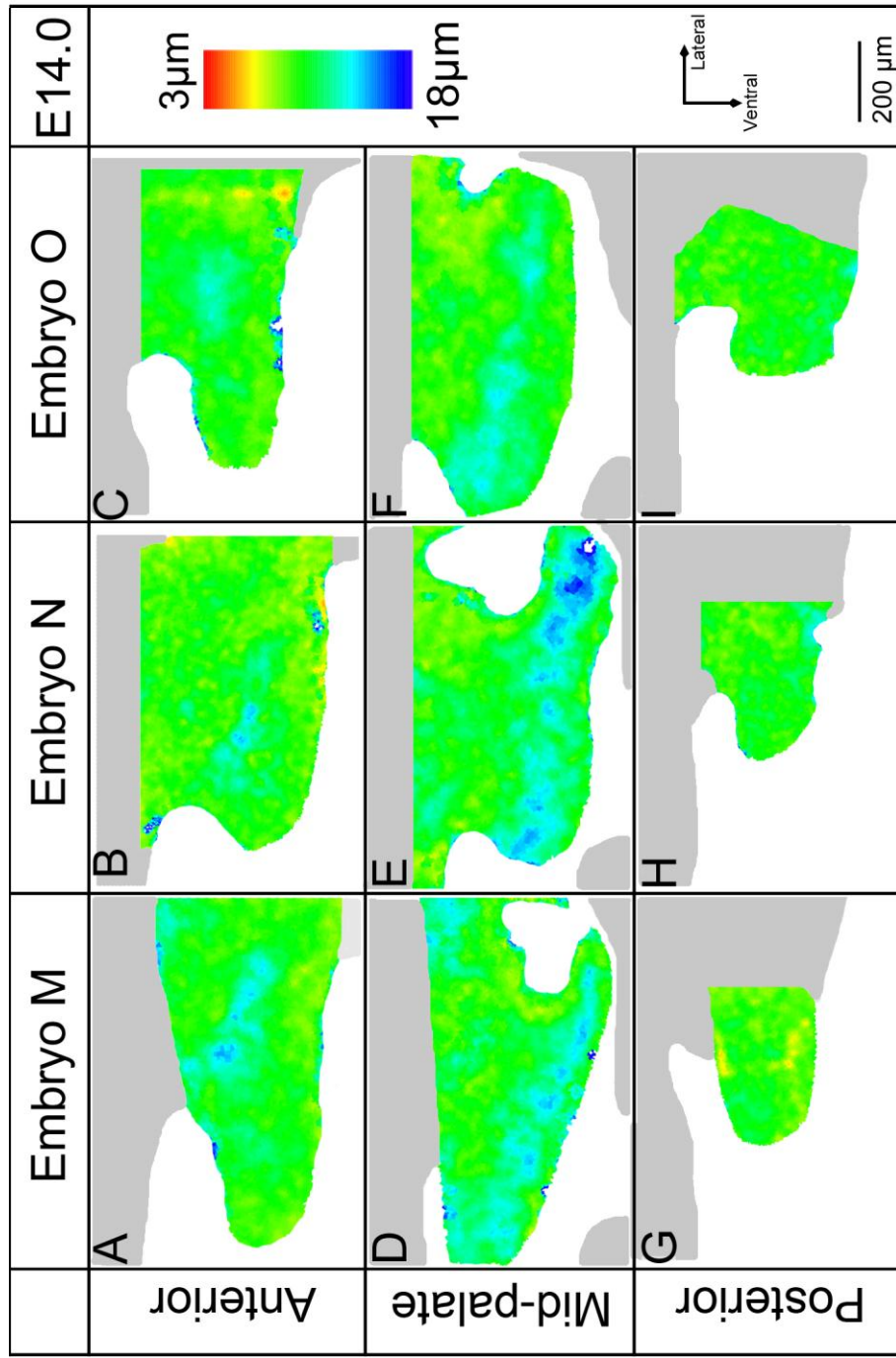


**Figure 7.9 Internuclear spacing heat maps of E14.0 palatal shelves** A-C) Heat maps of the anterior third of the palate D-F) Heat maps of the middle third of the palate G-I) Heat maps of the posterior third of the palate. Each heat map is an average of three individual sections and A, D and G; B, E and H and C, F and I are each from a different embryo, from at least two different litters. Scale bars represent 200 µm. The grey region on the heat maps represents the rest of the embryo away from the ROI, which was not included in the heat map.

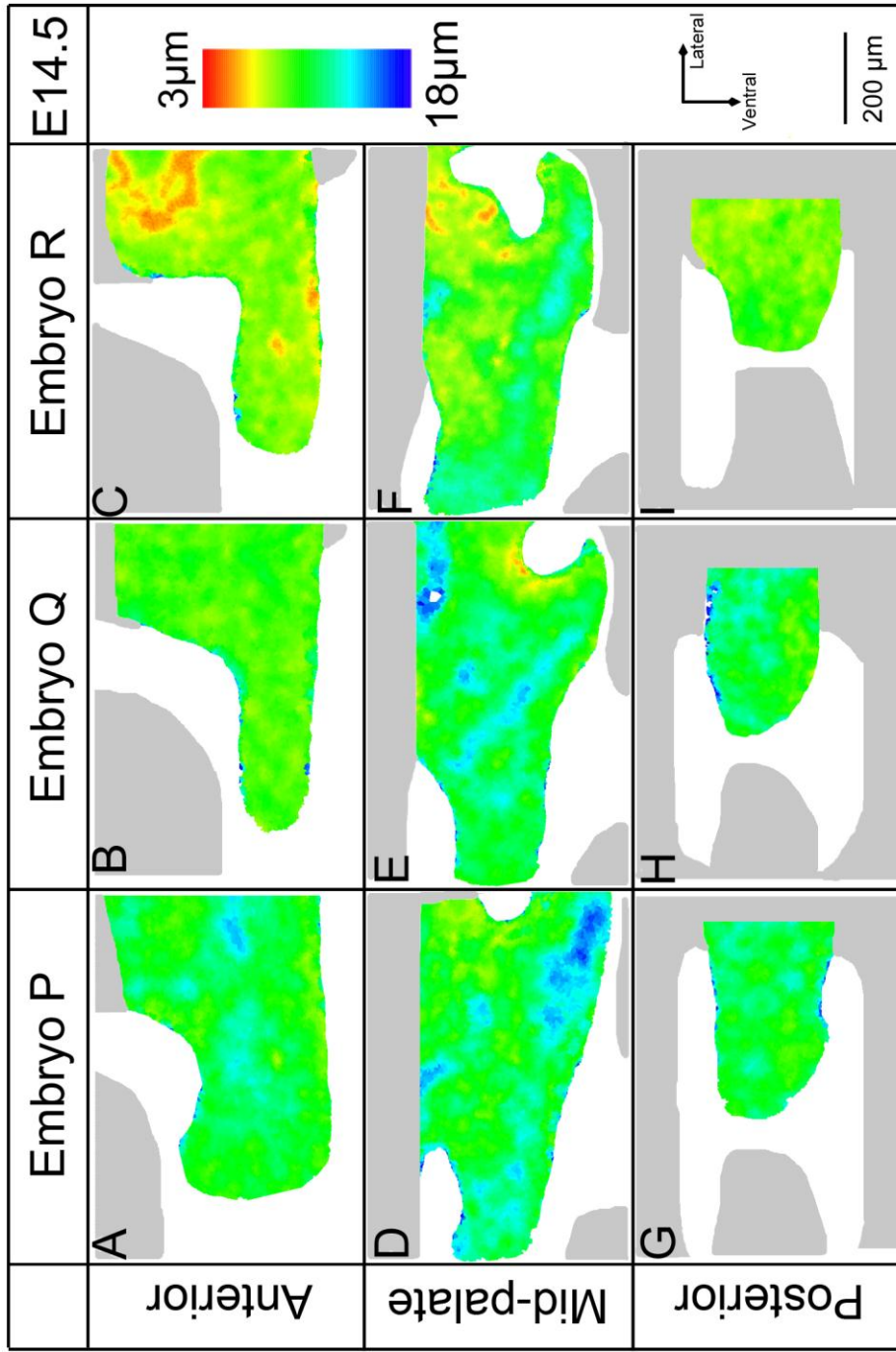


**Figure 7.10 Internuclear spacing heat maps of E14.5 palatal shelves** A-C) Heat maps of the anterior third of the palate D-F) Heat maps of the middle third of the palate G-I) Heat maps of the posterior third of the palate. Each heat map is an average of three individual sections and A, D and G; B, E and H and C, F and I are each from a different embryo, from at least two different litters. Scale bars represent 200 µm. The grey region on the heat maps represents the rest of the embryo away from the ROI, which was not included in the heat map.

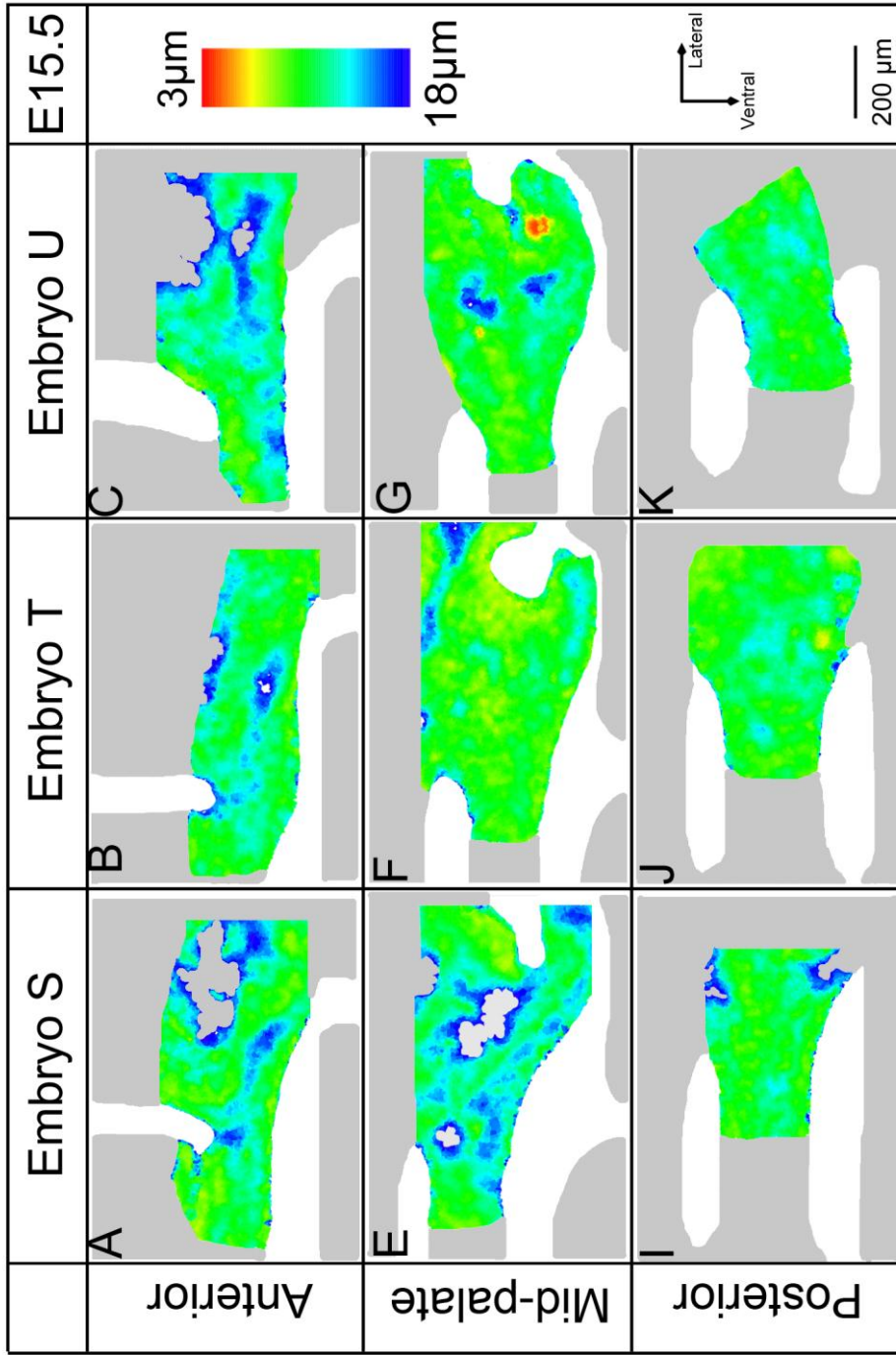


**Figure 7.11 Internuclear spacing heat maps of E15.5 palatal shelves** A-C) Heat maps of the anterior third of the palate D-F) Heat maps of the middle third of the palate G-I) Heat maps of the posterior third of the palate. Each heat map is an average of three individual sections and A, D and G; B, E and H and C, F and I are each from a different embryo, from at least two different litters. Scale bars represent 200  $\mu\text{m}$ . The grey region on the heat maps represents the rest of the embryo away from the ROI, which was not included in the heat map.

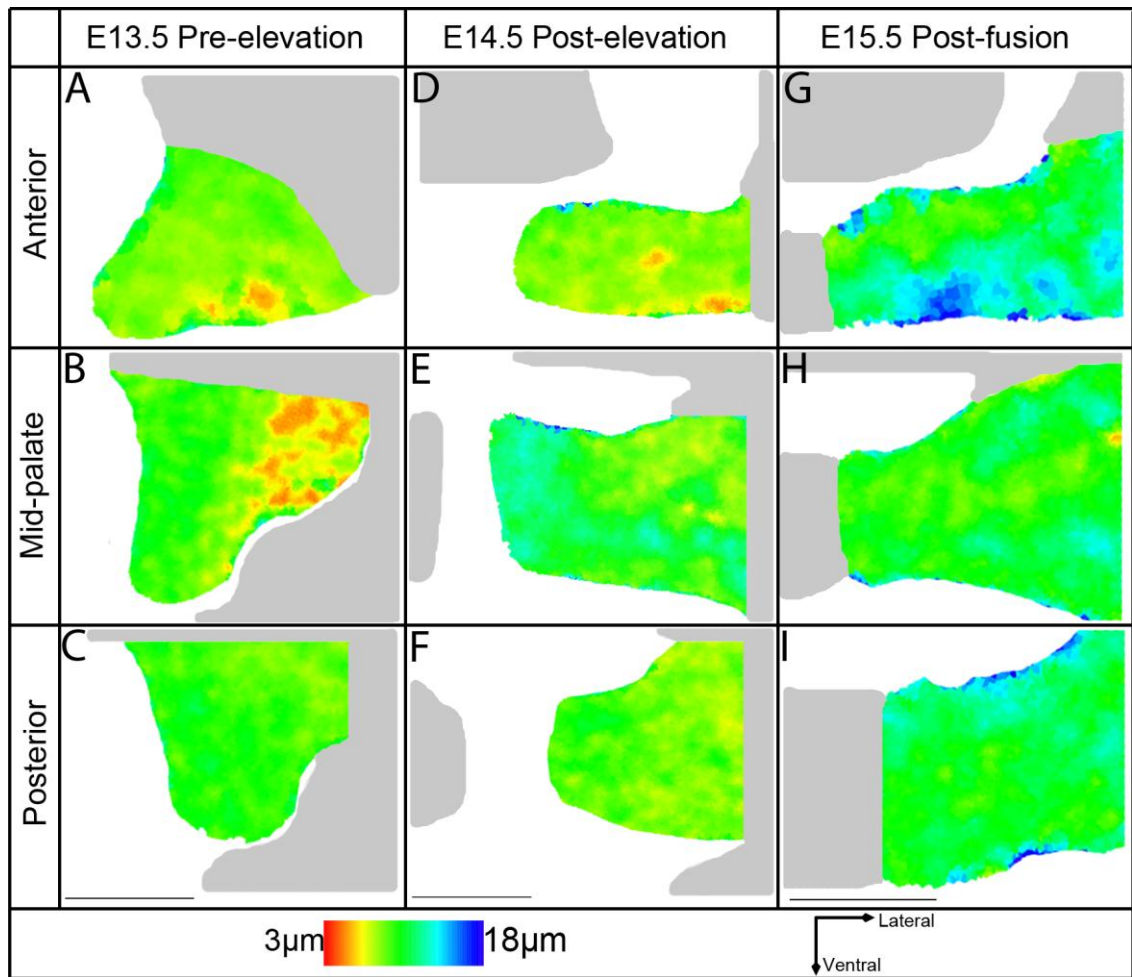


**Figure 7.12 Changes in cell density during post-elevational growth** A-C) Internuclear spacing heat map of the E13.5 palate A) Anterior B) Mid-palate C) Posterior D-F) Internuclear spacing heat map of the E14.5 palate D) Anterior; overall cell spacing is not very different from E13.5 E) Mid-palate; the cell's are more loosely packed and the mid-line growth is nearly complete in this region F) Posterior G-I) Internuclear spacing heat map of the E15.5 palate G) Anterior; the spacing is more loosely packed and the two shelves are now touching H) Mid-palate; palatal fusion has occurred and the spacing has become slightly more densely packed again I) Posterior. Scale bars represent 200  $\mu\text{m}$ . The grey region on the heat maps represents the rest of the embryo away from the ROI, which was not included in the heat map.

#### 7.3.4 Cell spacing changes along the oronasal axis

The rugae form along the oral side of the palatal epithelium and potentially these thickenings of cells are influencing the underlying mesenchyme. The mesenchyme was investigated in sagittal sections (Fig 7.13). On average, at E13.5, there did not appear to be distinct thickenings aligned with the rugae, but the mesenchyme on the ventral side of the anterior palate, where rugae are present, was more tightly packed than the rugae-free posterior palate (Fig 7.13A, anterior region is circled).

It has been suggested that one mechanism of elevation is by the palate remodelling itself rather than flipping up. The posterior palate did not match the spacing patterns of the anterior and mid-palate and it does not have the same epithelial structures present. Therefore it is likely that different mechanisms play a role in the development of the posterior palate. The spacing in the posterior palate remained a lot more constant and at a more slightly more compact level than the more anterior tissue but it is possible that local, very transient, changes contribute to elevation.

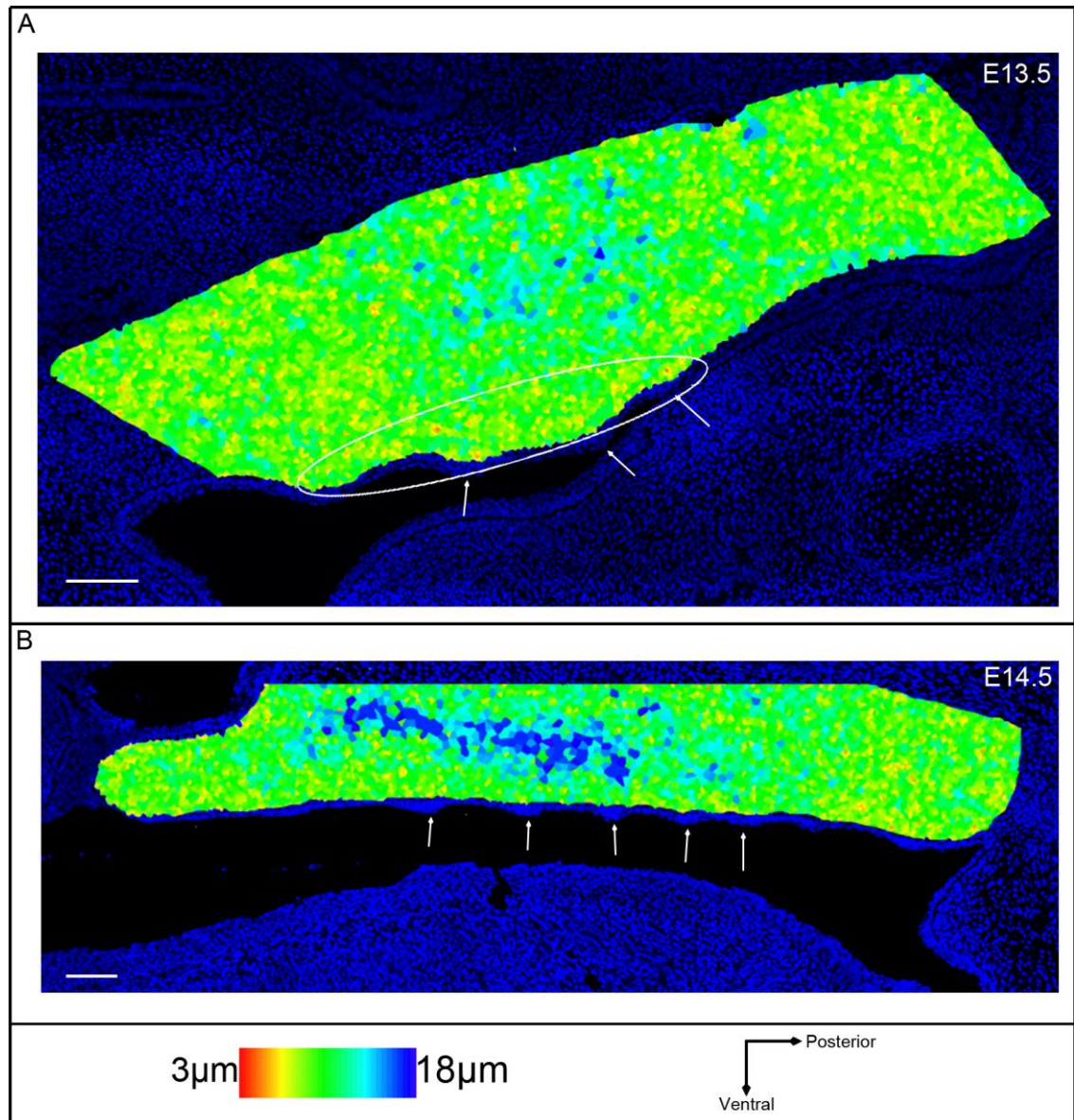


**Figure 7.13 Internuclear spacing heat maps in sagittal sections before and after elevation** A) E13.5 spacing heat map placed on top of a DAPI image of the embryo with the rugae present. White circle highlights the more tightly packed mesenchyme along the ventral side in the anterior of the palate B) E14.5 heat maps and DAPI image. White arrows are pointing at the rugal thickenings. Scale bar represents 200 μm.

## 7.4 Internuclear spacing: Discussion

### 7.4.1 Method used to investigate cell density

A simple DAPI stain is all that is required to create these spacing heat maps so this assay can be easily included while imaging other antibodies. For example here the same images produced cell spacing and cell proliferation data; this saved time and embryos.

Previous work on cell density has simply counted the number of cells in a certain area and calculated the density. Here a more localised method is used, using the distance between a cell and its neighbours. This also allows small changes in cell density to be detected and every cell is included in the calculation. It is also possible to average over more than one set of neighbours if the analyst chooses. This automated method of calculating and displaying cell density copes a lot better with tissues of different shapes and is a lot quicker than having to count cells by hand. The work of Brinkley and Bookstein tried to take into account every single cell, but they ended up having to weight, everything because they used a square grid that could not mould around the edges of the palate. They also used a series of black dots to show the different regions of spacing, but the scale is not particularly clear and requires some time to study, whereas the colours in the heat maps used in this study jump out at you.

The main limitation of the software used is that the values for the average distances between the neighbours remain hidden in R as it does the calculation and outputs a heat map without saving the distance values measured. These values would be useful to produce statistical output such as histograms. It should be possible in the future to extract the average spacing value in each heat map and use these to determine which are statistically significant. It would also be helpful to be able to know the spacing value for different regions within a heat map. Currently attempts to split the image up in R have proved too cumbersome for practical purposes. The long winded, extremely time consuming way would be to open the images and re-crop them in Volocity, create a new table of co-ordinates, input these to R and get it to calculate the average for that region, if a pattern is identified and the analyst wants to see if it is statistically different spacing from another region. Alternatively, once a pattern is identified from the first set of heat maps, the research group might choose to look in further detail at what is causing the change in cell spacing, for example cell size change or changes in ECM.

## 7.4.2 Cell spacing during palate development

Cell spacing remains fairly constant through the early stages of development (i.e. before E13.5) despite the fact that the maxillary process and palate are growing and changing shape rapidly. This means that other processes must be at work to maintain a constant level of spacing. There is potentially a feedback system so that any changes are quickly compensated for, either by changes in proliferation, ECM expansion or changes in cell shape.

There are very few distinctive changes in cell spacing until E13.5, which could mean that this change in spacing that has finally been allowed to happen has a significant role. Strikingly, the same region that has densely packed cells has lower levels of proliferation (compared fig. 4.8 in the chapter 4 with fig. 7.8). Therefore it could be possible that the cell density acts as a feedback mechanism similar to the cell density controlled proliferation proposed in the limb (Saunders, 1948).

The differences in cell packing seen in the anterior two-thirds at E13.5 could be contributing to the palate's flip-up mechanism. Having fewer cells on one side could allow the tissue to bend and flow more whilst the more tightly packed cells could be gathering on one side ready to produce a force that helps the palate flip-up and become straighter over the tongue.

The ECM between the cells could also be playing an important role at this point. The major component of the ECM in an E13.5 palate is hyaluronic acid, which is highly electrostatically charged, and this will provide strength and rigidity to the palate, helping it to elevate above the tongue. Changes in ECM will affect the viscosity of the mesenchyme and if the posterior palate does elevate by remodelling then it will need to be able to flow more than the anterior palate. Hence the posterior palate having more even packing as there is no extra ECM which would cause the cells to space out more. The more even packing may also benefit the remoulding process as the entire section of palate could be doing the same thing, or potentially it is driven by other mechanisms and therefore no change in spacing is seen prior to elevation.

After elevation the palate is described as reaching the midline, firstly in the mid-palate region and then zipping up along the AP axis. The mechanism behind this growth has

never been identified and proliferation is consistently low along the AP axis at this point therefore it is unlikely to be causing the growth. This study has identified an increase in the cell spacing that matches the post-elevational growth towards the midline. Cells become more loosely packed in the mid-palate, where the opposing shelves touch first. Twenty-four hour later, the anterior palate is also more loosely packed and the shelves are now touching here too.

Cell spacing seems to play a bigger role in the development of the anterior two-thirds of the palate compared to the posterior third. This is consistent with the model that anterior palate elevation is driven by expansion of ECM that in turn causes the tissue to “flip up”, while posterior elevation is less dependent or independent of this mechanism. Interestingly, within the anterior palate, the spacing increase is quite tightly restricted to a layer of cells a few cell diameters above the oral epithelium. This layer would have to act as a sort of piston and a more detailed study of the anisotropy of the spacing would perhaps reveal that it increases in the plane of this layer.

Changes in the epithelium could also be affecting cell spacing as it can alter the volume in which the cells have to space out. For example if the epithelium expands the mesenchyme has more space to fill. These changes could be driven by the epithelium or by the mesenchyme putting pressure on the covering cells. As well as this direct mechanical effect signalling from the epithelium could alter the behaviour of the mesenchymal cells. This could account for the more tightly packed cells along the oral edge of the palate. The rugae are epithelial cell thickenings and it is thought that they cause the mesenchyme directly below them to condense. It appears that potentially this also affects the mesenchyme but it is not as regimented. The mesenchyme along the oral edge in the anterior two thirds (where the rugae are present) is consistently more condensed than the mesenchyme adjacent or posterior to it. It is possible for the palatal shelves to elevate and fuse without rugae being present, such as in a Wnt beta-catenin knockout (Lin et al., 2011). It is also reported the oral side mesenchyme is not as condensed in this mutant. Therefore this change in sub-epithelial cell spacing does not appear to play a key role in palate development, but is under the control of signalling from the epithelium. The tongue is also smaller in the knockouts, posing less of a physical obstruction and allowing the palatal shelves to elevate as soon as the intrinsic factors reach their critical threshold. After elevation the gap between the two shelves is significantly smaller in the mutants. Consequently the shelves reach the midline sooner, and fusion, which is initiated by the two shelves touching, is complete by E14.5 in the mutants whereas it has barely started in the wild-



types at this stage. There is a cleft of the primary palate, which has formed incorrectly, and the secondary palate does not extend along its AP axis as much. The level of cell proliferation is considered normal. The lack of rugae and smaller tongue have removed some of the constraints placed on the mesenchyme, if the cells in the oral third are now more loosely packed the growth towards the midline can occur more swiftly. The earlier elevation due to the smaller tongue will mean that the shelves do not have as far to go to reach the midline, because the head will be smaller and as proliferation levels are following a normal pattern they will still be slightly higher than usual while the palate is growing towards the midline a stage early, which could also be contributing. A change in one factor can easily have knock on effects on how other mechanisms are affecting morphogenesis.

It will always be difficult to uncouple cell spacing from other cellular behaviours and tissue characteristics, but this must be included to complete the full story of cellular mechanisms that drive palatogenesis. It is especially important where elevational failure rather than altered size of the shelf is involved in a cleft palate. Ultimately, both genetic approaches and modelling all the properties of the tissue will be required. The following chapters investigate different mouse models with a cleft palate phenotype and demonstrate how these can provide further insight into the possible interactions between cellular mechanisms and how it is important to study a range of cellular behaviours in order to identify the potential cause of the cleft.

## 8.0 Palate Development in the *Tbx-1* Knockout Mouse

### 8.1 *Tbx-1*<sup>-/-</sup> Introduction

#### 8.1.1 *Tbx-1*<sup>-/-</sup> phenotype

DiGeorge syndrome (DGS), or velo-cardio-facial syndrome (VCFS), occurs in around one in 4000 births, and in humans is caused by a deletion of the region of chromosome 22q11. This region maps the *Tbx-1* gene, a member of the T-box family of binding domain transcription factors.

The T-box family of transcription factors are required for early cell fate decisions (Wilson and Conlon, 2002). Many of the symptoms have an origin in the neural crest. Therefore DGS is thought to be caused by anomalies occurring during migration of the neural crest cells (Merscher et al., 2001).

Humans with DGS can present a range of symptoms and a range of severities and in some mild cases the patient might not be diagnosed for a year or two. Symptoms include congenital heart defects, learning disorders, hearing loss and hypoparathyroidism leading to hypocalcemia. More specific craniofacial symptoms are cleft palate, a blunted nose, a receding or abnormal jaw (micrognathia), hypertelorism (wide set eyes), midface hypoplasia and vertical maxillary excess (Liao et al., 2004). Many of these defects are in structures that arise from the pharyngeal arches.

*Tbx-1* null mice do not survive postnatally, as the lungs fail to inflate upon birth, and they start to noticeably differ from wild-type litter mates at around E8.5 (Jerome and Papaioannou, 2001). By E9.5 the wild-type mice have three pharyngeal arches and pouches present but the mutant only has one (Fig. 8.1B). The severity of the mutation varies between mutant mice. For example around a third have the upper incisors missing or malformed and a short mandible. There are abnormalities in many different bones, including the palatine bone, and differences in the external and inner ear, none of which are seen in heterozygous mice. The heterozygous mice survive but can have fourth aortic arch anomalies and are considered to be on the autistic spectrum (Hiramoto et al., 2011).

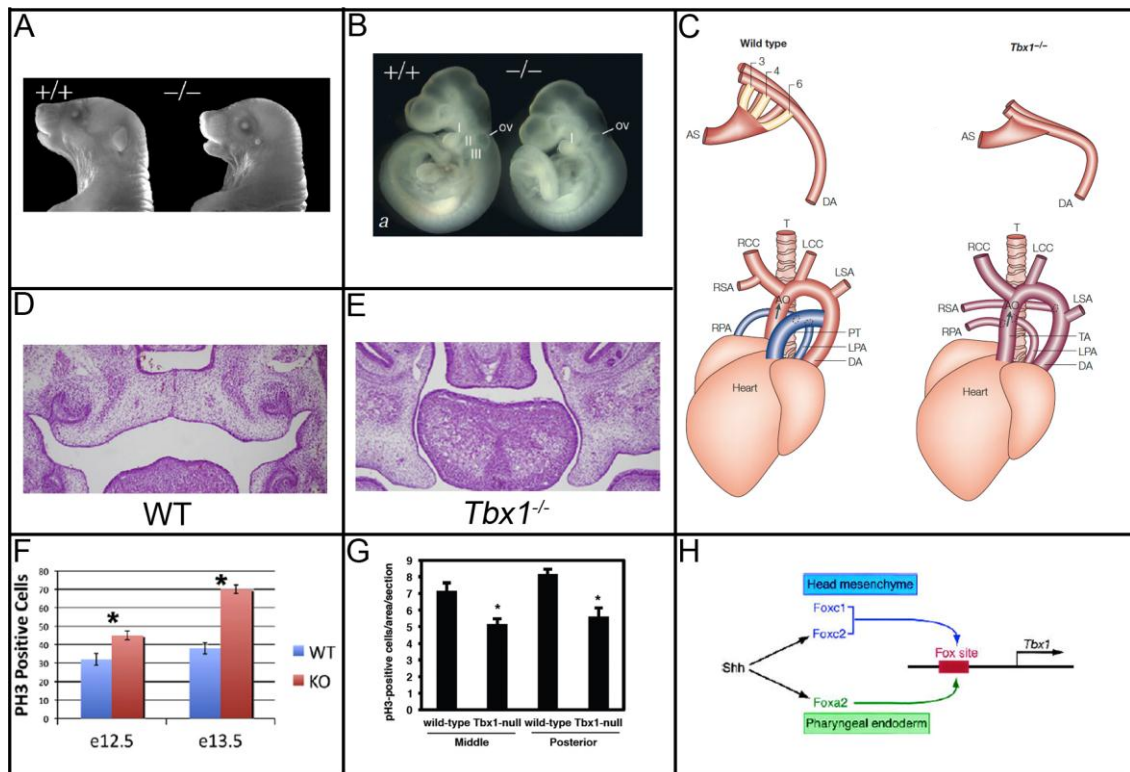


**Figure 8.1** *Tbx-1*<sup>-/-</sup> mutant mice and their defects A) Wild-type and *Tbx-1*<sup>-/-</sup> mutant neonates B) Wild-type and *Tbx-1*<sup>-/-</sup> mutant embryos at E9.5. A & B adapted from Jerome & Papaioannou 2001 C) Cardiac defects in the mutant embryo; there is no formation of the pharyngeal apparatus distal to arch two, as a result the other arches do not form and the aortic sac connects directly to the dorsal aorta. The *Tbx-1*<sup>-/-</sup> mutant also only has one artery leaving the heart instead of two. Adapted from Lindsay, 2001 D) Wild-type frontal section of an E14.5 elevated palate E) *Tbx-1*<sup>-/-</sup> mutant palate at E14.5, the palatal shelves have failed to elevate F) Graph of the level of proliferation from a PH-3 stain in the wild-type and *Tbx-1*<sup>-/-</sup> mutant at E12.5 and E13.5. D-F adapted from Goudy et al., 2010 G) Graph of the level of proliferation from a PH-3 stain in the wild-type and *Tbx-1*<sup>-/-</sup> mutant at E13.5 from the mid- and posterior palate. Adapted from Funato et al., 2012 H) A proposed model for the molecular regulation of *Tbx-1*. Adapted from Yamagishi et al., 2003.

## 8.1.2 *Tbx-1* in development

### 8.1.2.1 *Tbx-1* in the palate

All *Tbx-1*<sup>-/-</sup> mice display a cleft palate but the cause of this failure is still under debate (Fig. 8.1D & E). The palatal shelves have been shown to fuse in culture; therefore it is likely that the cleft is due to a failure in outgrowth or elevation. When the tongue was removed and the head cultured in a roller culture the palatal shelves did elevate but did not fuse due to never meeting in the midline. This could mean there was a failure in the outgrowth process. In the vast majority of mutant embryos the palatal shelves do not elevate. The tongue remains a lot higher in the oral cavity at E14.5 in the *Tbx-1*<sup>-/-</sup> mutant than in wild-type and the level of ECM, mainly hyaluronic acid, is a lot lower

in the mutant. This implies that both extrinsic and intrinsic factors have been affected by the *Tbx-1* mutation.

In the developing heart, loss of *Tbx-1* has been linked to a decrease in proliferation (Xu et al., 2004; Zhang et al., 2006) but proliferation in the palate seems to be less clear-cut. One study, using PH-3 staining, has shown the *Tbx-1*<sup>-/-</sup> mouse to have increased proliferation (Goudy et al., 2010) at E12.5 and E13.5 (Fig. 8.1F) compared to the wild-type. Another study looked more closely at the epithelium and found a slight increase in the level of proliferation, but only in the epithelium of the posterior palate at E14.5 and no significant difference in epithelial proliferation by E18.5 (Funato et al., 2012). In their supplementary data they also recorded the level of proliferation in the mesenchyme at E13.5 and found that it had significantly decreased (Fig. 8.1G). Previous work done in this lab, using a PH-3 proliferation assay, showed no significant difference in proliferation in the epithelium or mesenchyme at E13.5 (Zoupa, 2008).

The amount of apoptosis in the *Tbx-1*<sup>-/-</sup> mouse has also been published at conflicting levels with one study saying it increased in the *Tbx-1*<sup>-/-</sup> mouse at E13.5 (Goudy et al., 2010) and another claiming it never changes significantly from the wild-type in the mesenchyme at this stage or in the epithelium at E14.5 or E18.5 (Funato et al., 2012).

Often the palatal epithelium of *Tbx-1*<sup>-/-</sup> mice appears to fuse with the oral epithelium, particularly in the posterior palate, creating a physical barrier that prevents the palate from elevating but embryos where no fusion has occurred still present a cleft palate (Goudy et al., 2010). This observation suggested that *Tbx-1* has a role in epithelial integrity. In the *Tbx-1*<sup>-/-</sup> mutant *Fgf8* activity is affected in the same regions where palatal-oral epithelial fusions are observed. When investigated more closely the epithelium was shown to be thicker in the *Tbx-1*<sup>-/-</sup> mouse (Funato et al., 2012) and lacked distinct layers. Normally keratinocytes are restricted to the basal layer and differentiate into the spinous and granular layers as they migrate out, but in the *Tbx-1*<sup>-/-</sup> mouse keratinocytes were seen in disorganised masses (Funato et al., 2012) and cells were poorly differentiated.

Growth factors, known to be involved in palate development, which might be part of the *Tbx-1* signalling pathway, have been found to vary their expression in the *Tbx-1*<sup>-/-</sup> mouse (Rice et al., 2004). For example in situ hybridization has shown that *Fgf8* levels are decreased in the mutant at E13.5 whereas *Fgf10* expression was increased in both the midline of the tongue and the prospective nasal side of the palate (Goudy

et al., 2010). An *Fgf10* null mouse also has a cleft palate but in the double heterozygous *Tbx-1/Fgf10* mouse no cleft palate was observed so this was not a dosage dependant effect (Rice et al., 2004). In the *Tbx-1*<sup>-/-</sup> mouse *Shh* levels remained the same and *Tgfβ3* was still present in the MEE so these are either acting upstream of *Tbx-1* or are not in the *Tbx-1* signalling pathway.

#### **8.1.2.2 *Tbx-1* craniofacial defects derived from the pharyngeal arches**

A variety of craniofacial bones and muscles are deformed or missing in the *Tbx-1*<sup>-/-</sup> mouse, which are derived from the first through third pharyngeal arches. This results in facial dysmorphism, a shortened mandible and neck region, causing low set ears. Myogenesis of the striated muscles of the head and neck (branchiomic skeletal muscles) has been shown to be under the control of *Tbx-1*. These muscles include those involved in mastication, from the first pharyngeal arch, and in facial expressions, from the second, as well as those in the pharynx and larynx. Without *Tbx-1* expression the myogenic determinate genes, *Myf5* and *MyoD*, do not get activated in the pharyngeal mesoderm. This is required for the correct patterning of the neural crest cells to form the mandibular arch (Kelly et al., 2004).

DGS/VCFS patients often present with otitis media and conductive hearing loss, with some having sensorineural hearing loss as well and the pinnae (outer ear) can be abnormally folded. The most extreme cases in mouse can develop without the outer or middle ear structures at all. The inner ear develops from the otic vesicle, which appears smaller and thickened in the *Tbx-1* mutant. The middle ear ossicles are formed from the first pharyngeal arch and the external ear originates from the first and second pharyngeal arches (Jerome and Papaioannou, 2001).

#### **8.1.2.3 *Tbx-1* and heart development**

The abnormal development of the pharyngeal arches had consequences for the development of the heart and has linked the *Tbx-1* gene with the cardiovascular defects seen in DGS/VCFS (Jerome and Papaioannou, 2001). The two noticeable defects were incorrect aortic arch and outflow tract (Merscher et al., 2001). There should be visible branches of the aorta at E11.5 curving around the third, fourth and sixth pharyngeal arches but in the mutant there was only a single large aortic arch on each side. Normally the outflow tract should branch into the pulmonary and aortic

vessels, separated by the aorticopulmonary septum, but in the *Tbx-1*<sup>-/-</sup> mouse and DGS patients this septum was absent (Fig. 8.1C). The same deformities can be caused by ablating the cardiac neural crest cells that migrate into the pharyngeal arches (Kirby and Waldo, 1990) or a tissue specific knockdown of *Tbx-1* in the pharyngeal endoderm or mesoderm (Zhang et al., 2006).

A recent study has linked *Tbx-1* to the non-canonical *Wnt* signalling pathway with respect to heart formation (Choudhry and Trede, 2013). A mutation in *Wnt11r* (*Wnt11 related*), a member of the non-canonical *Wnt* pathway, caused similar cardiac outflow tract defects to those seen in the *Tbx-1* mutant. This led to levels of *Wnt11r* being measured in a zebrafish *Tbx-1*<sup>-/-</sup> mutant. *Wnt11r* is expressed in the same region as *Tbx-1* but it did not appear until just after *Tbx-1* and in the *Tbx-1* mutant there was 37% less *Wnt11r* expression. In comparison in a *Wnt11r* mutant the amount of *Tbx-1* did not change, supporting the theory that *Tbx-1* regulates heart formation through *WNT11r*. *Wnt11r* has been shown to target *Xenopus alcama*, which is present in the correct time and place to be involved in heart development and it is found to be down-regulated in both the *Tbx-1* and *Wnt11r* mutants, supporting the idea that it is downstream of *Tbx-1* and *Wnt11* (Choudhry and Trede, 2013). Rescue experiments have demonstrated that the cardiac defects can be corrected after ectopic over-expression of either *Wnt11r* or *alcama* to a *Tbx-1*<sup>-/-</sup>. Further analysis of this *Tbx-1*<sup>-/-</sup> mutant zebrafish showed that there were defects in cell shape, number and differentiation of cells in the primary heart field of the lateral plate mesoderm and a conserved location where heart formation commences. This work is beginning to link the genetic factors and cellular behaviours.

#### **8.1.2.4 *Tbx-1* in thyroid and parathyroid development**

Thyroid and parathyroid disorders are another common result of pharyngeal arch defects (Lindsay, 2001) and lead to the immune deficiencies seen in DGS. *Tbx-1*<sup>-/-</sup> mice have thyroid hypoplasia (Liao et al., 2004) and parathyroid gland aplasia. DGS/VCFS patients sometimes suffer from hypothyroidism; this can be caused by the normal bi-lobed thyroid developing as a single lobe.

The thyroid is an endocrine gland that is important in hormone secretion and consists of two distinct cell types that arise from specific regions of the pharyngeal endoderm, which then fuse later in development. The thyroid follicular cells develop in the ventral

pharyngeal endoderm whereas the parafollicular, or C-cells, come from the endoderm of the fourth-pharyngeal pouch. *Tbx-1* mutants do not develop the fourth-pharyngeal pouch, which meant they completely lack some components of the final organ. The impact of having no *Tbx-1* gene was seen when the required number of endoderm progenitors did not develop (Lania et al., 2009). *Tbx-1* has been shown to control the size of the developing thyroid (Fagman et al., 2007) through its expression in the adjacent mesoderm, which regulates the expression of *Fgf8*, which can interact with the endodermal thyrocyte progenitors. The same phenotype occurred if *Fgf8* was ablated as when *Tbx-1* was ablated (Lania et al., 2009) and addition of *Fgf8* was able to rescue the thyroid defect in the *Tbx-1* mutant.

### 8.1.3 *Tbx-1* Expression Pattern and signaling pathway

*Tbx-1* expression can be seen from early embryonic stages throughout gastrulation and at early organogenesis. It is expressed in the pharyngeal arches and pouches as well as the otic vesicle (Chapman et al., 1996). During early facial development *Tbx-1* is expressed in the epithelium of the frontonasal, medial and lateral nasal processes (Zoupa et al., 2006). *Tbx-1* is expressed in the epithelium of the palate (Fig. 8.2) throughout its initial outgrowth and elevation and is still expressed in the epithelial seam when the two palatal shelves touch in the midline. The expression in the palate is generally stronger in the anterior palate (Fig. 8.2). There are high levels of expression in the developing tooth buds and in the tongue intrinsic musculature and epithelium from E11.5 – E14.5. There is also *Tbx-1* expression in developing hair follicles (Zoupa et al., 2006).

Expression of *Tbx-1* is dependent on other factors, such as *Shh*, for example in the pharyngeal arch system (Garg et al., 2001). *Tbx-1* is co-expressed with *Shh* in the epithelium of several organs and they are both vital for the correct development of these organs. The role of these factors varies between organs. For example in the tooth the two are thought to be involved in the initiation of development (Cobourne et al., 2001; Gritli-Linde et al., 2002) whereas in hair follicle development they appear to have more of a role in growth and morphogenesis not maturation (Karlsson et al., 1999).

*Shh* is involved in the development of the craniofacial region as well as the correct development of the brain, spinal cord, axial skeleton and limbs (Chiang et al., 1996).

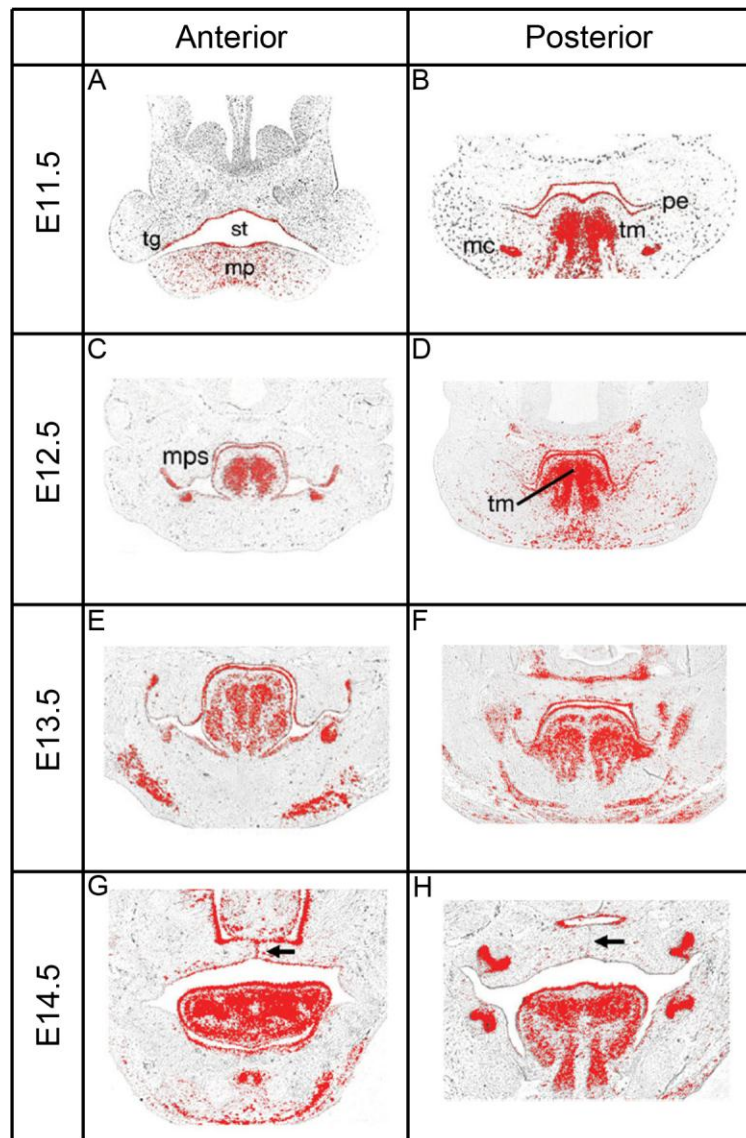


**Figure 8.2 Expression pattern of *Tbx-1* during palate development** A-B) *Tbx-1* is expressed in the oral epithelium at E11.5 C-D) *Tbx-1* is expressed in the oral epithelium and the tongue at E12.5 E-F) *Tbx-1* is expressed in the oral epithelium, tongue and the developing molar at E13.5 G-H) *Tbx-1* is expressed in the anterior oral epithelium, tongue, nasal cavity and developing molar at E14.5. Adapted from Zoupa et al., 2006.

In early development it is expressed in the pharyngeal region and its expression pattern overlaps with *Tbx-1*. In *Shh*<sup>-/-</sup> mutants *Tbx-1* becomes down-regulated in this region and ectopic addition of *Shh* led to over-expression of *Tbx-1* (Garg et al., 2001). Loss of *Shh* has quite significant impacts on the embryo (Chiang et al., 1996), including pharyngeal hypoplasia. Therefore expression of *Tbx-1* was also investigated in a model of pharyngeal arch hypoplasia, using mice lacking the transcription factor basic helix-loop-helix (bHLH) bHAND. *Tbx-1* expression did not alter in these mice, implying that it is due to the loss of *Shh* and not the hypoplasia that *Tbx-1* levels changed in the *Shh*<sup>-/-</sup> mouse (Garg et al., 2001).



In the pharyngeal mesoderm winged helix/forkhead box (Fox) transcription factors, *Foxa2*, *Foxc1* and *Foxc2*, have been identified as acting downstream of *Shh* and interacting with a critical *cis*-element upstream of *Tbx-1* resulting in transcription of *Tbx-1* in the endoderm and head mesenchyme (Hu et al., 2004; Yamagishi et al., 2003), (Fig. 8.2H). In *Foxc1*<sup>-/-</sup> or *Foxc2*<sup>-/-</sup> mice *Tbx-1* was partially down regulated but only in regions where they were co-expressed and this indicated a dose-dependent regulation. They also had aortic arch defects, similar to *Tbx-1*<sup>-/-</sup> mutants. *Shh* was thought to be necessary for the maintenance, not the induction, of the *Fox2a* signal in the pharyngeal endoderm but *Fox2a* mutants arrested too early to study *Tbx-1* expression (Chiang et al., 1996). *Foxa2* was also required downstream of *Tbx-1* to activate cardiac outflow precursors, so there appeared to be an auto-regulatory loop set up with respect to early heart development (Hu et al., 2004). This evidence suggests *Tbx-1* is a downstream target of *Shh*, acting via Fox transcription factors, in pharyngeal and otic development. It showed how a local change in gene regulation could potentially have a global impact on organogenesis.

*Fgfs* and their receptors have been linked to the regulation of several different cellular behaviours, including proliferation, survival, migration and differentiation. There are 18 ligands and 4 receptors in the *Fgf* family (Turner and Grose, 2010). *Fgf8* and *Fgf10* have been linked to *Tbx-1* activity, because they have partially overlapping expression regions and loss of *Tbx-1* altered their expression (Vitelli et al., 2002).

*Fgf8* is expressed in the epithelium of the pharyngeal arches and is involved with signalling to the mesenchyme and is thought to be dependent on *Tbx-1* expression. Loss of *Fgf8* activity in the pharyngeal arches led to increased apoptosis, supporting the theory that *Tbx-1* has a cell protective effect (Abu-Issa et al., 2002). Alterations to the expression levels of *Tbx-1* or *Fgf8*, or both, led to defects in the aortic arch. The more severe the loss in expression the more severe the defect was (Vitelli et al., 2002). *Fgf10* is lost in the secondary heart field in the *Tbx-1*<sup>-/-</sup> mouse and this was thought to be responsible for the outflow tract defects in the mutant (Aggarwal et al., 2006).

Vascular endothelial growth factor (*Vegf*) exists in several different isoforms and is known to be essential for angiogenesis. The knockout of one of these isoforms led to a phenotype very similar to the *Tbx-1*<sup>-/-</sup> mouse with defects in heart, craniofacial, thyroid and parathyroid development. This has led to the conclusion that *Tbx-1* interacts with isoforms of *Vegf* (Stalmans et al., 2003). Similarly the Bmp inhibitor

Chordin mutant has a comparable phenotype to the *Tbx-1* mutant. Chordin is important for dorsoventral patterning and pharyngeal development and its secretion by the mesendoderm is thought to be required for the correct expression of *Tbx-1* (Bachiller et al., 2003).

## 8.2 *Tbx-1*<sup>-/-</sup> palate development: Methods

Two heterozygous *Tbx-1*<sup>+/-</sup> mice were bred to produce *Tbx-1*<sup>-/-</sup> embryos. For the proliferation and cell spacing analysis the mothers were injected with IddU 2.5 hours prior to sacrifice and the embryos were removed, fixed, embedded, sectioned and stained as described in section 2.3.4-2.5. Every other section of the palate was imaged with an n=3 per stage for embryos at E11.5 – E15.5 and the images were analysed as described in sections 2.6-2.8. T-tests were performed to analyse the statistical significance of measurements made with p<0.05 counted as statistically significant.

For the analysis of the Golgi position and orientated cell division the embryos were processed for frozen sectioning. They were stained and imaged as described in sections 2.3-2.6 and the angles were measured as described in section 2.10. As the *Tbx-1*<sup>-/-</sup> mouse line did not have the mT/mG membrane stain a fibronectin antibody was also used to visualise the ECM, this was to aid the identification of corresponding Golgi and nuclei. Rose plots were created and Watson's U<sup>2</sup> test was performed to test for statistical significance (section 2.10 for further details) with p<0.05 counted as statistically significant. For this section different regions of the palatal outgrowth have been investigated as well as cells from the adjacent mesenchyme for comparisons. On the rose plots the 180° point represents the distal tip of the palate, where the plots are displayed on an outline of the palate they have been rotated so the 180° line matches distal point of the diagram. For the OCD data the rose plots are showing mirror-image symmetry to reflect the symmetry of the spindles because this helps to reduce visual bias that would be produced from a 180° plot. Also for the OCD data, prior to performing the Watson's U<sup>2</sup> test, which requires a distribution of angles spread over 360°, the value of each angle was doubled.

## 8.3 *Tbx-1*<sup>-/-</sup> palate development: Results

### 8.3.1 *Tbx-1*<sup>-/-</sup> phenotype

Significant differences between the wild-type and *Tbx-1*<sup>-/-</sup> palatal shelves were first seen at E11.5 when the mutant can be considered significantly wider than the wild-type palate (Fig. 8.3A & 8.4A). Yet, by E12.5 there was no significant difference in the height and width between the wild-type and mutant palatal shelves (Fig. 8.3B & 8.4A). Then at E13.5 the wild-type palatal shelves were significantly wider than the mutant ones (Fig. 8.3C & 8.4A). There is no significant difference in the height of the palatal shelves between the wild-type and the mutant until E14.5 when the mutant palate has failed to elevate (Fig. 8.3D & 8.4A). Although at this point the height measurement might not be comparable because the landmarks have changed. The *Tbx-1*<sup>-/-</sup> palate remains positioned vertically parallel to the tongue even at E15.5 (Fig. 8.3E) but was both significantly shorter and thinner than the wild-type (Fig. 8.4A).

When the height measurements were studied along the AP axis the main difference that stood out between the wild-type and mutant palates was a significant increase in height between E13.5 and E14.5 in the *Tbx-1*<sup>-/-</sup> palate, which never occurred in the wild-type (Fig. 8.4B & C). It is at this stage that the wild-type palate is elevating and the mutant palate remains vertical.

The main difference in the width of the palate between the wild-type and mutant also occurred around the time of wild-type palate elevation. The *Tbx-1*<sup>-/-</sup> palate increased its width significantly between E13.5 and E14.5 along the entire AP axis and in the wild-type this is only a significant change in the mid-palate (Fig. 8.4B & C). The wild-type displayed a significant increase in width along its entire AP axis between E14.5 and E15.5 where the *Tbx-1*<sup>-/-</sup> palate showed a decrease in width.

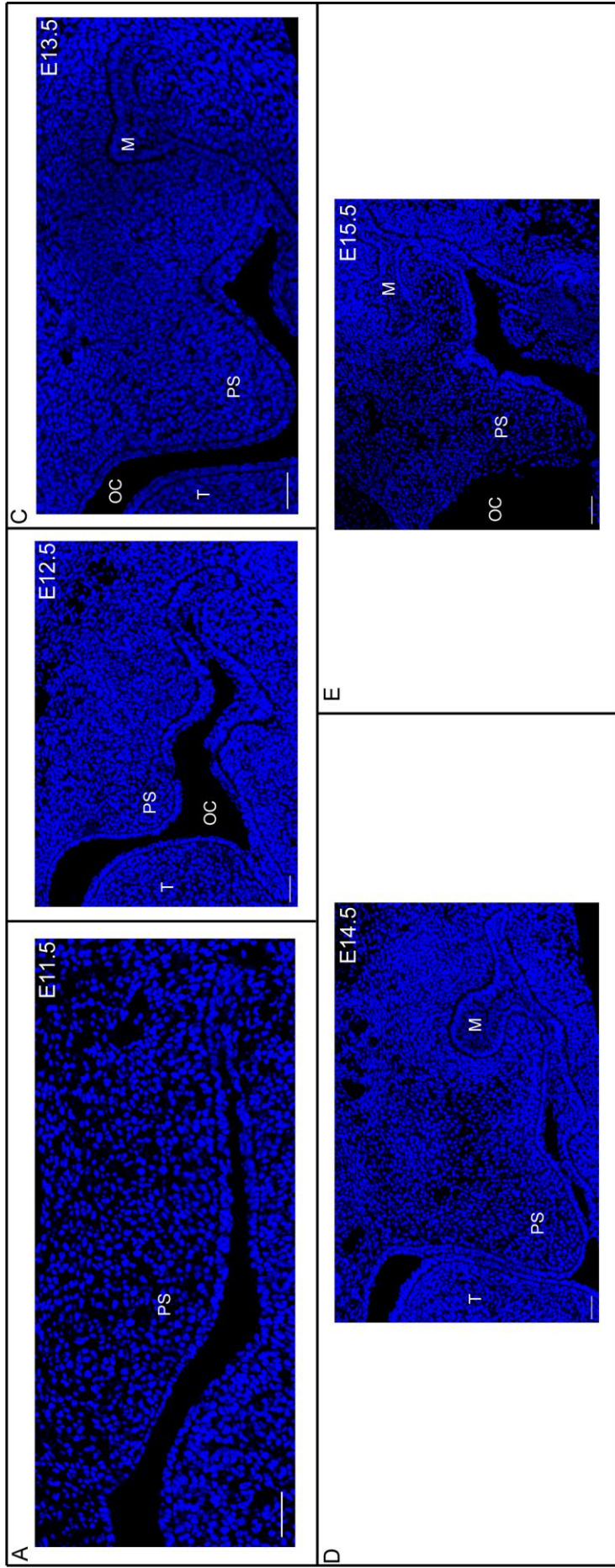


**Figure 8.3 DAPI images of *Tbx-1* mutant palate development** A) E11.5 B) E12.5 C) E13.5 D) E14.5, no elevation has occurred E) E15.5. Scale bars represent 200  $\mu\text{m}$ . M, molar tooth bud; OC, oral cavity; PS, palatal shelf; T, tongue.

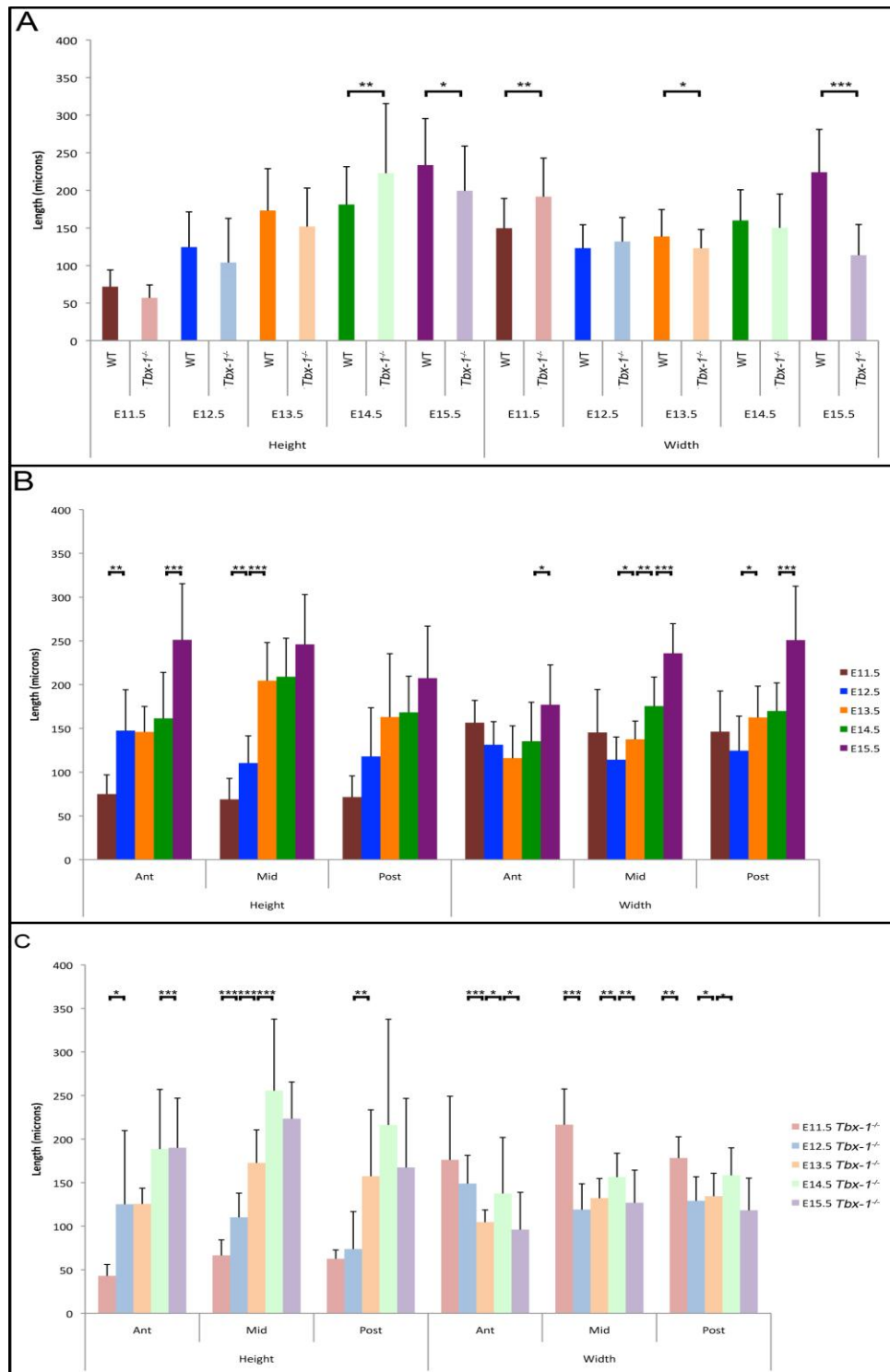


**Figure 8.4 Wild-type and *Tbx-1*<sup>-/-</sup> height and width measurements** A) Wild-type and *Tbx-1*<sup>-/-</sup> mutant palate measurements during development B) Changes in height and width along the AP axis during the development of the wild-type palate C) Changes in height and width along the AP axis during the development of the *Tbx-1*<sup>-/-</sup> mutant palate. A, anterior palate; P, posterior palate. Error bars display 1 standard deviation. Results of t-tests are shown \*p<0.05 \*\*p<0.01 \*\*\*p<0.001

### **8.3.2 Localised cell proliferation in the *Tbx-1*<sup>-/-</sup> mutant**

#### **8.3.2.1 Overview of localised cell proliferation during *Tbx-1*<sup>-/-</sup> palate development**

The *Tbx-1* mice were in a C57BL/6 background and these mice were smaller than the CD-1s used in the wild-type and *Msx-1*<sup>-/-</sup> study and overall lower levels of proliferation were observed.

The highest level of proliferation was seen at E11.5 in both the *Tbx-1*<sup>-/-</sup> mutant and wild-type palates (Fig. 8.5A) and in both genotypes there was a significant drop in the amount of proliferation by E12.5. Although the difference in the level of proliferation between the wild-type and *Tbx-1*<sup>-/-</sup> mutant palates was not significant different at E11.5 or E12.5 it is interesting to note that the mutant is displaying a slightly higher level of proliferation at both stages (Fig. 8.5A). The wild-type palatal outgrowth then displayed a significant increase of proliferation at E13.5 and this burst of proliferative activity did not occur in the *Tbx-1*<sup>-/-</sup> mutant leaving the mutant palate at a significantly lower level of proliferation. In fact the mutant had remained at a very similar level of proliferation to that seen at E12.5 (Fig. 8.5A). By E14.5 the amount of proliferation had fallen significantly in both genotypes and they were back at near identical levels of proliferation, although by this stage the wild-type palate will have elevated and these *Tbx-1*<sup>-/-</sup> mutant palates had not. As the wild-type palate reached the fusion stage of development at E15.5 the level of proliferation had significantly dropped once again but this time a greater drop had occurred in the *Tbx-1*<sup>-/-</sup> mutant leaving it at a significantly lower level than its wild-type counterpart (Fig. 8.5 A).

#### **8.3.2.2 Regionalised changes in cell proliferation along the AP axis of the *Tbx-1*<sup>-/-</sup> palate**

Even at E11.5 when the initial palatal outgrowth of the *Tbx1*<sup>-/-</sup> mutant is very small it had significantly higher proliferation in the anterior third compared to the remainder of the palate (Fig. 8.5B). There was no significant difference along the AP axis of the wild-type palate at E11.5. This pattern of decreasing proliferation from the anterior to posterior palate remained in the mutant palate through to E12.5, whereas there was

still no significant difference between the levels of proliferation in the wild-type along the AP axis (Fig. 8.5B).

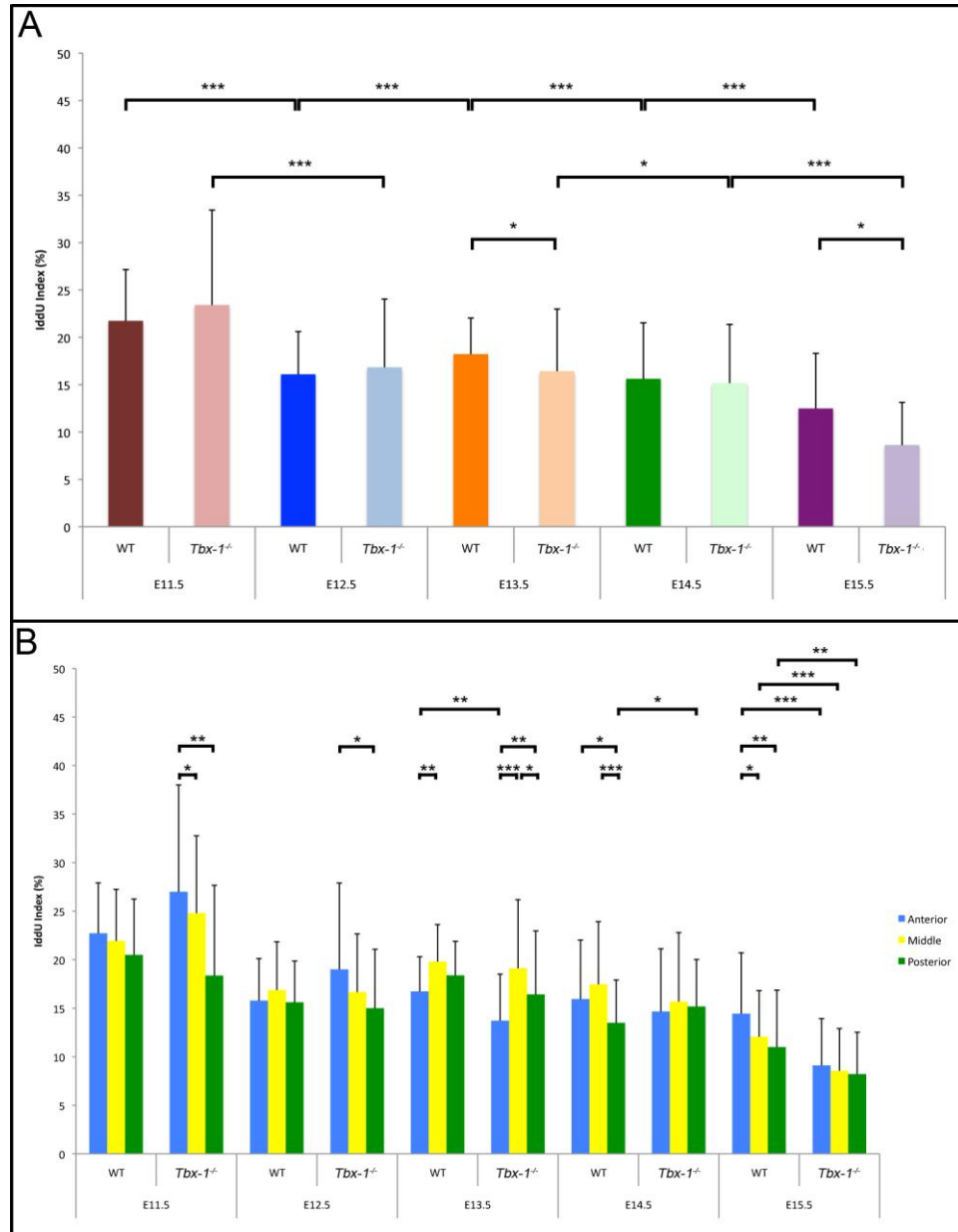


**Figure 8.5 Proliferation index results represented as graphs** A) Overall IddU index for wild-type and *Tbx-1*<sup>-/-</sup> mutant palates (E11.5 – E15.5) B) Average IddU index along the AP axis of the wild-type and *Tbx-1*<sup>-/-</sup> mutant palatal shelves comparing changes within the palate at each developmental stage, E11.5 – E15.5. Error bars display 1 standard deviation. Results of t-tests are shown \*p<0.05 \*\*p<0.01 \*\*\*p<0.001. Although overall the amount of proliferation was constant between E12.5 and E13.5 (Fig. 8.5A) in the *Tbx-1*<sup>-/-</sup> palate when looked at along the AP axis the proliferation dropped in the anterior region and increased in both the middle and posterior thirds of the palate (Fig. 8.5B). At E13.5 the level of proliferation in the anterior region of the

*Tbx-1*<sup>-/-</sup> mutant palate was significantly less than the wild-type palate, whereas levels were similar in the mid- and posterior palate. Both genotypes had their highest level of proliferation in the middle third of the AP axis (Fig. 8.5B).

There was no significant difference in the level of proliferation along the AP axis in the *Tbx-1*<sup>-/-</sup> mutant palate at E14.5 (Fig. 8.5B). In the wild-type palate the posterior third had significantly lower proliferation from the anterior and mid-palate (Fig. 8.5B). In addition the proliferation in the posterior third of the wild-type palate was significantly lower than in the posterior third of the *Tbx-1*<sup>-/-</sup> mutant palate at this stage.

By E15.5 each third of the *Tbx-1*<sup>-/-</sup> mutant palate was significantly lower than its wild-type counterpart (Fig. 8.5B). There was also no significant difference along the AP axis in the *Tbx-1*<sup>-/-</sup> mutant (Fig. 8.5B). Whereas at E15.5 the wild-type showed significantly higher proliferation in the anterior third compared to the rest of the palate.

### **8.3.2.3 Regionalised changes in cell proliferation shown in the heat maps of the *Tbx-1*<sup>-/-</sup> palate**

The mutant palate showed a slightly greater range in its level of proliferation along the mediolateral axis, with some patches of higher proliferation towards the lateral side of the outgrowth (Fig. 8.6). The level of proliferation in the maxillary tissue immediately dorsal to the palatal outgrowth appears to be at a fairly similar level in the wild-type and mutant.

At E12.5 the proliferation heat maps in both the mid- and posterior palate had a region of slightly lower proliferation on the prospective oral side and this could be seen in both the wild-type and *Tbx-1*<sup>-/-</sup> palate (Fig. 8.7, black arrows indicate regions of lower proliferation). In the wild-type palate there were consistently no blue patches, indicating lower proliferation, in the tip region of the mid- and posterior palate (Fig. 8.7B & C, black circles). This pattern did not stand out in the mutant palate. In the anterior palate the *Tbx-1*<sup>-/-</sup> palate, regions of increased proliferation were seen, generally towards the prospective oral side (Fig. 8.7D, ventral on the heat map), this accounts for the significant difference in the level of proliferation seen between the anterior and posterior palate at E12.5 in the *Tbx-1*<sup>-/-</sup> palate.



In the anterior third of both the wild-type and mutant palate at E13.5 a core of low proliferation could be seen (Fig. 8.8A, A', D, D', brackets indicate regions of lower proliferation). In the mid-palate there was a slight variation of proliferation across the prospective oronasal axis in both the wild-type and mutant palates. The prospective oral side had slightly lower levels of proliferation compared to the prospective nasal side (Fig. 8.8B & E, brackets indicate regions of lower proliferation). The posterior third of the wild-type palate was showing a very similar pattern of proliferation to the posterior third at E12.5 (Fig. 8.7C & 8.8C). The *Tbx-1*<sup>-/-</sup> mutant palate showed a more general low level of proliferation, subject to patches of noise that varied between specimens (Fig. 8.8F).

Proliferation at E14.5 in the wild-type palate showed no strong biases, with only potentially a slight increase towards the distal and nasal side (Fig. 8.9A-C, black arrows). Proliferation in the *Tbx-1*<sup>-/-</sup> mutant appeared to fluctuate randomly at E14.5 (Fig. 8.9D-F). At E14.5 the wild-type palate was lying horizontal across the top of the oral cavity whereas the *Tbx-1*<sup>-/-</sup> mutant was still vertical along side the tongue therefore it was not really possible to truly compare regions between the wild-type and mutant at this stage without lineage data.

In the anterior and posterior thirds of the wild-type E15.5 palate there was a region of slightly lower proliferation between the oral and nasal sides (Fig. 8.10A & C, brackets). The E15.5 *Tbx-1*<sup>-/-</sup> mutant palate was now displaying very low levels of proliferation throughout (Fig. 8.10D-F).

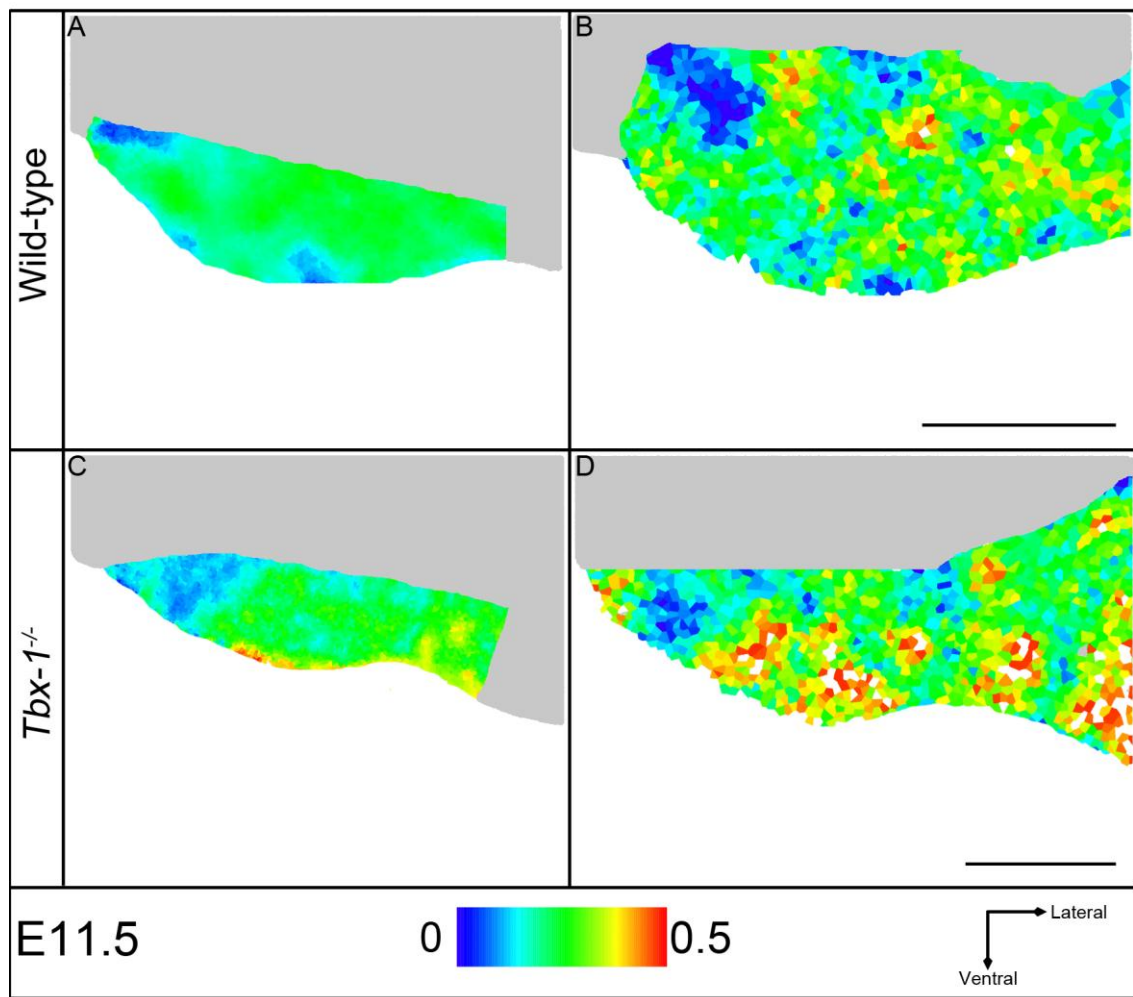


**Figure 8.6 Proliferation heat maps of E11.5 wild-type and *Tbx-1*<sup>-/-</sup> palatal shelves** A) Heat map of the wild-type palate B) Individual heat map of the wild-type palate C) Heat map of the *Tbx-1*<sup>-/-</sup> mutant palate D) Individual heat map of the *Tbx-1*<sup>-/-</sup> mutant palate. Each heat map is an average of three individual sections. Scale bars represent 200  $\mu$ m.

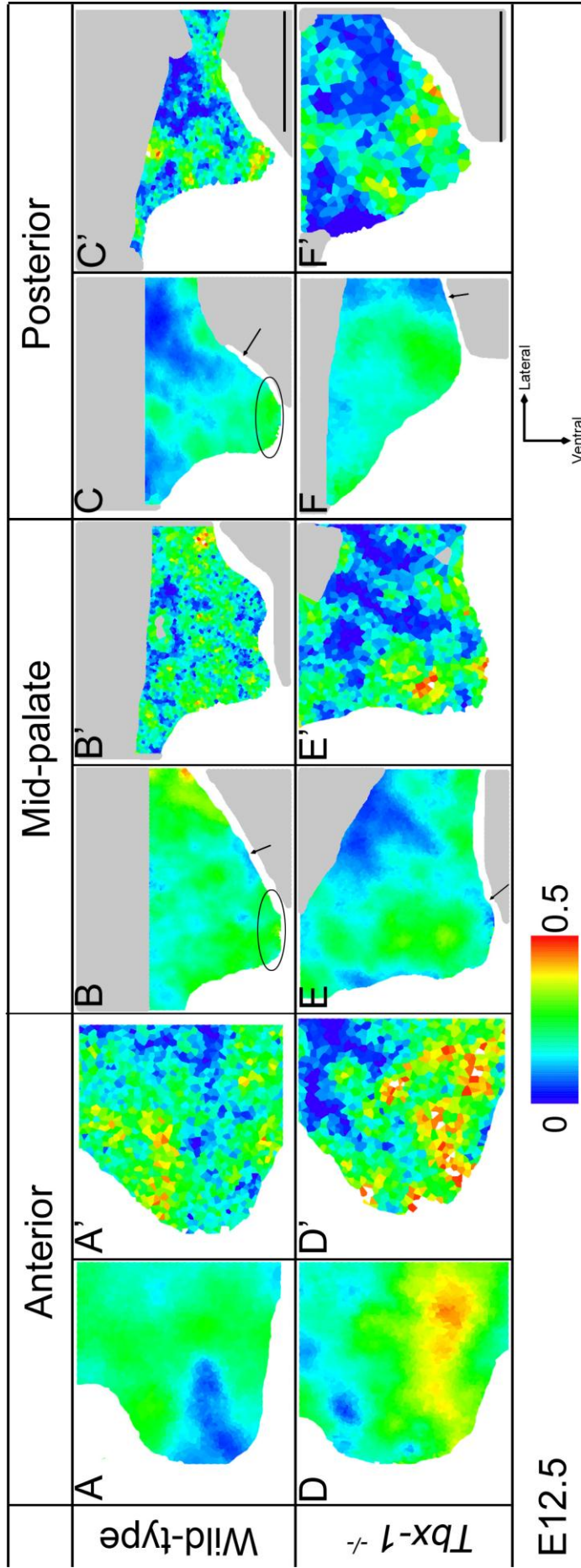


**Figure 8.7 Proliferation heat maps of E12.5 wild-type and *Tbx-1*<sup>-/-</sup> palatal shelves** A) Heat map of the wild-type anterior palate A') Individual heat map of the wild-type anterior palate B) Heat map of the wild-type mid-palate. Black circle highlights slightly higher proliferation towards the distal tip B') Individual heat map of the wild-type mid-palate. Black circle highlights slightly higher proliferation towards the distal tip C) Individual heat map of the wild-type posterior palate. Black circle highlights slightly higher proliferation towards the distal tip C') Individual heat map of the wild-type posterior palate D) Heat map of the *Tbx-1*<sup>-/-</sup> mutant anterior palate D') Individual heat map of the *Tbx-1*<sup>-/-</sup> mutant anterior palate E) Heat map of the *Tbx-1*<sup>-/-</sup> mutant mid-palate E') Individual heat map of the *Tbx-1*<sup>-/-</sup> mutant mid-palate F) Heat map of the *Tbx-1*<sup>-/-</sup> mutant posterior palate F') Individual heat map of the *Tbx-1*<sup>-/-</sup> mutant posterior palate. Each heat map is an average of three individual sections. Scale bars represent 200  $\mu$ m. Black arrows indicate regions of lower levels of proliferation.

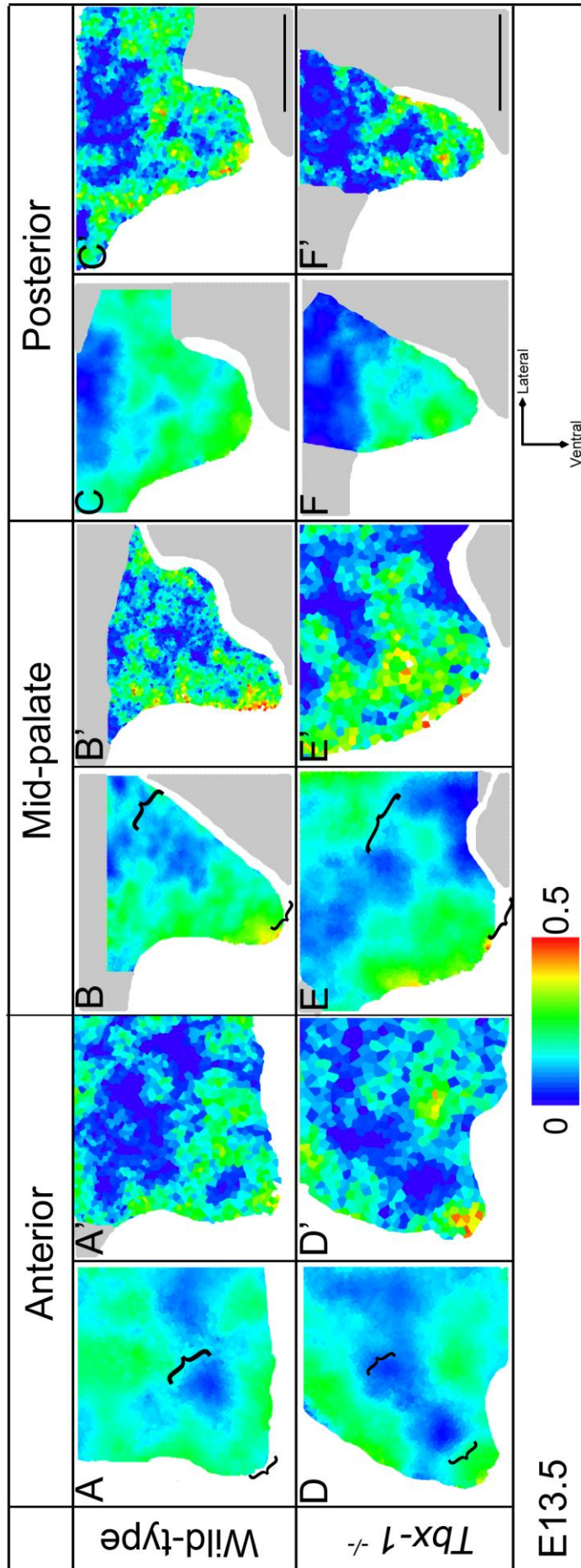


**Figure 8.8 Proliferation heat maps of E13.5 wild-type and *Tbx-1*<sup>-/-</sup> palatal shelves** A) Heat map of the wild-type anterior palate A') Individual heat map of the wild-type anterior palate B) Heat map of the wild-type mid-palate B') Individual heat map of the wild-type mid-palate C) Heat map of the wild-type posterior palate C') Individual heat map of the wild-type posterior palate D) Heat map of the *Tbx-1*<sup>-/-</sup> mutant anterior palate D') Individual heat map of the *Tbx-1*<sup>-/-</sup> mutant anterior palate E) Heat map of the *Tbx-1*<sup>-/-</sup> mutant mid-palate E') Individual heat map of the *Tbx-1*<sup>-/-</sup> mutant mid-palate F) Heat map of the *Tbx-1*<sup>-/-</sup> mutant posterior palate F') Individual heat map of the *Tbx-1*<sup>-/-</sup> mutant posterior palate. Each heat map is an average of three individual sections. Brackets indicate regions of low proliferation. Scale bars represent 200  $\mu$ m.

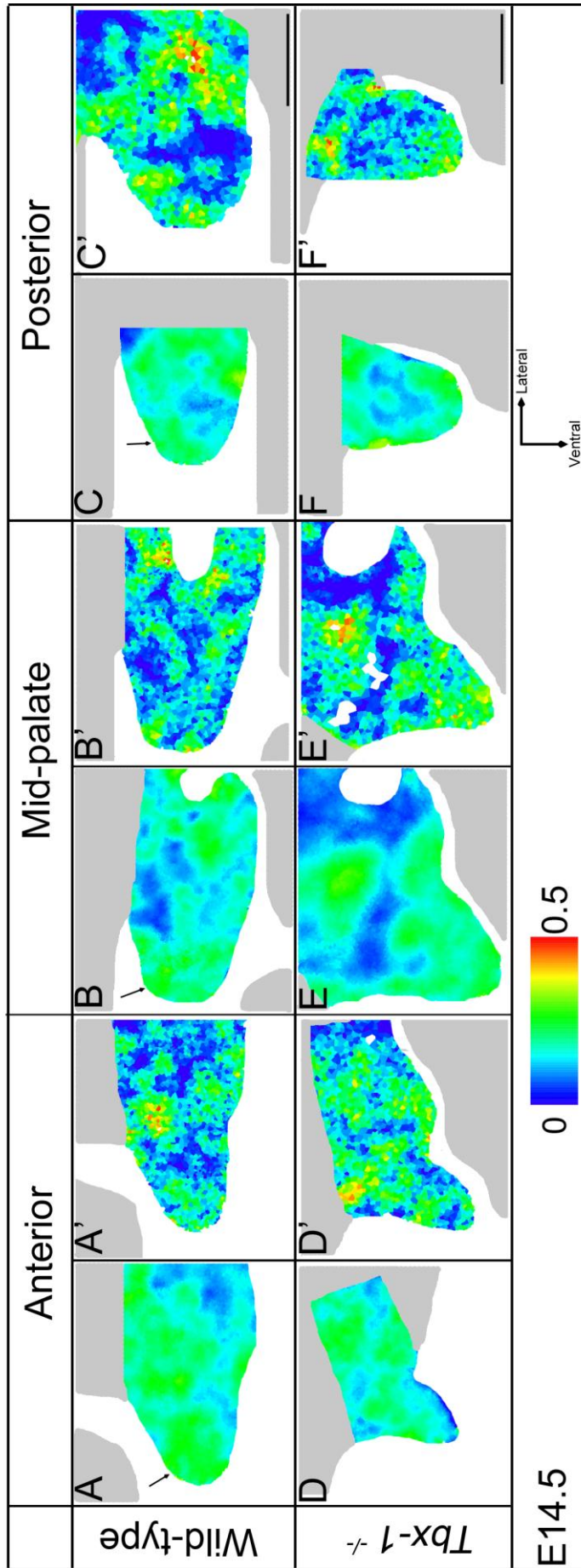


**Figure 8.9 Proliferation heat maps of E14.5 wild-type and *Tbx-1*<sup>-/-</sup> palatal shelves** A) Heat map of the wild-type anterior palate A') Individual heat map of the wild-type anterior palate B) Heat map of the wild-type mid-palate B') Individual heat map of the wild-type mid-palate C) Heat map of the wild-type posterior palate C') Individual heat map of the wild-type posterior palate D) Heat map of the *Tbx-1*<sup>-/-</sup> mutant anterior palate D') Individual heat map of the *Tbx-1*<sup>-/-</sup> mutant anterior palate E) Heat map of the *Tbx-1*<sup>-/-</sup> mutant mid-palate E') Individual heat map of the *Tbx-1*<sup>-/-</sup> mutant mid-palate F) Heat map of the *Tbx-1*<sup>-/-</sup> mutant posterior palate F') Individual heat map of the *Tbx-1*<sup>-/-</sup> mutant posterior palate. Black arrows in A-C indicate slightly more consistent green regions along the distal and nasal side of the wild-type palate. Each heat map is an average of three individual sections. Scale bars represent 200  $\mu$ m.

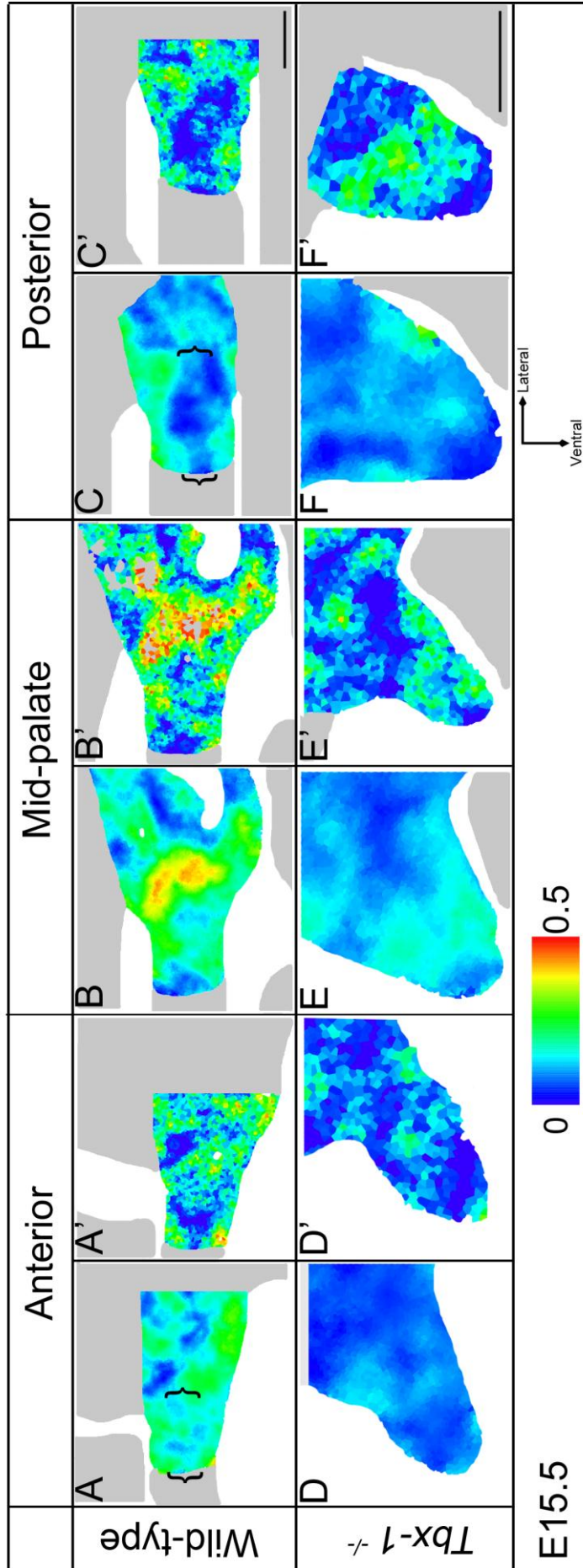


**Figure 8.10 Proliferation heat maps of E15.5 wild-type and *Tbx-1*<sup>-/-</sup> palatal shelves** A) Heat map of the wild-type anterior palate. Brackets indicate region of lower proliferation A') Individual heat map of the wild-type anterior palate B) Heat map of the wild-type mid-palate B') Individual heat map of the wild-type mid-palate C) Heat map of the wild-type posterior palate. Brackets indicate region of lower proliferation C') Individual heat map of the wild-type posterior palate D) Heat map of the *Tbx-1*<sup>-/-</sup> mutant anterior palate. Brackets indicate region of lower proliferation D') Individual heat map of the *Tbx-1*<sup>-/-</sup> mutant anterior palate E) Heat map of the *Tbx-1*<sup>-/-</sup> mutant mid-palate. Black circle highlights distal tip where levels of proliferation have fallen since E14.5 E') Individual heat map of the *Tbx-1*<sup>-/-</sup> mutant mid-palate F) Heat map of the *Tbx-1*<sup>-/-</sup> mutant posterior palate. Black circle highlights distal tip where levels of proliferation have fallen since E14.5 F') Individual heat map of the *Tbx-1*<sup>-/-</sup> mutant posterior palate. Each heat map is an average of three individual sections. Scale bars represent 200  $\mu$ m.

### 8.3.3 Golgi positioning in the *Tbx-1*<sup>-/-</sup> mutant

The orientation of the Golgi can provide information about the polarity of the cell and potential orientated cell behaviours. The full results of the statistical tests for the *Tbx-1* Golgi orientation data are listed in table 12.4 (See Appendix) and a  $p < 0.05$  is considered statistically significant.

#### 8.3.3.1 Golgi positioning during the initial outgrowth, E11.5-E12.5

In the initial palatal outgrowth at E11.5 both the wild-type and *Tbx-1*<sup>-/-</sup> mutant palate showed a distribution that was significantly different from a uniform distribution (Fig. 8.11). The *Tbx-1*<sup>-/-</sup> mutant palate actually showed a clearer ventral distribution, towards the palate's distal end (Fig. 8.11B), than the wild-type's rose plot that had a wider spread in both a medial and ventral direction (Fig. 8.11A). Despite the visual difference between the two rose plots the actual difference was not statistically significant in either the palatal outgrowth or the maxillary mesenchyme. Both the wild-type and *Tbx-1*<sup>-/-</sup> mutant maxillary process also displayed a distribution that was significantly different from a uniform distribution and had a bias in a ventral direction (Fig. 8.11C & D).

As the outgrowth continued to elongate downwards at E12.5 the wild-type displayed a distribution that was significantly different from a uniform distribution but a von Mises distribution cannot be rejected. Therefore it can be described as unimodal and directional (Fig. 8.12A). In contrast the overall distribution of the Golgi in the *Tbx-1*<sup>-/-</sup> mutant palate at E12.5 was not significantly different from a uniform distribution (Fig. 8.12B). Already the wild-type and mutant palatal outgrowths were displaying significantly different distributions of Golgi orientations ( $p < 0.01$ ).

At the tip of the palate at E12.5 the distribution of the Golgi in the wild-type palate shows a distribution that was significantly different from a uniform distribution with nearly half of the Golgi positioned in a ventral-lateral direction (Fig. 8.12H). The prospective oral and the prospective nasal thirds of the wild-type palate also had significantly non-uniform distributions with over half of their Golgi also directed in a ventral-lateral direction (Fig. 8.12E & G). In the *Tbx-1*<sup>-/-</sup> mutant palate the distribution of Golgi did vary significantly from a uniform distribution in both the distal tip region and prospective nasal side (Fig. 8.12K & N), but show different orientations from the

wild-type. The tip region of the *Tbx-1*<sup>-/-</sup> mutant showed a bilateral-like distribution, with Golgi pointing in both a medial-dorsal and ventral-lateral direction (Fig. 8.12N). Along the prospective nasal side the prevailing direction of Golgi was medial-ventral and this distribution was significantly different from the wild-type (Fig. 8.12K). The prospective oral side of the *Tbx-1*<sup>-/-</sup> mutant palate had a random distribution that did not vary significantly from a uniform one (Fig. 8.12M) but was significantly different from the prospective nasal side.

At E12.5 there was no significant difference between the anterior, middle and posterior thirds of the wild-type palate (Fig. 8.12O-Q). The distribution in the wild-type anterior and mid-palate could be described as unimodal and directional as a uniform distribution can be rejected but a von Mises one cannot (Fig. 8.12O-P). These two thirds had a bias in a ventral-lateral direction. In the *Tbx-1*<sup>-/-</sup> mutant palate only the distribution in the mid-palate differed significantly from a uniform distribution and was significantly different from the anterior third (Fig. 8.12R & S). The middle third is also significant different from the wild-type distribution because it had a ventral-medial bias whereas the wild-type has a ventral-lateral one (Fig. 8.12P & S).

### **8.3.3.2 Golgi positioning at the end of the outgrowth stage, E13.5**

At E13.5 the wild-type palate as a whole displayed a distribution that was significantly different from a uniform distribution (Fig 8.13A). In contrast the *Tbx-1*<sup>-/-</sup> mutant palate was not found to vary from a uniform distribution (Fig. 8.13B). The overall distribution of Golgi orientations between the wild-type and *Tbx-1*<sup>-/-</sup> mutant remained significantly different at E13.5 ( $p < 0.001$ )

At the tip of the wild-type palate the cells were displaying a bimodal distribution, clarified by the distribution varying significantly from both a uniform distribution and a von Mises distribution (Fig. 8.13H). The tip of the *Tbx-1*<sup>-/-</sup> mutant palate also appeared to display a bimodal distribution, but it had significantly different orientation from the wild-type. The distribution of the *Tbx-1*<sup>-/-</sup> mutant tip was closer to a mediolateral direction where the wild-type was in a dorsoventral one (Fig. 8.13H & N). In the wild-type each third of the palate along the prospective oronasal axis had a non-uniform distribution (Fig. 8.13E-G) whereas in the *Tbx-1*<sup>-/-</sup> mutant palate none of them varied significantly from a uniform distribution (Fig. 8.13K-M).



As previously mentioned in chapter 5, at E13.5 the Golgi in the wild-type posterior palate appeared to have switched their orientation and were now displaying a dorsal and lateral distribution. This is potentially important for the posterior palate to elevate using a remodelling mechanism. This distribution was significantly different from both the anterior and middle thirds of wild-type palate (Fig. 8.13O-Q). In contrast the *Tbx-1*<sup>-/-</sup> mutant palate displayed a random distribution in the posterior palate that was not significantly different from the rest of the palate (Fig. 8.13R-T). The anterior and middle thirds of the wild-type palate still had a slight ventral bias and both varied significantly from a uniform distribution. The middle third of the *Tbx-1*<sup>-/-</sup> mutant palate also had a non-uniform distribution but its orientation was slightly off ventral and significantly different from the distribution in the wild-type's middle third (Fig. 8.13P & S).

The distribution within the palate of the wild-type was significantly different from that of the adjacent mesenchyme too (Fig. 8.13A & D) and this difference was not seen in the mutant palate (Fig. 8.13B & J). The distribution of Golgi in the adjacent mesenchyme of the *Tbx-1*<sup>-/-</sup> mutant appeared to have potentially been disrupted as well because it was no longer displaying a non-uniform, random distribution like the wild-type.

### **8.3.3.3 Golgi positioning after failed elevation in the *Tbx-1*<sup>-/-</sup> mutant palate, E14.5**

The *Tbx-1*<sup>-/-</sup> mutant palate continued to display a significantly different orientation of Golgi at E14.5 after it had failed to elevate (Fig. 8.14). Overall the *Tbx-1*<sup>-/-</sup> mutant palate did not vary from a uniform distribution (Fig. 8.14B) whereas the wild-type palate did (Fig. 8.14A).

All of the regions across the oronasal axis appeared to display a medial and nasal bias in the elevated E14.5 wild-type palate (Fig. 8.14D, F & H). In the middle and oral thirds the distribution also varied significantly from a uniform one. There was no significant difference in distributions between different regions within the wild-type palate. In the *Tbx-1*<sup>-/-</sup> mutant palate the tip region varied significantly from the rest of the palatal outgrowth, displaying a dorsal bias on the rose plot (Fig. 8.14N). The remainder of the *Tbx-1*<sup>-/-</sup> mutant palate displayed a random distribution of Golgi orientation.

Along the AP axis of the wild-type palate the middle third had a non-uniform distribution with a medial-nasal bias (Fig. 8.14P). It was also significantly different from the distribution in the wild-type anterior palate (Fig. 8.14O & P). The *Tbx-1*<sup>-/-</sup> mutant palate had a significantly different distribution from the wild-type palate along its AP axis and none of the thirds varied significantly from a uniform distribution (Fig. 8.14P & S).

Significant differences in the orientation of the Golgi between the wild-type and *Tbx-1*<sup>-/-</sup> mutant palate were visible throughout palatogenesis. Therefore this could be a major contributor to the disrupted morphogenesis that leads to a cleft palate in the *Tbx-1*<sup>-/-</sup> mutant mouse.

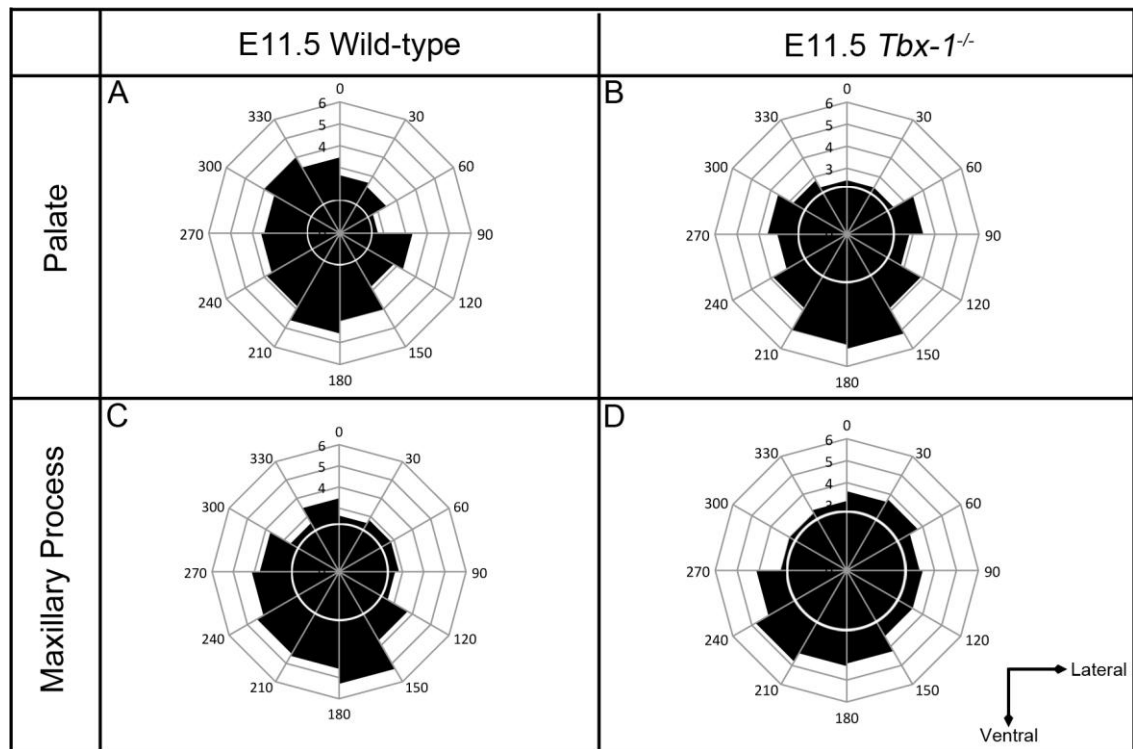


**Figure 8.11** Rose plots summarising Golgi angle in relation to the nuclear centre at E11.5 for wild-type and *Tbx-1*<sup>-/-</sup> palatal shelves A) Orientation of the Golgi in cells in the wild-type palatal outgrowth B) Orientation of the Golgi in cells in the *Tbx-1*<sup>-/-</sup> mutant palatal outgrowth C) Orientation of the Golgi in cells in the wild-type maxillary process D) Orientation of the Golgi in cells in the *Tbx-1*<sup>-/-</sup> mutant maxillary process. The white circle represents a uniform distribution. The 180° point is towards the distal tip of the palate.

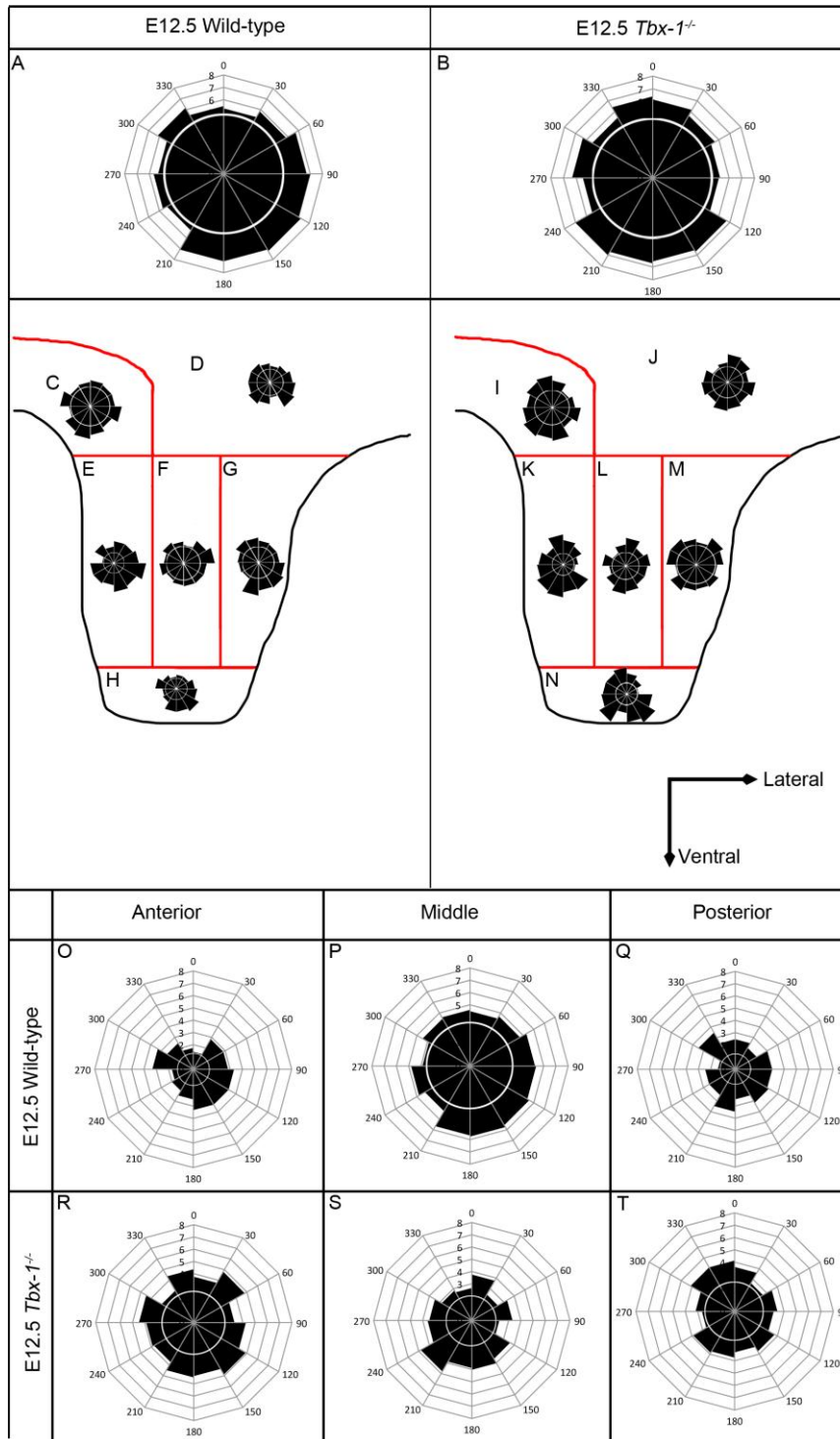


**Figure 8.12** Rose plots summarising Golgi angle in relation to the nuclear centre at E12.5 for wild-type and *Tbx-1*<sup>-/-</sup> palatal shelves A) Orientation of the Golgi in cells in the entire wild-type palatal outgrowth (E-H summed together) B) Orientation of the Golgi in cells in the entire *Tbx-1*<sup>-/-</sup> mutant palatal outgrowth (K-N summed together) C-H) Orientation of the Golgi in cells across different regions of the wild-type palate C) Shoulder region D) Mesenchymal cells adjacent to the palatal outgrowth E) Prospective nasal third F) Middle third G) Prospective oral third H) Tip I-N) Orientation of the Golgi in cells across different regions of the *Tbx-1*<sup>-/-</sup> mutant palate I) Shoulder region J) Mesenchymal cells adjacent to the palatal outgrowth K) Prospective nasal third L) Middle third M) Prospective oral third N) Tip O-P) Orientation of the Golgi in cells along the AP axis of the wild-type palate O) Anterior P) Mid-palate Q) Posterior R-T) Orientation of the Golgi in cells along the AP axis of the *Tbx-1*<sup>-/-</sup> mutant palate R) Anterior S) Mid-palate T) Posterior. The white circle represents a uniform distribution. The 180° point is towards the distal tip of the palate.

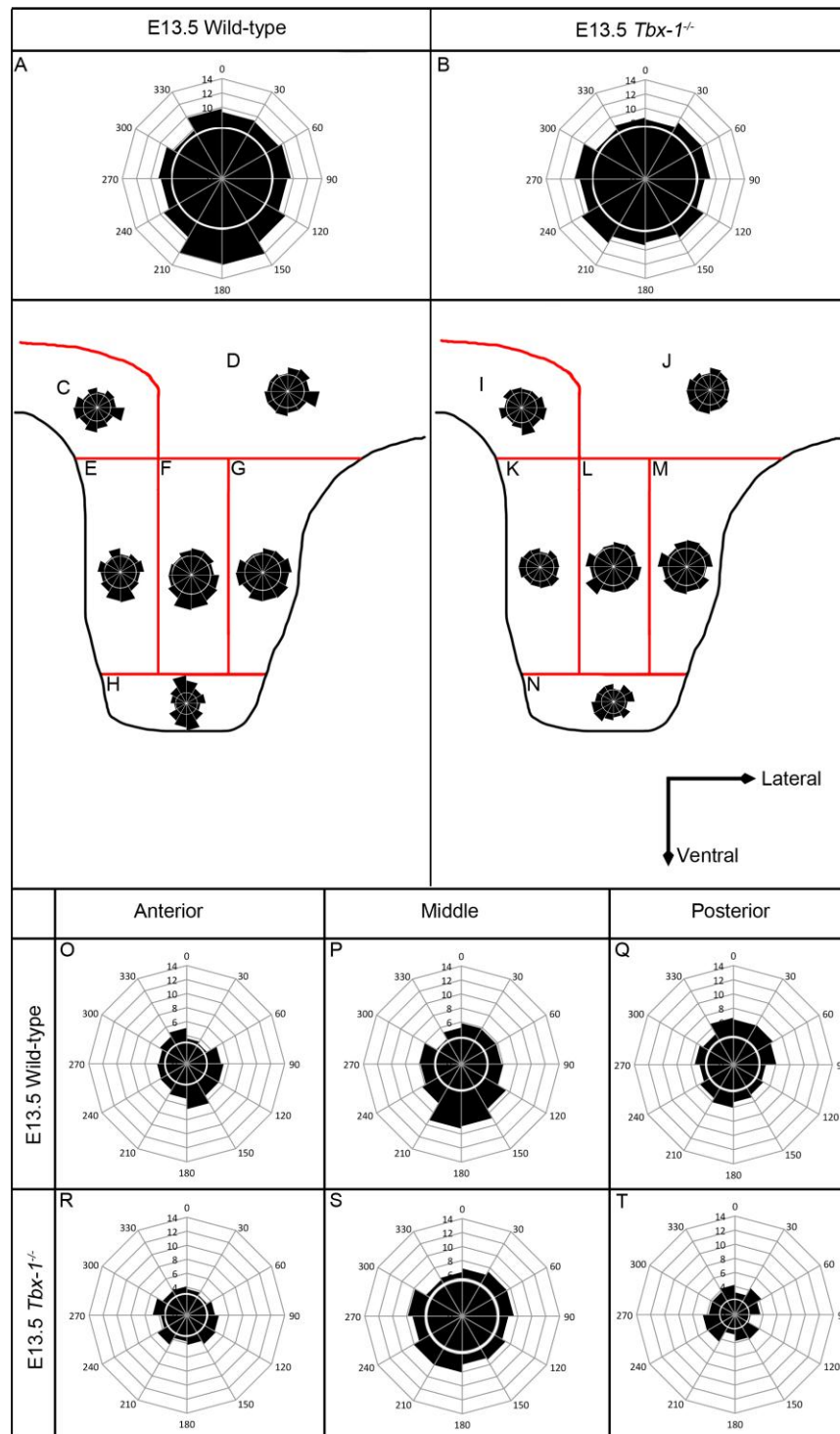


**Figure 8.13 Rose plots summarising Golgi angle in relation to the nuclear centre at E13.5 for wild-type and *Tbx-1*<sup>-/-</sup> palatal shelves** A) Orientation of the Golgi in cells in the entire wild-type palatal outgrowth (E-H summed together) B) Orientation of the Golgi in cells in the entire *Tbx-1*<sup>-/-</sup> mutant palatal outgrowth (K-N summed together) C-H) Orientation of the Golgi in cells across different regions of the wild-type palate C) Shoulder region D) Mesenchymal cells adjacent to the palatal outgrowth E) Prospective nasal third F) Middle third G) Prospective oral third H) Tip I-N) Orientation of the Golgi in cells across different regions of the *Tbx-1*<sup>-/-</sup> mutant palate I) Shoulder region J) Mesenchymal cells adjacent to the palatal outgrowth K) Prospective nasal third L) Middle third M) Prospective oral third N) Tip O-P) Orientation of the Golgi in cells along the AP axis of the wild-type palate O) Anterior P) Mid-palate Q) Posterior R-T) Orientation of the Golgi in cells along the AP axis of the *Tbx-1*<sup>-/-</sup> mutant palate R) Anterior S) Mid-palate T) Posterior. The white circle represents a uniform distribution. The 180° point is towards the distal tip of the palate.

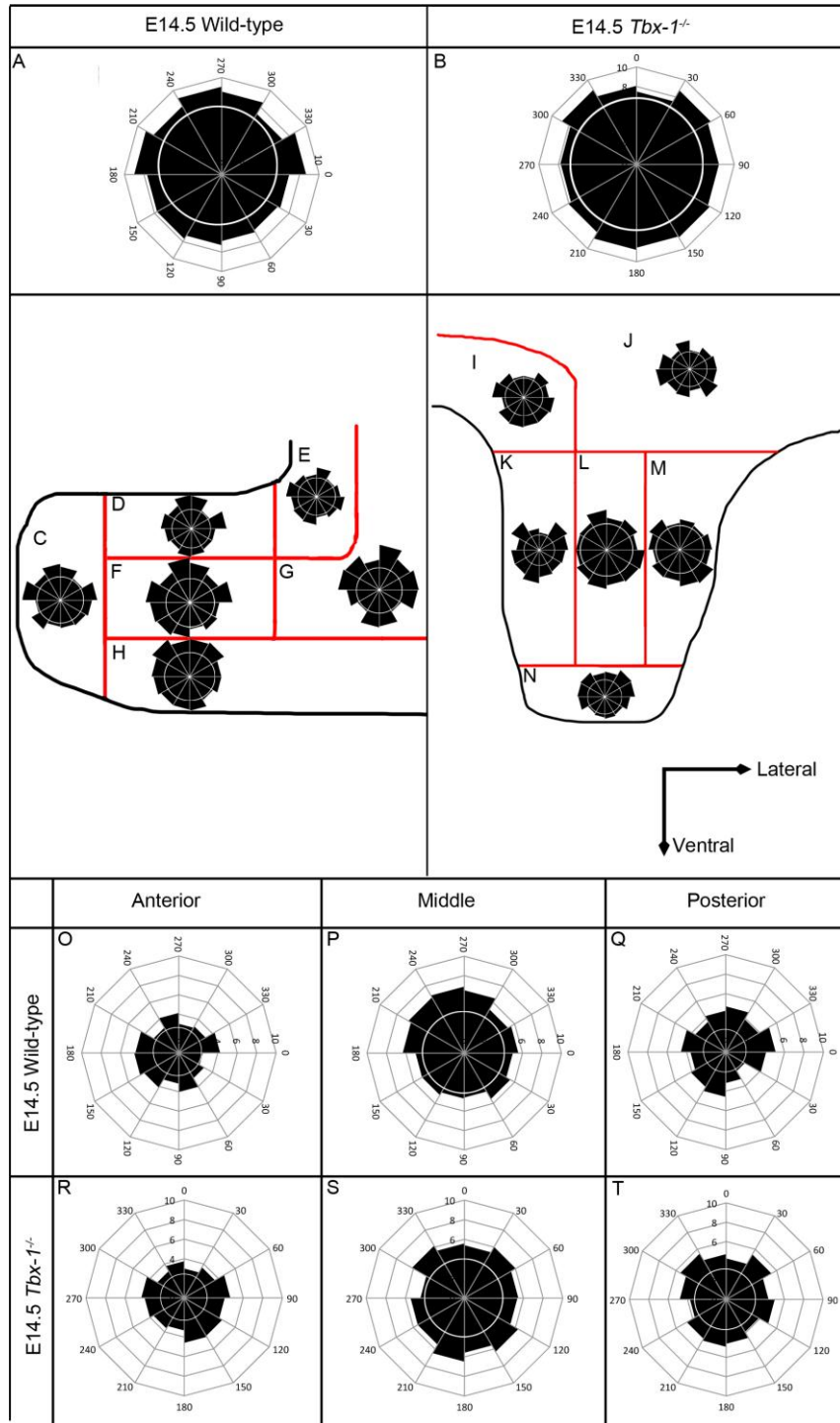


**Figure 8.14 Rose plots summarising Golgi angle in relation to the nuclear centre at E14.5 for wild-type and *Tbx-1*<sup>-/-</sup> palatal shelves** A) Orientation of the Golgi in cells in the entire wild-type palatal outgrowth (E-H summed together) B) Orientation of the Golgi in cells in the entire *Tbx-1*<sup>-/-</sup> mutant palatal outgrowth (K-N summed together) C-H) Orientation of the Golgi in cells across different regions of the wild-type palate C) Tip D) Nasal third E) Nasal Shoulder F) Middle third G) Mesenchymal cells adjacent to the palatal outgrowth H) Oral third I-N) Orientation of the Golgi in cells across different regions of the *Tbx-1*<sup>-/-</sup> mutant palate I) Shoulder region J) Mesenchymal cells adjacent to the palatal outgrowth K) Prospective nasal third L) Middle third M) Prospective oral third N) Tip O-P) Orientation of the Golgi in cells along the AP axis of the wild-type palate O) Anterior P) Mid-palate Q) Posterior R-T) Orientation of the Golgi in cells along the AP axis of the *Tbx-1*<sup>-/-</sup> mutant palate R) Anterior S) Mid-palate T) Posterior. The white circle represents a uniform distribution. The 180° point is towards the distal tip of the palate.

### 8.3.4 Orientated cell division in the *Tbx-1*<sup>-/-</sup> mutant

The full results of the statistical tests for the *Tbx-1* OCD data are listed in table 12.5 (See Appendix) and a  $p < 0.05$  was considered statistically significant. The number of mitotic events occurring in the *Tbx-1* mice was very low and this was probably the reason for the lack of statistical significance in the data in this section.

The E11.5 OCD data did not vary significantly between the wild-type and the *Tbx-1*<sup>-/-</sup> mutant palatal outgrowths. There did appear to be a slight dorsoventral bias in the wild-type's rose plot, with over half the mitotic divisions occurring in this plane (Fig. 8.15). In comparison the rose plot of the OCD in the wild-type maxillary process appeared to have a more random distribution of spindle orientations (Fig. 8.15C).

At E12.5 the palatal outgrowth of the *Tbx-1*<sup>-/-</sup> mutant had a distribution of spindle orientations that varied significantly from the mesenchyme of the adjacent maxillary process (Fig. 8.16B & G) although this difference was not seen in the wild-type mesenchyme. The mitotic cells in the tip region of the outgrowing palate at E12.5 appeared to have a fairly similar bias in the direction of spindle orientations between the mutant and the wild-type (Fig. 8.16F & K).

At E13.5 the overall distributions of the spindles, in both genotypes, did not vary from a uniform distribution (Fig. 8.17A & B). The rose plots for the wild-type palates did not vary significantly from a uniform distribution and did not have a visual correlation either (Fig. 8.17E-H). The distributions in the *Tbx-1*<sup>-/-</sup> mutant palate did appear different from the wild-type palate but alternatively the distributions of OCD were just as random (Fig. 8.18K-M). The orientation of spindles in the tip of the *Tbx-1*<sup>-/-</sup> mutant palate had rotated 90° clockwise compared to the tip region at E12.5 (Fig. 8.16N & 8.17N).

In the elevated wild-type palate at E14.5 spindles in the tip region were significantly different from a uniform distribution and were orientated along the mediolateral axis of the embryo (Fig. 8.18C). The spindles in the palate lateral to the tip region were showing a non-uniform distribution as well, and their combined distribution varied significantly from that of the cells in the tip region (Fig. 8.18C versus D, F & H).

After the *Tbx-1*<sup>-/-</sup> mutant palate had failed to elevate at E14.5 the prospective nasal side showed a distribution of spindle orientations that was significantly different from a uniform distribution (Fig. 8.18K). The direction of these spindles was slightly off from

the direction of elongation. The cells in the rest of the *Tbx-1*<sup>-/-</sup> palate had a similar weak bias in a variety of directions like that observed at previous stages (Fig. 8.18K-N).

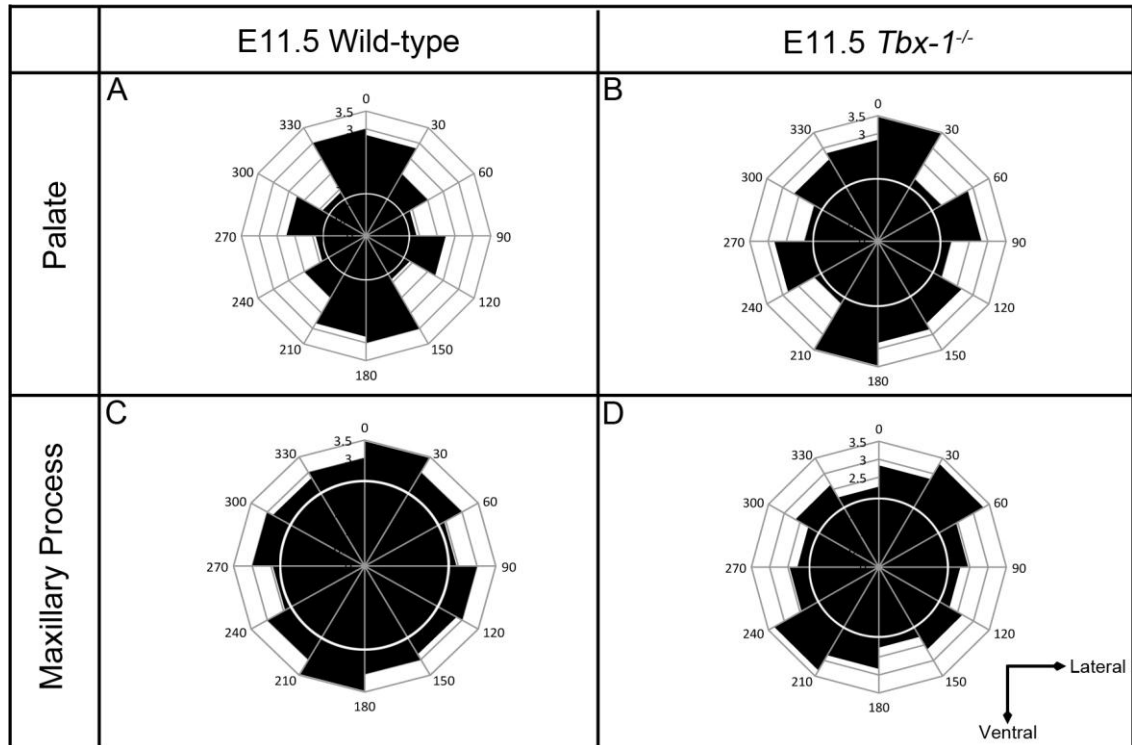


**Figure 8.15 Rose plots summarising the distribution of mitotic angles at E11.5 for wild-type and *Tbx-1*<sup>-/-</sup> palatal shelves** A) Distribution of mitotic spindle angles in the wild-type palatal outgrowth B) Distribution of mitotic spindle angles in the *Tbx-1*<sup>-/-</sup> mutant palatal outgrowth C) Distribution of mitotic spindle angles in the wild-type maxillary process D) Distribution of mitotic spindle angles in the *Tbx-1*<sup>-/-</sup> mutant maxillary process. The white circle represents a uniform distribution. The 180° point is towards the distal tip of the palate.

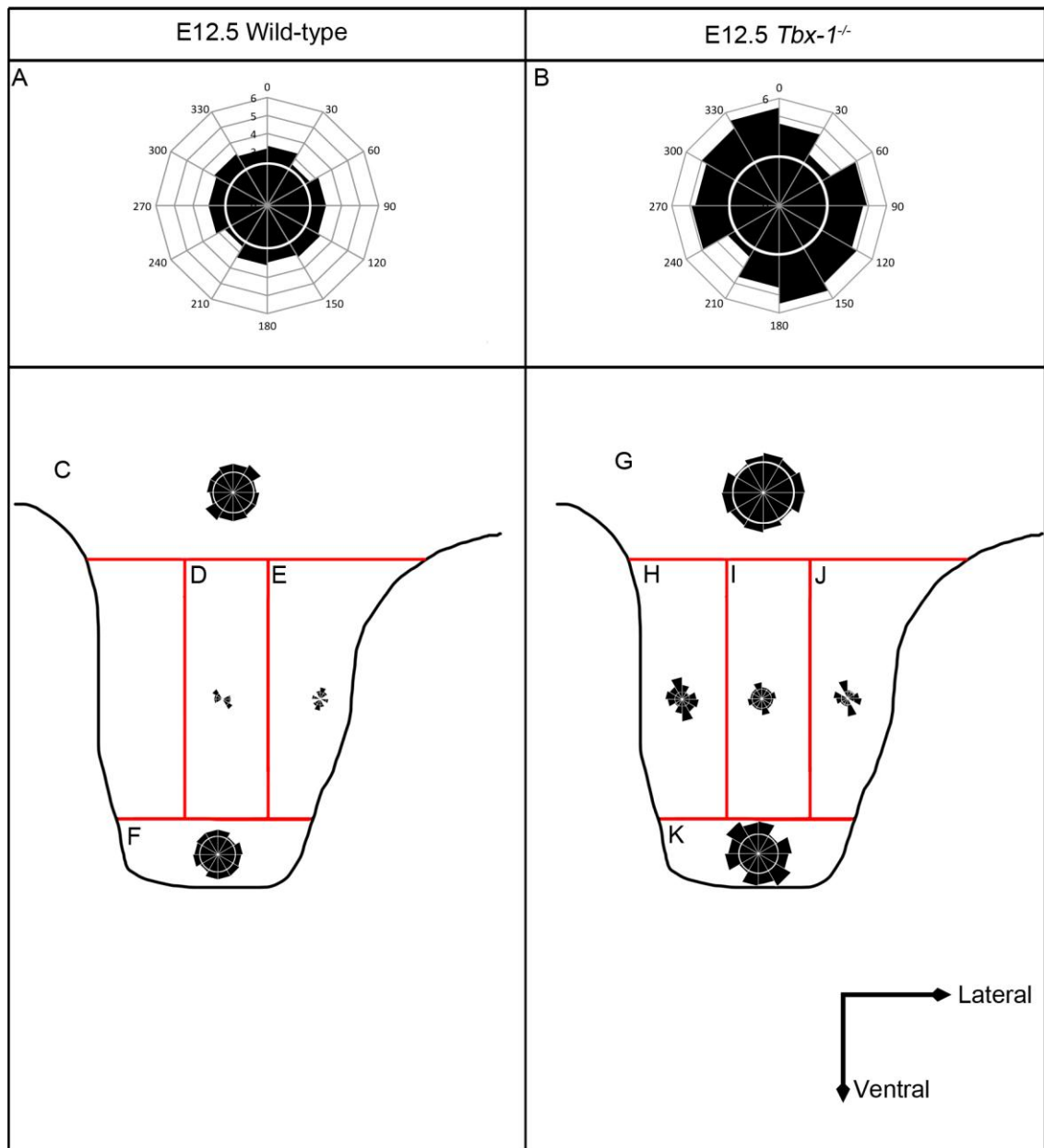


**Figure 8.16 Rose plots summarising the distribution of mitotic angles at E12.5 for wild-type and *Tbx-1*<sup>-/-</sup> palatal shelves** A) Distribution of mitotic spindle angles in the entire wild-type palatal outgrowth (D-F summed together) B) Distribution of mitotic spindle angles in cells in the entire *Tbx-1*<sup>-/-</sup> mutant palatal outgrowth (G-K summed together) C-F) Distribution of mitotic spindle angles in cells across different regions of the wild-type palate C) Mesenchymal cells adjacent to the palatal outgrowth D) Middle third E) Prospective oral third F) Tip G-K) Distribution of mitotic spindle angles in cells across different regions of the *Tbx-1*<sup>-/-</sup> mutant palate G) Mesenchymal cells adjacent to the palatal outgrowth H) Prospective nasal third I) Middle third J) Prospective oral third K) Tip. The white circle represents a uniform distribution. The 180° point is towards the distal tip of the palate.



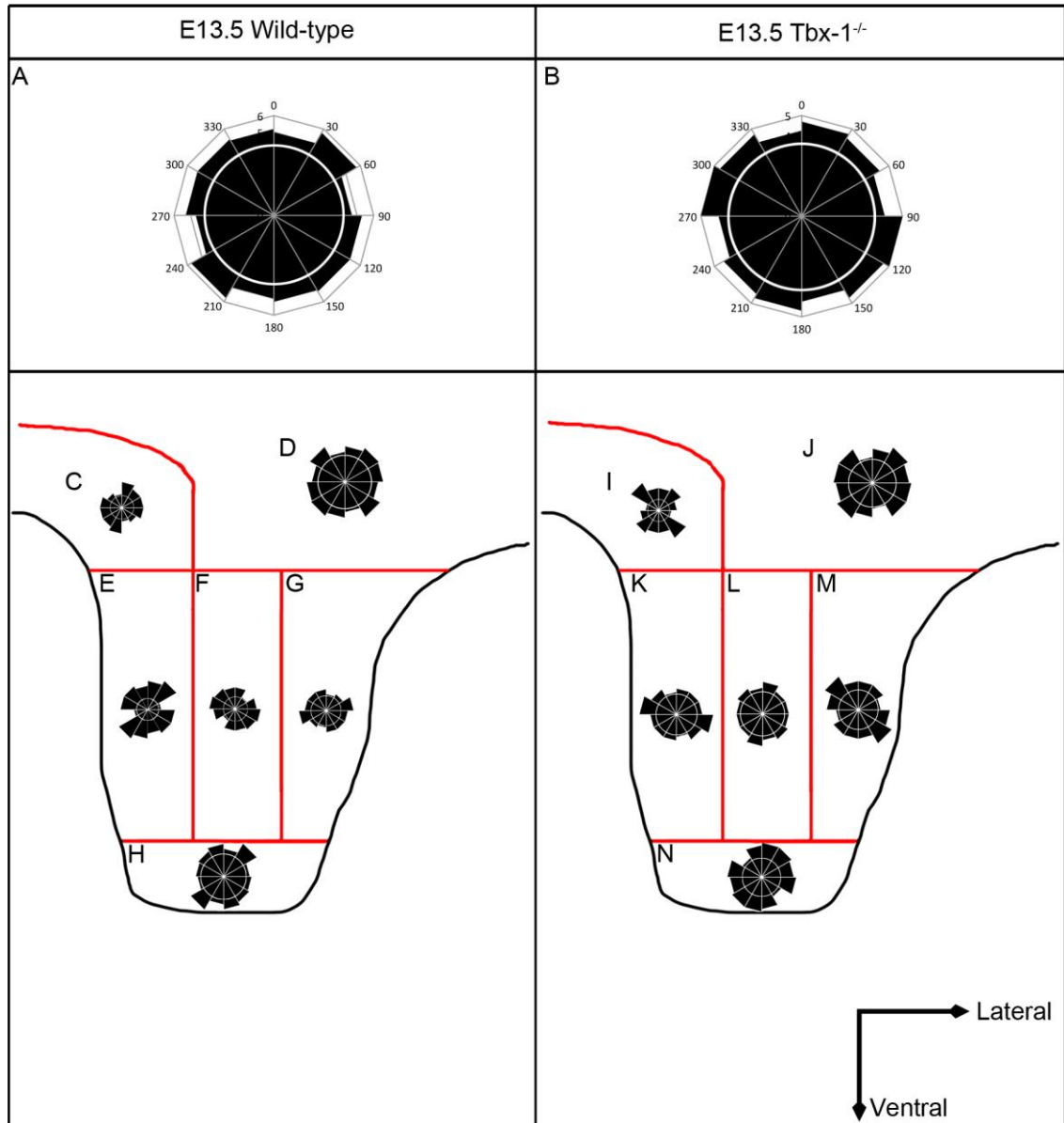


**Figure 8.17 Rose plots summarising the distribution of mitotic angles at E13.5 for wild-type and *Tbx-1*<sup>-/-</sup> palatal shelves** A) Distribution of mitotic spindle angles in the entire wild-type palatal outgrowth (E-H summed together) B) Distribution of mitotic spindle angles in the entire *Tbx-1*<sup>-/-</sup> mutant palatal outgrowth (K-N summed together) C-H) Distribution of mitotic spindle angles across different regions of the wild-type palate C) Shoulder region D) Mesenchymal cells adjacent to the palatal outgrowth E) Prospective nasal third F) Middle third G) Prospective oral third H) Tip I-N) Distribution of mitotic spindle angles across different regions of the *Tbx-1*<sup>-/-</sup> mutant palate I) Shoulder region J) Mesenchymal cells adjacent to the palatal outgrowth K) Prospective nasal third L) Middle third M) Prospective oral third N) Tip. The white circle represents a uniform distribution. The 180° point is towards the distal tip of the palate.

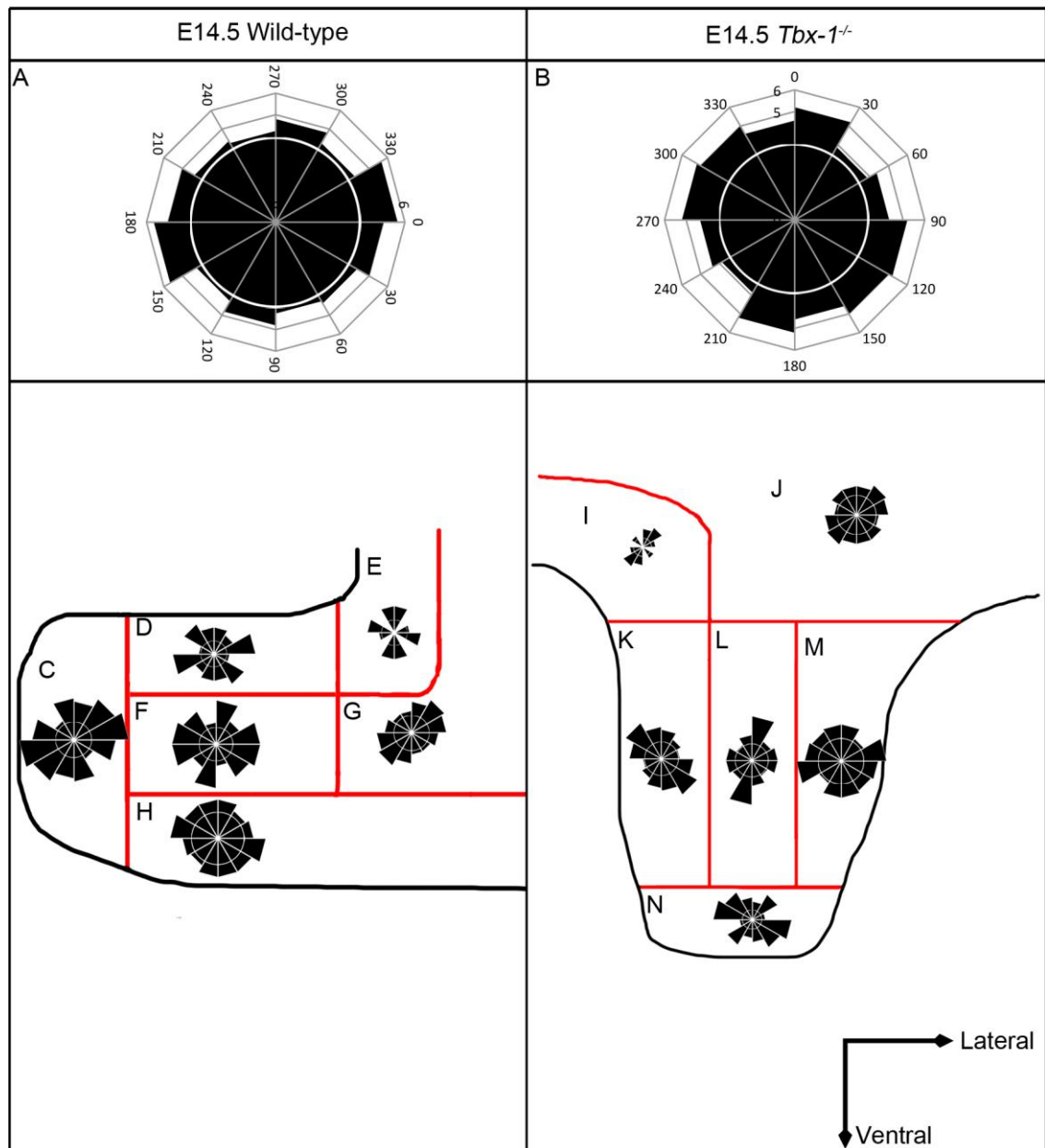


**Figure 8.18 Rose plots summarising the distribution of mitotic angles at E14.5 for wild-type and *Tbx-1*<sup>-/-</sup> palatal shelves** A) Distribution of mitotic spindle angles in the entire wild-type palatal outgrowth (E-H summed together) B) Distribution of mitotic spindle angles in the entire *Tbx-1*<sup>-/-</sup> mutant palatal outgrowth (K-N summed together) C-H) Distribution of mitotic spindle angles across different regions of the wild-type palate C) Tip D) Nasal third E) Nasal Shoulder F) Middle third G) Mesenchymal cells adjacent to the palatal outgrowth H) Oral third I-N) Distribution of mitotic spindle angles across different regions of the *Tbx-1*<sup>-/-</sup> mutant palate I) Shoulder region J) Mesenchymal cells adjacent to the palatal outgrowth K) Prospective nasal third L) Middle third M) Prospective oral third N) Tip. The white circle represents a uniform distribution. The 180° point is towards the distal tip of the palate.

### 8.3.5 Internuclear spacing in the *Tbx-1*<sup>-/-</sup> mutant

At E11.5 the *Tbx-1*<sup>-/-</sup> mutant palate was slightly less densely packed than the wild-type palate (Fig. 8.19) and it has already been noted that the wild-type palate was not as wide as the mutant at this stage (Fig. 8.4).

The level of cell density remained fairly constant as the palatal outgrowth proceeded to E12.5; the wild-type palate remained subtly more tightly packed than the *Tbx-1*<sup>-/-</sup> mutant palate (Fig. 8.20). There was also very little difference in the level of packing between the maxillary process and the palatal outgrowth in both genotypes (Fig. 8.20).

There were only very small differences in the cell packing by E13.5 seen in the anterior two-thirds of the wild-type palate (Fig. 8.21). There were regions of higher cell density in the anterior wild-palate whereas the packing in the anterior of *Tbx-1*<sup>-/-</sup> mutant palate remained more uniform (Fig. 8.21, black arrows). In the mid-palate of the wild-type the prospective oral side was more compact than the prospective nasal side and this extended towards the developing molar (Fig. 8.21B, dashed line separates the two different regions). This pattern was not seen in the *Tbx-1*<sup>-/-</sup> mutant palate (Fig. 8.21E). The anterior and posterior regions of the mutant palate are slightly more tightly packed than they were at E12.5, where the mid-palate does not seem to have changed (Fig. 8.20 versus 8.21). The posterior third of the *Tbx-1*<sup>-/-</sup> mutant palate is slightly more densely packed than its wild-type counterpart (Fig. 8.21C, C', F & F').

In both the elevated wild-type and non-elevated *Tbx-1*<sup>-/-</sup> mutant palate at E14.5 the cell density has decreased (Fig. 8.22). Within the palatal outgrowths themselves the mid-palate of the wild-type was the only place to have regions of blue, indicating more loosely packed cells (Fig 8.22B, black arrows). This is the region of the palate that grows and reaches the mid-line first. The cell density in the anterior and posterior regions was very similar at this stage (Fig. 8.22C, C', F & F').

By E15.5 the wild-type palate had extended towards the midline and fused and the packing was now less dense, compared to the *Tbx-1*<sup>-/-</sup> mutant in both the anterior and mid-palate (Fig. 8.23A, B, D & E). Between E14.5 and E15.5 the unelevated *Tbx-1*<sup>-/-</sup> mutant palate became more tightly packed along its entire AP axis (Fig. 8.23D-F) as it appeared gets slightly squashed in the gap left between the tongue and the mandible.

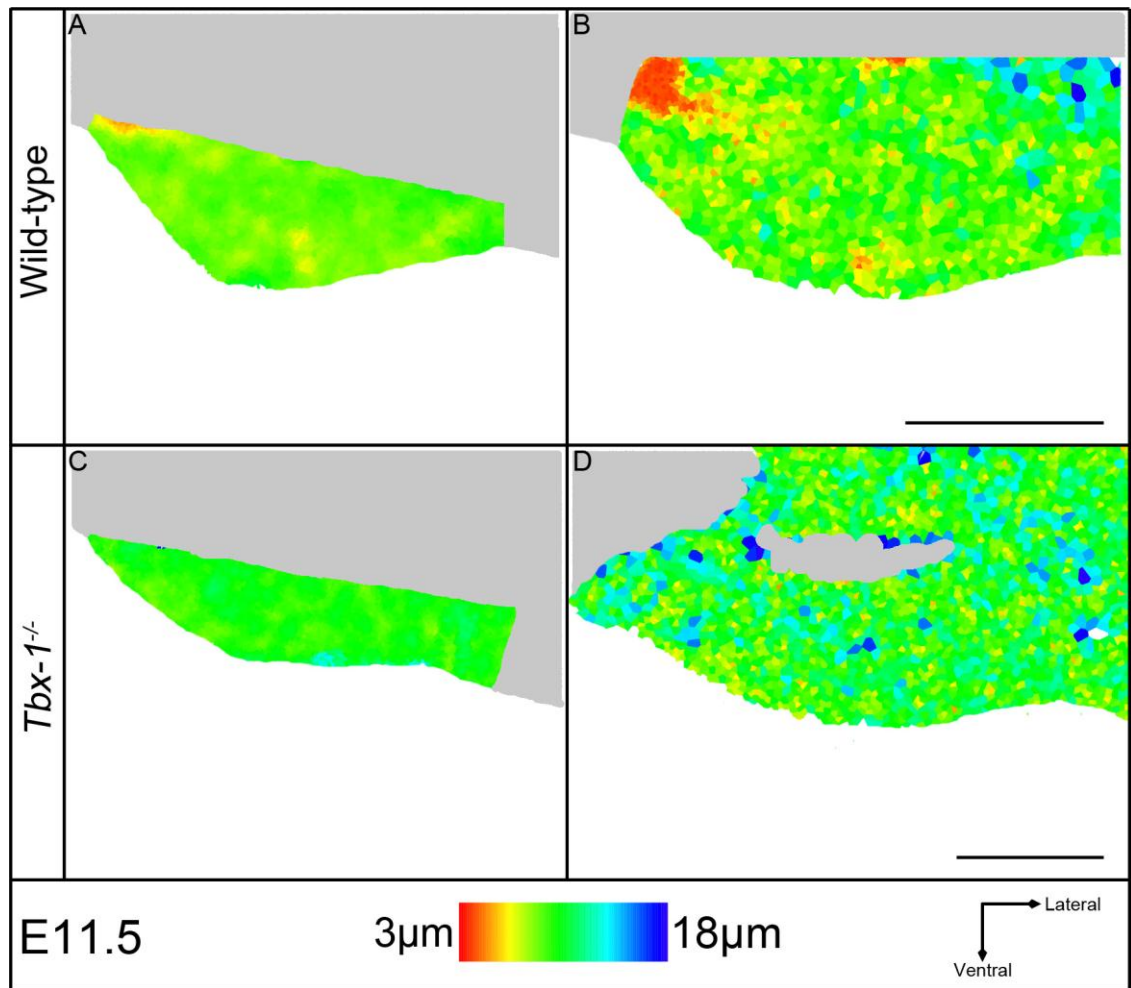


**Figure 8.19 Internuclear spacing heat maps of E11.5 wild-type and *Tbx-1*<sup>-/-</sup> palatal shelves** A) Heat map of the wild-type palate B) Individual heat map of the wild-type palate C) Heat map of the *Tbx-1*<sup>-/-</sup> mutant palate D) Individual heat map of the *Tbx-1*<sup>-/-</sup> mutant palate. Each heat map is an average of three individual sections. Scale bars represent 200 μm.

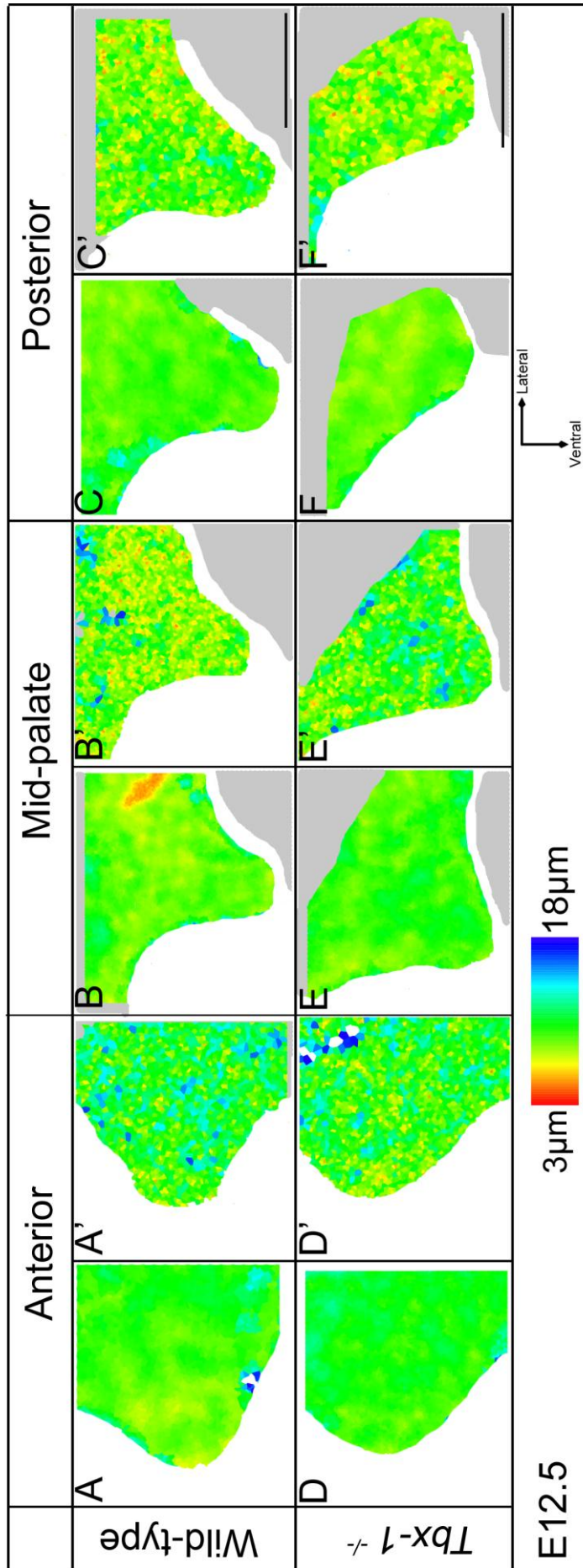


**Figure 8.20 Internuclear spacing heat maps of E12.5 wild-type and *Tbx-1*<sup>-/-</sup> palatal shelves** A) Heat map of the wild-type anterior palate A') Individual heat map of the wild-type anterior palate B) Heat map of the wild-type mid-palate B') Individual heat map of the wild-type mid-palate C) Heat map of the wild-type posterior palate C') Individual heat map of the wild-type posterior palate D) Heat map of the *Tbx-1*<sup>-/-</sup> mutant anterior palate D') Individual heat map of the *Tbx-1*<sup>-/-</sup> mutant anterior palate E) Heat map of the *Tbx-1*<sup>-/-</sup> mutant mid-palate E') Individual heat map of the *Tbx-1*<sup>-/-</sup> mutant mid-palate F) Heat map of the *Tbx-1*<sup>-/-</sup> mutant posterior palate F') Individual heat map of the *Tbx-1*<sup>-/-</sup> mutant posterior palate. Each heat map is an average of three individual sections. Scale bars represent 200 µm.

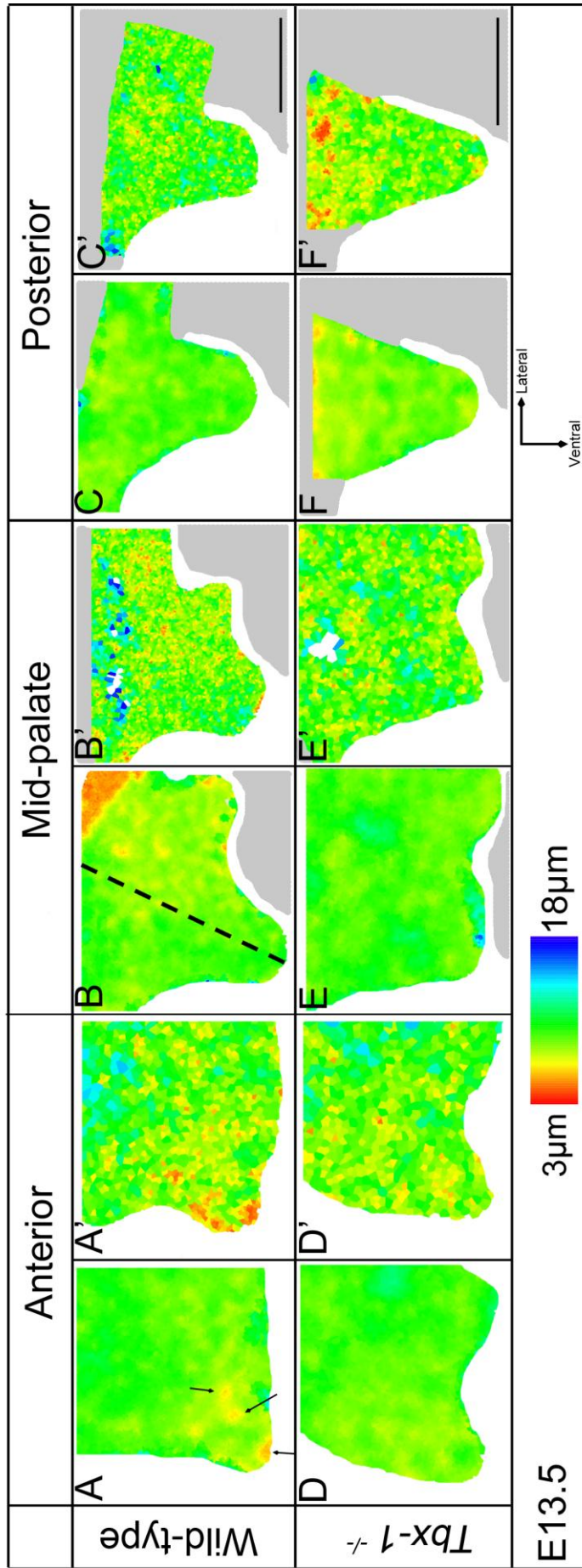


**Figure 8.21 Internuclear spacing heat maps of E13.5 wild-type and *Tbx-1*<sup>-/-</sup> palatal shelves** A) Heat map of the wild-type anterior palate. Black arrows indicate regions of more tightly packed cells. A') Individual heat map of the wild-type anterior palate B) Heat map of the wild-type mid-palate. Dashed line separates the slightly more tightly packed prospective oral side from the less densely packed cells on the prospective nasal side B') Individual heat map of the wild-type mid-palate C) Heat map of the wild-type posterior palate C') Individual heat map of the wild-type posterior palate D) Heat map of the *Tbx-1*<sup>-/-</sup> mutant anterior palate D') Individual heat map of the *Tbx-1*<sup>-/-</sup> mutant anterior palate E) Heat map of the *Tbx-1*<sup>-/-</sup> mutant mid-palate E') Individual heat map of the *Tbx-1*<sup>-/-</sup> mutant mid-palate F) Heat map of the *Tbx-1*<sup>-/-</sup> mutant posterior palate F') Individual heat map of the *Tbx-1*<sup>-/-</sup> mutant posterior palate. Each heat map is an average of three individual sections. Scale bars represent 200 µm.

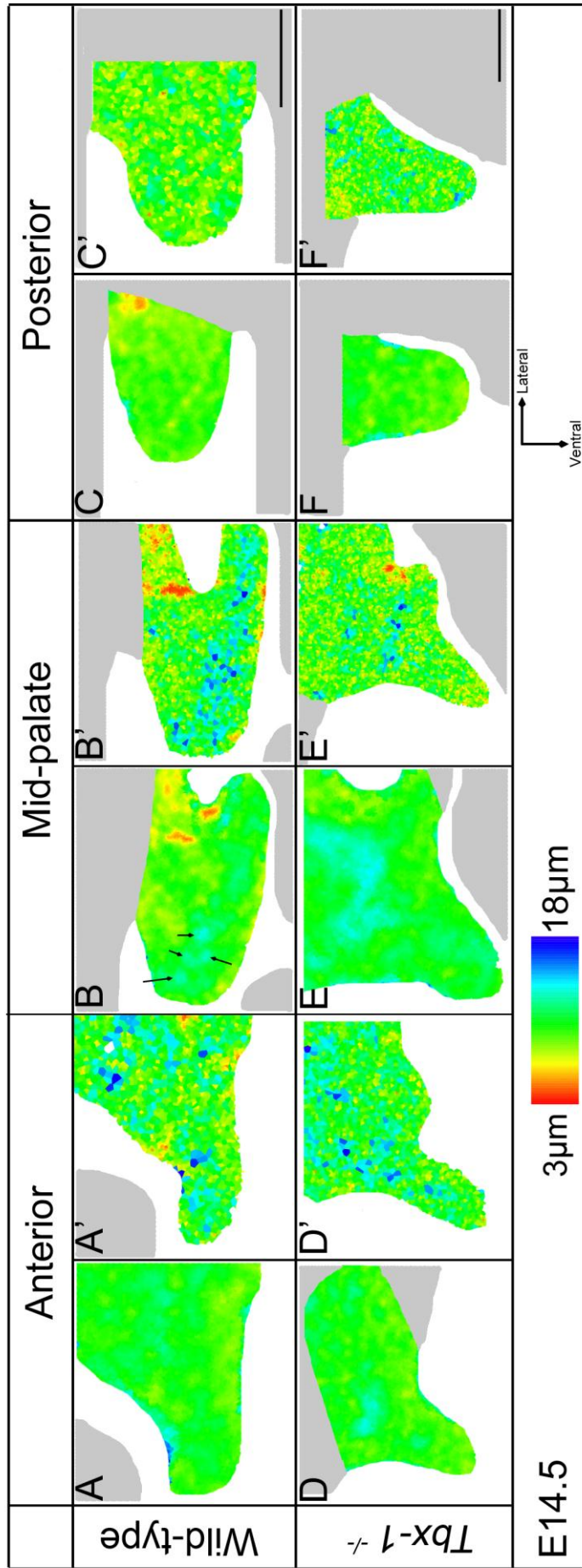


**Figure 8.22 Internuclear spacing heat maps of E14.5 wild-type and *Tbx-1*<sup>-/-</sup> palatal shelves** A) Heat map of the wild-type anterior palate A') Individual heat map of the wild-type anterior palate B) Heat map of the wild-type mid-palate. Black arrows indicate regions of more loosely packed cells B') Individual heat map of the wild-type mid-palate C) Heat map of the wild-type posterior palate C') Individual heat map of the wild-type posterior palate D) Heat map of the *Tbx-1*<sup>-/-</sup> mutant anterior palate D') Individual heat map of the *Tbx-1*<sup>-/-</sup> mutant anterior palate E) Heat map of the *Tbx-1*<sup>-/-</sup> mutant mid-palate E') Individual heat map of the *Tbx-1*<sup>-/-</sup> mutant mid-palate F) Heat map of the *Tbx-1*<sup>-/-</sup> mutant posterior palate F') Individual heat map of the *Tbx-1*<sup>-/-</sup> mutant posterior palate. Each heat map is an average of three individual sections. Scale bars represent 200 µm.

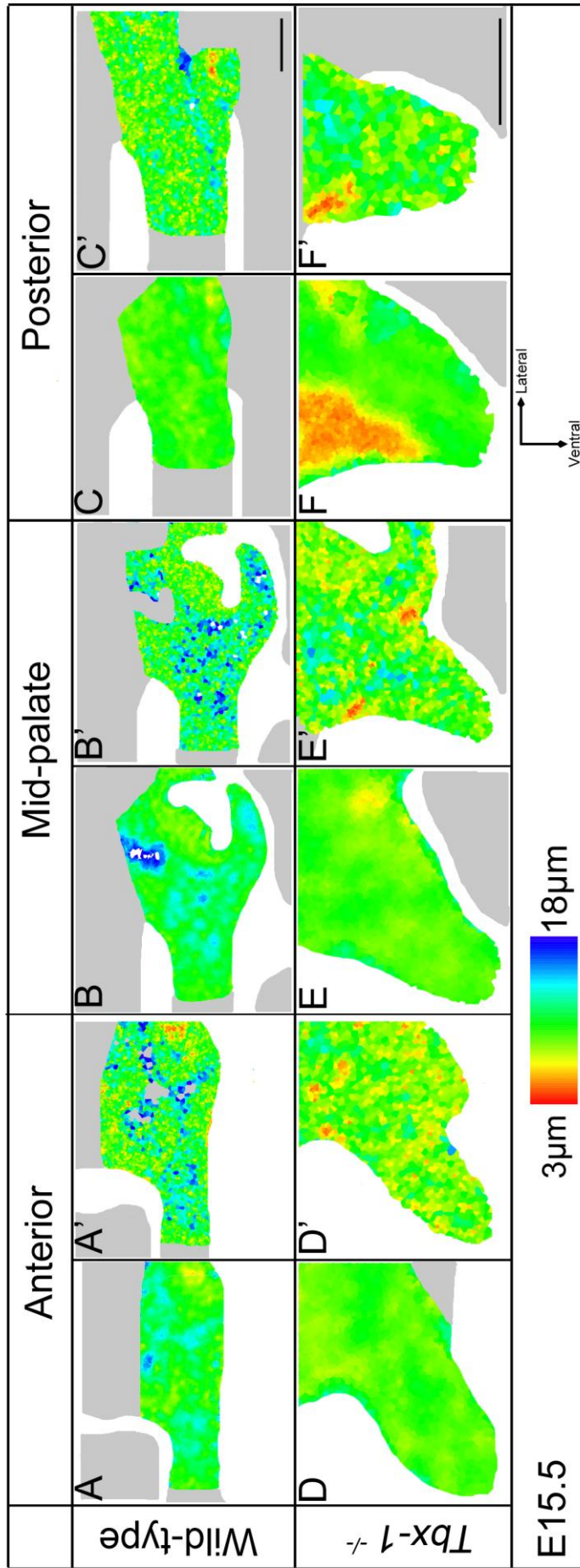


**Figure 8.23 Internuclear spacing heat maps of E15.5 wild-type and *Tbx-1*<sup>-/-</sup> palatal shelves** A) Heat map of the wild-type anterior palate A') Individual heat map of the wild-type anterior palate B) Heat map of the wild-type mid-palate B') Individual heat map of the wild-type mid-palate C) Heat map of the wild-type posterior palate C') Individual heat map of the wild-type posterior palate D) Heat map of the *Tbx-1*<sup>-/-</sup> mutant anterior palate D') Individual heat map of the *Tbx-1*<sup>-/-</sup> mutant anterior palate E) Heat map of the *Tbx-1*<sup>-/-</sup> mutant mid-palate E') Individual heat map of the *Tbx-1*<sup>-/-</sup> mutant mid-palate F) Heat map of the *Tbx-1*<sup>-/-</sup> mutant posterior palate F') Individual heat map of the *Tbx-1*<sup>-/-</sup> mutant posterior palate. Each heat map is an average of three individual sections. Scale bars represent 200 µm.



## 8.4 *Tbx-1*<sup>-/-</sup> palate development: Discussion

There is debate in the literature over the cause of the cleft in the *Tbx-1*<sup>-/-</sup> mouse. Studies identified both elevated and decreased proliferation at apparently the same stage compared to the wild-type (Funato et al., 2012; Goudy et al., 2010). A full high-resolution study of proliferation in the *Tbx-1*<sup>-/-</sup> mutant during palate development was required. By using IddU instead of PH-3 more information can be gained because slightly more cells are stained as once the IddU is incorporated into the DNA it remains there. Higher numbers of stained cells can help highlight statistically significant differences more reliably and, also importantly, from fewer embryos. This analysis revealed that levels of proliferation in the *Tbx-1*<sup>-/-</sup> mutant palate do vary significantly from the wild-type palate but only at two stages, E13.5 and E15.5, and the level of proliferation manages to normalise between these stages. This analysis also identified stages, E11.5 and E12.5, where the level of proliferation was higher in the mutant than the wild-type. Although this trend is not currently significant it could reach a statistically significant level with a higher n number. Also if other groups used a different strain or had slightly different staging criteria they might have reported this result in their E13.5 dataset. This demonstrates that something more complex and interesting than a mere decrease in proliferation is going on.

Merscher et al., (2001) linked DGS and the *Tbx-1* gene and proposed that the defect is in the migrating cranial NCC. These normally migrate into the palatal outgrowth at the base of the maxillary process and so if the defect was due to their improper migration the evidence should be clear at E11.5. This project identified no significant differences between the wild-type and mutant palate at E11.5 so it is unlikely that the defect is linked directly to the migration of the neural crest.

The main differences during palatal development between the wild-type and *Tbx-1*<sup>-/-</sup> mouse, in the processes studied here, were in the orientation of the Golgi. Significant differences in the distribution of the Golgi were seen between the wild-type and mutant palate from E12.5 onwards.

By E13.5 the statistically significant differences in Golgi orientation can be seen in small regions throughout the palate. As an aside, this potentially shows that if a pattern of the distribution being tested is significantly different a manageable number of measurements are needed. Therefore perhaps enough spindles have been

measured for the OCD data and the random distributions seen are true and will remain random even if the n number is hugely increased.

A possible mechanism being disrupted as a consequence of the incorrect orientation of the Golgi is cell migration. This is potentially particularly important in the posterior palate for the purpose of elevation by a remodelling mechanism. The wild-type cells in the posterior palate reorientate from a ventral to a more dorsal direction prior to elevation, possibly a sign that the cells are starting to retract from their position down the side of the tongue ready to flow across the top of the oral cavity. This change in orientation did not occur in the *Tbx-1*<sup>-/-</sup> mutant, the Golgi was orientated randomly and a cleft palate is formed.

An alternative mechanism that could have been disrupted, as well as or instead of, was the direction of cellular secretions. The composition of the ECM is also thought to be important in the process of palate elevation, particularly in the anterior palate. The cleft could be due to the incorrect composition or amount of ECM throughout the palate, particularly as this could be contributing to the stiffness of the palate, the posterior could become too stiff to remould or the anterior not rigid enough to flip upwards.

The *Tbx-1*<sup>-/-</sup> mouse has other craniofacial defects and these mean the extrinsic conditions may also not be correct to allow the palate to develop. Normally immediately prior to elevation the tongue drops ventrally, removing the physical block from the palatal shelves and providing more room for them once they are horizontal. Another symptom of DGS is micrognathia a small jaw, and if the jaw does not elongate properly the tongue has no room to move down and will remain high in the oral cavity blocking the palatal shelves (Jerome and Papaioannou, 2001). *Tbx-1*<sup>-/-</sup> mice have been shown to have a higher than normal tongue (Goudy et al., 2010). This would impact the potential flip-up mechanism of elevation that occurs in the anterior palate as it requires the tongue to move out of the way to elevate properly (assuming the intrinsic factors are all correct).

The *Tbx-1* palate has been shown to be able to fuse in culture therefore it is not a defect in the fusion process that is causing the cleft palate. Although occasionally abnormal epithelial fusions occur between the palatal shelf and oral or tongue epithelium, which do contribute to some cases of the cleft palate in the *Tbx-1*<sup>-/-</sup> mouse (Goudy et al., 2010).

Occasionally a *Tbx-1*<sup>-/-</sup> palatal shelf is able to elevate in vivo but a cleft palate still occurs due to a failure to reach the midline or the other shelf may not have elevated. This means that it is very likely that the defect occurs during the outgrowth process. Also because elevation sometimes occurs it may be that *Tbx-1* has a dose-dependent effect or something is partially compensating for the loss of *Tbx-1*.

The effect *Tbx-1* has on proliferation is often linked to *Fgf10* activity. An *Fgf10* null mouse also displays a cleft palate but the double heterozygous *Tbx-1/Fgf10* mouse does not have a cleft palate. Palate development can cope with reduced levels of *Tbx-1* and *Fgf10* signals but not a complete loss of either of them. Also the underlying level of proliferation appears to be more constant in the *Tbx-1*<sup>-/-</sup> palate compared to the wild-type which has a statistically significant change across every 24 hour time period tested. So *Tbx-1*, potentially through a pathway involving *Fgf10*, might be more involved in the final refinement of proliferation levels rather than being the key driving force behind proliferation in the palate.

The difference between the wild-type and mutant palate is most obvious in the E15.5 heat maps and this is potentially because often *Tbx-1*<sup>-/-</sup> embryos do not make it to full term so it is possible these embryos would have aborted naturally before they were born and we are seeing the first stages of this. The common deterioration seen in E15.5 embryos could be due to the cumulative effect of several different behaviours going wrong, this could mean the significantly lower proliferation at E15.5 was more of a consequence of the palatogenesis going wrong rather than a direct cause. Also by this stage perhaps some key signals have been missed that drive development. There also seemed to be a variation in the age when embryos were naturally aborted and variations in the extent of the phenotype. For example there are cases where one palatal shelf has been seen to elevate and others where the palatal epithelium fuses with the tongue (Goudy et al., 2010). This could account for variations or larger error bars in the mutants, because they are not all experiencing exactly the same reaction to the lack of *Tbx-1*. If levels of proliferation are varying slightly then this could account for different groups getting different results especially if they do not sample along the entire palate. For example at E13.5 the middle and posterior thirds of the palate do not vary significantly from the wild-type but only the anterior third is significantly lower. If an analyst sampled from just the posterior two thirds they would get different results from one that was biased towards the anterior third.

*Tbx-1* is expressed in the palatal epithelium, but it is possible that it has a significant effect on the developing mesenchyme as it has been shown to control the size of the thyroid gland by acting from the neighbouring mesodermal cells (Fagman et al., 2007). *Tbx-1* is expressed more strongly in the anterior of the palate (Zoupa et al., 2006) but the effects of losing *Tbx-1* are not restricted to the anterior third of the palate. For example although the non-uniform distribution of Golgi orientation is lost in the anterior thirds of the E12.5 and E13.5 *Tbx-1*<sup>-/-</sup> palates it is actually the middle third that displays a distribution of Golgi that varies significantly from the wild-type. Also at E14.5 it is only the posterior third of the palate that has a significantly different, and higher, level of proliferation from the wild-type embryos. This shows that *Tbx-1* possibly has different roles along the AP axis of the development of the palate. In the anterior it could be mediating the *Shh/Fgf10* interaction (Lan and Jiang, 2009) that has been shown to control mesenchymal proliferation. Whereas in the posterior it could be acting in or mediating a different pathway, particularly because *Shh* expression is restricted to the rugae that are not found in the posterior palate (Rice et al., 2006).

Loss of the *Tbx-1* gene results in a cleft palate as part of a DGS mouse model. *Tbx-1* appears to have a role in regulating several different mechanisms of morphogenesis. The cause of the cleft palate is a combination of factors leading to the improper outgrowth of the palate and a physical block against elevation from the tongue. The intrinsic mechanism of morphogenesis affected the most is the position of the Golgi within the cell, which is an indicator of cell polarity, and could affect the orientated cell behaviours required by the posterior palate to elevate by remodelling.

Importantly, this work has shown that not only must more than one mechanism of morphogenesis be studied but that it is important to consider the time series and the resolution at which the phenotype is analysed. At some stages proliferation is disrupted in the *Tbx-1*<sup>-/-</sup> mutant but Golgi orientation shows significant disruption throughout palate development. Also as the changes in proliferation were quite subtle conflicting results could be recorded if a sample is biased towards certain regions of the palate.

## 9.0 *Msx-1*<sup>-/-</sup> knockout mouse

### 9.1 Introduction to *MSX-1*

#### 9.1.1 *Msx-1*<sup>-/-</sup> phenotype

*Msx-1* is a vertebrate hox gene and was first isolated in *Drosophila* as *msh* (muscle segment homeobox) gene (Davidson, 1995; Satokata and Maas, 1994). *Msx-1* is involved in signalling between the epithelium and mesenchyme and is involved in the development of many different systems, for example the limb, Rathke's pouch, the mandible and tooth.

Homozygous *Msx-1*<sup>-/-</sup> mice display a range of defects and die very soon after birth (Fig. 9.1A). The defects include a complete cleft of the secondary palate; the palatal shelves of the *Msx-1*<sup>-/-</sup> mice do elevate but do not fuse with each other or the nasal septum (Fig. 9.1A-C). The upper incisors are missing altogether and both the maxillary and mandibular alveolar processes are missing. The molars also do not develop properly (Fig. 9.1D), at E14.5 the wild-type tooth has reach the cap stage whereas the *Msx-1*<sup>-/-</sup> tooth remains at the bud stage (Satokata and Maas, 1994). The mandible has a slightly reduced length and the frontal and parietal skull bones develop abnormally. The malleus of the middle ear is shorter than normal, but the incus and stapes develop normally.

Mutations in the human *MSX-1* gene have been linked to witkop syndrome, also known as tooth and nail syndrome (Jumlongras et al., 2001). It is a rare autosomal dominant disorder with an incidence of around 1:10,000 live births. The symptoms include ectodermal dysplasias and clefting.

The *Msx-1*<sup>-/-</sup> mouse is also a useful model of isolated secondary palate in humans, accompanied with oglodontia (a condition where fewer than a full complement of teeth develop). These defects also occur in Pierre Robin syndrome, which includes other symptoms such as micrognathia (undersized jaw) and glossoptosis (incorrect tongue position in the upper airway). This syndrome occurs in between 1:2,000 – 1:30,000 births depending on how it is defined, it does not always include a cleft palate but it

never includes a cleft lip. The similarities between the *Msx-1*<sup>-/-</sup> mice and human cases of isolated cleft palate are often seen alongside other craniofacial deficiencies, such as abnormal head size and cranial shape. This implies that the gene has a pleiotropic effect.

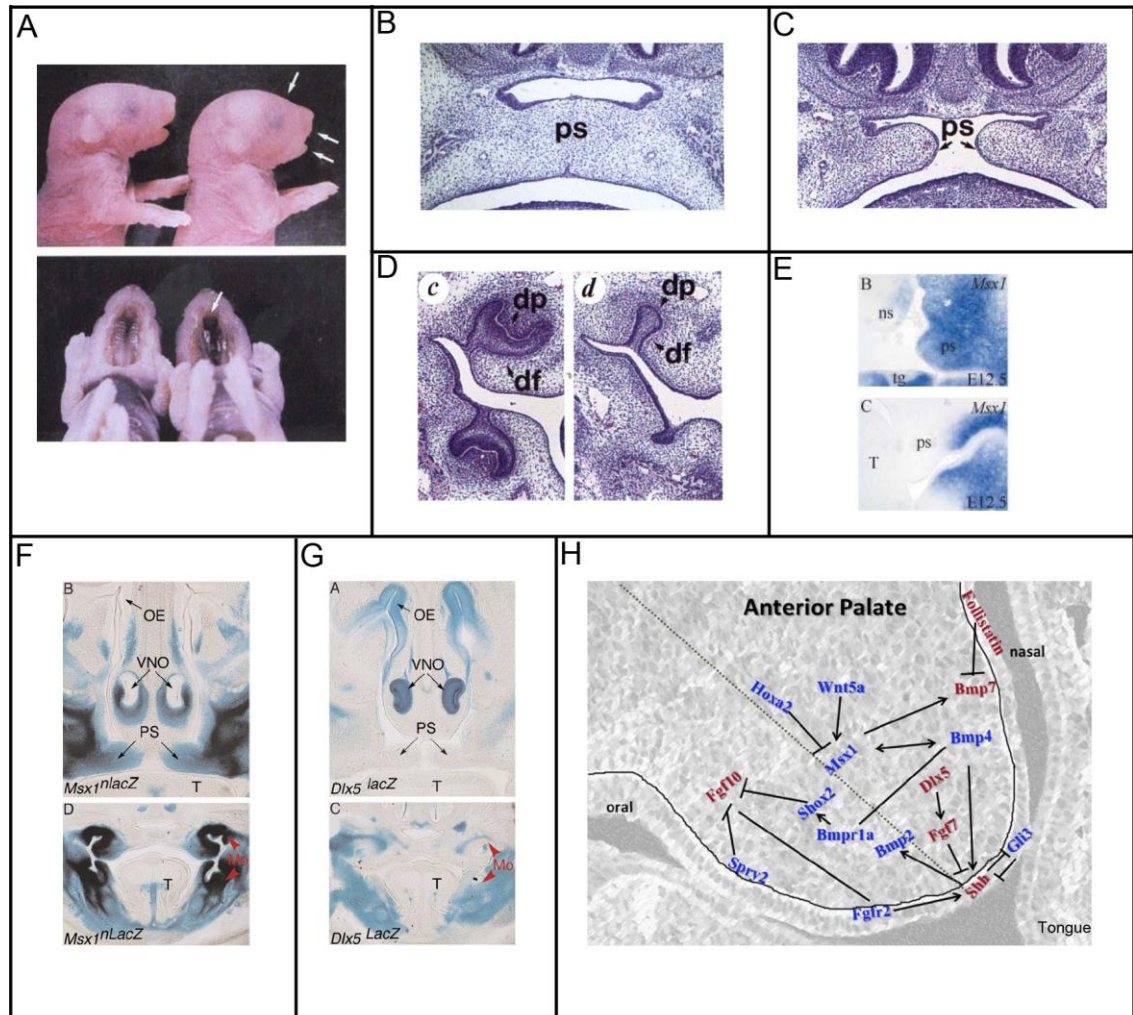


**Figure 9.1 *Msx-1*<sup>-/-</sup> mutant mice phenotype** A) Wild-type and *Msx-1*<sup>-/-</sup> new born mice. The mutant has a shortened maxilla and mandible, a more rounded frontal bone of the skull and a cleft secondary palate (white arrows) B) Frontal section of a wild-type E14.75 palate starting to fuse C) Frontal section of an *Msx-1*<sup>-/-</sup> mutant palate, the shelves have elevated but have not met in the midline D) Wild-type and *Msx-1*<sup>-/-</sup> mutant molar development; both upper and lower molar development is defective in the *Msx-1*<sup>-/-</sup> mutant. A-D adapted from Satokata & Maas, 1994 E) *Msx-1* is expressed in the mesenchyme of the anterior but not the posterior palate at E12.5. Adapted from Hilliard et al., 2005 F) Expression of *Msx-1*<sup>nlacZ</sup> by X-gal staining in the anterior (top) and posterior (bottom) palate and surrounding craniofacial structures at E14.5 G) Expression of *Dlx-5*<sup>lacZ</sup> by X-gal staining in the anterior (top) and posterior (bottom) palate and surrounding craniofacial structures at E14.5. Adapted from Levi et al., 2006 H) Diagram of the potential signaling pathways, involving *Msx-1*, regulating the development of the anterior palate. Adapted from Smith et al., 2013. Df, dental follicle mesenchyme; dp, dental papilla mesenchyme; Mo, molar buds; OE, olfactory epithelium; Ps, palatal shelf; T, tongue; VNO, vomeronasal organ

### 9.1.2 *Msx-1* expression pattern

The defects displayed by *Msx-1*<sup>-/-</sup> mice are mainly in bone and tooth development and in structures that develop from the first pharyngeal arch and involve the cranial neural crest. Around E9 – E10 *Msx-1* is expressed in the cranial NCC as they begin to migrate. The tooth defect has been linked to a lack of *Msx-1* in the dental mesenchyme to respond to the *Bmp-4* signal from the dental epithelium that, in wild-type, induces tooth development. *Msx-1* is also required for the progression of tooth development from bud to cap stage as this process fails to occur. *Msx-1* is normally expressed at E12.5 in the mesenchyme of the anterior palate (Fig. 9.1E), which is defined as anterior to the first molar (Hilliard et al., 2005).

### 9.1.3 *Msx-1* pathway in palatal development

*Msx-1*<sup>-/-</sup> mice, which have a cleft palate, have reduced proliferation in the anterior palate (Zhang et al., 2002) at E12.5 and E13.5. It is not due to a failure to elevate or fuse but the initial outgrowth is incorrect so the later stages cannot occur correctly. The two *Msx-1*<sup>-/-</sup> palatal shelves were capable of fusion when they were placed together in culture (Zhang et al., 2002). These results also suggested that palatal fusion occurs in a zip-up mechanism where the posterior palate, unaffected by the loss of *Msx-1*, cannot fuse until the more anterior palate has done so. This mouse mutant has been included in the following work to act as a control, to make sure our assays produce the same result and potentially to learn something more about the role *Msx-1* plays in palate development.

*Msx-1* is required for the correct expression of *Bmp-4* and *Bmp-2* in the palatal mesenchyme and *Shh* in the MEE. Ectopic *Bmp-4* can rescue the cleft palate and return *Bmp-2* and *Shh* expression to normal (Zhang et al., 2002). *Shh* is thought to promote *Bmp-2* activity, which increases cell proliferation and it is thought that the *Bmp-2* affects the cell's mitotic activity, this was shown by placing beads on explanted anterior palatal mesenchyme from wild-type and *Msx-1*<sup>-/-</sup> mice. When the beads were soaked in *Bmp-2* the level of proliferation increased in both the wild-type and mutant tissue after just 8 hours (Zhang et al., 2002). When the beads were soaked in *Shh* no change in proliferation was seen for 24 hours, when it increased, again in both genotypes, indicating that *Shh* may be acting via an indirect mechanism. The Bmp-inhibitor, noggin, is capable of decreasing proliferation in the anterior palate of wild-

type embryos. This is evidence that *Bmp-2* is probably acting downstream of *Shh* to control proliferation in the anterior palate. *Bmp-2* had no effect on proliferation in the posterior palate. This growth factor network is supported by the expression patterns of *Bmps* and *Shh* in both the wild-type and *Msx-1*<sup>-/-</sup> mice (Fig. 9.1H); with the protein from each gene transporting the message between the epithelium and mesenchyme.

Since the work of Zhang et al. (2002) other genes have been added to the anterior palate regulatory network and some have been shown to be restricted to just one side of the palate. As well as contributing to proliferation through the described linear pathway *Msx-1* also affects proliferation through *Bmp-7* and its antagonist Follistatin (Levi et al., 2006), but just along the prospective nasal epithelium. *Bmp-7* is expressed along the entire anteroposterior axis and loss of *Msx-1* leads to it being down-regulated in the anterior palate but up-regulated in the posterior palate.

*Msx-1* is downstream of the *Foxe-1* gene and deletion of this gene leads to reduced expression of *Msx-1* (Venza et al., 2011). In contrast decreased *Spry2* expression leads to increased *Msx-1* expression and increased proliferation in the palate (Welsh et al., 2007), linking *Msx-1* and *Fgf* activity. *Fgf10* null palates do not display altered *Msx-1* expression but *Fgf9* or *Fgf7* may also be involved in *Spry2* regulation. Whether working alongside or completely separate from *Fgfs*, it has been shown that *Msx-1* expression is also under the control of *Hoxa2* (Smith et al., 2009). The majority of *Hoxa2* null mice display a cleft palate with elevated *Msx-1*, *Bmp-4* and proliferation levels. Interestingly this gene is not expressed in the first branchial arch, from which the NCC that contribute to the palate arise so the strict regulation of these genes changes temporally.

*Msx-1* and *Dlx5*, another homeobox gene, have different expression patterns that only overlap in regions where they act independently on morphogenesis (Fig. 9.1F-G) (Levi et al., 2009). In the double knockout of these genes the cleft palate seen in the *Msx-1* mutant mouse is partially rescued. Both genes affect the expression domains and levels of *Shh*, *Fg-7* and *Follistatin* (Han et al., 2009). Work has indicated that *Dlx5* regulated *Fgf-7*, which represses *Shh* and a feedback loop is thought to be involved in regulating the exact levels of the expression of these genes and their products. Therefore in the double knockout the loss of *Shh* activity from the loss of *Msx-1* was compensated for by an up-regulation of *Shh* via *Fgf-7* due to the loss of the *Dlx5*, and leading to an overall increase in proliferation so the normal *Msx-1*<sup>-/-</sup> cleft palate phenotype was not seen.



Other genes and transcription factors have been described as having a role in palate development and this also includes further interactions with the genes discussed here. These have recently been fully reviewed by Smith et al., 2012. These genes have been shown to interact in other developing systems, such as the limb (Laufer et al., 1994) and the gut (Robert et al., 1989) and they are thought to control different cell behaviours when contributing to the formation of different organs.

The Msx-1 protein undergoes post-translational alterations. This is another stage at which something could be going wrong and contributes to the cleft palate. The protein undergoes sumoylation (Gupta and Bei, 2006) which affects its ability to bind with other proteins, although its exact role in mouse and human normal or cleft palate is unclear (Zhang et al., 2008).

## **9.2 *Msx-1*<sup>-/-</sup> Methods**

Two heterozygous *Msx-1*<sup>+/-</sup> mice were bred to produce *Msx-1*<sup>-/-</sup> embryos. The mothers were injected with IddU 2.5 hours prior to sacrifice and the embryos were removed, fixed, embedded, sectioned and stained as described in section 2.3.4-2.5. Every other section of the palate was imaged with an n=3 per stage for embryos at E11.5-E14.5 and the images were analysed as described in sections 2.6-2.8.

## **9.3 *Msx-1*<sup>-/-</sup> Results**

### **9.3.1 *Msx-1*<sup>-/-</sup> phenotype**

During the processes of palate development some regions were able to maintain more similarities to the wild-type mice than others; this may also be affected by the extremity of the phenotype. On average the wild-type palatal outgrowth was significantly wider than the mutant at E11.5 but there was no significant difference in the height (Fig. 9.2A & B). The same pattern between the two genotypes could be seen at E12.5.

By E13.5 the mutant palate was significantly shorter than the wild-type palate and there was no significant difference in width (Fig. 9.2A). From observations of the

palate at E13.5 it can sometimes look squarer, more like a wild-type E14.0, having lost its characteristic “U” shape (Fig. 9.2D).

*Msx-1*<sup>-/-</sup> palatal shelves are capable of elevating but do not always do so by E14.5. The embryos used for the E14.5 stage in this project had, at least partially, elevated. The mutant palates were now significantly shorter and narrower than the wild-types of the same age (Fig. 9.2A & E).

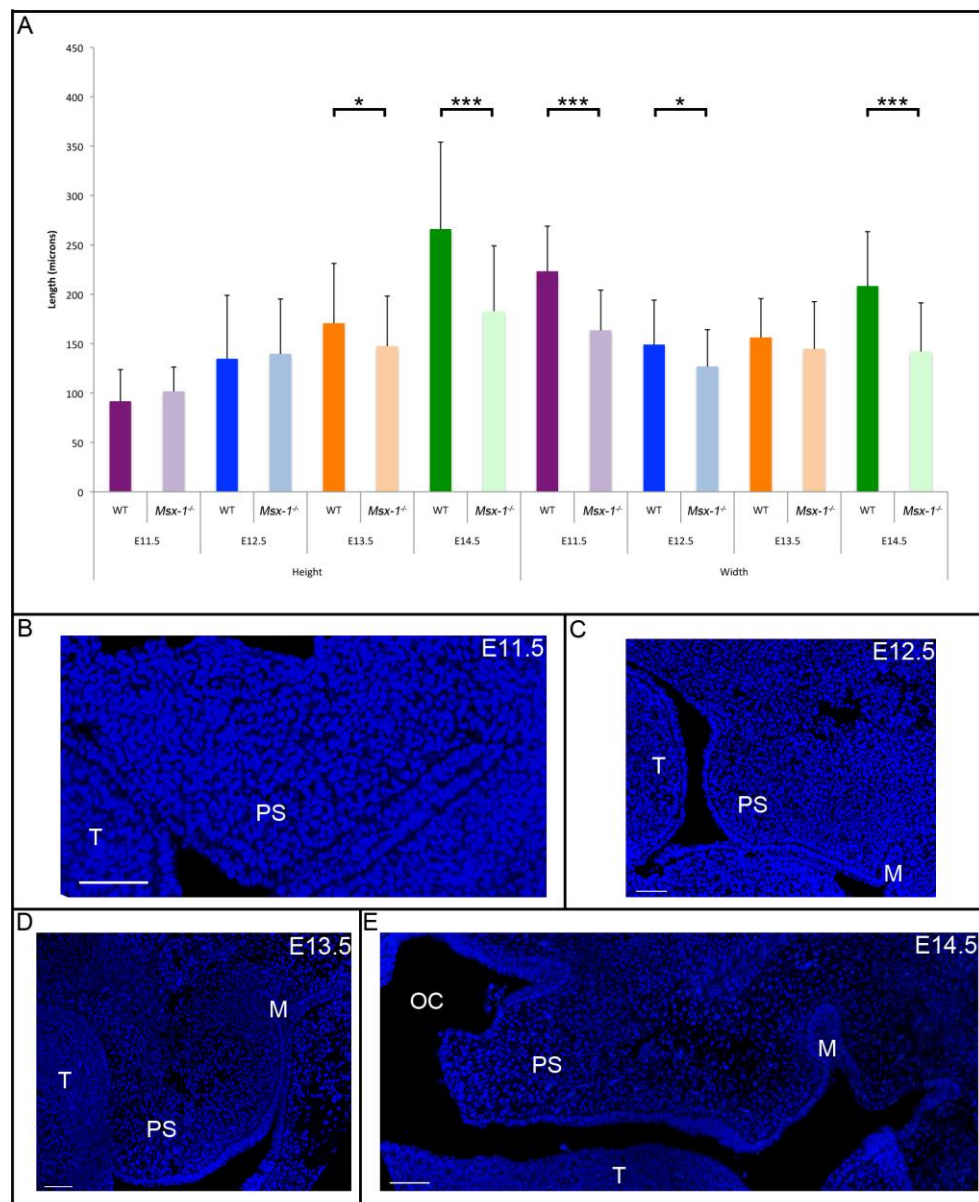


**Figure 9.2 Wild-type and *Msx-1*<sup>-/-</sup> height and width measurements and DAPI images of *MSX-1*<sup>-/-</sup> palate development** A) Wild-type and *Msx-1*<sup>-/-</sup> mutant palate measurements during development. Results of t-tests are shown \**p*<0.05 \*\**p*<0.01 \*\*\**p*<0.001 B) *MSX-1*<sup>-/-</sup> palate at E11.5 C) *Msx-1*<sup>-/-</sup> palate at E12.5 D) *Msx-1*<sup>-/-</sup> palate at E13.5 E) *Msx-1*<sup>-/-</sup> palate at E14.5. Error bars display 1 standard deviation. Scale bars represent 200 μm. M, molar tooth bud; OC, oral cavity; PS, palatal shelf; T, tongue.

### 9.3.2 Localised cell proliferation in the *Msx-1*<sup>-/-</sup> palate

#### 9.3.2.1 Localised cell proliferation overview

The initial level of proliferation at E11.5 was the same in both wild-type and *Msx-1*<sup>-/-</sup> palatal shelves but a significant difference between the two can be seen by E12.5 when proliferation in the *Msx-1*<sup>-/-</sup> palatal shelf has dropped significantly (Fig. 9.3). In fact, every 24 hours the amount of proliferation in the *Msx-1*<sup>-/-</sup> palate changed significantly. As the outgrowth phase continues the proliferation in the mutant palate remained significantly lower than the wild-type. The level of proliferation in the wild-type steadily decreased as development progresses. In contrast there was a small but significant rise in proliferation in the *Msx-1*<sup>-/-</sup> mouse between E12.5 and E13.5 (Fig. 9.3).

By E14.5, whether the palatal shelves have elevated or not, the levels of proliferation has dropped in both the wild-type and *Msx-1*<sup>-/-</sup> mutant (Fig. 9.3). The amount of proliferation was still significantly lower in the mutant mouse, but the difference between the two appears much less, due to the large drop in proliferation in the wild-type between E13.5 and E14.5.

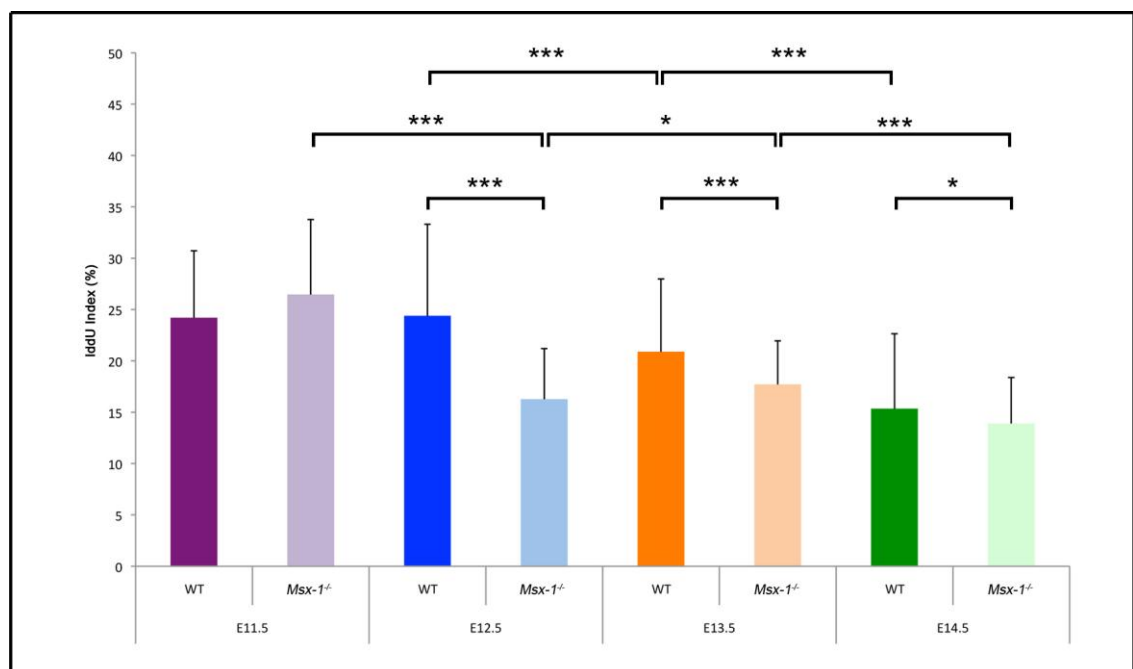


**Figure 9.3 Wild-type and *Msx-1*<sup>-/-</sup> proliferation index results** Overall IddU index for wild-type and *Msx-1*<sup>-/-</sup> mutant palates (E11.5 – E14.5). Error bars display 1 standard deviation. Results of t-tests are shown \*p<0.05 \*\*p<0.01 \*\*\*p<0.001

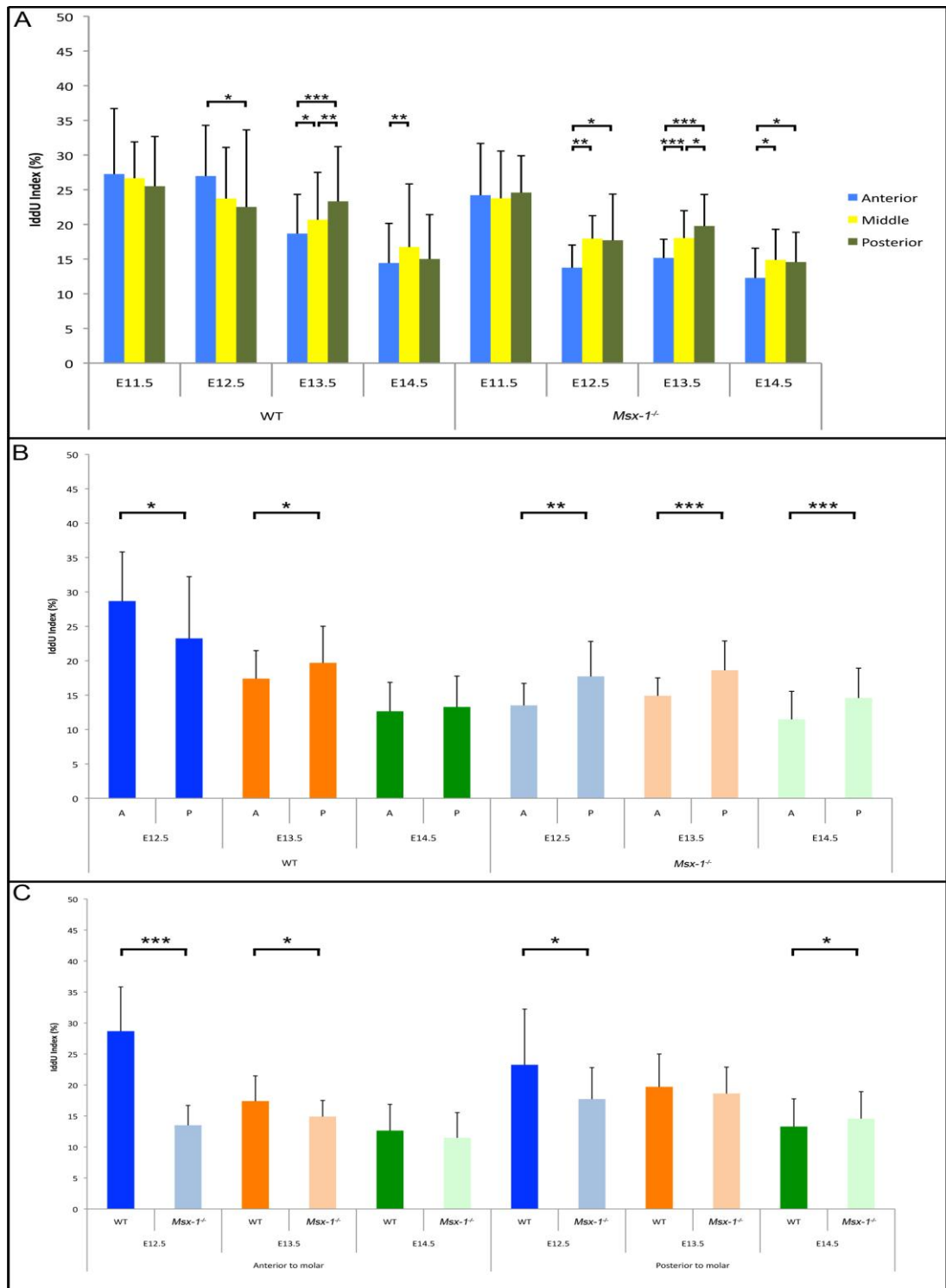


**Figure 9.4 Wild-type and *Msx-1*<sup>-/-</sup> proliferation index results along the AP axis** A) Changes in the IddU index along the AP axis for wild-type and *Msx-1*<sup>-/-</sup> mutant palates (E11.5 – E14.5). B) *Msx-1* is expressed strongly anterior to the molar so the palate was divided in two and the amount of proliferation compared between the anterior and posterior sections C) Differences in proliferation anterior or posterior to the molar between the wild-type and *Msx-1*<sup>-/-</sup> palate. A, anterior to molar; P, posterior to molar. Error bars display 1 standard deviation. Results of t-tests are shown \*p<0.05 \*\*p<0.01 \*\*\*p<0.001

### 9.3.2.2 Proliferation along the AP axis in *Msx-1*<sup>-/-</sup> mice

*Msx-1* is expressed in the palatal shelves anterior to the first upper molar. Therefore, as well as looking at the equal thirds along the AP axis, a comparison was made by dividing the palate into anterior and posterior halves, using the first section that the molar tooth bud appears on as the first “posterior” section (Fig. 9.4B & C).

When the palate was divided into thirds no difference in the level of proliferation was seen along the AP axis in either the wild-type and *Msx-1*<sup>-/-</sup> mutant palate at E11.5 (Fig. 9.4A). By E12.5 both the wild-type and *Msx-1*<sup>-/-</sup> mutant palate had significant variations in the level of proliferation along their AP axis, but in the wild-type the highest level of proliferation was in the anterior whereas in the *Msx-1*<sup>-/-</sup> mutant the posterior was displaying the highest level (Fig. 9.4A & B). Also the level of proliferation in the *Msx-1*<sup>-/-</sup> mutant was significantly lower in both the anterior and posterior compared to the wild-type (Fig. 9.4C).

In the *Msx-1*<sup>-/-</sup> mutant palate there appeared to be very little variation along the AP between E12.5 and E13.5 but the level of proliferation had increased in the posterior palate and it is no longer significantly different from the wild-type posterior palate (Fig. 9.4C). Both the wild-type and mutant displayed significantly different levels of proliferation between their anterior and posterior regions but both now have the highest proliferation in the posterior (Fig. 9.4A & B).

By E14.5 there was no longer a significant difference between the level of proliferation occurring in the anterior palate in the wild-type and *Msx-1*<sup>-/-</sup> mutant (Fig. 9.4C), but the posterior *Msx-1*<sup>-/-</sup> palate had significantly higher levels of proliferation compared to the wild-type so the loss of *Msx-1* could be having different effects along the AP axis. There was still a significant difference between the anterior and posterior regions of the palate in the *Msx-1*<sup>-/-</sup> mutant at E14.5 (Fig. 9.4B) whereas the wild-type displayed a more uniform level of proliferation.

### 9.3.2.3 Distribution of proliferation in the *Msx-1*<sup>-/-</sup> palate

There was again a fair amount of noise in the proliferation E11.5 heat maps of both the wild-type and *Msx-1*<sup>-/-</sup> mutant (Fig. 9.5). In the anterior palate at E12.5 where the proliferation was normally higher along the ventral side it was very low in the *Msx-1*<sup>-/-</sup>

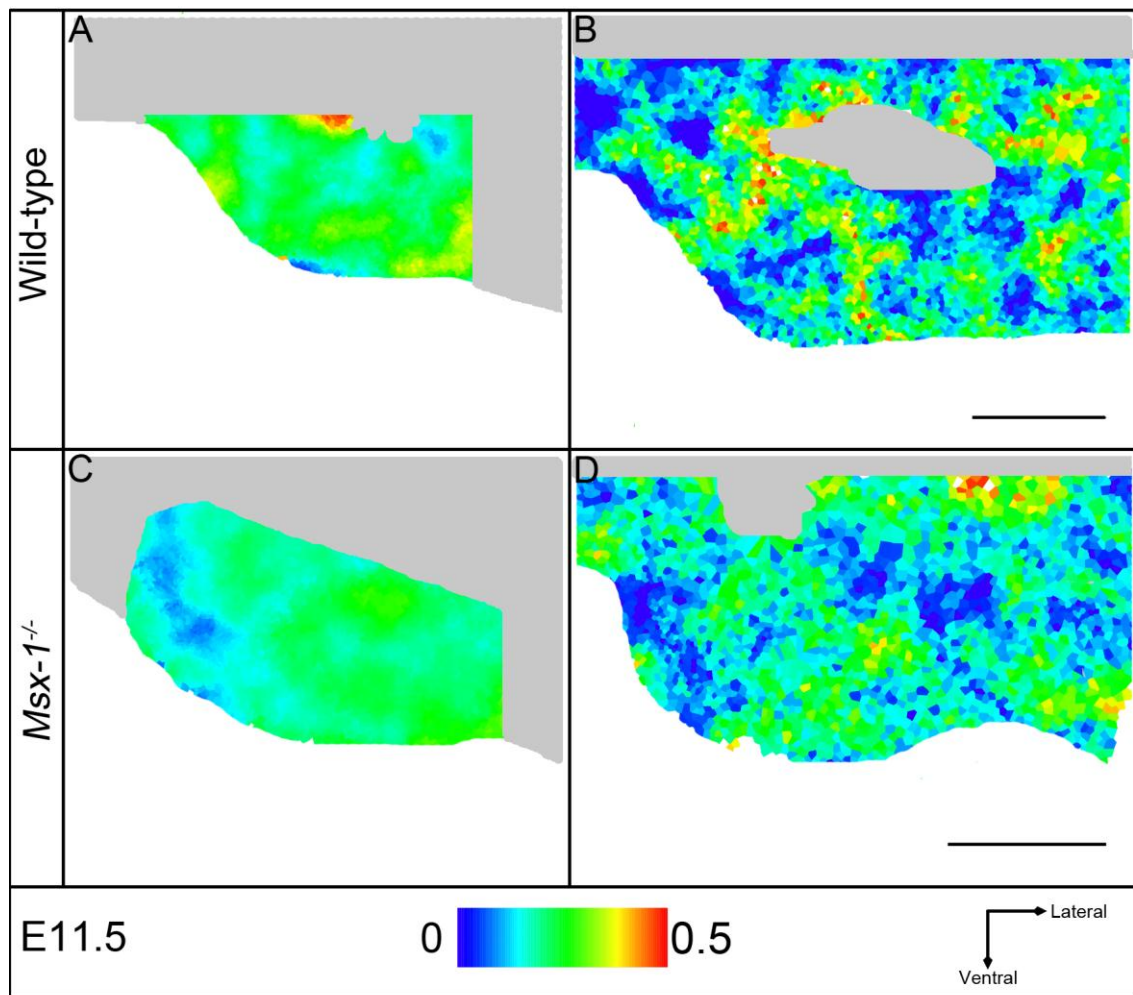


**Figure 9.5 Proliferation heat maps of E11.5 wild-type and *Msx-1*<sup>-/-</sup> palatal shelves** A) Heat map of the wild-type palate B) Individual heat map of the wild-type palate C) Heat map of the *Msx-1*<sup>-/-</sup> mutant palate D) Individual heat map of the *Msx-1*<sup>-/-</sup> mutant palate. Each heat map is an average of three individual sections. Scale bars represent 200  $\mu$ m.

mutant (Fig. 9.6A, A', D & D', brackets). In the middle third of the palate the wild-type heat map showed regions of higher proliferation around the edges of the palatal shelf whereas this is where it is lowest in the mutant (Fig. 9.6B, B', E & E', black arrows). The heat maps show that the proliferation is lower in the *Msx-1*<sup>-/-</sup> palates but they also highlight regional variations indicating that *Msx-1* may not have a uniform effect across the mesenchyme.

The distribution of proliferation across the palate in the mutant was a lot more similar to the wild-type at E13.5 (Fig. 9.7). Although the level was lower overall in the *Msx-1*<sup>-/-</sup> mutant the patterns of proliferation can be picked out. For example in the middle third, where there was lower proliferation on the prospective oral side of the palate (Fig. 9.7A, B, D & E, brackets indicate region of lower proliferation), and proliferation in the posterior was subtly higher at the distal tip of the palate compared to more proximal regions (Fig. 9.7C & F, black circles).

At E14.5 the heat maps show the low level of proliferation in both genotypes varying fairly randomly across the palatal shelves. Potentially the region of slightly higher proliferation at the tip of the *Msx-1*<sup>-/-</sup> mutant palate is the cause of the significantly higher proliferation in this region (Fig. 9.8C & F, black circles).

Overall there was less localised cell proliferation happening in the *Msx-1*<sup>-/-</sup> palatal shelves compared to the wild-type. This drop in proliferation was mainly seen in the mesenchyme anterior to the first molar, but the posterior mesenchyme still varied significantly from the wild-type at times. The distribution of relative levels of proliferation does not vary greatly between the wild-type and *Msx-1*<sup>-/-</sup> palate.

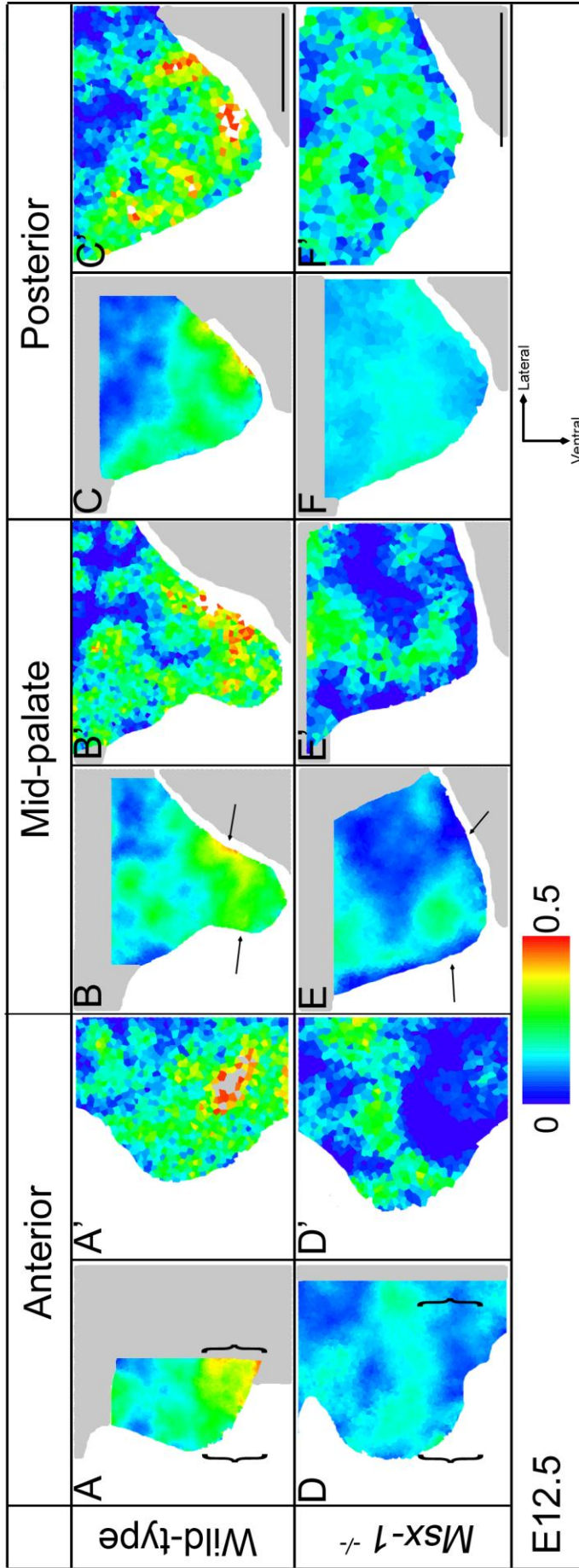


**Figure 9.6 Proliferation heat maps of E12.5 wild-type and *Msx-1*<sup>-/-</sup> palatal shelves** A) Heat map of the wild-type anterior palate. Brackets highlight region of higher proliferation A') Individual heat map of the wild-type anterior palate B) Heat map of the wild-type mid-palate. Arrows indicate regions of higher proliferation B') Individual heat map of the wild-type mid-palate C) Heat map of the wild-type posterior palate C') Individual heat map of the wild-type posterior palate D) Heat map of the *Msx-1*<sup>-/-</sup> mutant anterior palate. Brackets highlight region where proliferation is high in the wild-type but low in the mutant D') Individual heat map of the *Msx-1*<sup>-/-</sup> mutant anterior palate E) Heat map of the *Msx-1*<sup>-/-</sup> mutant mid-palate. Arrows indicate regions of lower proliferation, which are higher in the wild-type E') Individual heat map of the *Msx-1*<sup>-/-</sup> mutant mid-palate F) Heat map of the *Msx-1*<sup>-/-</sup> mutant posterior palate F') Individual heat map of the *Msx-1*<sup>-/-</sup> mutant posterior palate. Each heat map is an average of three individual sections. Scale bars represent 200  $\mu$ m.



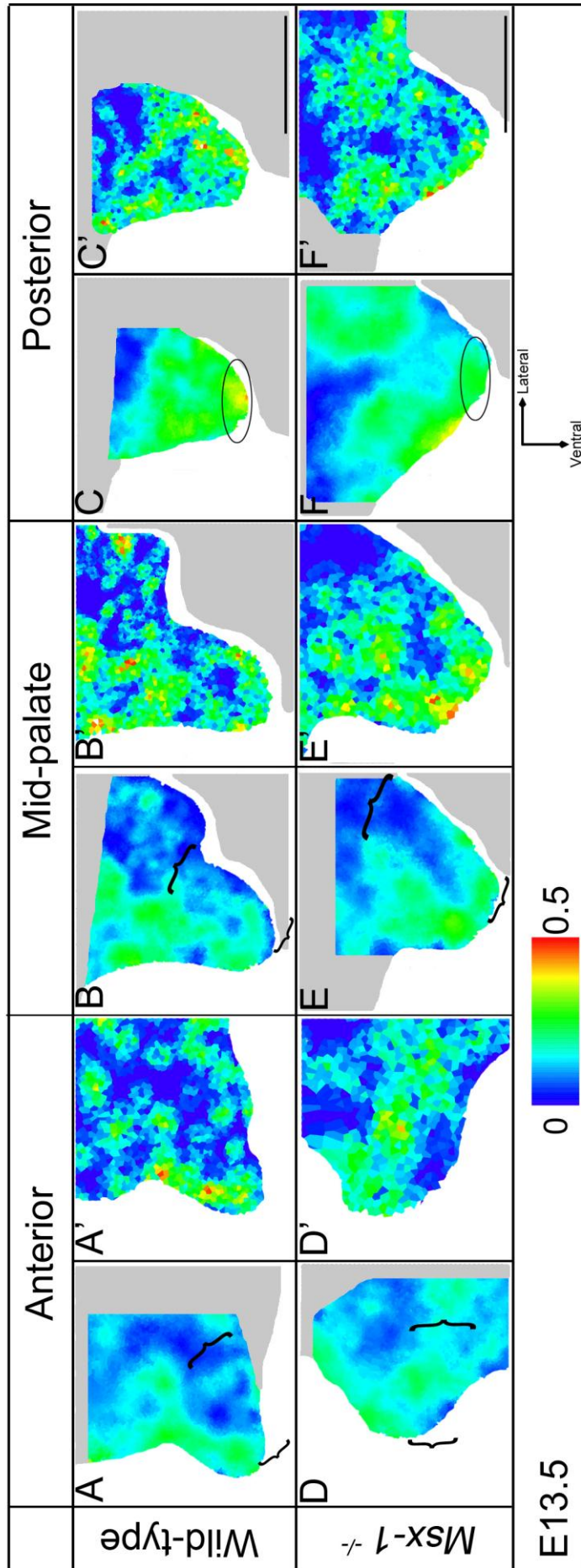


**Figure 9.7 Proliferation heat maps of E13.5 wild-type and *Msx-1<sup>-/-</sup>* palatal shelves** A) Heat map of the wild-type anterior palate A') Individual heat map of the wild-type anterior palate A') Heat map of the wild-type mid-palate B) Heat map of the wild-type mid-palate B') Individual heat map of the wild-type mid-palate C) Heat map of the wild-type posterior palate C') Individual heat map of the wild-type posterior palate C') Heat map of the *Msx-1<sup>-/-</sup>* mutant anterior palate D) Heat map of the *Msx-1<sup>-/-</sup>* mutant anterior palate D') Individual heat map of the *Msx-1<sup>-/-</sup>* mutant anterior palate E) Heat map of the *Msx-1<sup>-/-</sup>* mutant mid-palate E') Individual heat map of the *Msx-1<sup>-/-</sup>* mutant mid-palate F) Heat map of the *Msx-1<sup>-/-</sup>* mutant posterior palate F') Individual heat map of the *Msx-1<sup>-/-</sup>* mutant posterior palate. Each heat map is an average of three individual sections. Scale bars represent 200  $\mu\text{m}$ . Brackets show regions of lower proliferation. Black circles highlight regions of higher proliferation.

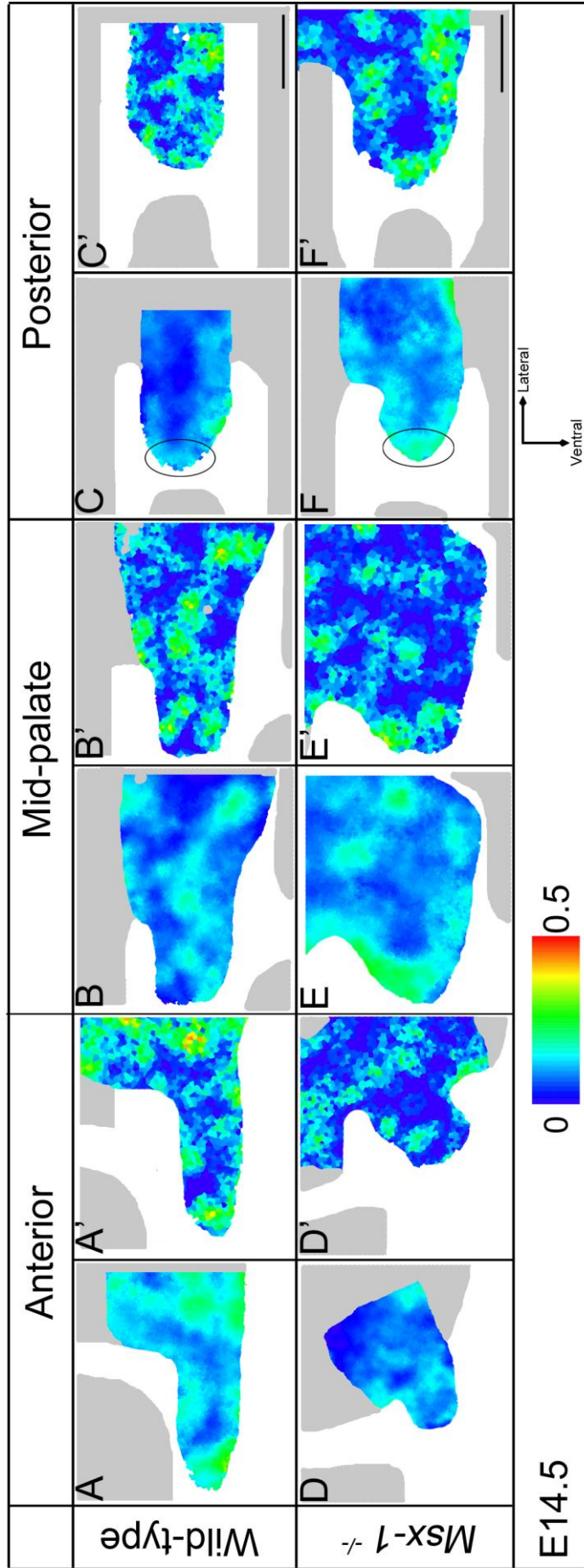


**Figure 9.8 Proliferation heat maps of E14.5 wild-type and *Msx-1<sup>-/-</sup>* palatal shelves** A) Heat map of the wild-type anterior palate A') Individual heat map of the wild-type anterior palate A') Individual heat map of the wild-type mid-palate B') Individual heat map of the wild-type mid-palate C) Heat map of the wild-type posterior palate C') Individual heat map of the wild-type posterior palate C') Heat map of the *Msx-1<sup>-/-</sup>* mutant anterior palate D') Individual heat map of the *Msx-1<sup>-/-</sup>* mutant anterior palate D') Individual heat map of the *Msx-1<sup>-/-</sup>* mutant anterior palate E) Heat map of the *Msx-1<sup>-/-</sup>* mutant mid-palate E') Individual heat map of the *Msx-1<sup>-/-</sup>* mutant mid-palate F) Heat map of the *Msx-1<sup>-/-</sup>* mutant posterior palate F') Individual heat map of the *Msx-1<sup>-/-</sup>* mutant posterior palate. Each combined heat map is an average of three individual sections. Scale bars represent 200  $\mu\text{m}$ . Black circles highlight region of raised proliferation at the medial edge of the mutant.

### 9.3.3 Internuclear spacing in the *Msx-1*<sup>-/-</sup> palate

In the *Msx-1*<sup>-/-</sup> palate at E11.5 the cells were more tightly packed than in the wild-type, and on average cells were more densely packed on the medial side (Fig. 9.9, black arrow). The palate remained slightly more densely packed in the mutant compared to the wild-type at E12.5 (Fig. 9.10). The *Msx-1*<sup>-/-</sup> heat maps displayed a greater range of cell spacing across the palate (Fig. 9.10D-F, colours varied from red through to green). In the anterior third the dorsal and distal edges had more tightly packed cells (Fig. 9.10A & D, arrows). In the posterior palate the prospective nasal side also had more densely packed cells (Fig. 9.10C & F, brackets) than the wild-type.

By E13.5 the difference in the cell spacing between the mutant and the wild-type was still evident (Fig. 9.11). In the anterior two-thirds the mutant remained more tightly packed than the wild-type but the *Msx-1*<sup>-/-</sup> mutant also displayed more uniform cell packing within the palatal outgrowth. Whereas by this stage the wild-type was displaying slightly higher proliferation on its prospective oral side (Fig. 9.11A & B, dashed lines separate the two differently spaced sides). In the posterior palate both the wild-type and mutant showed a more uniform packing, but the *Msx-1*<sup>-/-</sup> palate remains more tightly packed.

By E14.5 the spacing in the wild-type and the *Msx-1*<sup>-/-</sup> mutant palate had decreased compared to E13.5. The *Msx-1*<sup>-/-</sup> heat maps were now looking greener but they were still more tightly packed than the wild-type palate, which was displaying regions of cooler colours (Fig. 9.12). At this stage of development the palatal shelves should be growing towards the midline to meet and fuse but this never happens in the *Msx-1*<sup>-/-</sup> mouse so growth at this point could be disrupted. The difference in spacing was more noticeable in the outgrowth of the mid-palate, where the wild-type palate has completed its growth towards the midline and is touching the opposing shelf at this stage (Fig. 9.12B & E). An increase in cell spacing potentially contributes to this post elevation growth (as discussed in chapter 8). The *Msx-1*<sup>-/-</sup> posterior palate still displayed a similar pattern of spacing to the wild-type, even though the mutant palate was more tightly packed, with the oral and nasal sides being marginally more densely packed than the mesenchyme in the centre of the outgrowth (Fig. 9.12C, C', F & F").

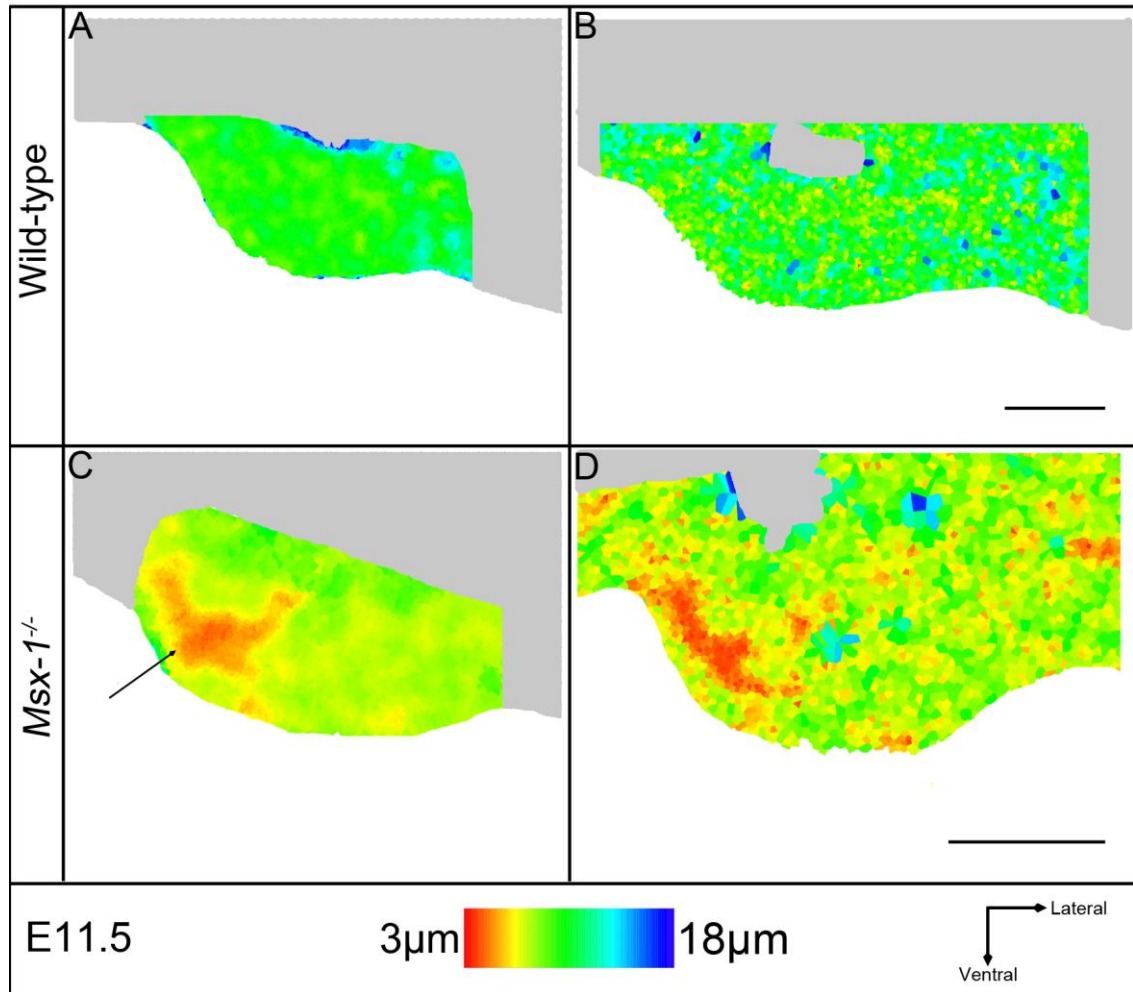


**Figure 9.9 Internuclear spacing heat maps of E11.5 wild-type and *Msx-1*<sup>-/-</sup> palatal shelves** A) Heat map of the wild-type palate B) Individual heat map of the wild-type palate C) Heat map of the *Msx-1*<sup>-/-</sup> mutant palate. Arrow indicates region of more densely packed cells D) Individual heat map of the *Msx-1*<sup>-/-</sup> mutant palate. Each heat map is an average of three individual sections. Scale bars represent 200 μm.

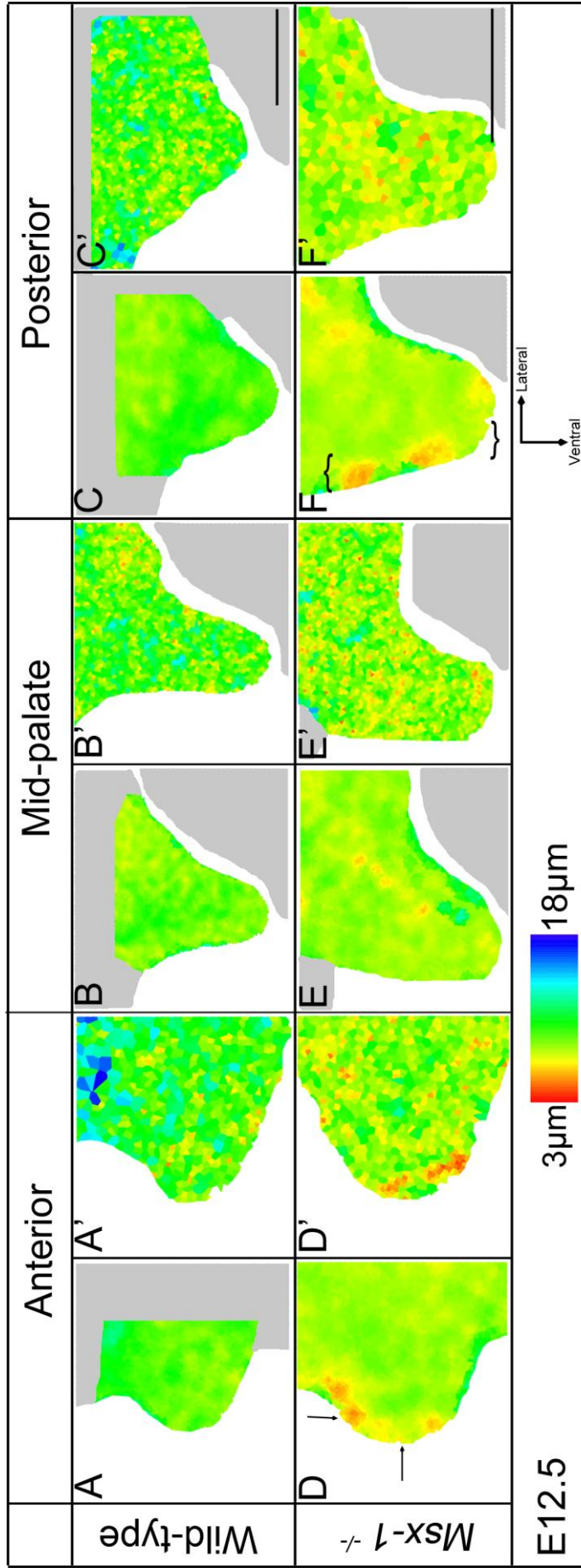


**Figure 9.10 Internuclear spacing heat maps of E12.5 wild-type and *Msx-1<sup>-/-</sup>* palatal shelves** A) Heat map of the wild-type anterior palate A') Individual heat map of the wild-type anterior palate B) Heat map of the wild-type mid-palate B') Individual heat map of the wild-type mid-palate C) Heat map of the wild-type posterior palate C') Individual heat map of the wild-type posterior palate along the dorsal and distal edges D') Individual heat map of the *Msx-1<sup>-/-</sup>* mutant anterior palate D) Heat map of the *Msx-1<sup>-/-</sup>* mutant anterior palate along the dorsal and distal edges E') Individual heat map of the *Msx-1<sup>-/-</sup>* mutant mid-palate E) Heat map of the *Msx-1<sup>-/-</sup>* mutant mid-palate F') Individual heat map of the *Msx-1<sup>-/-</sup>* mutant posterior palate F) Heat map of the *Msx-1<sup>-/-</sup>* mutant posterior palate. Brackets highlight region of more tightly packed cells along the prospective nasal edge F') Individual heat map of the *Msx-1<sup>-/-</sup>* mutant posterior palate. Each heat map is an average of three individual sections. Scale bars represent 200 µm.

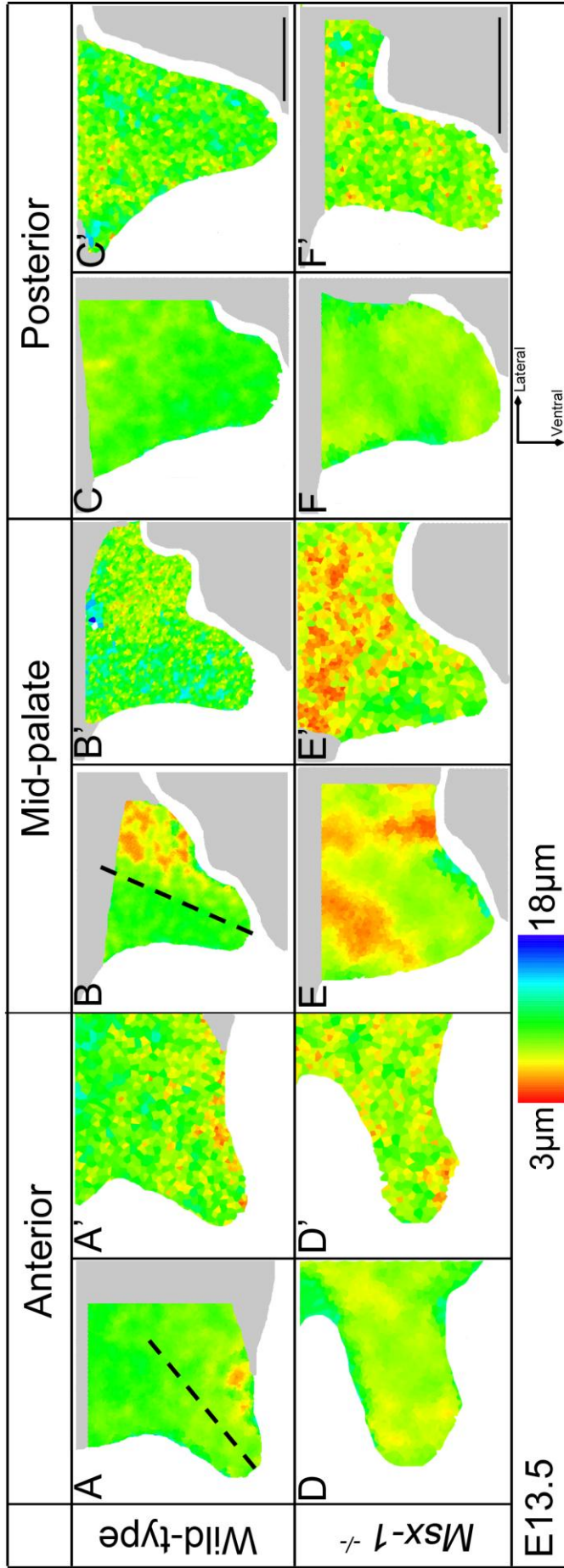


**Figure 9.11 Internuclear spacing heat maps of E13.5 wild-type and *Msx-1*<sup>-/-</sup> palatal shelves** A) Heat map of the wild-type anterior palate. Dashed line separates the loosely packed prospective nasal side from the tightly packed prospective oral side A') Individual heat map of the wild-type anterior palate B) Heat map of the wild-type mid-palate. Dashed line separates the loosely packed prospective nasal side from the tightly packed prospective oral side B') Individual heat map of the wild-type mid-palate C) Heat map of the wild-type posterior palate C') Individual heat map of the *Msx-1*<sup>-/-</sup> mutant anterior palate D) Heat map of the wild-type posterior palate D') Individual heat map of the *Msx-1*<sup>-/-</sup> mutant anterior palate E) Heat map of the *Msx-1*<sup>-/-</sup> mutant mid-palate E') Individual heat map of the *Msx-1*<sup>-/-</sup> mutant mid-palate F) Heat map of the *Msx-1*<sup>-/-</sup> mutant posterior palate F') Individual heat map of the *Msx-1*<sup>-/-</sup> mutant posterior palate. Each heat map is an average of three individual sections. Scale bars represent 200 µm.

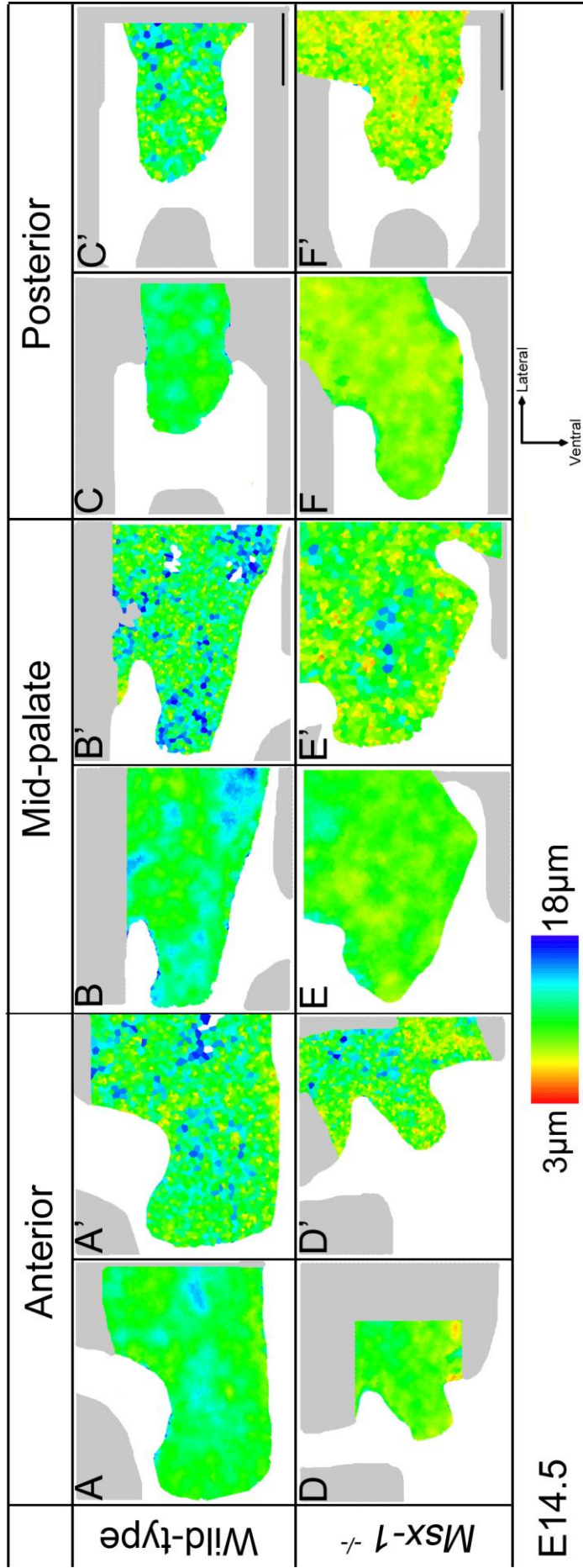


Figure 9.12 Internuclear spacing heat maps of E14.5 wild-type and *Msx-1<sup>-/-</sup>* palatal shelves A) Heat map of the wild-type anterior palate A') Individual heat map of the wild-type anterior palate A) Heat map of the wild-type mid-palate B) Heat map of the wild-type mid-palate B') Individual heat map of the wild-type mid-palate B') Heat map of the wild-type posterior palate C) Heat map of the wild-type posterior palate C') Individual heat map of the wild-type posterior palate C') Heat map of the *Msx-1<sup>-/-</sup>* mutant anterior palate D) Heat map of the *Msx-1<sup>-/-</sup>* mutant anterior palate D') Individual heat map of the *Msx-1<sup>-/-</sup>* mutant anterior palate D') Heat map of the *Msx-1<sup>-/-</sup>* mutant mid-palate E) Heat map of the *Msx-1<sup>-/-</sup>* mutant mid-palate E') Individual heat map of the *Msx-1<sup>-/-</sup>* mutant mid-palate E') Heat map of the *Msx-1<sup>-/-</sup>* mutant posterior palate F) Heat map of the *Msx-1<sup>-/-</sup>* mutant posterior palate F') Individual heat map of the *Msx-1<sup>-/-</sup>* mutant posterior palate. Each heat map is an average of three individual sections. Scale bars represent 200  $\mu\text{m}$ .

#### 9.4 *Msx-1*<sup>-/-</sup> Discussion

The palate of the *Msx-1*<sup>-/-</sup> mouse had lower proliferation and more tightly packed cells during development. The palate is often able to elevate but a cleft still forms. This cleft was most likely due to the small size of the palate meaning the shelves do not meet in the midline. The results shown in the proliferation assay here are in agreement with work done by other groups studying the *Msx-1*<sup>-/-</sup> mouse (Han et al., 2009; Satokata and Maas, 1994). This confirms that the assay protocols used in this thesis were working and in addition were able to provide a more detailed analysis of proliferation and internuclear spacing.

The decrease in proliferation occurred in the anterior of the palate and this matched the expression pattern of *Msx-1*. This means the signalling cascade involving *Msx-1* in the anterior palate is involved in the up-regulation of proliferation. The loss of proliferation leads to a significantly smaller palate, which was too short to meet its counterpart in the midline. Therefore the two palatal shelves never touched to be able to fuse, resulting in a cleft palate.

The palate is still able to elevate showing that proliferation is either not a vital mechanism for this process or the palate has been able to compensate for a significant loss of proliferation and the required intrinsic forces are still generated by the more smaller palate with more tightly packed mesenchymal cells. The patterns of proliferation do not vary greatly, unlike the amount of proliferation between the wild-type and *Msx-1*<sup>-/-</sup>, so the relative amounts in the smaller palate might be enough to allow the palate to elevate.

There was a difference in cell spacing after the palates have elevated and the wild-type palatal shelves had grown and were touching in the midline. If the post elevational growth towards the midline is due to an increase in cell spacing, then the lack of this decrease in cell density in the mutant could be contributing to the cleft.

During the initial outgrowth, at E11.5, the tight packing of cells seen in both genotypes could be due to the arrival of migrating NCC. The *Msx-1*<sup>-/-</sup> palate than fails to elongate while cells are still entering the palate from the maxillary process causing the *Msx-1*<sup>-/-</sup> palate to have more cells occupying a smaller volume therefore the packing appears tighter.



This work potentially indicates a link between cellular mechanisms of morphogenesis, where there is lower proliferation there are often more tightly packed cells. These two mechanisms could be regulating in a similar way to that proposed in limb development (Saunders, 1948). Somewhat oddly, in wild-type palatogenesis regions of low proliferation often also had more tightly packed cells, such as the prospective nasal side of the palate at E13.5. The cell packing could potentially be a feedback mechanism for the level of proliferation.

The tightly packed cells could lead to differences in both signalling received and cell-cell/cell-ECM contact. Diffusible signals may struggle to get through the tightly packed cells or different signals may get through any extra cell contacts that exist in the mutants. It is possible the tight packing is due to a lack of ECM. The population of cells responsible for producing ECM may not exist due to the low level of proliferation or they never receive the signals to induce the production of ECM. It would also be interesting to look at how much the amount and the composition of the ECM in the *Msx-1*<sup>-/-</sup> palate varies.

*Msx-1* is not expressed in the posterior of the palate yet the proliferation and the cell spacing both vary from the wild-type in the *Msx-1*<sup>-/-</sup> palate. By E14.5 the posterior of the *Msx-1*<sup>-/-</sup> palate has higher levels of proliferation compared to the wild-type so *Msx-1* could be having a slight indirect repressive effect in the posterior palate. By E14.5 the difference is being seen in the higher level of proliferation. It is thought that the complete cleft of the *Msx-1*<sup>-/-</sup> palate is due to the posterior palate requiring the more anterior regions to fuse first, but this evidence shows that morphogenesis in the posterior region is disrupted more directly by the loss of *Msx-1*.

## 10.0 *Wnt1-Cre;ERK2<sup>fl/fl</sup>* Mutant Mouse

### 10.1 Introduction to *Wnt1-Cre;Erk2<sup>fl/fl</sup>* phenotype

The extracellular signalling-regulating kinase (Erk) 2 knockout mouse phenotype falls into a category of neuro-cardio-facial-cutaneous syndromes (NCFCS), where the defect is in structures derived from the neural crest. In humans these syndromes are often linked to a gain of function in the *Erk* pathway but through studying them it has been shown just how sensitive the development of these systems is to changes in *Erk1* and *Erk2* activity. To study the contribution of the *Erks* during development various mouse models have been created (Newbern et al., 2008). The double *Erk1* knockout is viable, with no detectable phenotype, mostly likely because *Erk2* is able to compensate for the loss of *Erk1*. In contrast the homozygous conditional knockout of *Erk2* produces mice with embryonic lethality, but the heterozygous knockout of *Erk2* allows normal Mendelian postnatal survival rates of mutant mice. When the heterozygous conditional knockout of *Erk2* is combined with loss of one or both alleles of *Erk1* the phenotype of the mutant embryos increases in severity showing that the *Erks* regulate development in a gene dosage dependent manner.

The mouse used in this study was the *Wnt1-Cre;Erk2<sup>fl/fl</sup>* mutant, which caused embryonic lethality, but the embryos can survive through to late gestation. They display a range of anomalies (Fig. 10.1 A-F) including a cleft palate, shortened maxilla, mandibular hypoplasia and conotruncal cardiac defects. Despite the deletion being more distal and involving different genes many of these defects are very similar to those seen in the chromosome 22q11 micro-deletion that has been linked to DiGeorge syndrome (Kobrynski and Sullivan, 2007). Other common symptoms in DiGeorge syndrome are defects in the thymus and thyroid gland development; in the *Wnt1-Cre;Erk2<sup>fl/fl</sup>* mice the thymus and thyroid develop normally the majority of the time. Defects are only seen in the more severe knockouts (Newbern et al., 2008). A similar pattern is seen in patients, a small deletion rarely leads to thymus and thyroid defects, but large deletions of the 22q11 region can cause the glands to develop a single lobe or not appear at all. The ability of the mouse model to mimic the human syndrome demonstrates that it is worthwhile using mouse models in medical research.

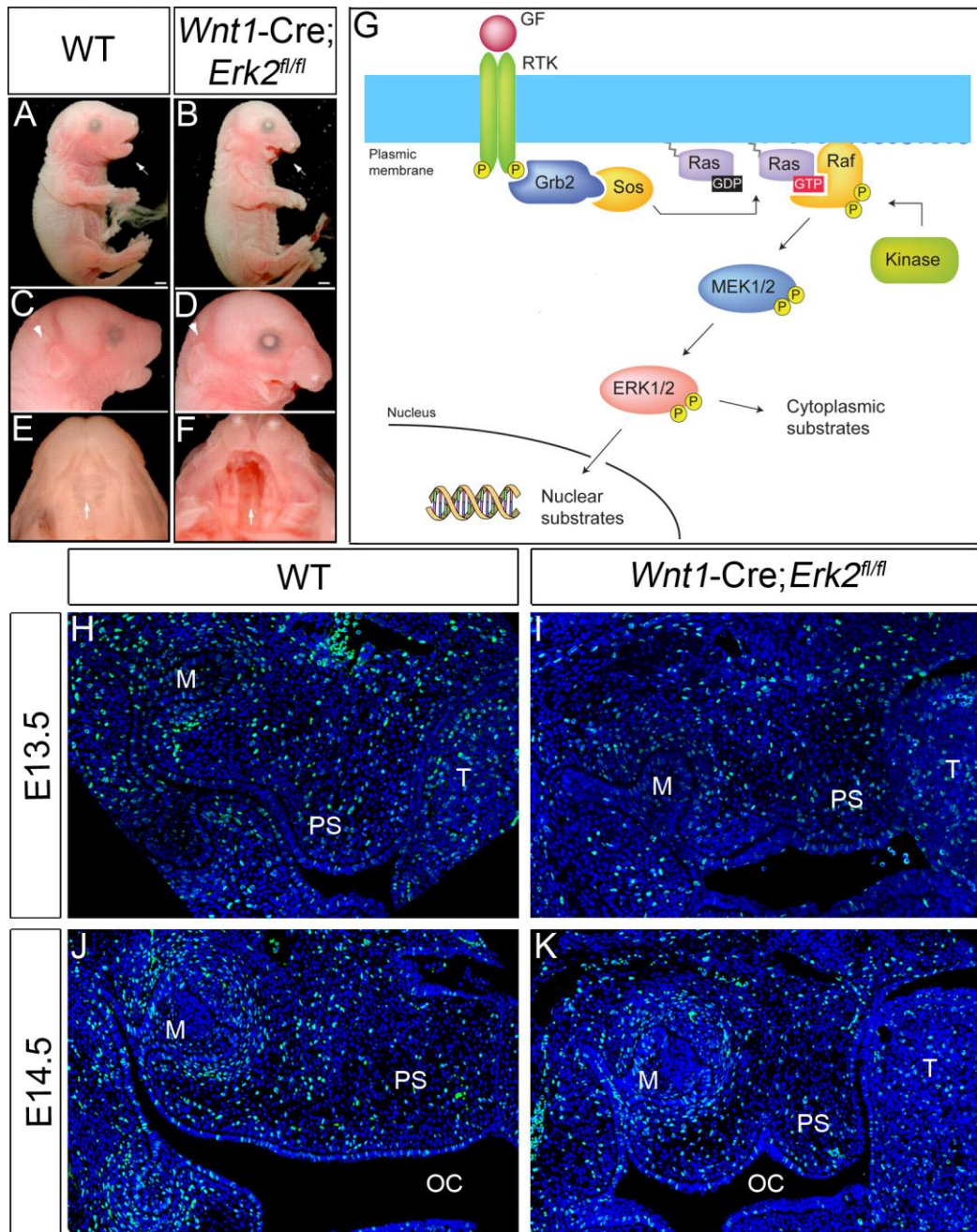


**Figure 10.1 *Wnt1-Cre;Erk2<sup>fl/fl</sup>* phenotype** A) Wild-type E17.5 embryo B) *Wnt1-Cre;Erk2<sup>fl/fl</sup>* E17.5 embryo C) Wild-type maxilla and mandible formation D) *Wnt1-Cre;Erk2<sup>fl/fl</sup>* displays defects in its maxilla and mandible formation E) Wild-type palate development F) *Wnt1-Cre;Erk2<sup>fl/fl</sup>* has a cleft palate. Scale bars 2mm. Adapted from Newbern et al., 2008 G) Diagram of the upstream signaling pathway to Erk2. Adapted from Frémin & Meloche, 2010 H) DAPI and BrdU labeled wild-type E13.5 palate I) DAPI and BrdU labeled *Wnt1-Cre;Erk2<sup>fl/fl</sup>* E13.5 palate J) DAPI and BrdU labeled wild-type E14.5 palate K) DAPI and BrdU labeled *Wnt1-Cre;ERK2<sup>fl/fl</sup>* E14.5 palate. GF, growth factor; RTK, receptor tyrosine kinase. M, molar tooth bud; OC, oral cavity; PS, palatal shelf; T, tongue.

There are also cardiac outflow tract symptoms; these also display variable penetrance from double-outlet right ventricles, ventricular septal defects and other defects resulting from the improper formation of the septum (Newbern et al., 2008). These structures form from the cardiac neural crest and these defects are common in DGS patients as well.

A similar range of symptoms are seen when either the upstream regulators of *Erk2*, such as the *Meks* or *Raf* components, or the downstream effectors, including the transcription factor serum response factor (SRF) are disrupted. These also have compensatory isoforms, for example only when all isoforms of *Mek1* and *Mek2* are deleted is a phenotype seen, but this will have all the most extreme NCFCS defects and is lethal to the embryo. Embryos with *B-Raf* and *C-Raf* conditionally inactivated display mandibular and maxilla hypoplasia and decreased crown-rump length, similar to the *Wnt1-Cre;Erk2<sup>fl/fl</sup>* mouse. It is thought the third isoform, *A-RAF* is able to compensate and produce low levels of *Erk1/2* activity preventing the most extreme phenotype (Newbern et al., 2008).

### **10.1.2 The *Erk2* pathway**

*Erk2* is an intracellular mediator involved in a signalling cascade to transmit signals from extracellular factors to their cytoplasmic and nuclear effectors. It is one of four *mitogen-activated protein kinase (MAPK)* signalling pathways, which have been shown to be involved in many cellular processes from proliferation and differentiation to cell survival and apoptosis (Liu et al., 2004). More specifically *Erk2* has been identified as having a role in cell growth and differentiation.

#### **10.1.2.1 Upstream of *Erk2***

The signalling cascade involving *Erk2* is initiated by an extracellular growth factor, such as *Fgf8*, binding to a receptor embedded in the cell surface membrane. There are a variety of extracellular growth factor receptors, for example it can be a G-protein coupled receptor (GPCRs) or a receptor tyrosine kinase (RTK) (Fremin and Meloche, 2010). This activation causes the assembly of multiple adaptor protein complexes, for example Growth Factor Receptor Bound Protein-2 (GRB2), SHO2 and CRK-Like

(CRKL), which form a link to the three-tiered protein cascade (Fig 10.1G). The adaptor protein allows the signalling cascade to progress by bringing a nucleotide exchange factor, like Son of Sevenless (SOS), close to the membrane bound small GTP binding protein (Ras) resulting in guanine exchange and converting the GTPase to its active conformation. The active Ras works as another adaptor that is responsible for recruiting the first of the core signalling modules, Raf Murine Sarcoma Viral Oncogene Homolog (Raf) kinase, to the cell membrane (Fig 10.1G). The phosphorylated Raf activates the second core module, a MAPK kinase, such as Mek, by phosphorylating at two different sites. Partial activity can be achieved by single site activation (Fig 10.1G) (Fremin and Meloche, 2010).

The final core signalling module, Erk, requires both of its phosphorylation sites to be activated for it to be fully active. This also helps control the signal through factors that dephosphorylate Erk. When Erk2 is inactive it can be found in the cytoplasm bound to Mek but once the activated Raf phosphorylates Mek it dissociates from Erk and phosphorylates it. This stimulation causes around half of the endogenous Erk2 to remain in the cytoplasm attached to the microtubule cytoskeleton (Reszka et al., 1995) while the rest dimerizes apparently allowing it to translocate to the nucleus. The attachment to the cytoskeleton not only regulates the spatial activity of Erk but it increases the specificity and efficiency of Erk signalling.

#### **10.1.2.2 Downstream of *Erk2***

The *Erk* pathway is involved in cell proliferation and survival and hyperactivity and has been linked to human cancers (Fremin and Meloche, 2010). Effectors of the *Erk* pathway are often transcription factors, which can be activated directly or indirectly via targets in both the cytoplasm and the nucleus. Erk2 activates its targets by acting as a proline directed protein kinases and phosphorylating serine or threonine residues that are next to proline residues. Activated Erk is able to regulate its own pathway through several negative feedback loops via the phosphorylation of components, such as SOS. The Erks have an indirect effect on translation in the cell by inducing both tRNA and rRNA synthesis, which are involved in protein synthesis that the cell requires to grow.

Targets in the cytoplasm include the phosphorylation of Ribosomal Protein S6 Kinases (RSKs). These then translocate to the nucleus where they in turn phosphorylate transcription factors such as serum response factor (SRF) and cyclic AMP response

element-binding protein (CREB). When Erk itself translocates to the nucleus it targets more transcription factors. Often these are ternary complex factors (TCFs). For example Ets1-like (Elk-1) and these then interact with SRF. Other targets include RSK-related kinase, mitogen- and stress-activated protein kinases (MSKs).

### 10.1.3 *Erk2* is required for neural crest development

Neural crest development relies upon and is very sensitive to extracellular signals, especially *Fgf8*. It has been shown that neural crest development is also critically dependent on the *Raf/Mek/Erk/SRF* signalling pathway (Newbern et al., 2008) and that many of the defects in NCFCS patients are due to deficiencies in neural crest *Erk2* signalling. Mice lacking *Fgf8* also show an array of cardiac and craniofacial defects similar to the *Wnt1-Cre;Erk2<sup>fl/fl</sup>* mouse and DGS mouse models, like *Tbx-1<sup>-/-</sup>*. Deficiencies in other parts of the pathway also result in similar craniofacial defects, such as *Mek1/2* or *B-Raf/C-Raf*. Many of these signalling molecules also have roles outside of the described pathway but the effects seen are consistent with them acting in the *Erk1/2* pathway (Hindley and Kolch, 2002).

A cleft palate has been identified among the deficiencies in the *Wnt1-Cre;Erk2<sup>fl/fl</sup>* mouse but the cellular processes that have been disrupted have not yet been rigorously studied. Preliminary work suggests that levels of apoptosis are normal, and that when placed together in culture the shelves are able to fuse, but a Ki67 analysis of proliferation showed that there might be disruption in the mesenchyme of the *Wnt1-Cre;Erk2<sup>fl/fl</sup>* palate (Parada, 2013).

## 10.2 *Wnt1-Cre;Erk2<sup>fl/fl</sup>* Materials and Methods

The *Wnt1-Cre;Erk2<sup>fl/fl</sup>* mouse was generated by inserting Lox-P sites either side of exon 3 of *Erk2* and mating these animals with those expressing a *Wnt1-Cre* transgene (Newbern et al., 2008). This resulted in animals without *Erk2* activity in the neural crest.

Carolina Parada, from Prof. Yang Chai's research group based at the University of Southern California, provided these samples. The pregnant mothers were injected with 50mg/kg BrdU 150 minutes before sacrifice. The embryos were embedded in

paraffin, as described in section 2.3.8, and three wild-type and three *Wnt1-Cre;Erk2<sup>fl/fl</sup>* embryos at both E13.5 and E14.5 were delivered from the University of Southern California to Kings College London. The samples were then sectioned and stained against DAPI and BrdU as described in section 2.4.1, 2.5.1 (excluding the IddU antibody). The images were then processed as described in section 2.7 to identify the amount and the location of proliferating cells and leading to the production of heat maps and data on which t-tests were performed and  $p < 0.05$  was considered statistically significant.

### **10.3 *Wnt1-Cre;Erk2<sup>fl/fl</sup>* Results**

#### **10.3.1 Palate development in the *Wnt1-Cre;Erk2<sup>fl/fl</sup>* mouse**

At E13.5 there was no difference in the width of the palate between the wild-type and the mutant, but the *Wnt1-Cre;Erk2<sup>fl/fl</sup>* palate was significantly shorter in height (Fig. 10.2). In contrast at E14.5 there was no significant difference in the length of the outgrowth, despite the wild-type having elevated, but it was now significantly wider than the *Wnt1-Cre;Erk2<sup>fl/fl</sup>* palate. The E14.5 *Wnt1-Cre;Erk2<sup>fl/fl</sup>* palate was now nearly exactly the same length as the outgrowth in the wild-type a stage earlier, E13.5 (Fig. 10.2). There was an increase in length of the wild-type palatal outgrowth between stages E13.5 and E14.5 of around 17  $\mu\text{m}$  but the change in the length of the *Wnt1-Cre;Erk2<sup>fl/fl</sup>* palatal shelf between these stages was over three times this. The trend was very different when considering the width of the palatal shelf between E13.5 and E14.5; in this case the wild-type palate expanded by about 44  $\mu\text{m}$  but the width of the mutant palate increased by only half of this.

#### **10.3.2 Localised cell proliferation in the *Wnt1-Cre;Erk2<sup>fl/fl</sup>* palate**

##### **10.3.2.1 Quantity of proliferation**

There was very little difference in the amount of proliferation between the *Wnt1-Cre;Erk2<sup>fl/fl</sup>* mice and their wild-type litter mates. At E13.5, the end of the outgrowth stage, the amount of proliferation was the same in the anterior and middle thirds but

there was significantly less proliferation in the posterior third of the *Wnt1-Cre;Erk2<sup>fl/fl</sup>* mutant compared to the wild-type (Fig. 10.3B). This was the same at E14.5 but the

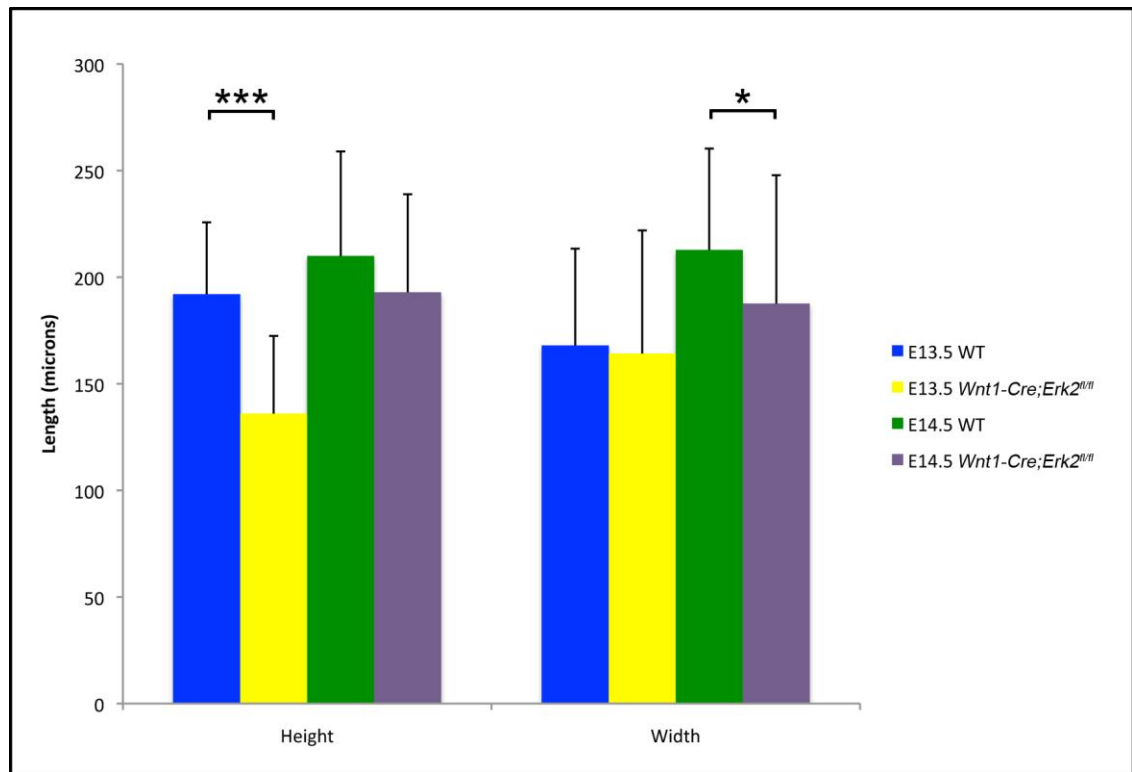


**Figure 10.2 Wild-type and *Wnt1-Cre;Erk2<sup>fl/fl</sup>* height and width measurements** Wild-type and *Wnt1-Cre;Erk2<sup>fl/fl</sup>* mutant palate measurements before and after wild-type elevation. Error bars display 1 standard deviation. Results of t-tests are shown \* $p < 0.05$  \*\* $p < 0.01$  \*\*\* $p < 0.001$

difference was greater in the posterior proliferation reached the  $p < 0.05$  level of significance (Fig. 10.3A). As the *Wnt1-Cre;Erk2<sup>fl/fl</sup>* palate continued to develop proliferation dropped significantly across the wild-type mouse only showed a middle third of the palate (Fig. 10.3B).

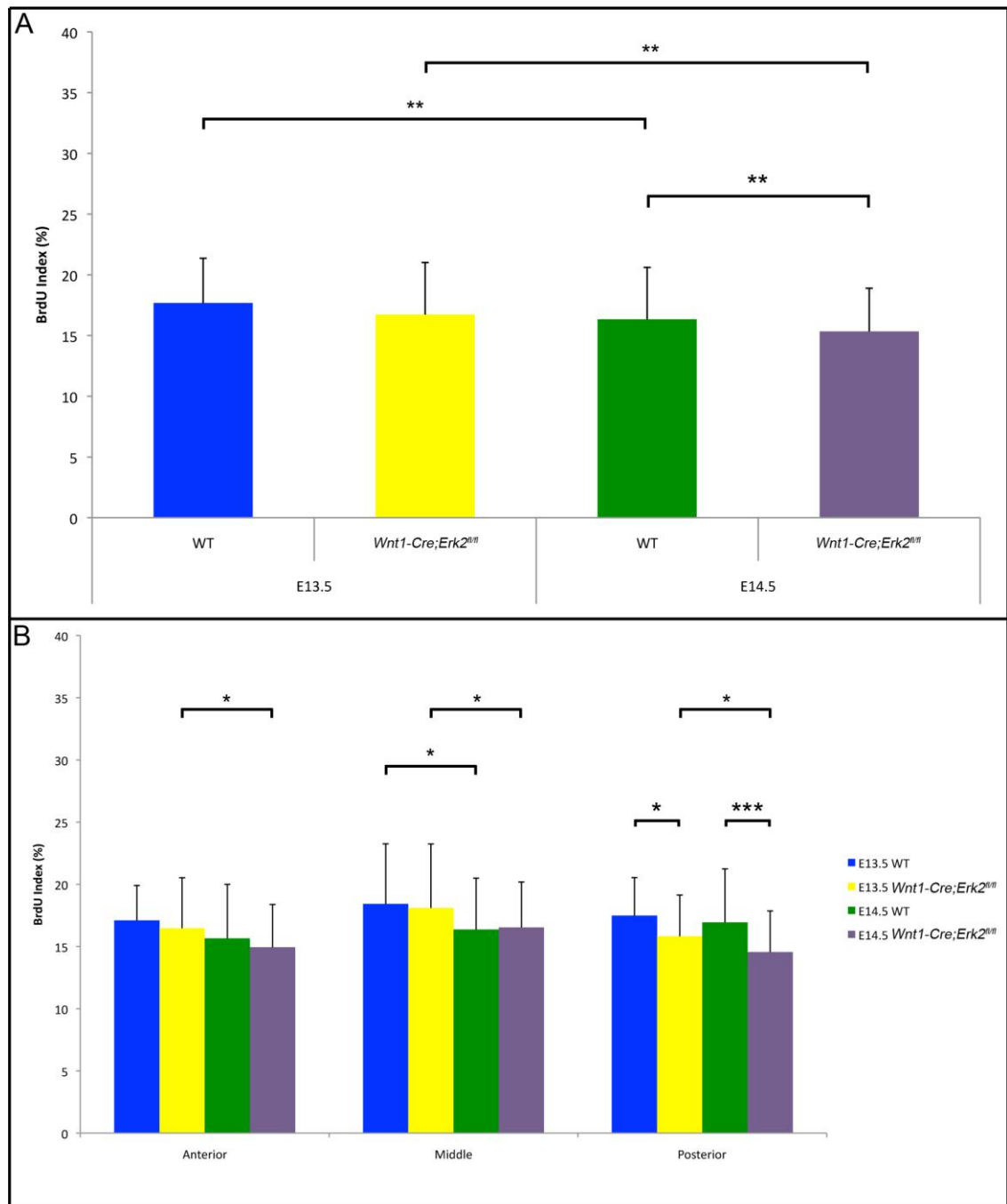
third and the overall difference in proliferation reached the  $p < 0.05$  level of significance (Fig. 10.3A). As the *Wnt1-Cre;Erk2<sup>fl/fl</sup>* palate continued to develop proliferation dropped significantly across the wild-type mouse only showed a middle third of the palate (Fig. 10.3B). In contrast significant drop in proliferation in the

### 10.3.2.2 Distribution of proliferation

There were regional differences in proliferation observed across the frontally orientated heat maps of the *Wnt1-Cre;Erk2<sup>fl/fl</sup>* palates. In the wild-type at E13.5 there was slightly increased proliferation on the prospective nasal side of the palate and proliferation was higher towards the tip of the palatal outgrowth compared to the more dorsal tissue. The overall pattern of proliferation was very similar between the wild-



type and the *Wnt1-Cre;Erk2<sup>fl/fl</sup>* mutant palate at E13.5, with a prospective oronasal difference still visible, but the *Wnt1-Cre;Erk2<sup>fl/fl</sup>* palatal outgrowth was slightly higher in the tip region (Fig. 10.4A, B, E & F).



In

**Figure 10.3 Wild-type and *Wnt1-Cre;Erk2<sup>fl/fl</sup>* proliferation index results** A) Overall BrdU index for wild-type and *Wnt1-Cre;Erk2<sup>fl/fl</sup>* mutant palates (E13.5 and E14.5) B) Changes in proliferation along the AP axis between the wild-type and *Wnt1-Cre;Erk2<sup>fl/fl</sup>* palate. Error bars display 1 standard deviation. Results of t-tests are shown \* $p < 0.05$  \*\* $p < 0.01$  \*\*\* $p < 0.001$  the wild-type at E14.5 the elevated palatal shelf displayed slightly higher proliferation along the oral side compared to the nasal side (Fig. 10.4C & G). The highest level was in the medial-oral region and the lowest was dorsal to this in the medial nasal

region. At E14.5 the mutant palate had not elevated but the pattern of proliferation had varied since E13.5. The tip of the palate appeared to have higher proliferation than the rest of the palate whereas in the wild-type the tip did not stand out as a distinct region on its own (Fig. 10.4C-D). There appeared to be less of a difference between the prospective nasal and prospective oral sides of the palate in the *Wnt1-Cre;Erk2<sup>fl/fl</sup>* mutant (Fig. 10.4H).

### 10.3.3 Internuclear spacing in the *Wnt1-Cre;Erk2<sup>fl/fl</sup>* palate

There were variations in the cell packing clearly visible across the frontal sections at E13.5 and E14.5 in both the wild-type and mutant embryos (Fig. 10.5). At E13.5, in the wild-type, the cells were less densely packed on the prospective nasal side and this pattern stretched from the tip region to the dorsal end of the palatal outgrowth (Fig. 10.5A & E). Post elevation, at E14.5, there was a large decrease in cell packing in the outgrowth with the nasal side showing slightly decreased packing (Fig. 10.5 C & G). The cells were more tightly packed the further they were from the distal tip of the palate in the wild-type at E14.5.

In the *Wnt1-Cre;Erk2<sup>fl/fl</sup>* palate at E13.5 a prospective oral/nasal variation was still observed, with the packing on the prospective oral side being at similar levels to the wild-type despite the overall height of the palatal outgrowth being significantly smaller. The cell spacing seen in the *Wnt1-Cre;Erk2<sup>fl/fl</sup>* mutant was constant between E13.5 and E14.5, except in the tip region, which changes to mimic the mesenchyme dorsal to it, so the prospective nasal side becomes slightly more tightly packed and the prospective oral side is slightly less tightly packed. This change meant the E14.5 *Wnt1-Cre;Erk2<sup>fl/fl</sup>* palate more closely resembled the E13.5 wild-type palate.

The differences appeared to be fairly subtle in the assays studied here between the *Wnt1-Cre;Erk2<sup>fl/fl</sup>* mouse and its wild-type littermates but they resulted in a cleft palate. It is also worth noting that the Chai group who provided these samples have observed that the palate of the *Wnt1-Cre;Erk2<sup>fl/fl</sup>* mouse does eventually elevate at around E15.5-E16.5 but still forms a cleft.

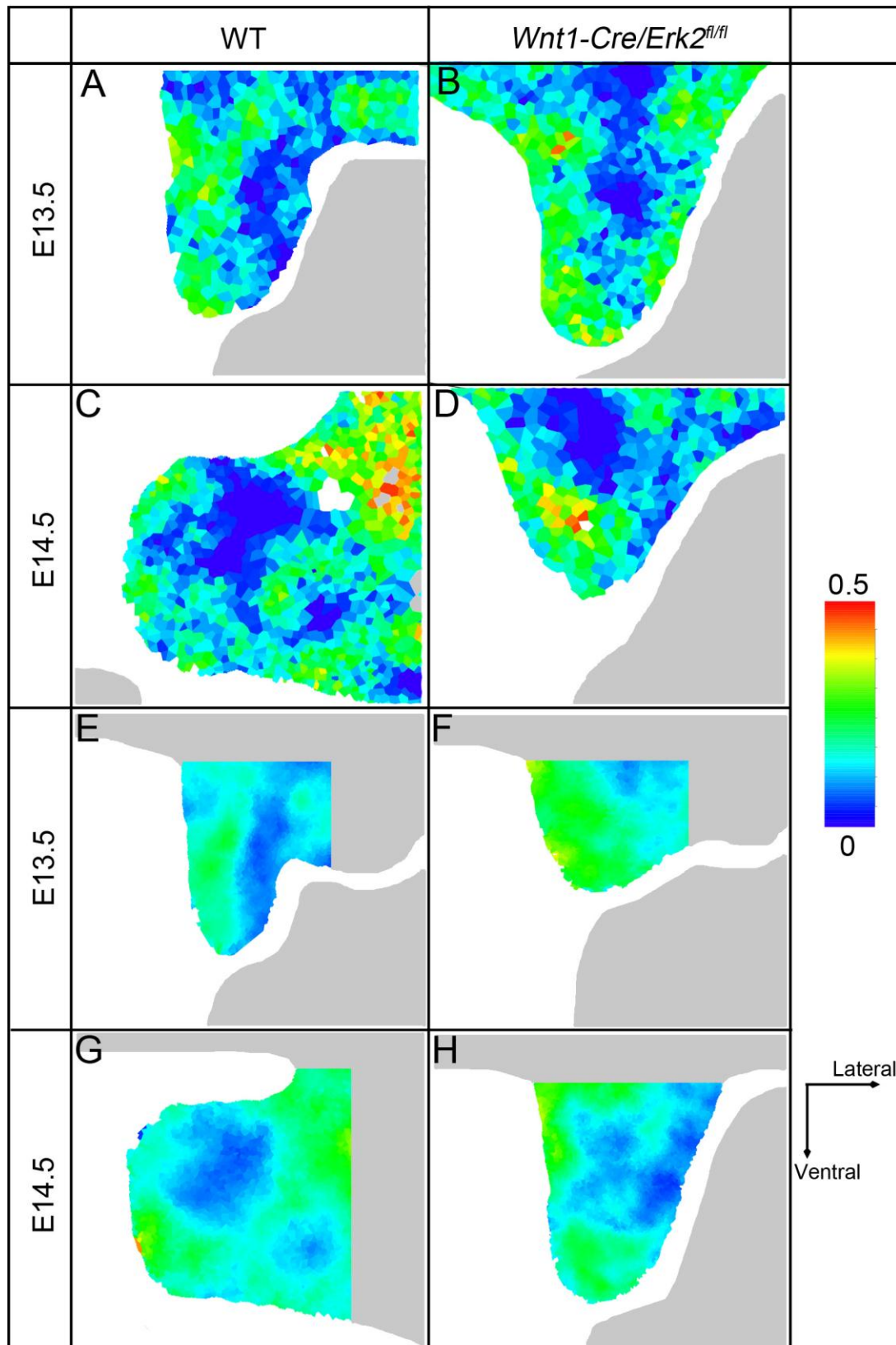


**Figure 10.4 Proliferation heat maps of E13.5 and E14.5 wild-type and *Wnt1-Cre;Erk2<sup>fl/fl</sup>* palatal shelves** A) Individual heat map of E13.5 wild-type palate B) Individual heat map of E13.5 *Wnt1-Cre;Erk2<sup>fl/fl</sup>* palate C) Individual heat map of E14.5 wild-type palate D) Individual heat map of E14.5 *Wnt1-Cre;Erk2<sup>fl/fl</sup>* palate E) Heat map of E13.5 wild-type palate F) Heat map of E13.5 *Wnt1-Cre;Erk2<sup>fl/fl</sup>* palate G) Heat map of E14.5 wild-type palate H) Heat map of E14.5 *Wnt1-Cre;Erk2<sup>fl/fl</sup>* palate. Each heat map is an average of three individual sections.

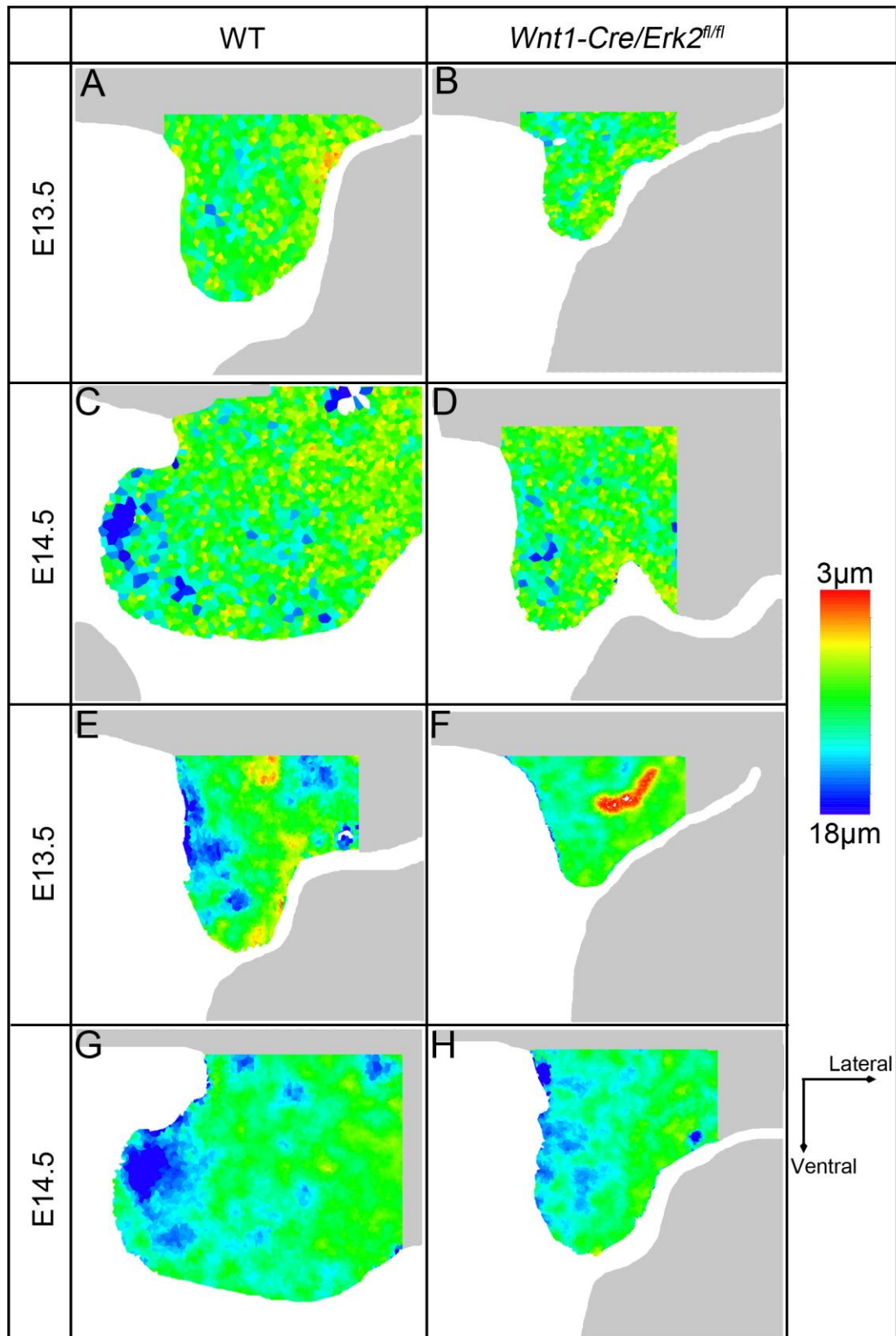


**Figure 10.5 Internuclear spacing heat maps of E13.5 and E14.5 wild-type and *Wnt1-Cre;Erk2<sup>fl/fl</sup>* palatal shelves** A) Individual heat map of E13.5 wild-type palate B) Individual heat map of E13.5 *Wnt1-Cre;Erk2<sup>fl/fl</sup>* palate C) Individual heat map of E14.5 wild-type palate D) Individual heat map of E14.5 *Wnt1-Cre;Erk2<sup>fl/fl</sup>* palate E) Heat map of E13.5 wild-type palate F) Heat map of E13.5 *Wnt1-Cre;Erk2<sup>fl/fl</sup>* palate G) Heat map of E14.5 wild-type palate H) Heat map of E14.5 *Wnt1-Cre;Erk2<sup>fl/fl</sup>* palate. Each heat map is an average of three individual sections.

## 10.4 *Wnt1-Cre;Erk2<sup>fl/fl</sup>* Discussion

Disruption of *Erk2* led to defects in a couple of cellular behaviours with a disruption to the distribution of proliferation and a delay in the patterning of cell density. The palatal shelves are smaller than normal and the process of elevation is delayed. Overall, the *Wnt1-Cre;Erk2<sup>fl/fl</sup>* palate phenotype seen at E14.5 closely resembles the E13.5 wild-type palate. There is still evidence of downstream activity, normally caused by *Erk2* in the mutant, because *Erk1*, which can activate the same downstream targets, is still functioning. Mutants with *Erk1<sup>+/-</sup>* and *Wnt1-Cre;Erk2<sup>fl/fl</sup>* show a more severe phenotype and ones with the double knockout *Erk1<sup>-/-</sup>* and *Wnt1-Cre;Erk2<sup>fl/fl</sup>* display an even more severe phenotype. *Erk2* is able to fully compensate for the loss of *Erk1* shown by the *Erk1<sup>-/-</sup>* mutant does not display a phenotype, but the same is not the case for *Erk1* in the *Wnt1-Cre;Erk2<sup>fl/fl</sup>* as a clear phenotype has been described. *Erk* activity is dose dependent. Therefore different degrees of severity are seen as more of *Erk1* and *Erk2* is knocked out. This has been shown in a culture experiment where EGF (Yamamoto et al., 2003), which increases *Erk* activity, caused increased proliferation and inhibited the normal palatal fusion process. For example epithelial bridges were left in the palate after the palate should have fused. To rescue the EGF-induced cleft palate an inhibitor of *Erk* activity was added to the culture system, this decreased proliferation in the MEE in a dose-dependent manner. The dose needed to stop proliferation in the MEE, where normally there is very little, was the same as the dose needed to rescue the EGF-induced cleft palate.

During normal palate development the level of *Erk* activity and the consequential cell proliferation are tightly regulated and the consequences of disrupting *Erk* signaling include a cleft palate. TGF-beta signaling has been shown to be very important in the epithelium around the tip region at the time of fusion and this is thought to inhibit the effect of *Erk2*. One reason for a different level of proliferation at the tip of the E14.5 palate in the *Wnt1-Cre;Erk2<sup>fl/fl</sup>* mutant could be that changing the dose of one signal has a knock-on the effect on another signal and its downstream pathway.

The lower dosage of *Erk1* that is still operating could be why the E14.5 *Wnt1-Cre;Erk2<sup>fl/fl</sup>* resembles the E13.5 wild-type palate in terms of cell spacing, proliferation and dimensions. Before the palate can elevate a certain force from intrinsic factors needs to be generated and this takes longer to occur with such low levels of *Erk* signaling which is how the shelves do eventually elevate.

Palate elevation also depends on extrinsic factors and these are affected by the loss of *Erk2* signalling such as in the tongue and mandible. Around the time of palate elevation the mandible is undergoing elongation and the tongue appears to drop, creating space for the palate to elevate. An E13.5 palate in a dissected out embryo can be made to elevate by depressing the mandible and tongue with a blunt probe but upon release the tongue rises again and the palatal shelves return to their original vertical position (Ferguson, 1978). The loss of *Erk2* in the *Wnt1-Cre;Erk2<sup>fl/fl</sup>* mutant also impacts mandible and tongue development, it is possible that the low levels of *Erk1* are able to compensate for this in a similar way and on a similar time scale as the palate which is how the palate is eventually able to elevate. Both intrinsic and extrinsic factors must be correct for the process to occur.

Some of the changes seen here are quite subtle but the overall impact on palate development is quite dramatic. These changes might have been missed if the original proliferation analysis was just taken from a sample region of the palate and the pattern of the staining not observed. It would be very interesting to see if the pattern of cell spacing and the level of proliferation in the *Wnt1-Cre;Erk2<sup>fl/fl</sup>* palate ever catches up with the wild-type, or if it falls further behind as development continues. Other mechanisms of morphogenesis might also be disrupted and it would be useful to look at some of these as well. For example the orientation of the Golgi, which is the main defect in the *Tbx-1<sup>-/-</sup>* palate as similarities between the symptoms caused by the disruption of *Erk2* and DGS have already been noted.

## **11.0 General Discussion and Future Considerations**

### **11.1 General discussion on palatogenesis**

This project focused on the cellular mechanisms that contribute to palatogenesis. It is necessary to firstly understand how these contribute to the normal development of the palate to further learn about what has gone wrong in cases of cleft palate. This thesis has developed a set of techniques that allowed cellular behaviours to be qualitatively and quantitatively determined from sectioned material and examined. A necessary cell phenotype dataset for the normal development of the palatal mesenchyme has been produced at a higher resolution per palate than previously done in the field. It included all the stages from the initial outgrowth through to the beginning of palatal shelf fusion. These assays were then used to compare cellular behaviours in three mouse models with a cleft palate phenotype against the normal cellular behaviours contributing to palatogenesis. A combination of factors was found to be contributing to wild-type palate development and the genetic knockout models used in this project showed that a defect in any of a range of mechanisms can result in a cleft palate.

#### **11.1.1 Cellular behaviours contributing to initial palatal outgrowth**

This project has identified a combination of high levels of proliferation and directional cell behaviours that are behind the initial outgrowth of the palatal shelves at the base of the maxillary process at E11.5. The orientation of Golgi presented by E11.5 had a significant ventral bias, which could be interpreted as suggesting that cells are migrating towards the distal tip of the palatal outgrowth. These migrating cells would be cranial NCC that were travelling anteriorly towards the tip of the maxillary outgrowth. Something would have needed to have caused the direction of these cells to change by 90°. One possibility is that this is happening in response to a chemoattractant. The presence of a chemoattractant would not be a new idea in either the development of an outgrowth or of the palate itself. There is evidence of directional cell behaviours in response to a chemoattractant contributing to the outgrowth of the limb bud (Wyngaarden et al., 2010) and evidence has been presented of a chemoattractant being present in the palate later on in development (He et al., 2008). Future work on the initial outgrowth stage of palate development

should aim to identify the presence of any possible chemoattractant molecules. The strong directional bias displayed by the Golgi at E11.5 gave way to a more random distribution at E12.5 except in the distal tip region. If the cell orientation is indeed directed by a chemoattractant gradient, one might expect the tip/edge region to be the location of its highest and therefore longest lasting concentration.

The palatal shelves continued to elongate down either side of the tongue for over sixty hours. The length increased steadily, and, after the wider initial outgrowth seen at E11.5, the palate formed its more characteristic “U” shape outline, when viewed in frontal sections, at E12.5. This initial decrease in width potentially contributed to the increase in length by cells intercalating, perhaps by convergent extension. The distribution of Golgi in the palate at E12.5 did not show a bias towards the midline but a closer look at the cell shape and taking samples between E11.5 and E12.5 would be a starting point for investigating this further.

The high level of proliferation that was evident at E12.5 and the constant cell spacing means that the new cells must be contributing to the increase in length of the palate. The data obtained in this project – which is more complete than any previously reported in the literature – showed that proliferation varies significantly along the AP axis and there is a lot of noise across the prospective oral-nasal axis of the palate. Therefore in proliferation studies of the palate care needs to be taken when deciding where to sample and how many samples to take in order to avoid misleading results. The ideal way to avoid error or bias is to do a high-resolution examination of proliferation in the palate. This would be made easier by using automated cell identification and counting macros, like those used in this thesis.

There did not appear to be any consistent orientated cell division at these early stages of palatal shelf outgrowth. It therefore seems highly unlikely that OCD contributes towards the outgrowth of the palatal shelf. Given the low sample size, a weak trend might not have reached statistical significance but it is difficult to know how many would be needed to identify a true random distribution from one with too few spindles. The rose plots mapping the OCD data showed a very weak bias along the proximodistal axis of the palate. At this stage, and in general, the OCD could be actively regulated or passively responding to external-force-driven cell shape change. Therefore this weak bias could be the consequence of other directional behaviours pulling on the cell and causing it to become elongated along the proximodistal axis.



This would cause the slight bias seen in the rose plots because of the tendency for cells to divide along their long axis.

As palatal outgrowth continued this project found evidence of further directional behaviours occurring across the palate's prospective oral-nasal axis. This is consistent with previous work that claimed that cells in the anterior palate migrate towards the prospective oral side of the palate (He et al., 2008). There is not a clear link between this movement and the initial outgrowth but this directional behaviour, along with subtle patterns across the prospective oral-nasal axis in localised cell proliferation and cell density, could be related to palate elevation (see below).

The internuclear spacing heat maps showed that cell density remained fairly constant throughout the initial outgrowth phase despite the noisy distribution of proliferation and evidence pointing towards cell movements occurring. Although to know the true meaning of these data information on the contributing factors such as cell shape and ECM volume are required.

This work has contributed to a more detailed picture of the mechanisms behind the initial palatal outgrowth. The leading theory for palate elevation says the two ends of the palate elevate using different mechanism (Bush & Jiang, 2012) and this work has shown there are significant differences along the AP axis, visible from just twenty-four hours after the palate was first visible.

### **11.1.2 Palatal elevation**

The extensive literature on the process of palatal elevation has already been introduced showing that there is still debate over the exact mechanism by which the process of elevation occurs. The leading theory is that the anterior palate develops by a flip-up mechanism while the posterior palate relies on a remodelling mechanism (Larson, 1962; Ferguson, 1978). A failure of palate elevation is evident in many mouse models with a cleft palate, indicating that many genes are involved, but the relationship between the many genes and the actual mechanisms remains unclear. Palatal elevation is a rapid process. It is too rapid for it to be due to regrowth of the palate (Walker and Fraser, 1956), but the palate spends hours preparing for it. Palatal elevation is asynchronous, both shelves do not always elevate together. Both intrinsic and extrinsic factors contribute to palatal elevation, and if any of these are disrupted

the palatal shelves will remain vertical and the embryo will develop a cleft palate. The extrinsic factors involve the proper development of the structures surrounding the palate. The mandible needs to elongate correctly allowing the tongue to form normally and to drop into a resting position lower in the oral cavity. This removes a physical barrier from the palate allowing it to move upwards, and creates space for it to lie horizontally at the top of the oral cavity.

The analysis in the preceding chapters has shown that the anterior palate displays multiple differences across the prospective oral-nasal axis at E12.5 and E13.5. The main overall growth of the palate at these stages is in a ventral direction and it is tricky to see how differences across the prospective oral-nasal axis would contribute to this. It is more plausible that these changes are in preparation for palatal elevation. Proliferation was slightly greater on the prospective nasal side and the cells were subtly more loosely packed here, whereas there was relatively less proliferation and comparatively more tightly packed cells on the prospective oral side.

The slight variation in cell density across the palate at E13.5 could have been due to both the previously discussed movement of cells across from the prospective nasal to the prospective oral side, and a change in the amount of ECM. Of particular interest in the ECM is the GAG content which has previously been measured and shown to peak at E13.5 (Foreman et al., 1991) and which would cause the cells to be more spaced out. The increased levels of GAG, particularly the highly electrostatically charged hyaluronic acid, would cause a change in the osmotic potential of the palate as well. All of these small, but consistent changes and movements happening in the small and confined space of the palatal mesenchyme could contribute to creating the forces required for the anterior palate to flip-up and remain horizontal above the tongue. The build-up of cells on the prospective oral side of the palate could be like a spring that is pulled back and then when it is released by the removal of the tongue or another signal, the cells spring back towards the other side of the palate. This might create enough force to help flip the palate upwards.

Cleft palate has been found in mutant models where the behaviours along the prospective oral-nasal axis were disrupted and there is evidence from more molecular work that some genes only act on one half of the palate (Smith et al., 2012; Hilliard et al., 2005). This provides support for what could otherwise be considered very weak variations in behaviours along the prospective oral-nasal axis in the palate at E13.5. Mouse mutants, different from those studied here, have contributed evidence to the

molecular control of palatal elevation. There was reduced accumulation of GAGs in the *FgfR2* mutant (Snyder-Warwick et al., 2010). These mutant mice also had increased proliferation along the prospective nasal side of the anterior palate. These changes resulted in a cleft palate. There was also a failure of elevation leading to a cleft palate in the *Osr2*<sup>-/-</sup> mutant (Lan et al., 2004), which had reduced proliferation on the prospective nasal side of the palate. These models of cleft palate all demonstrate the importance of the differences across the prospective oral-nasal axis during palatal development.

It has been proposed that elevation of the posterior palate occurred due to a remodelling mechanism (Bush and Jiang, 2012) and the work in this thesis has provided further evidence to support this theory. At E12.5 there was no significant difference in the orientation of directional behaviours along the AP axis but by E13.5 the posterior third had a significantly different distribution from not just the previous stage, but also the anterior two-thirds of the E13.5 palate. The cells in the posterior region switched from a ventral to a dorsal and lateral bias. The dorsal aspect of this new direction could mean the cells were now migrating towards the palate's proximal end before they flowed over the top of the tongue resulting in an elevated palate. The slight lateral bias is harder to explain as eventually the cells need to move medially but the medial movement could be initiated after the E13.5 time point measured here. In fact, a histomorphological study has been carried out that shows the remodelling event occurs around E14.0 to E14.5 between time points studied here (Yu and Ornitz, 2011). Refining the time course further would be a key focus of future work.

The cells remained more evenly packed in the posterior palate. Immediately prior to elevation (E13.75) the GAG content in the posterior palate has been shown to be uniform (Brinkley & Morris-Wiman, 1987) this would provide a matrix and allow the cells to migrate, contributing to the remodelling process.

The PCP pathway has been linked to cell polarity behaviours and cell movement. This pathway involves the Wnt receptors frizzled 1 and frizzled 2 (*Fzd1* and *Fzd2*). The double knockout *Fzd1*<sup>-/-</sup>/*Fzd2*<sup>-/-</sup> mouse exhibits a cleft palate, sometimes due to a failure to elevate (Yu et al., 2010). The *Wnt5A* mutant mouse also has a cleft palate and the shelves do not manage to elevate (He et al., 2010). Therefore the PCP pathway could be involved in palatal development potentially driving the polarised cell behaviours, such as cell migration, that could be contributing to palatal elevation. This molecular evidence is consistent with the cellular behaviours observed in some ex-vivo

experiment (He et al., 2010). However, it would be interesting to apply the same cell polarity orientation analysis to these mutants to determine whether the orientations uncovered in this project were indeed disrupted in the mutant mesenchyme.

### **11.1.3 Post-elevational growth**

Once the palatal shelves elevate the two opposing shelves need to grow towards the midline. The mid-palate region reaches the midline first. The mid-palate starts off being longer than the anterior and posterior regions so it does not have as far to grow. This work has provides evidence of cellular behaviours occurring in the mid-palate before they happen elsewhere. Perhaps surprisingly, higher cell proliferation is not one of these; between E13.5, which is before elevation, and E14.5, which is after elevation, proliferation decreased by twice as much as it did in any other 24-hour interval. Therefore it is unlikely that proliferation was a major contributor to the directional post-elevational growth towards the midline. Rather, the dataset in this thesis shows evidence that post-elevational growth was due to an increase in cell spacing and medially directed polarity, potentially symptomatic of cell migration, towards the midline. The increase in cell spacing could first be seen in the mid-palate at E14.0, immediately after shelf elevation (several other embryos in the same litter had not elevated at E14.0 and there was a gap between the two elevated shelves along the entire AP axis of those embryos that had elevated). It was even more evident by E14.5 when the two shelves were touching in the midline but not yet fusing. The spacing in the anterior and posterior regions did not show this increase until a stage later, E15.5, at which point they were also touching in the midline. In the palate at E14.5 over half the cells were displaying polarised behaviours towards the medial tip. This included cells in the mesenchyme adjacent to the palatal outgrowth. Therefore cells could have been migrating into the palate and towards the medial tip driving the elongation towards the midline. There was evidence of an increase in cell spacing along the entirety of the AP axis suggesting that this could be a mechanism for post-elevation medial growth throughout, despite other differences between anterior, middle and posterior palate. The exact timings seemed to vary slightly along the AP axis and between embryos, but this is consistent with the different timing of elevation and there is debate over the order in which the process of elevation occurs along the AP axis (Walker and Fraser, 1956; Yu and Ornitz, 2011). A more detailed time series with a larger number of embryos is required to start to fully understand the extent to which these cellular behaviours contribute to post-elevational growth.

#### **11.1.4 Epithelial influence on the mesenchyme**

The palatal mesenchyme does appear to be driving the thinning of the epithelium along the nasal side as it expands beneath it (Luke, 1989). The overall control of palate morphogenesis involves signalling pathways that go between the mesenchyme and the epithelium, but the individual behaviours are generally more restricted to one or the other (Economou et al., 2013). The distal tip of the palate when it is growing vertically is not the medial edge after elevation in the posterior palate (Jin et al., 2008); this is further evidence that the mesenchyme and the epithelium are growing independently. Vital signalling could be coming from the epithelium, because it is more spatially consistent. The exact location of behaviours seems to be very important in the development of the palate, and so the signalling behind these behaviours needs to reach the correct areas. For example it was proposed that the posterior palate elevates by remodelling itself, which might have required the cells to move. Therefore signals originating from these mesenchymal cells might not be in the correct place. In contrast the epithelium was a lot more spatially constant, demonstrated by the continual appearance of the rugae. So signalling pathways that required the epithelium ensured that the correct region of the palate performed the correct mechanism at the correct time.

#### **11.1.5 Mouse models of cleft palate**

Several genes have been shown to have different expression patterns along the AP and the mediolateral axis (Bush and Jiang, 2012; Smith et al., 2012). These match patterns seen in the cell behaviours. By disrupting these signalling pathways both their role and the role of the cell behaviour they contribute to in palatal development could be identified. This helps our understanding of not just normal palate development but also how these behaviours can go wrong and result in a cleft palate.

A mutant in the *Tbx-1* gene has been linked to DiGeorge syndrome and symptoms include a cleft palate. *Tbx-1* is expressed in the epithelium throughout palatal development (Zoupa et al., 2006). Previous studies into the cellular mechanism behind this cleft palate have been inconsistent in their findings (Funato et al., 2012; Goudy et al., 2010). They have shown that a standard high-resolution toolset is required to analyse the cellular mechanisms behind cleft palate. By performing a high-

resolution study of the *Tbx-1*<sup>-/-</sup> mouse this work has shown that there is a significant difference in the level of proliferation between the wild-type and the mutant, but only at E13.5 and E15.5. By E15.5 the decreased proliferation could have been due to the cumulative effect of other aspects of development going wrong. Perhaps the mutant embryo was starting to abort. Consequently any cellular behaviours measured might be disrupted indirectly. Interestingly, during very early palate development of the *Tbx-1*<sup>-/-</sup> mouse the palate displayed slightly higher levels of proliferation than the wild-type. The discrepancies in proliferation levels found by different groups in the field could be due to low n numbers, variations between strains or slightly different stage criteria used. More unexpected than the transient differences in proliferation was the significant difference in the orientation of the Golgi identified by this study. This significant change in distribution means the cleft in the *Tbx-1*<sup>-/-</sup> mouse could be as much due to the disruption of polarised cell behaviours, as due to a proliferation defect.

The *Msx-1*<sup>-/-</sup> mutant failed to proliferate enough to form an outgrowth large enough to reach the midline when relying on normal post-elevational growth behaviours, such as an increase in cell spacing and the directional cell behaviours. Therefore it never got a chance to fuse, despite being able to do so in culture. Sometimes it even fused with the tongue therefore it is able to fuse but needs to make contact with another epithelium for it to happen. The fact that it sometimes fused with the tongue could mean that the integrity of the palate had been disrupted. It was not able to hold itself horizontally above the tongue, or the elevation process, which does sometimes fail in *Msx-1*<sup>-/-</sup> mice, had not been completed and the palatal shelves had come into contact with the tongue, at which point the epithelium started the fusion process. This could have been due to not having enough cells but it is also likely that there was not enough ECM was present, as demonstrated by the data showing that the *Msx-1*<sup>-/-</sup> mutant palates had more tightly packed cells than the wild-type. The *Msx-1*<sup>-/-</sup> mutant palate may have been able to elevate the majority of the time because overall the size of the palate was significantly smaller than the wild-type. Therefore potentially smaller forces were required and there was less distance to remodel over; indicating that proliferation contributes to the outgrowth of the palate but not the process of elevation. *Msx-1* expression is restricted to the anterior palate (Satokata and Maas, 1994). This is where the more severe alterations to the level of proliferation were shown, but the posterior palate also had significant differences between the wild-type and mutant palate. This could mean there are links, maybe indirect ones, between the

developmental processes contributing to directional growth in the different regions of the palate.

Analysis of the *Wnt1-Cre;Erk2<sup>fl/fl</sup>* mutant gave results suggesting that the signalling pathways involved in palatal development sometimes act in a dose dependent manner or redundantly. There are predicted to be still low levels of *Erk*-dependent signaling taking place in the *Wnt1-Cre;Erk2<sup>fl/fl</sup>* mutant due to the presence of *Erk1*, which activates the same pathway, but not as efficiently or as strongly. It has been demonstrated that the cleft caused by the *Erk* inhibitor EGF can be rescued in a dose dependent manner by the addition of an *Erk* inhibitor (Yamamoto et al., 2003). The palatal shelves in the *Wnt1-Cre;Erk2<sup>fl/fl</sup>* mutant reportedly show delayed elevation (Parada, 2013). Results in Chapter 10 demonstrate that the cell behaviours in the palate occurred as in wild type, but not until a stage later than normal. The *Wnt1-Cre;Erk2<sup>fl/fl</sup>* mutant palate is also slightly smaller than the wild-type. These results hint at the possibility that *Erk*-dependent signalling acts in some sense as a developmental clock: lower amounts delay the timing rather than the outcome of developmental processes. However, this may be over-simplistic: *Erk* signaling affects palate, mandible and tongue development, so both intrinsic and extrinsic factors could be disrupted in a way that merely appears to be a developmental delay.

All of these mutants display a defect in the level of proliferation at some point during palate development. This work has identified other cellular behavioural defects in each mutant demonstrating the importance of performing more than just a proliferation assay.

These mutants showed that a defect in just a single gene, however small its role in palatal development might be, could cause a cleft palate. Some genes act in a dose dependent manner, but even when they are compensated for, it only takes a slight deviation from the normal levels and a cleft palate is formed.

## **11.2 General discussion on assays and possible future improvements**

### **11.2.1 How to improve/develop these assays**

#### **11.2.1.1 Proliferation**

The proliferation assay could be developed further to calculate the cell cycle time. The controls and different interval lengths tested for the IddU and BrdU double labelling experiment are shown in the appendix. Instead of using IddU and BrdU, a marker for a different part of the cell cycle could be used, because with IddU and BrdU there was very little difference in the number of cells marked at E13.5. Calculating how many cells are proliferating at each stage, possibly by using a marker such as Ki67, and then weighting the cell cycle time calculation and changing the assumptions, might work at different stages (as a different proportion of cells likely to be proliferating at each stage).

#### **11.2.1.2 Heat map analysis**

Individual heat maps display such a high resolution that they can appear quite noisy. A way of creating an automated summary diagram could be developed, but would require the images to be very accurately registered so that the correct regions were picked out of each image. The registration techniques already exist and are well established in fields such as brain imaging (Crum et al., 2004; Schmitt et al., 2007; Zitova and Flusser, 2003). When a non-rigid registration is required this would have to be careful linked back to the original spacing data so that the values are not distorted. Alternatively the registration could be done after the heat maps have been created in greyscale. The greyscale value can then be used to average between the images but so far it has not been possible to reapply the same colour scale back to the heat maps that R was using.

The heat maps are an appropriate way of representing cell spacing data. Changes over small areas can be seen or the data can be averaged over a larger number of neighbours to give a more smoothed average. Unfortunately, the macro used in this project did not output the map data in a numerical form that would of allowed statistical analysis. The user has an idea of the spacing values as they have set the scale, but



being able to perform statistical tests would identify which are the significant differences in cell spacing. Extracting the information manually from enough individual sections to perform valid statistical analysis would be hugely time consuming due to the time taken to extract each image and highlight and extract the data from a single specific area at a time.

### **11.2.1.3 Measuring orientation of the Golgi or spindles**

It should be possible to automate the measurements of the angle of Golgi relative to the cell nucleus. The biggest hurdle that needs to be overcome is ensuring the computer correctly identifies which Golgi belongs to which nucleus in a tightly packed block of cells. A good membrane stain, either with an antibody or using the mT/mG mouse line, should allow this to be programmed. Use of an antibody, or better still a chemical stain, which might be cheaper and more widely available than the long-term maintenance of a mouse line, would be preferable as part of a standardised toolset for phenotype analysis.

This study did not have enough spindles, particularly in anaphase, to be able to do statistical analysis and draw conclusive results about any contribution OCD might have to palatal development. This can simply be overcome by including more samples, both from each palate and from more embryos. It is difficult to know exactly how many more samples are needed to be confident enough to tell the difference between a true random distribution and one because the sample number is too low. More than ten times the number of Golgi than spindles were used measured for the wild-type dataset but this would mean around thirty mice would be required and ten times the number of hours on the confocal microscope.

### **11.2.2 Further investigations**

Investigating cellular mechanisms of morphogenesis leads to more detailed questions about the development of the palate, some which could be more easily investigated than others. Although once the toolset developed here has been applied to a mouse mutant the next steps a research group takes will depend on their individual findings.

There are some fairly large changes in palate morphology occurring between the time points focused on here and in many studies of palatal development and so to better

understand how different mechanisms are contributing to palatal development more closely spaced time points. This would not only help refine understanding of events such as rapid anterior palate elevation but also pinpoint the earliest signs of abnormality, and therefore the likely first cause of failure, in cleft mutants. Ideally an ex-vivo culture technique could be developed to allow the time points to be more controlled, as even embryos within the same litter display variation in the stage of palatal development. Other factors than the presumed time from conception used in this project could be used to stage the embryos (e.g. weight, limb development) because the further away from conception the embryo is the more it could be varying from its littermates.

It has been strongly implied that cell migration is contributing to palatal development. Ideally a culture system that allows live imaging of individually labelled cells could be set up and their movements tracked. A sparse labelling of cells from a tamoxifen injected mT/mG mice could be used, as a low level of Cre recombinations would create a few green fluorescent cells that could easily be visualised. However, this live imaging technique pushes the limits of current microscopy due to the thickness of the tissue and the smallness of the cells. Culture systems, such as rolling head and perfusion-chamber systems, may allow the palate to grow normally but are problematic optically. Also the palate does not grow properly as an explant on its own or as part of a head slice culture.

Changes in cell density have been identified and it would be interesting to see how the adhesions between cells change over time as well. In order for the mesenchyme to flow more easily around the time of elevation, particularly in the posterior region, the number of cell-cell adhesions might decrease. If the number of cell-cell adhesions decreases the cells might be relying more on diffusible signalling molecules. This could be evident from gradients of cell behaviours leading to the source of the signal, and could help identify any signal control centres set up during palatal development. This could be done initially by looking at different adhesion markers, such as cadherins for cell-cell adhesions; cell-matrix adhesion molecules could also be looked at.

A lot of the stages of palatal development that have been investigated here show the palate potentially making intrinsic changes to allow it to produce the forces required for elevation. It may also soon be possible to take force measurements using atomic force microscopy (AFM) to measure the nanoforces occurring in the cells (Stewart et al., 2011). If a culture technique that allows the palate to elevate as it would in vivo is

developed, then the actual forces present in different regions and at different times could be measured and provide a greater understanding of the mechanism behind palatal elevation.

This study has focussed on the impact of the mesenchyme on palatal development but there is always scope to look at the epithelium as well. As well as investigating these cellular behaviours in epithelial development its contribution too palatal elevation could be analysed. There are two key shoulder regions, one of which becomes more tightly bent and the other straightens out during elevation. These could be a consequence of mesenchymal movements or they could contribute independently to the elevation process.

To work out the interplay between intrinsic and extrinsic forces during palatal development experiments similar to those carried out by Ferguson in the 1980s could be performed followed by the assays used here. For example the changes in cell spacing seen after elevation could be a result of the movement occurring in palatal elevation and not driving the growth. One way to test this would be to make the palate elevate earlier than normal by depressing the mandible and tongue with a blunt probe. The tissue could be fixed immediately, sectioned, stained with DAPI and imaged. Then cell spacing could be looked at in a situation where it would not of been possible for it to react to a new molecular signal. Preliminary experiments (see appendix) to this effect were carried out, but in many cases the fixing process was not quick enough to maintain the shelves in a vertical position, even when the tongue and mandible was removed. Sometimes the shelves appeared folded or damaged. This may have happened during sectioning. Perhaps the presence of the mandible normally offers protection during the sectioning process. In any case, as reported by Ferguson, the stability of the shelves in an elevated position increases as the normal elevation stage is approached, so optimisation may simply involve obtaining exactly the right staged embryo. Interestingly in none of the experiments did the posterior palate elevate. This could have been due to the mandible not being depressed enough (if it was pushed too much the tissue would split) but a more appealing explanation is that while anterior flip-up depends on rapid release of stored elastic force, posterior elevation requires cell movements that take place on a much slower time scale.

### 11.2.3 Other assays that could be included

The analytical “tool set” used in this project and in the Green lab currently focuses on four cellular behaviours, but they are not the only cellular mechanisms that could be contributing to palatogenesis.

Changes in cell shape could be contributing to directional growth, if they all elongate along the same axis. This could be affecting the OCD as well, because cells have been shown to divide along their long axis often. Differences and similarities in different regions across the palate could be providing information about any of the key stages of palatal development and the forces that might be acting on the cells. The mT/mG mice could be used from the images taken for the Golgi/OCD analysis to start look at cell shapes. A low level of Cre recombinations could be induced so that a random sampling of individual cells is highlighted, making cell shapes easier to see. Changes in cell shape particularly around the shoulder region, where one study (Babiarz et al., 1979) has already claimed there are changes during elevation, could be identified and more accurately recorded in 3D.

Abnormal apoptosis could be contributing to the morphogenesis of the cleft palates. This mechanism has mainly been studied with respect to palatal fusion. There is little evidence of it occurring during normal palatal outgrowth. It could be occurring in models of cleft palate and can be easily measured using a TUNEL stain.

The distribution and composition of the ECM has been shown to change during palatal development and altering either of these factors could result in a cleft palate (Brinkley and Morriswiman, 1987; Foreman et al., 1991; Knudsen et al., 1985). Therefore it would be useful to investigate how the amount of ECM varies in normal palatal development and to investigate any changes in the ECM of cleft palate models. This study did use a fibronectin antibody to help identify which Golgi corresponded to which nuclei in the *Tbx-1*<sup>-/-</sup> mutant, but to do this it was not imaged in a way that the amount of ECM could be quantified because as the z-stacks were quickly set up some regions were slightly over-exposed and as the deeper regions were imaged the brightness captured faded off dramatically. It could still be used to identify cell boundaries in these conditions but not to quantify the amount of ECM accurately. In the future well-imaged z-stacks could be used to work out the volume of ECM present by measuring the stained area at different stages.

A way of looking at the number of cell intercalations taking place is to use the mT/mG mice treated with a low dose of tamoxifen for at least the length of one entire cell cycle before they were sacrificed. Then the relative number of doublets and singlets in different regions could be counted. If there are lots of doublets it would mean that the daughter cells are remaining near each other after proliferation whereas if there are mainly singlets present then it would mean that cells are intercalating soon after division. This approach has been used in the Green lab and has correlated well with patterns of growth inferred from other types of measurement (Economou et al., 2013). Of course careful titration is required to ensure that touching cells are mostly or entirely clonal siblings to avoid independent recombinations occurring in two cells very close together. At stages when cell proliferation is low not many divisions will be occurring and so not much data can be gathered.

Cells are potentially migrating from the posterior to the anterior of the palate. This would require the angle of “elevation” to be measured from the z-stacks with the Golgi stained. Volocity is already recording this angle so this analysis could very easily be included to see if polarised cell behaviours are occurring along the AP axis.

Studying palatal development in mouse mutants with a cleft palate phenotype does more than further our understanding of what has gone wrong. It can also teach us about normal development in more detail. For example in the *Wnt5a*<sup>-/-</sup> mutant the anterior palate has raised levels of proliferation while levels have fallen in the posterior palate (He et al., 2008). The same paper suggests that cells migrate from the posterior palate to the anterior with *Wnt5a* acting as a chemoattractant. Therefore no migration occurs in these mutants. Cell density could be controlling the level of proliferation occurring. Where there are fewer than normal cells in the anterior the palate tries to compensate by increasing proliferation. Proliferation decreases in the posterior palate when it is no longer losing cells by migration. Performing the analyses used in this project on other cleft mutants could prove to be a useful diagnostic tool and among the mutants the *Wnt5a*<sup>-/-</sup> cleft mutant would be among the most interesting.

### 11.3 Summary of findings

- Very early palate outgrowth of the secondary palate was due to high levels of proliferation and polarised cells orientated towards the distal tip of the palate.
- Small yet consistent changes in cell spacing, proliferation and directional cell behaviours across the prospective oronasal axis were observed.
- The posterior palate reorientated concomitantly with a change in the direction of cell polarisation consistent with a cell-migration or cell-rearrangement-dependent elevation mechanism.
- Post-elevational growth towards the midline was correlated with an increase in cell spacing and polarised cell behaviours directed towards the medial tip of the palatal outgrowth consistent with a non-proliferation-dependent mechanism.
- Cleft palate seen in the *Tbx-1* null mouse was associated with palate cell orientation as well as proliferation being significantly disrupted.
- The *Msx-1*<sup>-/-</sup> cleft palate was associated with reduced proliferation and abnormal cell density associated with palatal shelves being able to elevate but being too small to meet in the midline.
- In the *Wnt1;Cre-Erk2*<sup>f/f</sup> cleft palate delayed elevation was associated with the level of proliferation being normal, but the distribution of proliferation and density of the cells being disrupted.

## 12.0 Appendix

### 12.1 *Pbx-1*<sup>-/-</sup> mouse development

This work was performed on samples received from Licia Selleri's group at Cornell University, New York, USA. The Selleri group had a variety of *Pbx* family knock-out mice, which they have generated to look at the role of *Pbx* in mammalian development. The *Pbx* family encode homeodomain proteins and regulate transcription in numerous cell types (Schnabel et al., 2001). *Pbx* has been linked to the correct patterning and morphogenesis of the axial, craniofacial and limb skeleton, as well as many internal organs.

The knockout mouse in these heat maps is the *Pbx-1*<sup>-/-</sup>;*Pbx-2*<sup>+/-</sup>;*Cre*<sup>Cre</sup> mutant, and had no *Pbx-1* and reduced *Pbx-2* activity (Ferretti et al., 2011). The phenotype included a cleft lip and palate (Fig. 12.1A & B). Unlike previous E11.5 heat maps these were in sagittal section as indicated in figure 12.1C. There was reduced proliferation in the *Pbx-1*<sup>-/-</sup>;*Pbx-2*<sup>+/-</sup>;*Cre*<sup>Cre</sup> palate at E11.5 (Fig. 12.1D & E, brackets) compared to the wild-type. The cells were more tightly packed in the *Pbx-1*<sup>-/-</sup>;*Pbx-2*<sup>+/-</sup>;*Cre*<sup>Cre</sup> palate than in the wild-type at this early stage. This investigation needed to include many more samples and several extra time points before the role of *Pbx* in controlling cellular behaviours involved in palate development can be deciphered. The *Pbx* family have been shown to play several hierarchical and overlapping roles in limb development (Capellini et al., 2011). This work in the limb recognises the need to link molecular networks with cellular behaviours and this is exactly what the work in this thesis is striving towards.

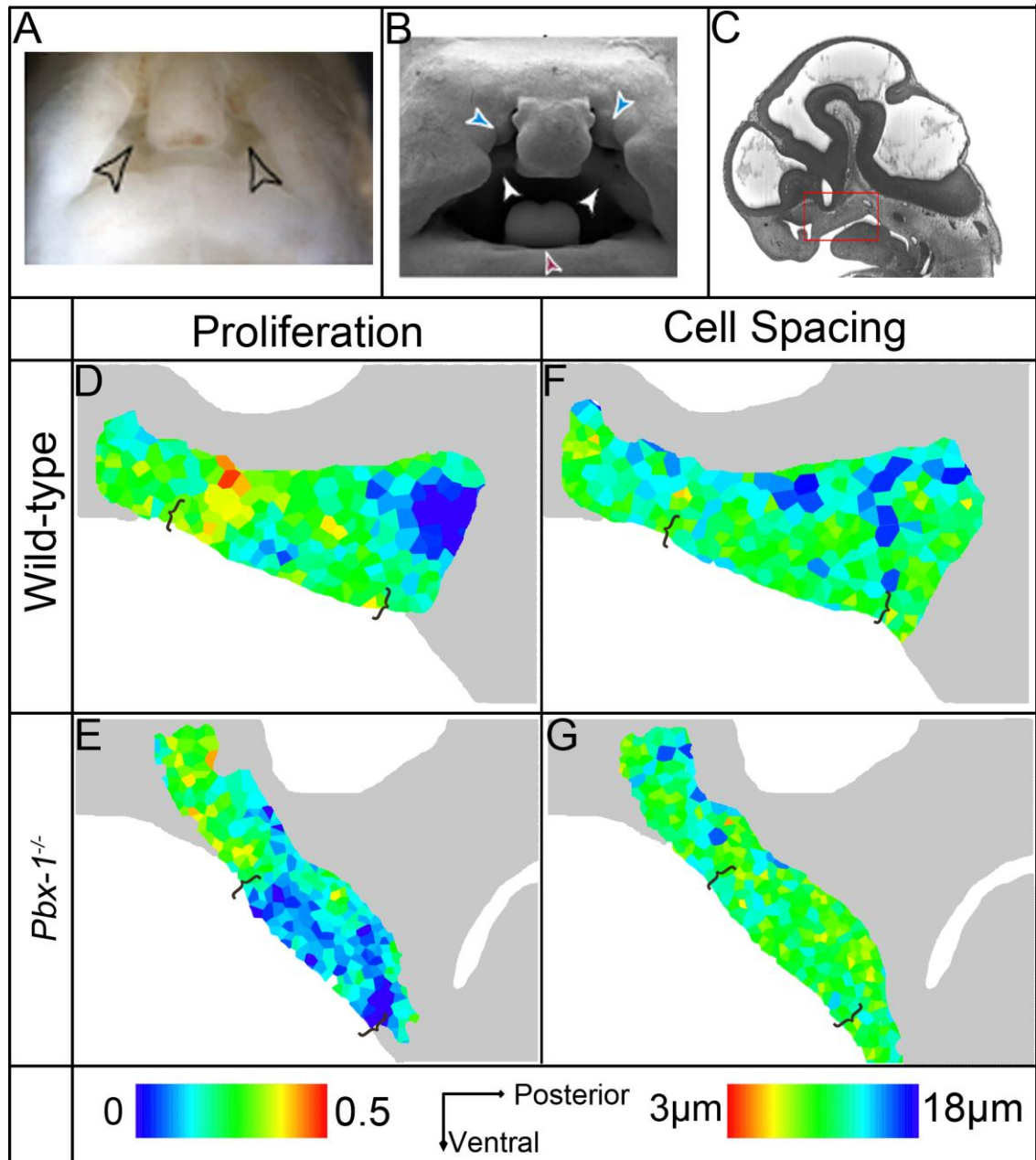


**Figure 12.1 *Pbx-1*<sup>-/-</sup>;*Pbx-2*<sup>+/-</sup>;*Cre*<sup>Cre</sup> and wild-type proliferation and internuclear spacing heat maps** A) *Pbx-1*<sup>-/-</sup>;*Pbx-2*<sup>+/-</sup>;*Cre*<sup>Cre</sup> mutant has a cleft lip as indicated by the empty arrow heads B) SEM of *Pbx-1*<sup>-/-</sup>;*Pbx-2*<sup>+/-</sup>;*Cre*<sup>Cre</sup> mouse head in frontal view showing cleft lip (azure arrowheads), cleft palate (blue arrowheads) and mandibular hypoplasia (pink arrowhead). A & B adapted from Ferretti et al., 2011 C) Sagittal view of an E11.5 wild-type mouse embryo. Red box indicates the region represented by the heat maps in D-G. Image from [www.embryoimaging.org](http://www.embryoimaging.org) D) Proliferation heat map of a wild-type palate. Brackets indicate the palate where proliferation was higher than in the mutant E) Proliferation heat map of a *Pbx-1*<sup>-/-</sup>;*Pbx-2*<sup>+/-</sup>;*Cre*<sup>Cre</sup> palate. Brackets indicate the palate where the proliferation was lower than the wild-type F) Internuclear spacing heat map of a wild-type palate. Brackets indicate the palate where cells were less densely packed than in the mutant E) Internuclear spacing heat map of a *Pbx-1*<sup>-/-</sup>;*Pbx-2*<sup>+/-</sup>;*Cre*<sup>Cre</sup>. Brackets indicate the palate where the cells were more densely packed than the wild-type. Each heat maps represents a single image. All heat maps are in sagittal view.



## 12.2 Palate and Mandible development in *Wnt1Cre-Tgfβ2<sup>fl/fl</sup>* mice

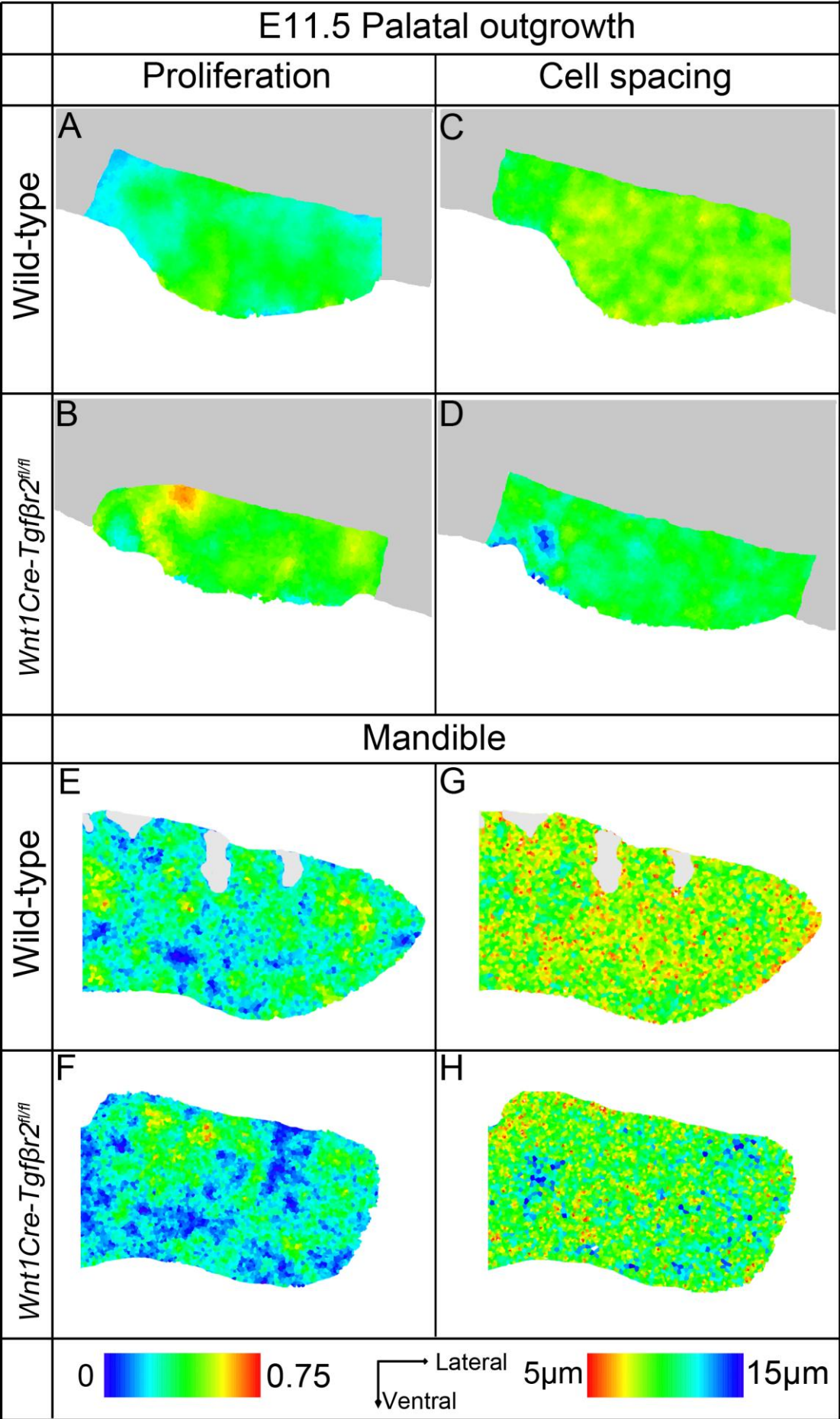
This work was done to set up a collaboration between Yang Chai's group at the University of Southern California and the Green Lab at KCL and was featured on a recently submitted NIH grant proposal.

One research interest of the Chai lab was cranial NCC and craniofacial malformations. Work has shown that *Tgf-β* plays an important role in regulating the fate of NCC. The Chai lab are now looking at *Tgf-β* type II receptor (*Tgfβ2*) in a conditional knockout mouse, *Wnt1Cre-Tgfβ2<sup>fl/fl</sup>* (Ito et al., 2003). This mutant displayed a cleft palate, small mandible and other craniofacial defects (Oka et al., 2007). Preliminary investigations showed that the *Wnt1Cre-Tgfβ2<sup>fl/fl</sup>* mandibles had a lower level of proliferation. From these preliminary heat maps it became evident that although in the mandible the proliferation in the mutant was lower the proliferation (Fig. 12.2E & F) in the palatal outgrowth is higher in the *Wnt1Cre-Tgfβ2<sup>fl/fl</sup>* palate than in the wild-type (Fig. 12.2A & B).

Heat maps showing cell spacing were also produced. Cell spacing was found to be much lower in both the developing mandible and palate (Fig. 12.2C, D, G & H). This could mean that cell spacing is not linked to proliferation or the mechanisms contributing to growth are working differently in the palate and mandible at E11.5.

This work validates the techniques developed in this thesis and shows how important looking with this sort of resolution can be. It is laying down new foundation for the future of thorough phenotype characterisation.

**Figure 12.2 Heat maps showing the proliferation and internuclear spacing in wild-type and *Wnt1Cre-Tgfβ2<sup>fl/fl</sup>* palatal outgrowths and mandibles at E11.5** A) Proliferation heat map of wild-type palatal outgrowth B) Proliferation heat map of *Wnt1Cre-Tgfβ2<sup>fl/fl</sup>* palatal outgrowth with slightly higher proliferation than the wild-type C) Internuclear spacing heat map of the wild-type palatal outgrowth D) Internuclear spacing heat map of the *Wnt1Cre-Tgfβ2<sup>fl/fl</sup>* palatal outgrowth with more loosely packed cells compared to the wild-type. A-D) Each heat map is an average of three individual sections. The grey region on the heat maps represents the rest of the embryo away from the ROI, which was not included in the heat map. E) Proliferation heat map of a wild-type mandible F) Proliferation heat map of a *Wnt1Cre-Tgfβ2<sup>fl/fl</sup>* mandible with slightly lower proliferation G) Internuclear spacing heat map of a wild-type mandible H) Internuclear spacing heat map of a *Wnt1Cre-Tgfβ2<sup>fl/fl</sup>* mandible with slightly more loosely packed cells. E-H) Each heat map is from an individual section. Grey regions are where the tissue folded.



### 12.3 Mouse probe experiment

A series of experiments were carried out to investigate whether the change in cell spacing seen after elevation was due to the elevational movement of the palate or a slower response that could be driving growth. Late E13.5 embryos were removed in PBS and their heads were removed. The embryo was held still using a needle pushed through the brain, away from the palate, oral cavity and mandible. A blunt probe and sharp needles were used and the following experiments were performed:

- A – Mouth held open with blunt probe until the palatal shelves were seen to rise
- B – The mandible and tongue were removed
- C – As much anterior and lateral mandible was removed as possible while leaving the tongue in place
- D – Tongue removed and mandible left
- E – Pushed down on the mandible and caused it to split in two, which allowed the tongue to rise again
- F – Push down on tongue and mandible and then left for ten minutes before fixing

With the exception of embryos in experiment F, each head was fixed immediately after treatment in 4% PFA overnight. The heads were processed and embedded for wax sectioning. 8 µm thick sections were cut and mounted. The sections were dewaxed and incubated with DAPI (as described in section 2.5) and cover slipped with Mowiol. Images were taken on the confocal microscope and heat maps showing the cell spacing created. If the change in cell spacing is simply a consequence of the elevation process then any palates in a horizontal position would display a decrease in cell spacing. Alternatively if the increase in cell spacing was a response to a molecular signal after the palate has elevated then no or very little change in cell spacing would occur.

Only three out of the nine embryos tested had palatal shelves that remained partially horizontal after fixing, even though all were seen to elevate before they were placed in fixative solution.

Embryo 1 underwent experiment A. The anterior palate remained horizontal after fixing but the posterior palate was vertical (Fig 12.3A, A', D & D'). The mid-palate appeared to have half elevated; it was an unusual shape and looked flattened against the tongue (Fig. 12.3 D').

Embryo 2 underwent experiment F. The result was the same as for embryo 1, the anterior was horizontal and the mid-palate had risen out of its normal position while the posterior remained vertical (Fig. 12.3B, B', E & E').

Embryo 3 underwent experiment D. Where the tongue had been removed the palatal shelves were no longer fully vertical but they had not managed to maintain a horizontal position either (Fig. 12.3C & C'). In the more posterior region of the palate the tongue had not been removed and the shelves remained vertical (Fig. 12.3F & F').

Many of the sections produced from these embryos had rips, folds or regions overlapping and therefore very few heat maps could be produced (Fig. 12.3A'-F'). The heat maps of the elevated shelves display cells that were more tightly packed than they normally were at E13.5 or E14.0 (Fig. 12.3A-F). This could be an artefact from the experiment or could be a sub-stage of palate development that has not been caught before. This result, and the high number of problems encountered, could have been due to a bad batch of fixative or possibly the mandible normally offers the palatal shelves some protection during section. Further experiments need to be carried out to see when the change in cell spacing occurs.

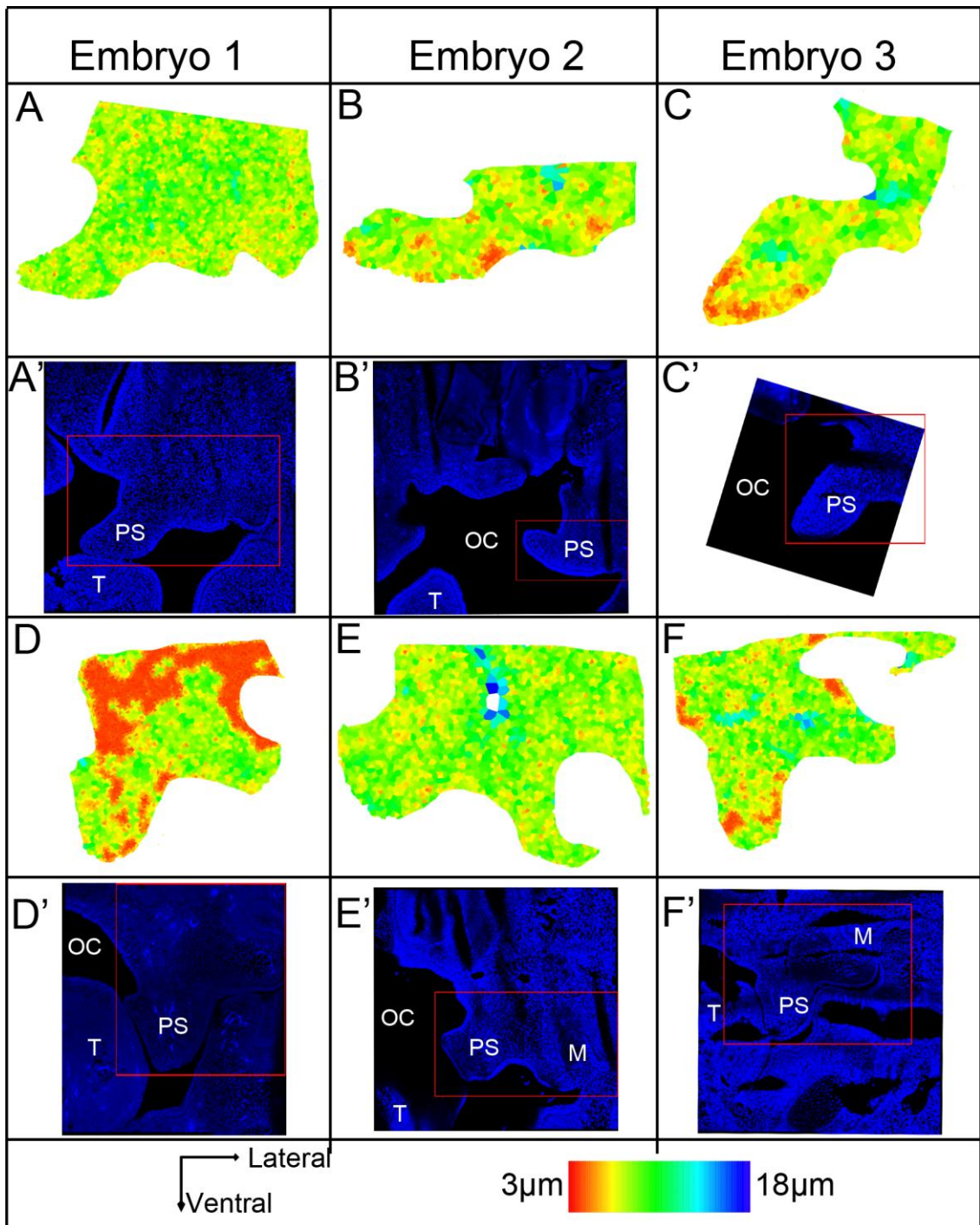


Figure 12.3 Internuclear heat maps and DAPI images from preliminary experiments when elevation was induced to investigate changes in Internuclear spacing A) Spacing heat map of an anterior section from embryo A A') DAPI image of an anterior section from embryo A B) Spacing heat map of an anterior section from embryo B B') DAPI image of an anterior section from embryo B C) Spacing heat map of an anterior section from embryo C C') DAPI image of an anterior section from embryo C D) Spacing heat map of a posterior section from embryo A D') DAPI image of a posterior section from embryo A E) Spacing heat map of a posterior section from embryo B E') DAPI image of a posterior section from embryo B F) Spacing heat map of a posterior section from embryo C F') DAPI image of a posterior section from embryo C. Each heat map is from an individual section. Red boxes on the DAPI images indicate the region featured in the heat map. T, tongue; PS, palatal shelves; OC, oral cavity; M, molar

## 12.4 The R macro

The proliferation and cell spacing heat maps were created in R using a macro written by Andrew Economou (Green Lab, KCL). R is a software package that offers a language and environment for data manipulation, graphical representation and statistical analysis to be performed. It is free and open source and there are various packages that can be added on to increase its capabilities.

The heat maps were based on the data extracted from the fluorescent images by Volocity (see chapter 3). Volocity created a table of co-ordinates of the centroid (centre of mass) of every cell it identified. This table was exported from Volocity and read directly into R. Each table contained information from all the images of a single embryo and R produced a heat map for each individual image. It automatically saved each heat map as a portable document format (PDF) file in a user-specified folder and moved on to the next image in the table.

Once the data table and Andrew Economou's macro was read into R and the "deldir" (Turner, 2007), "tripack" (A. Gebhardt, 2009) and "sp" (Bivand, 2012) packages were loaded the following macro-specific commands can be used:

**read.volocity** – read the Volocity table. It identified each column of data and whether each column was text or numbers. For each point in the table it extracted the parent image name and the XY co-ordinates are put into a data frame.

**Extract** – this allowed all the data points with the same image name to be extracted and worked on. This was used by the computer, as part of the automatic cycle, to create the heat maps for an entire dataset. It was also used to manually extract images before they were registered and a combined heat map created.

**CellSpacing** – this was used to automatically create cell spacing heat maps for all the images in a dataset. The centroid of every cell in an image was extracted by R (Fig. 12.4A), using the Extract function above. The neighbours of each centroid were identified using a Delaunay triangulation. The average distance between a centroid and each of its neighbours (as defined by the Delaunay triangulation) was calculated (Fig. 12.4C). The triangulation ignored centroids on the boundary, which formed the convex hull, because these did not have a full set of neighbours. The average distance between the centroid of interest and its neighbours was assigned a colour according to

the user-defined colour scale (Fig. 12.4F) and a voronoi tessellation was used to calculate the region around the centroid that was allocated this colour. The perimeter of the colour confined the region that was closer to the current centroid of interest than any other centroid (Fig. 12.4B). Sometimes the voronoi polygon would form a large spike that stuck out of the side of the heat map. Although the colour assigned to this region from the Delauney triangulation was correct they were distracting and messy. To prevent these spikes appearing a “mask” was used, which changed any final coloured regions on the heat map  $>300\mu\text{m}^2$  to white.

**ProliferationMap** – this was used to create cell proliferation heat maps for all the images in the dataset. The co-ordinates of the centroids from every nucleus in the image and positive IddU/BrdU nuclei were in separate tables. R matched up each centroid with the centroids from the proliferating cells by calculating which two centroids have the minimum distance between them (Fig. 12.4D). R assigned a centroid with true if a proliferation centroid was closest to it or a false if no proliferation centroid was nearby. R calculated the labelling index for the centroid of interest and two sets of neighbours and used a voronoi tessellation to create the coloured region (Fig. 12.4E).

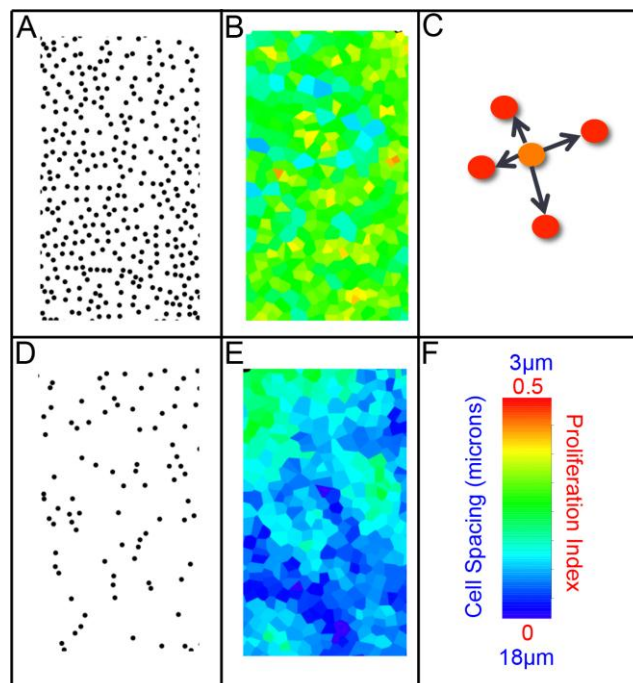


**Figure 12.4 Creating the heat maps** A) The table of co-ordinates was read by R and can be then mapped, each black dot represents the centroid of a different cells. This is an example of the when looking at the internuclear spacing B) An example of an internuclear spacing heat map C) R calculates the cell spacing by calculating the average distance between each cell and its neighbours D) An example of the centroid mapping from the IddU or BrdU positive cells E) A heat map is created by calculating the labeling index for a cell and two sets of neighbours F) The scale for the heat maps

**Rotate** – this function rotated all the data points by a certain value. This was used to align different images before they were combined into a single heat map. This was necessary because when the wax ribbon of sections was mounted on to the slide, out of the waterbath, each ribbon was not at exactly the same angle. Only a maximum of five images were ever combined, more commonly three images were used. These images were from adjacent sections therefore the registration only required rotations and translations (see below).

**Translate** – this function translated all the data points by a certain value. This was used to align different images before they were combined into a single heat map. This was necessary because the palate did not always appear in exactly the same place on every image.

**CombineSpace** – this was used to combine several cell spacing heat maps after the images had been registered. To combine three images they were registered, using the rotate and translate functions above, and a list created of the new co-ordinates of each registered centroid. This function used a Delauney triangulation to calculate the average spacing for each image, as described in the CellSpacing function. The lists of centroid co-ordinates and their spacing value were then combined into a single list. Polygons were then created from this combined dataset and these are then smoothed using the closest neighbours from the combined dataset. Finally it removed any data points that lay outside of the combined convex hull.

**CombineProlif** – this was used to combine several cell proliferation heat maps after the heat maps had been registered. This used a similar technique to CombineSpace except that it calculates the proliferation index for each individual image before combining them, as described in the ProliferationMap function.

Below is a copy of the R macro as it was when used in this thesis. There are other ways of doing the same functions and the Andrew Economou is continually developing it.

```
read.volocity.XY<-function(table) {  
  V<-table  
  V<-V[-1,] #to remove header line  
  N<-as.character(V[[3]])  
  X<-as.numeric(as.character(V[[6]])) #to get back to numbers
```



```

Y<-as.numeric(as.character(V[[7]]))
V<-data.frame(N,X,Y)
V
}

#extracted section named "name" from a read velocity table and
output in same format as read.velocity
extract<-function(table, name){
V<-table
N<-V[[1]]
X<-V[[2]]
Y<-V[[3]]
for(i in 1:length(N)){
  if(name!=N[i]){
    X[i]<-NA
    Y[i]<-NA
  }
}
X<-X[!is.na(X)]
Y<-Y[!is.na(Y)]
V<-cbind(X,Y)
V
}

CellSpacing<-function(XY){
N<-as.character(XY[[1]])
UN<-unique(N)
for(i in 1:length(UN)){
  E<-extract(XY,UN[i])
  if(length(E[,1])>=3){ #needed at least 3 points for the
triangulation
    print(i) #allowed the user to follow the computer's
progress
    CD<-centroid.displacement(E,0)
    CS<-centroid.spacing(CD)
    D<-deldir(E[,1],E[,2]) #Calculated Delaunay
triangulation and the voronoi tessellation
    T<-tile.list(D) #A list of pologons, the co-ordinates
outlining each coloured region
    pdf(file = paste("/Users/Lara/Desktop/IddU and BrdU

```

```

labelling/E13.5 embryos/E13.5 cell spacing
R/",UN[i],".pdf",sep="")
  centroid.map(E,CS,T,3,18)
  mask(E,T,300) #The edges appeared as peaks at first,
this removed the peaks
  dev.off()
}
}
}

```

```

ProliferationMap<-function(XY,XY2,S=1){
N<-as.character(XY[[1]])
UN<-unique(N)
for(i in 1:length(UN)){
  E<-extract(XY,UN[i])
  E2<-extract(XY2,UN[i])
  if(length(E[,1])>=3){
    print(i)
    P<-proliferation(E,E2)
    PI<-proliferation.index(E,P,S)
    D<-deldir(E[,1],E[,2])
    T<-tile.list(D)
    pdf(file = paste("/Users/Lara/Desktop/IddU and BrdU
labelling/E13.5 embryos/E13.5 cell spacing
R/",UN[i],".pdf",sep=""))
    centroid.map(E,PI,T,-0.000001,0.75000001)
    mask(E,T,300)
    dev.off()
  }
}
}

```

```

#rotation matrix, clockwise in degrees
rotate<-function(XY,theta){
XYT<-t(XY)
  R<-matrix (c(cos((-theta*pi)/180),-sin((-
theta*pi)/180),sin((-theta*pi)/180),cos((-
theta*pi)/180)),byrow=TRUE,nr=2,nc=2)
  XYR<-R%*%XYT
  XY<-t(XYR)

```

```

    XY
  }

translate<-function(XY,x,y){
  XY<-cbind(XY[,1]+x,XY[,2]+y)
  XY
}

CombineSpace<-function(XY,C=1,plot=TRUE){
  l<-length(XY) #XY is a list of XY coordinates of each slice
  CD<-list(l)
  CS<-list(l)
  for(i in 1:l){
    CD[[i]]<-centroid.displacement(XY[[i]])
    CS[[i]]<-centroid.spacing(CD[[i]])
  }
  cXY<-XY[[1]] #Concatenated XY coordinates
  cCS<-CS[[1]] #Concatenated XY coordinates
  for(i in 1:(l-1)){
    cXY<-rbind(cXY,XY[[i+1]])
    cCS<-c(cCS,CS[[i+1]])
  }
  D<-deldir(cXY[,1],cXY[,2])
  T<-tile.list(D)
  CSm<-centroid.smoothing(cXY,cCS,C)
  Tr<-list(l)
  CH<-list(l)
  PIP<-list(l)
  for(i in 1:l){
    Tr[[i]]<-tri.mesh(XY[[i]][,1],XY[[i]][,2])
    CH[[i]]<-convex.hull(Tr[[i]])
    PIP[[i]]<-
point.in.polygon(cXY[,1],cXY[,2],CH[[i]]$x,CH[[i]]$y)
    CSm[PIP[[i]]==0]<-NA
  }
  if(plot==TRUE){
    pdf("/Users/Lara/Desktop/IddU and BrdU labelling/E13.5
embryos/E13.5 cell spacing R/heat map.pdf")
    centroid.map(cXY,CSm,T,3,18)
    mask(cXY,T,300)
  }
}

```

```

        #P1<-polygon(CH1$x,CH1$y)
        #P2<-polygon(CH2$x,CH2$y)
        dev.off()
    }
CSm
"Complete"
}

CombineProlif<-function(XY,XY2,C=1,plot=TRUE){
  l<-length(XY) #XY is a list of XY coordinates of each slice
  PI<-list(l)
  for(i in 1:l){
    P<-proliferation(XY[[i]],XY2[[i]])
    PI[[i]]<-proliferation.index(XY[[i]],P,C)
  }
  cXY<-XY[[1]] #Concatenated XY coordinates
  cPI<-PI[[1]] #Concatenated XY coordinates
  for(i in 1:(l-1)){
    cXY<-rbind(cXY,XY[[i+1]])
    cPI<-c(cPI,PI[[i+1]])
  }
  D<-deldir(cXY[,1],cXY[,2])
  T<-tile.list(D)
  PIm<-centroid.smoothing(cXY,cPI,C)
  Tr<-list(l)
  CH<-list(l)
  PIP<-list(l)
  for(i in 1:l){
    Tr[[i]]<-tri.mesh(XY[[i]][,1],XY[[i]][,2])
    CH[[i]]<-convex.hull(Tr[[i]])
    PIP[[i]]<-
point.in.polygon(cXY[,1],cXY[,2],CH[[i]]$x,CH[[i]]$y)
    PIm[PIP[[i]]==0]<-NA
  }
  if(plot==TRUE){
    pdf("/Users/Lara/Desktop/IddU and BrdU labelling/E13.5
embryos/E13.5 cell spacing R/heat map.pdf")
    centroid.map(cXY,PIm,T,0,1)
    mask(cXY,T,300)
    #P1<-polygon(CH1$x,CH1$y)
    #P2<-polygon(CH2$x,CH2$y)

```

```

        dev.off()
    }
PIm
"Complete"
}

#input XY list of points
centroid.neighbours<-function(XY){
x<-XY[,1]
y<-XY[,2]
T<-tri.mesh(x,y) #Calculated the number of triangulations
neighbours
N<-neighbours(T) #Identified each triangulation neighbour
C<-convex.hull(T) #blanked the points of the convex hull as
these were not surrounded by neighbours
B<-C[[3]]
Bsort<-rev(B[order(B)])
#boundary nodes in N made blank
for(i in 1:length(Bsort)){
    Bi<-Bsort[i]
    N[Bi]<-NA
}
#boundary nodes neighbours made blank
for(i in 1:length(N)){
    for(j in 1:length(Bsort)){
        if(Bsort[j] %in% N[[i]])
            N[i]<-NA
    }
}
N
}

#input XY list and number of coronae of neighbours
corona.neighbours<-function(XY,C=0){
N<-centroid.neighbours(XY)
NC<-list(length(N))
#copy in neighbours
for(i in 1:length(N)){
    if(is.na(N[i])==FALSE){
        NC[i]<-N[i]
    }
}
}

```

```

else{
  NC[i]<-NA
}
}
#added neighbours of neighbours for each point
#C gives number of iterations
if(C!=0){
  for(i in 1:C){
    for(j in 1:length(NC)){
      if(is.na(NC[j])==FALSE){
        for(k in 1:length(NC[[j]])){
          NC[[j]]<-c(NC[[j]],N[[NC[[j]][k]]])
        }
        if(NA %in% NC[[j]]){
          NC[j]<-NA
        }
      }
    }
    #removed original point, duplicated, sort
    for(j in 1:length(NC)){
      if(is.na(NC[j])==FALSE){
        NC[[j]]<-NC[[j]][NC[[j]]!=j]
        NC[[j]]<-unique(NC[[j]])
        NC[[j]]<-sort(NC[[j]])
      }
    }
  }
}
NC
}

```

```

centroid.displacement<-function(XY,C=0){
  #made list of neighbours
  N<-centroid.neighbours(XY)
  x<-XY[,1]
  y<-XY[,2]
  #list of X and Y displacements
  dx<-list(length(N))
  dy<-list(length(N))
  if(C==0){
    for(i in 1:length(N)){
      if(is.na(N[i])==FALSE){

```

```

        dx[i]<-list(x[i]-x[N[[i]])]
        dy[i]<-list(y[i]-y[N[[i]])]
    }
    else{
        dx[i]<-NA
        dy[i]<-NA
    }
}
}
else{
    #made list of corona neighbours (one shell less than C)
    NC<-corona.neighbours(XY, (C-1))

    for(i in 1:length(NC)){
        if(is.na(NC[i])==TRUE){
            dx[i]<-NA
            dy[i]<-NA
        }
        else{
            #made temporary list of neighbours of point
            NT<-list()
            NT[[1]]<-N[[i]]
            for(j in 1:(length(NC[[i]]))){
                NT[[j+1]]<-N[[NC[[i]][j]]]
            }
            #put neighbours of boundary node neighbours as NA
            if(TRUE %in% is.na(NT)){
                dx[i]<-NA
                dy[i]<-NA
            }
            else{
                #removed repeats
                #removed the centroid itself from the list of
neighbours

                for(j in 1:length(NC[[i]])){
                    if(i %in% NT[[j+1]]){
                        NT[[j+1]]<-NT[[j+1]][!NT[[j+1]]==i]
                    }
                }
                #removed other repeats between neighbours
                for(j in 1:length(NC[[i]])){
                    for(k in 1:length(NC[[i]])){

```

```

        if(NC[[i]][k] %in% NT[[j+1]]){
            NT[[k+1]]<-
NT[[k+1]][!NT[[k+1]]==NC[[i]][j]]
        }
    }
    TX<-list(length(NT))
    TY<-list(length(NT))
    TX[1]<-list(x[i]-x[N[[i]])]
    TY[1]<-list(y[i]-y[N[[i]])]
    for(j in 1:length(NC[[i]])){
        TX[j+1]<-list(x[NC[[i]][j]]-x[NT[[j+1]])]
        TY[j+1]<-list(y[NC[[i]][j]]-y[NT[[j+1]])]
    }
    dx[[i]]<-unlist(TX)
    dy[[i]]<-unlist(TY)
}
}
}
dxy<-list(dx,dy)
dxy
}

#input displacement between adjacent centroids, uses pythagoras
to calculate the hypotenuse
centroid.spacing<-function(D){
L<-list(length(D[[1]]))
for(i in 1:length(D[[1]])){
    if(is.na(D[[1]][i])==FALSE){
        L[i]<-list(sqrt((D[[1]][[i]]^2+(D[[2]][[i]]^2))
        L[i]<-mean(L[[i]])
    }
    else{
        L[i]<-NA
    }
}
L<-unlist(L)
L
}

```



```

#makes voronoi heat map from XY list, measurement list and tile
list from deldir
#needed to input min and max values for heat map
centroid.map<-function(XY,L,T,min,max){
plot(XY,cex=0.5,pch=16,asp=1,ylim=c(max(XY[,2]),min(XY[,2])),
col="white") #R and Volocity used different origins, this
flipped the co-ordinates in R to match Volocity
for(i in 1:length(T)){
  if(is.na(L[i])==FALSE){
    if((min<L[i])&(L[i]<max)){
      polygon(T[[i]]$x,T[[i]]$y,col=hsv(0.7*((L[i]-
min)/(max-min)),1,1),border=NA)
#      polygon(T[[i]]$x,T[[i]]$y,col=grey((L[i]-
min)/(max-min)),border=NA) #This is used to produce a
greyscale heat map
    }
  }
}
}

```

```

#input list of centroids and list of centroids for a
proliferation marker, returned a list with TRUE/FALSE whether
the centroid had a marker based on shortest distance

```

```

proliferation<-function(D,P){
#create output list
M<-logical(length(D[,1]))
#found position of centroid closest to each marker
for(i in 1:length(P[,1])){
  #make a list of index
  L<-seq(1:length(D[,1]))
  #calculate distances
  XDiff<-D[,1]-P[i,1]
  YDiff<-D[,2]-P[i,2]
  Dist<-sqrt(XDiff^2+YDiff^2)
  #found list position of closest centroid
  Min<-L[Dist==min(Dist)]
  #mark that centroid as TRUE
  M[Min]<-TRUE
}
}

```

M

```

}

#input list of centroids (to calculate neighbours) and
TRUE/FALSE list and neighbours to smooth over, output list of
proliferation indices
proliferation.index<-function(D,M,S=1){
  #calculate neighbours
  CN<-corona.neighbours(D,S)
  I<-list(length(D[,1]))
  for(i in 1:length(D[,1])){
    if(is.na(CN[i])==FALSE){
      Total<-length(CN[[i]])
      Labelled<-length(M[CN[[i]]][M[CN[[i]]]==TRUE])
      I[i]<-Labelled/Total
    }
    else{
      I[i]<-NA
    }
  }
  I<-as.numeric(I)
  I
}

mask<-function(XY,T,tresh){
  V<-voronoi.mosaic(XY[,1],XY[,2])
  VA<-voronoi.area(V)
  VA[VA>tresh]<-NA
  for(i in 1:length(VA)){
    if(is.na(VA[i])==TRUE){
      polygon(T[[i]]$x,T[[i]]$y,col="white",border="white")
    }
  }
}

centroid.smoothing<-function(XY,CS,C=1){
  S<-numeric(length(XY[,1]))
  if(C==0){
    CN<-corona.neighbours(XY,0)
    for(i in 1:length(S)){
      if(is.na(CN[i])==FALSE){

```

```

        S[i]<-CS[i]
    }
else{
    S[i]<-NA
}
}
}
else{
C<-C-1 #smoothing with size 0 has one set of neighbours
CN<-corona.neighbours(XY,C)
for(i in 1:length(S)){
    if(is.na(CN[i])==FALSE){
        CN1<-c(i,CN[[i]])
        L1<-length(CN1)
        CN2<-CN1[!is.na(CS[CN1])] #removed excluded objects
that are not removed by filter
        L2<-length(CN2)
        S[i]<-mean(CS[CN2])
    }
else{
    S[i]<-NA
}
}
}
S
}

```

## 12.5 Investigating a double injection protocol

A protocol previously described and used in limb developed was applied to the palate to calculate cell cycle times (Boehm et al., 2010; Shibui et al., 1989). The stage E13.5 was tested first. The cell cycle time was coming out as 159 hours, which does not make biological sense. Controls were carried out to ensure both the injection and staining was working correctly and to make sure no unexpected cross-reactions were happening.

Both the IddU and the BrdU were injected individually, the amount of the injection was doubled and the time between injections was doubled. Table 12.1 showed that both the IddU and BrdU produced the same labelling index whether the other was present or not. Doubling the amount injected or the interval between injections increased the labelling index as expected.

Next the interval between injections was varied from 30 to 700 minutes. An E11.5 palate and an E11.5 hindlimb were also tested with a 120 minutes interval between injections (Fig. 12.5). The cell cycle time for the hindlimb was within the range found in another limb study (Boehm et al., 2010). This showed that the experiment and the calculation were both correct. The E11.5 palate produced a very similar cell cycle time to the limb. In comparison the cell cycle time calculated for the E13.5 palate increased as the time interval increased and does not appear to saturate within 700 minutes. Therefore the double injection protocol can be applied to the palate at stages where the assumptions are met but the calculation does not fit older datasets where fewer cells are proliferating.

<b>Table 12.1 Table of proliferation labelling index and cell cycle times for different injection protocols</b>			
All samples from E13.5 palatal shelves	IddU labelling index (%)	BrdU labelling index (%)	Cell cycle time (hours)
Double injection	21	24	159
IddU only	20	NA	NA
BrdU only	NA	23	NA
Double interval time between injections	29	22	89
Double amount injected	27	25	135

For every different condition or time point tested a slide for each of the following controls was included:

Only IddU primary and secondary antibodies

Only BrdU primary and secondary antibodies

IddU primary and BrdU secondary antibodies  
 BrdU primary and IddU secondary antibodies  
 Only primary antibodies  
 Only secondary antibodies  
 No antibodies

All control slides produced the correct result.

Calculation for cell cycle time (Boehm et al., 2010):

$$T^C = T^I \times \frac{N^T}{(N^{IddU} - N^{BrdU})}$$

$T^C$  – Cell cycle time (minutes)

$T^I$  – Interval time (minutes)

$N^T$  – Total number of cells

$N^{IddU}$  – Total number of IddU stained cells

$N^{BrdU}$  – Total number of BrdU stained cells

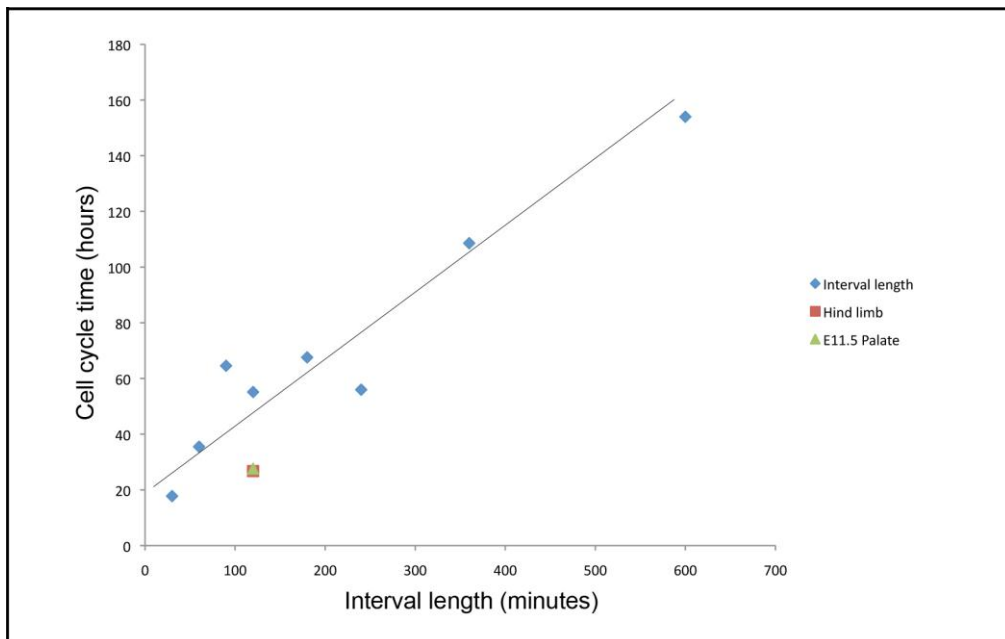


**Figure 12.5 Graph to show the cycle time** The cell cycle time increased as the interval length between the IddU and BrdU injection increased in an E13.5 palate. The red square represents the cell cycle for an E11.5 mouse hindlimb with a 120-minute injection interval. The green triangle represents the cell cycle time for an E11.5 mouse palate with a 120-minute injection interval. The line of best fit was drawn by hand referring only to the blue data points from the E13.5 palate data.

## **12.6 Tables of p-values from Watson $U^2$ statistical tests for Golgi and spindle, wild-type and *Tbx-1* orientation datasets**

The Watson  $U^2$  test was used, as described in chapter 2, to test the statistical significance of distributions of orientated cell behaviours. The letters refer to the regions shown in figure 2.1. These statistical tests were performed in R and a  $p < 0.05$  was considered statistically significant.

**Table 12.2 Table of p-values from statistical tests on the wild-type Golgi orientation data**

(A)	VS uniform distribution	VS von Mises distribution		VS uniform distribution	VS von Mises distribution
<b>E11.5</b>					
<b>TIP</b>	p<0.01	p<0.01			
<b>K</b>	p<0.01	p<0.01			
<b>E12.5</b>					
<b>TIP</b>	p<0.01	p>0.1	<b>E12.5 Ant</b>		
<b>K</b>	p<0.01	p<0.05	<b>BC</b>	p>0.1	p>0.1
<b>B</b>	p>0.1	p>0.1	<b>EFG</b>	p<0.01	p>0.1
<b>C</b>	p<0.01	p>0.1	<b>HIJ</b>	p>0.1	p>0.1
<b>D</b>	p<0.01	p>0.1	<b>TIP</b>	p>0.1	p>0.1
<b>E</b>	p>0.1	p<0.01			
<b>F</b>	p>0.1	p>0.1	<b>E12.5 mid</b>		
<b>G</b>	p>0.1	p>0.1	<b>BC</b>	p<0.01	p>0.1
<b>H</b>	p>0.1	p>0.1	<b>EFG</b>	p>0.1	p>0.1
<b>I</b>	p<0.01	p>0.1	<b>HIJ</b>	p>0.05	p>0.1
<b>J</b>	p<0.1	p>0.1	<b>TIP</b>	p<0.05	p>0.1
<b>BC</b>	p<0.01	p>0.1			
<b>EFG</b>	p<0.05	p>0.1	<b>E12.5 post</b>		
<b>HIJ</b>	p>0.1	p>0.1	<b>BC</b>	p>0.1	p>0.1
<b>B-J</b>	p<0.01	p>0.1	<b>EFG</b>	p<0.01	p>0.1
<b>B-J TIP</b>	p<0.01	p>0.1	<b>HIJ</b>	p>0.1	p>0.1
<b>Anterior</b>	p<0.01	p>0.1	<b>TIP</b>	p<0.01	p>0.1
<b>Middle</b>	p<0.01	p>0.1			
<b>Posterior</b>	p<0.01	p>0.1			
<b>E13.5</b>			<b>E13.5 Ant</b>		
<b>TIP</b>	p>0.1	p>0.1	<b>BC</b>	p>0.05	p>0.05
<b>K</b>	p<0.1	p>0.1	<b>EFG</b>	p<0.01	p>0.1
<b>B</b>	p>0.1	p>0.1	<b>HIJ</b>	p>0.1	p>0.1
<b>C</b>	p<0.1	p>0.1	<b>TIP</b>	p>0.1	p>0.1
<b>D</b>	p<0.1	p>0.1			

<b>E</b>	p<0.01	p<0.01	<b>E13.5 mid</b>		
<b>F</b>	p<0.1	p<0.01	<b>BC</b>	p>0.1	p>0.1
<b>G</b>	p<0.01	p<0.01	<b>EFG</b>	p<0.01	p<0.01
<b>H</b>	p>0.1	p>0.1	<b>HIJ</b>	p>0.1	p>0.05
<b>I</b>	p>0.1	p>0.1	<b>TIP</b>	p>0.1	p>0.1
<b>J</b>	p<0.01	p>0.1			
<b>BC</b>	p>0.1	p>0.1	<b>E13.5 post</b>		
<b>EFG</b>	p<0.01	p<0.01	<b>BC</b>	p>0.05	p>0.1
<b>HIJ</b>	p>0.1	p>0.1	<b>EFG</b>	p<0.01	p<0.01
<b>B-J</b>	p<0.01	p<0.01	<b>HIJ</b>	p>0.1	p>0.1
<b>B-J TIP</b>	p<0.01	p<0.01	<b>TIP</b>	p>0.1	p>0.1
<b>Anterior</b>	p<0.01	p>0.05			
<b>Middle</b>	p<0.05	p<0.01			
<b>Posterior</b>	p<0.01	p<0.01			
<b>Post B-J</b>	p<0.01	p<0.01			
<b>E14.5</b>			<b>E14.5 Ant</b>		
<b>TIP</b>	p>0.1	p>0.1	<b>BC</b>	p<0.01	p>0.05
<b>K</b>	p<0.05	p>0.1	<b>EFG</b>	p>0.05	p>0.1
<b>B</b>	p<0.01	p<0.01	<b>HIJ</b>	p>0.1	p>0.05
<b>C</b>	p>0.05	p<0.01	<b>TIP</b>	p>0.1	p>0.1
<b>D</b>	p<0.01	p>0.05			
<b>E</b>	p<0.01	p>0.1	<b>E14.5 mid</b>		
<b>F</b>	p<0.05	p>0.1	<b>BC</b>	p<0.01	p<0.01
<b>G</b>	p<0.01	p>0.1	<b>EFG</b>	p<0.01	p>0.1
<b>H</b>	p<0.01	p>0.1	<b>HIJ</b>	p<0.01	p>0.1
<b>I</b>	p>0.1	p>0.1	<b>TIP</b>	p>0.05	p>0.1
<b>J</b>	p<0.01	p>0.1			
<b>BC</b>	p<0.01	p<0.01	<b>E14.5 post</b>		
<b>EFG</b>	p<0.01	p>0.1	<b>BC</b>	p<0.01	p>0.1
<b>HIJ</b>	p<0.01	p>0.1	<b>EFG</b>	p>0.05	p>0.1
<b>B-J</b>	p<0.01	p<0.01	<b>HIJ</b>	p<0.01	p>0.1
<b>B-J TIP</b>	p<0.01	p<0.01	<b>TIP</b>	p<0.01	p>0.1
<b>Anterior</b>	p<0.01	p>0.1			
<b>Middle</b>	p<0.01	p>0.05			
<b>Posterior</b>	p<0.01	p<0.01			
<b>(B) Internal regions</b>	<b>Watson U<sup>2</sup> Test</b>		<b>Watson U<sup>2</sup> Test</b>		<b>Watson U<sup>2</sup> Test</b>



<b>E11.5</b>					
<b>Tip Vs K</b>	p>0.1				
<b>E12.5</b>		<b>E13.5</b>		<b>E14.5</b>	
<b>Tip Vs B-J</b>	p<0.05	<b>Tip Vs B-J</b>	p>0.1	<b>Tip Vs B-J</b>	p<0.01
<b>TIP VS K</b>	p<0.05	<b>TIP VS K</b>	p<0.05	<b>TIP VS K</b>	p>0.1
<b>B-J TIP VS K</b>	p>0.1	<b>B-J TIP VS K</b>	p>0.1	<b>B-J TIP VS K</b>	p>0.1
<b>B VS H</b>	p>0.1	<b>B VS H</b>	p>0.1	<b>B VS H</b>	p>0.05
<b>C VS I</b>	p>0.1	<b>C VS I</b>	p>0.1	<b>C VS I</b>	p>0.1
<b>BC VS EFG</b>	p>0.1	<b>BC VS EFG</b>	p>0.05	<b>BC VS EFG</b>	p<0.05
<b>EFG VS HIJ</b>	p>0.1	<b>EFG VS HIJ</b>	p>0.05	<b>EFG VS HIJ</b>	p<0.01
<b>HIJ VS BC</b>	p>0.1	<b>HIJ VS BC</b>	p>0.1	<b>HIJ VS BC</b>	p<0.01
<b>Ant Vs Mid</b>	p>0.1	<b>Ant Vs Mid</b>	p<0.01	<b>Ant Vs Mid</b>	p>0.1
<b>Mid Vs Post</b>	p<0.05	<b>Mid Vs Post</b>	p>0.1	<b>Mid Vs Post</b>	p<0.01
<b>Post Vs Ant</b>	p>0.1	<b>Post Vs Ant</b>	p<0.01	<b>Post Vs Ant</b>	p>0.1
<b>E12.5 Ant Vs post</b>		<b>Post tip vs Post B-J</b>	p>0.1		
		<b>E13.5 Ant vs post</b>		<b>E14.5 Ant vs post</b>	
<b>BC</b>	p>0.1	<b>BC</b>	p<0.05	<b>BC</b>	p<0.001
<b>EFG</b>	p>0.1	<b>EFG</b>	p<0.001	<b>EFG</b>	p>0.1
<b>HIJ</b>	p>0.1	<b>HIJ</b>	p>0.1	<b>HIJ</b>	p>0.1
<b>TIP</b>	p>0.1	<b>TIP</b>	p>0.1	<b>TIP</b>	p<0.01
		<b>E13.5 Post vs Mid</b>			
		<b>BC</b>	p>0.1	<b>E14.5 ANt Vs Mid</b>	
		<b>EFG</b>	p>0.1	<b>BC</b>	p>0.05
		<b>HIJ</b>	p>0.1	<b>EFG</b>	p<0.05
		<b>TIP</b>	p>0.1	<b>HIJ</b>	p>0.1
				<b>TIP</b>	p>0.05
				<b>E14.5 Post vs Mid</b>	
				<b>BC</b>	p<0.001
				<b>EFG</b>	p<0.05
				<b>HIJ</b>	p>0.1
				<b>TIP</b>	p<0.001

<b>(C) Between stages</b>					
	<b>Watson U<sup>2</sup> Test</b>		<b>Watson U<sup>2</sup> Test</b>		<b>Watson U<sup>2</sup> Test</b>
<b>TIP</b>		<b>G</b>		<b>B-J</b>	
<b>E11.5 Vs E12.5</b>	p<0.05	<b>E12.5 Vs E13.5</b>	p>0.1	<b>E12.5 Vs E13.5</b>	p<0.05
<b>E12.5 Vs E13.5</b>	p<0.001	<b>E13.5 Vs E14.5</b>	p<0.01	<b>E13.5 Vs E14.5</b>	p<0.0001
<b>E13.5 Vs E14.5</b>	p>0.1				
		<b>H</b>		<b>B-J TIP</b>	
<b>K</b>		<b>E12.5 Vs E13.5</b>	p>0.1	<b>E12.5 Vs E13.5</b>	p<0.01
<b>E11.5 Vs E12.5</b>	p<0.01	<b>E13.5 Vs E14.5</b>	p<0.0001	<b>E13.5 Vs E14.5</b>	p<0.0001
<b>E12.5 Vs E13.5</b>	p<0.01				
<b>E13.5 Vs E14.5</b>	p>0.1	<b>I</b>		<b>Anterior</b>	
		<b>E12.5 Vs E13.5</b>	p>0.1	<b>E12.5 Vs E13.5</b>	p>0.1
<b>B</b>		<b>E13.5 Vs E14.5</b>	p>0.1	<b>E13.5 Vs E14.5</b>	p>0.1
<b>E12.5 Vs E13.5</b>	p>0.1				
<b>E13.5 Vs E14.5</b>	p<0.05	<b>J</b>		<b>Middle</b>	
		<b>E12.5 Vs E13.5</b>	p>0.1	<b>E12.5 Vs E13.5</b>	p<0.05
<b>C</b>		<b>E13.5 Vs E14.5</b>	p>0.1	<b>E13.5 Vs E14.5</b>	p<0.01
<b>E12.5 Vs E13.5</b>	p<0.001				
<b>E13.5 Vs E14.5</b>	p<0.05	<b>BC</b>		<b>Posterior</b>	
		<b>E12.5 Vs</b>	p<0.05	<b>E12.5 Vs E13.5</b>	p<0.001

		<b>E13.5</b>			
<b>D</b>		<b>E13.5 Vs E14.5</b>	$p < 0.01$	<b>E13.5 Vs E14.5</b>	$p > 0.1$
<b>E12.5 Vs E13.5</b>	$p > 0.05$				
<b>E13.5 Vs E14.5</b>	$p < 0.01$	<b>EFG</b>		<b>E12.5 vs E13.5 anterior</b>	
		<b>E12.5 Vs E13.5</b>	$p > 0.05$	<b>BC</b>	$p > 0.1$
<b>E</b>		<b>E13.5 Vs E14.5</b>	$p > 0.1$	<b>EFG</b>	$p > 0.1$
<b>E12.5 Vs E13.5</b>	$p > 0.1$			<b>HIJ</b>	$p > 0.1$
<b>E13.5 Vs E14.5</b>	$p > 0.1$	<b>HIJ</b>		<b>TIP</b>	$p > 0.1$
		<b>E12.5 Vs E13.5</b>	$p > 0.1$		
<b>F</b>		<b>E13.5 Vs E14.5</b>	$p < 0.0001$	<b>E12.5 vs E13.5 middle</b>	
<b>E12.5 Vs E13.5</b>	$p > 0.1$			<b>BC</b>	$p < 0.01$
<b>E13.5 Vs E14.5</b>	$p > 0.1$			<b>EFG</b>	$p > 0.1$
				<b>HIJ</b>	$p > 0.1$
				<b>TIP</b>	$p > 0.05$
				<b>E12.5 vs E13.5 posterior</b>	
				<b>BC</b>	$p > 0.05$
				<b>EFG</b>	$p < 0.001$
				<b>HIJ</b>	$p > 0.1$
				<b>TIP</b>	$p < 0.001$

**Table 12.3 Table of p-values from statistical tests on the wild-type spindle orientation data**

<b>(A)</b>	<b>VS uniform distribution</b>	<b>VS von Mises distribution</b>
<b>E11.5</b>		
<b>TIP</b>	p>0.1	p>0.1
<b>K</b>	p>0.1	p>0.1
<b>E12.5</b>		
<b>TIP</b>	p>0.1	p>0.1
<b>K</b>	p>0.1	p>0.1
<b>B</b>	n too small	p>0.1
<b>H</b>	p>0.1	p>0.1
<b>BEH</b>	p>0.1	p>0.1
<b>BEH tip</b>	p>0.1	p>0.1
<b>Ant</b>	p>0.1	p>0.1
<b>Mid</b>	p>0.1	p>0.1
<b>Post</b>	p>0.1	p>0.05
<b>E13.5</b>		
<b>TIP</b>	p>0.1	p>0.1
<b>K</b>	p>0.1	p>0.1
<b>B</b>	p>0.1	p>0.1
<b>H</b>	p>0.1	p>0.1
<b>BEH</b>	p>0.1	p>0.1
<b>BEH tip</b>	p>0.1	p>0.1
<b>Ant</b>	p>0.1	p>0.1
<b>Mid</b>	p>0.1	p>0.05
<b>Post</b>	p>0.1	p>0.1
<b>EH</b>	p>0.05	p>0.1
<b>E14.5</b>		
<b>TIP</b>	p>0.1	p>0.1
<b>K</b>	p>0.1	p>0.1

<b>B</b>	p>0.05	p>0.1
<b>H</b>	p>0.1	p>0.1
<b>BEH</b>	p>0.1	p>0.1
<b>BEH tip</b>	p>0.1	p>0.1
<b>Ant</b>	p>0.1	p>0.1
<b>Mid</b>	p>0.1	p>0.1
<b>Post</b>	p>0.1	p>0.1
<b>(B) Internal regions</b>	<b>Watson U<sup>2</sup> Test</b>	
<b>E11.5</b>		
<b>Tip Vs K</b>	p>0.1	
<b>E12.5</b>		
<b>Tip Vs BEH</b>	p>0.1	
<b>B Vs H</b>	p>0.1	
<b>Tip Vs K</b>	p>0.1	
<b>TIP BEH Vs K</b>	p>0.1	
<b>Ant Vs Mid</b>	p>0.1	
<b>Mid Vs Post</b>	p>0.1	
<b>Ant Vs Post</b>	p>0.1	
<b>E13.5</b>		
<b>Tip Vs BEH</b>	p>0.1	
<b>B Vs H</b>	p>0.1	
<b>Tip Vs K</b>	p>0.1	
<b>TIP BEH Vs K</b>	p>0.1	
<b>Ant Vs Mid</b>	p>0.1	
<b>Mid Vs Post</b>	p>0.1	
<b>Ant Vs Post</b>	p>0.1	
<b>B Vs EH</b>	p>0.1	
<b>E14.5</b>		
<b>Tip Vs BEH</b>	p>0.1	
<b>B Vs H</b>	p<0.01	

<b>Tip Vs K</b>	p>0.1	
<b>TIP BEH Vs K</b>	p>0.1	
<b>Ant Vs Mid</b>	p>0.1	
<b>Mid Vs Post</b>	p>0.1	
<b>Ant Vs Post</b>	p>0.1	
<b>(C) Between stages</b>	<b>Watson U<sup>2</sup> Test</b>	
<b>TIP</b>		
<b>E11.5 Vs E12.5</b>	p>0.1	
<b>E12.5 Vs E13.5</b>	p>0.1	
<b>E13.5 Vs E14.5</b>	p>0.1	
<b>B</b>		
<b>E12.5 Vs E13.5</b>	p>0.05	
<b>E13.5 Vs E14.5</b>	p>0.1	
<b>BEH</b>		
<b>E12.5 Vs E13.5</b>	p>0.1	
<b>E13.5 Vs E14.5</b>	p>0.1	
<b>H</b>		
<b>E12.5 Vs E13.5</b>	p>0.1	
<b>E13.5 Vs E14.5</b>	p>0.1	
<b>TIP BEH</b>		
<b>E12.5 Vs E13.5</b>	p>0.1	
<b>E13.5 Vs E14.5</b>	p>0.1	
<b>Anterior</b>		
<b>E12.5 Vs E13.5</b>	p>0.1	
<b>E13.5 Vs E14.5</b>	p>0.1	
<b>Middle</b>		
<b>E12.5 Vs E13.5</b>	p>0.1	

<b>E13.5 Vs E14.5</b>	$p > 0.1$	
<b>Posterior</b>		
<b>E12.5 Vs E13.5</b>	$p > 0.1$	
<b>E13.5 Vs E14.5</b>	$p > 0.1$	
<b>TIP BEH Vs Tip</b>	$p > 0.1$	
<b>E12.5 Vs E11.5</b>	$p > 0.1$	
<b>K</b>		
<b>E12.5 Vs E11.5</b>	$p > 0.1$	
<b>E13.5 Vs E14.5</b>	$p > 0.1$	

**Table 12.4 Table of p-values from statistical tests on the *Tbx-1* wild-type and mutant Golgi orientation data**

(A)	Wild-type	TBX-1 <sup>-/-</sup>	Wild-type	TBX-1 <sup>-/-</sup>
	VS uniform distribution	VS uniform distribution	Vs von Mises distribution	Vs von Mises distribution
<b>E11.5</b>				
<b>TIP</b>	p<0.01	p<0.01	p>0.1	p>0.05
<b>K</b>	p<0.01	p<0.05	p>0.1	p>0.1
<b>E12.5</b>				
<b>TIP</b>	p<0.01	p<0.05	p>0.1	p>0.1
<b>K</b>	p>0.1	p>0.1	p>0.1	p>0.1
<b>B</b>	p<0.05	p<0.01	p>0.1	p>0.1
<b>C</b>	NA	p>0.1	NA	p>0.1
<b>D</b>	p>0.1	p>0.1	p>0.1	p>0.1
<b>E</b>	p>0.1	p>0.1	p>0.1	p>0.1
<b>F</b>	NA	NA	NA	NA
<b>G</b>	p>0.1	p>0.1	p>0.1	p>0.1
<b>H</b>	p>0.1	p>0.1	p>0.1	p>0.1
<b>I</b>	NA	p<0.05	NA	p>0.1
<b>J</b>	p>0.05	p>0.1	p>0.1	p>0.1
<b>BC</b>	NA	p<0.05	NA	p>0.1
<b>EFG</b>	p>0.1	p>0.1	p>0.1	p>0.1
<b>HIJ</b>	p<0.05	p>0.1	p>0.1	p>0.1
<b>B-J</b>	p<0.01	p>0.1	p>0.1	p>0.1
<b>B-J TIP</b>	p<0.01	p>0.05	p>0.1	p>0.1
<b>Ant</b>	p<0.05	p>0.1	p>0.1	p>0.1
<b>Mid</b>	p<0.01	p<0.01	p>0.1	p>0.1
<b>Post</b>	p>0.1	p>0.1	p>0.1	p>0.1
<b>E13.5</b>				
<b>TIP</b>	p<0.05	p>0.1	p<0.01	p>0.1
<b>K</b>	p<0.05	p>0.1	p>0.1	p>0.1



<b>B</b>	p<0.01	p>0.1	p>0.1	p>0.1
<b>C</b>	p>0.1	NA	p>0.1	NA
<b>D</b>	p<0.05	p>0.05	p>0.1	p>0.1
<b>E</b>	p<0.01	p>0.1	p<0.01	p>0.05
<b>F</b>	NA	NA	NA	NA
<b>G</b>	p<0.01	p>0.1	p>0.1	p>0.1
<b>H</b>	p>0.05	p>0.1	p>0.1	p>0.1
<b>I</b>	NA	NA	NA	NA
<b>J</b>	p>0.1	p>0.1	p>0.1	p>0.1
<b>BC</b>	p<0.01	NA	p>0.1	NA
<b>EFG</b>	p<0.01	p>0.05	p>0.05	p>0.1
<b>HIJ</b>	p<0.05	p>0.1	p>0.1	p>0.1
<b>B-J</b>	p<0.01	p>0.05	p>0.05	p>0.1
<b>B-J TIP</b>	p<0.01	p<0.05	p<0.01	p>0.1
<b>Ant</b>	p<0.01	p>0.1	p>0.05	p>0.1
<b>Mid</b>	p<0.01	p<0.05	p<0.01	p>0.05
<b>Post</b>	p<0.05	p>0.1	p>0.05	p>0.1
<b>E14.5</b>				
<b>TIP</b>	p>0.1	p>0.05	p>0.1	p>0.1
<b>K</b>	p>0.1	p>0.1	p>0.1	p>0.1
<b>B</b>	p>0.1	p>0.05	p>0.1	p>0.1
<b>C</b>	NA	p>0.1	NA	p>0.1
<b>D</b>	p>0.1	p>0.1	p>0.1	p>0.1
<b>E</b>	p>0.05	p>0.1	p>0.1	p>0.1
<b>F</b>	NA	NA	NA	NA
<b>G</b>	p>0.1	p>0.1	p>0.1	p>0.1
<b>H</b>	p>0.1	p>0.1	p>0.1	p>0.1
<b>I</b>	NA	p>0.05	NA	p>0.1
<b>J</b>	NA	p<0.01	NA	p>0.1
<b>BC</b>	NA	p>0.1	NA	p>0.1
<b>EFG</b>	p<0.05	p>0.1	p>0.1	p>0.1
<b>HIJ</b>	p<0.05	p>0.1	p>0.1	p>0.1
<b>B-J</b>	p<0.01	p>0.05	p>0.1	p>0.1
<b>B-J TIP</b>	p<0.01	p>0.1	p>0.1	p>0.1

<b>Ant</b>	p>0.05	p>0.05	p>0.1	p>0.1
<b>Mid</b>	p<0.01	p>0.1	p>0.1	p>0.1
<b>Post</b>	p>0.1	p>0.1	p>0.1	p>0.1
<b>(B) Internal regions</b>	<b>Watson U<sup>2</sup> Test</b>	<b>Watson U<sup>2</sup> Test</b>		
	<b>Wild-type</b>	<b>TBX-1<sup>-/-</sup></b>		
<b>E11.5</b>				
<b>Tip Vs K</b>	p>0.1	p>0.05		
<b>E12.5</b>				
<b>Tip Vs B-J</b>	p>0.1	p>0.1		
<b>TIP VS K</b>	p>0.1	p>0.1		
<b>B-J TIP VS K</b>	p>0.1	p>0.1		
<b>B VS H</b>	p>0.1	p<0.05		
<b>C VS I</b>	NA	p>0.05		
<b>BC VS EFG</b>	NA	p>0.05		
<b>EFG VS HIJ</b>	p>0.1	p>0.1		
<b>HIJ VS BC</b>	NA	p>0.1		
<b>Ant Va Mid</b>	p>0.1	p<0.05		
<b>Mid Vs Post</b>	p>0.1	p>0.05		
<b>Post Vs Ant</b>	p>0.1	p>0.1		
<b>E13.5</b>				
<b>Tip Vs B-J</b>	p<0.05	p>0.1		
<b>TIP VS K</b>	p<0.05	p>0.1		
<b>B-J VS K</b>	p<0.05	p>0.1		
<b>B-J TIP VS K</b>	p<0.05	p>0.1		
<b>B VS H</b>	p>0.1	p>0.1		
<b>C VS I</b>	p>0.1	NA		
<b>BC VS EFG</b>	p>0.1	NA		
<b>EFG VS HIJ</b>	p>0.1	p>0.1		
<b>HIJ VS BC</b>	p>0.1	NA		
<b>Ant Va Mid</b>	p<0.05	p>0.1		
<b>Mid Vs Post</b>	p<0.001	p>0.1		

<b>Post Vs Ant</b>	p<0.001	p>0.1		
<b>E14.5</b>				
<b>Tip Vs B-J</b>	p>0.1	p<0.05		
<b>TIP VS K</b>	p>0.1	p<0.05		
<b>B-J TIP VS K</b>	p>0.1	p>0.1		
<b>B VS H</b>	p>0.1	p>0.1		
<b>C VS I</b>	NA	p>0.1		
<b>BC VS EFG</b>	NA	p>0.1		
<b>EFG VS HIJ</b>	p>0.1	p>0.1		
<b>HIJ VS BC</b>	p>0.1	p>0.1		
<b>Ant Va Mid</b>	p<0.01	p>0.1		
<b>Mid Vs Post</b>	p>0.1	p>0.1		
<b>Post Vs Ant</b>	p>0.1	p>0.05		
<b>(C) Wild-type Vs TBX-1<sup>-/-</sup></b>	<b>Watson U<sup>2</sup> Test</b>		<b>Watson U<sup>2</sup> Test</b>	
<b>Tip</b>				
<b>E11.5</b>	p>0.05	<b>EFG</b>		
<b>E12.5</b>	p>0.1	<b>E12.5</b>	p>0.1	
<b>E13.5</b>	p<0.05	<b>E13.5</b>	p<0.05	
<b>E14.5</b>	p<0.05	<b>E14.5</b>	p<0.05	
<b>B</b>		<b>HIJ</b>		
<b>E12.5</b>	p<0.01	<b>E12.5</b>	p>0.05	
<b>E13.5</b>	p>0.1	<b>E13.5</b>	p>0.05	
<b>E14.5</b>		<b>E14.5</b>	p>0.1	
<b>D</b>		<b>TIP B-J</b>		
<b>E12.5</b>	p>0.1	<b>E12.5</b>	p<0.05	
<b>E13.5</b>	p>0.1	<b>E13.5</b>	p<0.01	
<b>E14.5</b>	p>0.1	<b>E14.5</b>	p<0.01	
<b>E</b>		<b>B-J</b>		

<b>E12.5</b>	p>0.1	<b>E12.5</b>	p<0.01	
<b>E13.5</b>	p<0.05	<b>E13.5</b>	p<0.001	
<b>E14.5</b>	p>0.05	<b>E14.5</b>	p<0.001	
<b>G</b>		<b>Anterior</b>		
<b>E12.5</b>	p>0.1	<b>E12.5</b>	p>0.1	
<b>E13.5</b>	p>0.1	<b>E13.5</b>	p>0.1	
<b>E14.5</b>	p>0.1	<b>E14.5</b>	p>0.1	
<b>H</b>		<b>Middle</b>		
<b>E12.5</b>	p>0.1	<b>E12.5</b>	p<0.01	
<b>E13.5</b>	p>0.1	<b>E13.5</b>	p<0.001	
<b>E14.5</b>	p>0.1	<b>E14.5</b>	p<0.001	
<b>J</b>		<b>Posterior</b>		
<b>E12.5</b>	p>0.1	<b>E12.5</b>	p>0.1	
<b>E13.5</b>	p>0.1	<b>E13.5</b>	p>0.1	
<b>E14.5</b>	NA	<b>E14.5</b>	p>0.1	
<b>K</b>				
<b>E11.5</b>	p>0.1			
<b>E12.5</b>	p>0.1			
<b>E13.5</b>	p<0.05			
<b>E14.5</b>	p>0.1			

**Table 12.5 Table of p-values from statistical tests on the *Tbx-1* wild-type and mutant spindle orientation data**

<b>(A)</b>	<b>Wild-type</b>	<b>TBX-1<sup>-/-</sup></b>	<b>Wild-type</b>	<b>TBX-1<sup>-/-</sup></b>
	<b>VS uniform distribution</b>	<b>VS uniform distribution</b>	<b>Vs von Mises distribution</b>	<b>Vs von Mises distribution</b>
<b>E11.5</b>				
<b>TIP</b>	p>0.1	p>0.1	p>0.1	p>0.1
<b>K</b>	p>0.1	p>0.1	p>0.1	p>0.1
<b>E12.5</b>				
<b>TIP</b>	p>0.1	p>0.1	p>0.1	p>0.1
<b>K</b>	p>0.1	p>0.1	p>0.1	p>0.1
<b>B</b>	NA	p>0.1	NA	p>0.1
<b>H</b>	NA	p>0.1	NA	p>0.1
<b>BEH</b>	p>0.1	p>0.1	p>0.1	p>0.1
<b>BEH tip</b>	p>0.1	p>0.05	p>0.1	p>0.1
<b>Ant</b>	p>0.1	p>0.1	p>0.1	p>0.1
<b>Mid</b>	p>0.1	p>0.1	p>0.1	p>0.1
<b>Post</b>	p>0.1	p>0.1	p>0.1	p>0.1
<b>E13.5</b>				
<b>TIP</b>	p>0.1	p>0.1	p>0.1	p>0.1
<b>K</b>	p>0.1	p>0.1	p>0.1	p>0.1
<b>B</b>	p>0.1	p>0.1	p>0.05	p>0.1
<b>H</b>	p>0.1	p>0.1	p>0.1	p>0.1
<b>BEH</b>	p>0.1	p>0.1	p>0.1	p>0.1
<b>BEH tip</b>	p>0.1	p>0.1	p>0.1	p>0.1
<b>E14.5</b>				
<b>TIP</b>	p<0.05	p>0.1	p>0.1	p>0.1
<b>K</b>	p>0.1	p>0.1	p>0.1	p>0.1
<b>B</b>	p>0.1	p<0.05	p>0.1	p>0.1
<b>H</b>	p>0.1	p>0.1	p>0.1	p>0.1
<b>BEH</b>	p>0.05	p>0.1	p>0.1	p>0.1

<b>BEH tip</b>	p>0.1	p>0.1	p>0.1	p>0.1
<b>(B) Internal regions</b>	<b>Watson U<sup>2</sup> Test</b>	<b>Watson U<sup>2</sup> Test</b>		
	<b>Wild-type</b>	<b>TBX-1<sup>-/-</sup></b>		
<b>E11.5</b>				
<b>Tip Vs K</b>	p>0.1	p>0.1		
<b>E12.5</b>				
<b>Tip Vs BEH</b>	p>0.1	p>0.1		
<b>B Vs H</b>	NA	p>0.1		
<b>Tip Vs K</b>	p>0.1	p>0.05		
<b>TIP BEH Vs K</b>	p>0.1	p<0.05		
<b>Ant Vs Mid</b>	p>0.1	p>0.1		
<b>Mid Vs Post</b>	p>0.1	p>0.1		
<b>Ant Vs Post</b>	p>0.1	p>0.1		
<b>E13.5</b>				
<b>Tip Vs BEH</b>	p>0.1	p>0.1		
<b>B Vs H</b>	p>0.1	p>0.1		
<b>Tip Vs K</b>	p>0.1	p>0.1		
<b>TIP BEH Vs K</b>	p>0.1	p>0.1		
<b>E14.5</b>				
<b>Tip Vs BEH</b>	p<0.05	p>0.1		
<b>B Vs H</b>	p>0.1	p>0.05		
<b>Tip Vs K</b>	p>0.1	p>0.1		
<b>TIP BEH Vs K</b>	p>0.1	p>0.1		
<b>(C) Wild-type Vs TBX-1<sup>-/-</sup></b>	<b>Watson U<sup>2</sup> Test</b>		<b>Watson U<sup>2</sup> Test</b>	
<b>TIP</b>				
<b>E11.5</b>	p>0.1	<b>K</b>		
<b>E12.5</b>	p>0.1	<b>E11.5</b>	p>0.1	

<b>E13.5</b>	p>0.1	<b>E12.5</b>	p>0.1	
<b>E14.5</b>	p>0.1	<b>E13.5</b>	p>0.1	
		<b>E14.5</b>	p>0.1	
<b>B</b>				
<b>E12.5</b>	NA	<b>BEH</b>		
<b>E13.5</b>	p>0.1	<b>E12.5</b>	p>0.1	
<b>E14.5</b>	p>0.1	<b>E13.5</b>	p>0.1	
		<b>E14.5</b>	p>0.1	
<b>H</b>				
<b>E12.5</b>	NA	<b>Anterior</b>		
<b>E13.5</b>	p>0.1	<b>E12.5</b>	p>0.1	
<b>E14.5</b>	p>0.1			
		<b>Middle</b>		
<b>TIP BEH</b>		<b>E12.5</b>	p>0.1	
<b>E12.5</b>	p>0.1			
<b>E13.5</b>	p>0.1	<b>Posterior</b>		
<b>E14.5</b>	p>0.1	<b>E12.5</b>	p>0.1	

## 13.0 References

- A. Gebhardt, S.E., S. Zuyev, D. White (2009). Triangulation of irregularly spaced data, pp. A constrained two-dimensional Delaunay triangulation package.
- Abu-Issa, R., Smyth, G., Smoak, I., Yamamura, K., and Meyers, E.N. (2002). Fgf8 is required for pharyngeal arch and cardiovascular development in the mouse. *Development* 129, 4613-4625.
- Adams, R.J. (1996). Metaphase spindles rotate in the neuroepithelium of rat cerebral cortex. *J Neurosci* 16, 7610-7618.
- Ads, A.H., Piddington, R., Goldman, A.S., and Herold, R. (1983). Cortisol Inhibition of Development of Various Lysosomal-Enzymes in Cultured Palatal Shelves from Mouse Embryos. *Archives of Oral Biology* 28, 1115-1119.
- Aggarwal, V.S., Liao, J., Bondarev, A., Schimmang, T., Lewandoski, M., Locker, J., Shanske, A., Campione, M., and Morrow, B.E. (2006). Dissection of Tbx1 and Fgf interactions in mouse models of 22q11DS suggests functional redundancy. *Human Molecular Genetics* 15, 3219-3228.
- Agostinelli, U.L.a.C. (2009). *Circular Statistics*.
- Ahringer, J. (2003). Control of cell polarity and mitotic spindle positioning in animal cells. *Curr Opin Cell Biol* 15, 73-81.
- Alappat, S.R., Zhang, Z.Y., Suzuki, K., Zhang, X.Y., Liu, H.B., Jiang, R.L., Yamada, G., and Chen, Y.P. (2005). The cellular and molecular etiology of the cleft secondary palate in Fgf10 mutant mice. *Developmental Biology* 277, 102-113.
- Babiarz, B.S., Wee, E.L., and Zimmerman, E.F. (1979). Palate Morphogenesis .3. Changes in Cell-Shape and Orientation during Shelf Elevation. *Teratology* 20, 249-&.
- Bachiller, D., Klingensmith, J., Shneyder, N., Tran, U., Anderson, R., Rossant, J., and De Robertis, E.M. (2003). The role of chordin/Bmp signals in mammalian pharyngeal development and DiGeorge syndrome. *Development* 130, 3567-3578.
- Bagci, U., and Bai, L. (2008). Fully automatic 3D reconstruction of histological images. *I S Biomed Imaging*, 991-994.
- Bao, X.D., Xu, D.H., Toumoulin, C., and Luo, L.M. (2007). Volume reconstruction based on non-rigid registration. *P Ann Int IEEE Embs*, 6536-6539.
- Barone, V., and Heisenberg, C.P. (2012). Cell adhesion in embryo morphogenesis. *Curr Opin Cell Biol* 24, 148-153.
- Beningo, K.A., Dembo, M., Kaverina, I., Small, J.V., and Wang, Y.L. (2001). Nascent focal adhesions are responsible for the generation of strong propulsive forces in migrating fibroblasts. *Journal of Cell Biology* 153, 881-887.
- Bergin, T.M. (1991). A Comparison of Goodness-of-Fit Tests for Analysis of Nest Orientation in Western Kingbirds (*Tyrannus-Verticalis*). *Condor* 93, 164-171.



Bivand, E.P.R. (2012). Classes and methods for spatial data, pp. A package that provides classes and methods for spatial data. The classes document where the spatial location information resides, for 2D or 3D data. Utility functions are provided, e.g. for plotting data as maps, spatial selection, as well as methods for retrieving coordinates, for subsetting, print, summary, etc.

Boehm, B., Westerberg, H., Lesnicar-Pucko, G., Raja, S., Rautschka, M., Cotterell, J., Swoger, J., and Sharpe, J. (2010). The role of spatially controlled cell proliferation in limb bud morphogenesis. *PLoS Biol* 8, e1000420.

Bollert, J.A., and Hendrick, A.G. (1971). Morphogenesis of Palate in Baboon (*Papio-cynocephalus*). *Teratology* 4, 343-8.

Brinkley, L.L., and Bookstein, F.L. (1986). Cell distribution during mouse secondary palate closure. II. Mesenchymal cells. *J Embryol Exp Morphol* 96, 111-130.

Brinkley, L.L., and Morriswiman, J. (1987). Computer-Assisted Analysis of Hyaluronate Distribution during Morphogenesis of the Mouse Secondary Palate. *Development* 100, 629-635.

Bulleit, R.F., and Zimmerman, E.F. (1985). The influence of the epithelium on palate shelf reorientation. *J Embryol Exp Morphol* 88, 265-279.

Burdett, D.N., Waterfield, J.D., and Shah, R.M. (1988). VERTICAL DEVELOPMENT OF THE SECONDARY PALATE IN HAMSTER EMBRYOS FOLLOWING EXPOSURE TO 6-MERCAPTOPYRIMIDINE. *Teratology* 37, 591-597.

Bush, J.O., and Jiang, R. (2012). Palatogenesis: morphogenetic and molecular mechanisms of secondary palate development. *Development* 139, 231-243.

Bush, J.O., and Soriano, P. (2010). Ephrin-B1 forward signaling regulates craniofacial morphogenesis by controlling cell proliferation across Eph-ephrin boundaries. *Genes Dev* 24, 2068-2080.

Byun, T.K.J. (2008). ITCN: Image-based Tool for Counting Nuclei, pp. ITCN is an ImageJ plugin for automatically counting the number cells within an image. The inputs are: (1) an estimation of the diameter of a cell, (2) an estimation of the minimum distance between cells, and (3) either a region of interest (ROI) selected with ImageJ's selection tools or a black and white mask image that is white in regions that are to be counted.

Capellini, T.D., Zappavigna, V., and Selleri, L. (2011). Pbx homeodomain proteins: TALENTed regulators of limb patterning and outgrowth. *Dev Dyn* 240, 1063-1086.

Carette, M.J., and Ferguson, M.W. (1992). The fate of medial edge epithelial cells during palatal fusion in vitro: an analysis by Dil labelling and confocal microscopy. *Development* 114, 379-388.

Castanon, I., and Gonzalez-Gaitan, M. (2011). Oriented cell division in vertebrate embryogenesis. *Curr Opin Cell Biol* 23, 697-704.

Castilla, P.M.E. (2001). Global registry and database on craniofacial anomalies. In Report of a WHO Registry Meeting on Craniofacial Anomalies (World Health Organisation).

Chai, Y., Jiang, X.B., Ito, Y., Bringas, P., Han, J., Rowitch, D.H., Soriano, P., McMahon, A.P., and Sucov, H.M. (2000). Fate of the mammalian cranial neural crest during tooth and mandibular morphogenesis. *Development* 127, 1671-1679.

Chapman, D.L., Garvey, N., Hancock, S., Alexiou, M., Agulnik, S.I., GibsonBrown, J.J., CebraThomas, J., Bollag, R.J., Silver, L.M., and Papaioannou, V.E. (1996). Expression of the T-box family genes, Tbx1-Tbx5, during early mouse development. *Developmental Dynamics* 206, 379-390.

Chen, Y.P., He, F.L., Xiong, W., Yu, X.Y., Espinoza-Lewis, R., Liu, C., Gu, S.P., Nishita, M., Suzuki, K., Yamada, G., *et al.* (2008). Wnt5a regulates directional cell migration and cell proliferation via Ror2-mediated noncanonical pathway in mammalian palate development. *Development* 135, 3871-3879.

Chiang, C., Ying, L.T.T., Lee, E., Young, K.E., Corden, J.L., Westphal, H., and Beachy, P.A. (1996). Cyclopia and defective axial patterning in mice lacking Sonic hedgehog gene function. *Nature* 383, 407-413.

Chou, M.J., Kosazuma, T., Takigawa, T., Yamada, S., Takahara, S., and Shiota, K. (2004). Palatal shelf movement during palatogenesis: a fate map of the fetal mouse palate cultured in vitro. *Anatomy and Embryology* 208, 19-25.

Choudhry, P., and Trede, N.S. (2013). DiGeorge syndrome gene tbx1 functions through wnt11r to regulate heart looping and differentiation. *Plos One* 8, e58145.

Christensen, K., Juel, K., Herskind, M., and Murray, J.C. (2004). Long term follow up study of survival associated with cleft lip and palate at birth. *Brit Med J* 328, 1405-1406.

Cobourne, M.T., Hardcastle, Z., and Sharpe, P.T. (2001). Sonic hedgehog regulates epithelial proliferation and cell survival in the developing tooth germ. *Journal of Dental Research* 80, 1974-1979.

Coleman, R.D. (1965). Development of the Rat Palate. *Anat Rec* 151, 107-117.

Concha, M.L., and Adams, R.J. (1998). Oriented cell divisions and cellular morphogenesis in the zebrafish gastrula and neurula: a time-lapse analysis. *Development* 125, 983-994.

Costantini, F., and Lacy, E. (1981). Introduction of a Rabbit Beta-Globin Gene into the Mouse Germ Line. *Nature* 294, 92-94.

Crum, W.R., Hartkens, T., and Hill, D.L.G. (2004). Non-rigid image registration: theory and practice. *Brit J Radiol* 77, S140-S153.

Cui, X.M., Chai, Y., Chen, J., Yamamoto, T., Ito, Y., Bringas, P., and Shuler, C.F. (2003). TGF-beta3-dependent SMAD2 phosphorylation and inhibition of MEE proliferation during palatal fusion. *Dev Dyn* 227, 387-394.

D'Angelo, M., and Greene, R.M. (1991). Transforming growth factor-beta modulation of glycosaminoglycan production by mesenchymal cells of the developing murine secondary palate. *Dev Biol* 145, 374-378.

Daley, W.P., and Yamada, K.M. (2013). ECM-modulated cellular dynamics as a driving force for tissue morphogenesis. *Curr Opin Genet Dev.* 23,408-414.

Davidson, D. (1995). The function and evolution of Msx genes: pointers and paradoxes. *Trends Genet* 11, 405-411.

Deng, M., Kleinert, R., Huang, H., He, Q., Madrahimova, F., Dirsch, O., and Dahmen, U. (2009). Statistical and Economical Efficiency in Assessment of Liver Regeneration Using Defined Sample Size and Selection in Combination With a Fully Automated Image Analysis System. *Journal of Histochemistry & Cytochemistry* 57, 1075-1085.

Dennis, S. (1977). Reduction of the rate of outgrowth, cell density, and cell division following removal of the apical ectodermal ridge of the chick limb-bud. *J Embryol Exp Morphol* 40, 1-21.

Dibiase, M.C.A. (2010). *Handbook of Orthodontics* (Elsevier Limited).

Diewert, V.M. (1985). Development of human craniofacial morphology during the late embryonic and early fetal periods. *Am J Orthod* 88, 64-76.

Dixon, M.J., Foreman, D., Schor, S., and Ferguson, M.W.J. (1993). Epidermal Growth-Factor and Transforming Growth-Factor-Alpha Regulate Extracellular-Matrix Production by Embryonic Mouse Palatal Mesenchymal Cells Cultured on a Variety of Substrata. *Roux Arch Dev Biol* 203, 140-150.

Druckenbrod, N.R., and Epstein, M.L. (2005). The pattern of neural crest advance in the cecum and colon. *Developmental Biology* 287, 125-133.

Druckenbrod, N.R., and Epstein, M.L. (2007). Behavior of enteric neural crest-derived cells varies with respect to the migratory wavefront. *Developmental Dynamics* 236, 84-92.

Economou, A.D., Ohazama, A., Porntaveetus, T., Sharpe, P.T., Kondo, S., Basson, M.A., Gritti-Linde, A., Cobourne, M.T., and Green, J.B.A. (2012). Periodic stripe formation by a Turing mechanism operating at growth zones in the mammalian palate. *Nature Genetics* 44, 348-U163.

Economou, A.D., Brock, L.J., Cobourne, M.T., Green, J.B.A., (2013) Whole population cell analysis of a landmark-rich mammalian epithelium reveals multiple elongation mechanisms. *Development* 140, 4740-4750.

Elul, T., and Keller, R. (2000). Monopolar protrusive activity: A new morphogenic cell behavior in the neural plate dependent on vertical interactions with the mesoderm in *Xenopus*. *Developmental Biology* 224, 3-19.

Fagman, H., Liao, J., Westerlund, J., Andersson, L., Morrow, B.E., and Nilsson, M. (2007). The 22q11 deletion syndrome candidate gene *Tbx1* determines thyroid size and positioning. *Human Molecular Genetics* 16, 276-285.

Ferguson, M.W. (1977). The mechanism of palatal shelf elevation and the pathogenesis of cleft palate. *Virchows Arch A Pathol Anat Histol* 375, 97-113.

Ferguson, M.W. (1978). Palatal shelf elevation in the Wistar rat fetus. *J Anat* 125, 555-577.

Ferguson, M.W.J. (1988). PALATE DEVELOPMENT. *Development* 103, 41-60.

Ferretti, E., Li, B.S., Zewdu, R., Wells, V., Hebert, J.M., Karner, C., Anderson, M.J., Williams, T., Dixon, J., Dixon, M.J., *et al.* (2011). A Conserved Pbx-Wnt-p63-Irf6 Regulatory Module Controls Face Morphogenesis by Promoting Epithelial Apoptosis. *Developmental Cell* 21, 627-641.

Foreman, D.M., Sharpe, P.M., and Ferguson, M.W. (1991). Comparative biochemistry of mouse and chick secondary-palate development in vivo and in vitro with particular emphasis on extracellular matrix molecules and the effects of growth factors on their synthesis. *Arch Oral Biol* 36, 457-471.

Fremin, C., and Meloche, S. (2010). From basic research to clinical development of MEK1/2 inhibitors for cancer therapy. *J Hematol Oncol* 3.

Funato, N., Nakamura, M., Richardson, J.A., Srivastava, D., and Yanagisawa, H. (2012). Tbx1 regulates oral epithelial adhesion and palatal development. *Hum Mol Genet*.

Furukawa, S., Usuda, K., Abe, M., and Ogawa, I. (2004). Histopathological findings of cleft palate in rat embryos induced by triamcinolone acetonide. *Journal of Veterinary Medical Science* 66, 397-402.

Garg, V., Yamagishi, C., Hu, T.H., Kathiriya, I.S., Yamagishi, H., and Srivastava, D. (2001). Tbx1, a DiGeorge syndrome candidate gene, is regulated by Sonic hedgehog during pharyngeal arch development. *Developmental Biology* 235, 62-73.

Gillies, T.E., and Cabernard, C. (2011). Cell Division Orientation in Animals. *Current Biology* 21, R599-R609.

Godt, D., and Laski, F.A. (1995). Mechanisms of Cell Rearrangement and Cell Recruitment in Drosophila Ovary Morphogenesis and the Requirement of Bric-a-Brac. *Development* 121, 173-187.

Gong, Y., Mo, C., and Fraser, S.E. (2004). Planar cell polarity signalling controls cell division orientation during zebrafish gastrulation. *Nature* 430, 689-693.

Goudy, S., Law, A., Sanchez, G., Baldwin, H.S., and Brown, C. (2010). Tbx1 is necessary for palatal elongation and elevation. *Mechanisms of Development* 127, 292-300.

Greene, R.M., and Pratt, R.M. (1976). Developmental Aspects of Secondary Palate Formation. *Journal of Embryology and Experimental Morphology* 36, 225-245.

Grenier, J., Teillet, M.A., Grifone, R., Kelly, R.G., and Duprez, D. (2009). Relationship between Neural Crest Cells and Cranial Mesoderm during Head Muscle Development. *Plos One* 4.

Griffith, C.M., and Hay, E.D. (1992). Epithelial-Mesenchymal Transformation during Palatal Fusion - Carboxyfluorescein Traces Cells at Light and Electron-Microscopic Levels. *Development* 116, 1087-1099.

Gritli-Linde, A. (2007). Molecular control of secondary palate development. *Developmental Biology* 301, 309-326.

Gritli-Linde, A., Bei, M., Maas, R., Zhang, X.Y.M., Linde, A., and McMahon, A.P. (2002). Shh signaling within the dental epithelium is necessary for cell proliferation, growth and polarization. *Development* 129, 5323-5337.

Grobstein, C., and Cohen, J. (1965). Collagenase: effect on the morphogenesis of embryonic salivary epithelium in vitro. *Science* 150, 626-628.

Gros, J., Hu, J.K.H., Vinegoni, C., Feruglio, P.F., Weissleder, R., and Tabin, C.J. (2010). WNT5A/JNK and FGF/MAPK Pathways Regulate the Cellular Events Shaping the Vertebrate Limb Bud. *Current Biology* 20, 1993-2002.

- Guest, E., and Baldock, R. (1995). Automatic reconstruction of serial sections using the finite element method. *Bioimaging|Bioimaging* 3, 154-167.
- Gupta, V., and Bei, M. (2006). Modification of Msx1 by SUMO-1. *Biochem Bioph Res Co* 345, 74-77.
- Hamachi, T., Sasaki, Y., Hidaka, K., and Nakata, M. (2003). Association between palatal morphogenesis and Pax9 expression pattern in CL/Fr embryos with clefting during palatal development. *Archives of Oral Biology* 48, 581-587.
- Han, J., Mayo, J., Xu, X., Li, J.Y., Bringas, P., Maas, R.L., Rubenstein, J.L.R., and Chai, Y. (2009). Indirect modulation of Shh signaling by Dlx5 affects the oral-nasal patterning of palate and rescues cleft palate in Msx1-null mice. *Development* 136, 4225-4233.
- Hayward, A.F. (1969). Ultrastructural changes in the epithelium during fusion of the palatal processes in rats. *Arch Oral Biol* 14, 661-678.
- He, F., Xiong, W., Yu, X., Espinoza-Lewis, R., Liu, C., Gu, S., Nishita, M., Suzuki, K., Yamada, G., Minami, Y., *et al.* (2008). Wnt5a regulates directional cell migration and cell proliferation via Ror2-mediated noncanonical pathway in mammalian palate development. *Development* 135, 3871-3879.
- He, F.L., Popkie, A.P., Xiong, W., Li, L., Wang, Y., Phiel, C.J., and Chen, Y.P. (2010). Gsk3 beta Is Required in the Epithelium for Palatal Elevation in Mice. *Developmental Dynamics* 239, 3235-3246.
- Hehn, B.M., Young, A.V., and Shah, R.M. (1995). Analysis of cell proliferation kinetics during the secondary palate development in quail. *Histol Histopathol* 10, 697-702.
- Heisenberg, C.P., Tada, M., Rauch, G.J., Saude, L., Concha, M.L., Geisler, R., Stemple, D.L., Smith, J.C., and Wilson, S.W. (2000). Silberblick/Wnt11 mediates convergent extension movements during zebrafish gastrulation. *Nature* 405, 76-81.
- Hilliard, S.A., Yu, L., Gu, S., Zhang, Z., and Chen, Y.P. (2005). Regional regulation of palatal growth and patterning along the anterior-posterior axis in mice. *J Anat* 207, 655-667.
- Hindley, A., and Kolch, W. (2002). Extracellular signal regulated kinase (ERK)/mitogen activated protein kinase (MAPK)-independent functions of Raf kinases. *J Cell Sci* 115, 1575-1581.
- Hiramoto, T., Kang, G., Suzuki, G., Satoh, Y., Kucherlapati, R., Watanabe, Y., and Hiroi, N. (2011). Tbx1: identification of a 22q11.2 gene as a risk factor for autism spectrum disorder in a mouse model. *Human Molecular Genetics* 20, 4775-4785.
- Hu, T.H., Yamagishi, H., Maeda, J., McAnally, J., Yamagishi, C., and Srivastava, D. (2004). Tbx1 regulates fibroblast growth factors in the anterior heart field through a reinforcing autoregulatory loop involving forkhead transcription factors. *Development* 131, 5491-5502.
- Huang, C.W., and Hales, B.F. (2002). Role of Caspases in murine limb bud cell death induced by 4-hydroperoxycyclophosphamide, an activated analog of cyclophosphamide. *Teratology* 66, 288-299.
- Humphrey, T. (1969). Relation between Human Fetal Mouth Opening Reflexes and Closure of Palate. *Am J Anat* 125, 317-&.

Hurle, J.M., Ros, M.A., Climent, V., and Garcia-Martinez, V. (1996). Morphology and significance of programmed cell death in the developing limb bud of the vertebrate embryo. *Microsc Res Tech* 34, 236-246.

Ito, Y., Yeo, J.Y., Chytil, A., Han, J., Bringas, P., Jr., Nakajima, A., Shuler, C.F., Moses, H.L., and Chai, Y. (2003). Conditional inactivation of *Tgfb2* in cranial neural crest causes cleft palate and calvaria defects. *Development* 130, 5269-5280.

Jerome, L.A., and Papaioannou, V.E. (2001). DiGeorge syndrome phenotype in mice mutant for the T-box gene, *Tbx1*. *Nature Genetics* 27, 286-291.

Jin, J.Z., Li, Q., Higashi, Y., Darling, D.S., and Ding, J. (2008). Analysis of *Zfhx1a* mutant mice reveals palatal shelf contact-independent medial edge epithelial differentiation during palate fusion. *Cell Tissue Res* 333, 29-38.

Jin, J.Z., Tan, M., Warner, D.R., Darling, D.S., Higashi, Y., Gridley, T., and Ding, J.X. (2010). Mesenchymal Cell Remodeling During Mouse Secondary Palate Reorientation. *Developmental Dynamics* 239, 2110-2117.

Johnston, M.C. (1966). A radioautographic study of the migration and fate of cranial neural crest cells in the chick embryo. *Anat Rec* 156, 143-155.

Jumlongras, D., Bei, M., Stimson, J.M., Wang, W.F., DePalma, S.R., Seidman, C.E., Felbor, U., Maas, R., Seidman, J.G., and Olsen, B.R. (2001). A nonsense mutation in *MSX1* causes Witkop syndrome. *Am J Hum Genet* 69, 67-74.

Kafri, R., Levy, J., Ginzberg, M.B., Oh, S., Lahav, G., and Kirschner, M.W. (2013). Dynamics extracted from fixed cells reveal feedback linking cell growth to cell cycle. *Nature* 494, 480-483.

Kapur, J.N., Sahoo, P.K., and Wong, A.K.C. (1985). A New Method for Gray-Level Picture Thresholding Using the Entropy of the Histogram. *Comput Vision Graph* 29, 273-285.

Karlsson, L., Bondjers, C., and Betsholtz, C. (1999). Roles for PDGF-A and sonic hedgehog in development of mesenchymal components of the hair follicle. *Development* 126, 2611-2621.

Keller, R. (2006). Mechanisms of elongation in embryogenesis. *Development* 133, 2291-2302.

Keller, R., Davidson, L., Edlund, A., Elul, T., Ezin, M., Shook, D., and Skoglund, P. (2000). Mechanisms of convergence and extension by cell intercalation. *Philos T R Soc B* 355, 897-922.

Kelly, R.G., Jerome-Majewska, L.A., and Papaioannou, V.E. (2004). The del22q11.2 candidate gene *Tbx1* regulates branchiomic myogenesis. *Human Molecular Genetics* 13, 2829-2840.

Kim, H.J., Schleiffarth, J.R., Jessurun, J., Sumanas, S., Petryk, A., Lin, S., and Ekker, S.C. (2005). *Wnt5* signaling in vertebrate pancreas development. *Bmc Biol* 3.

Kirby, M.L., and Waldo, K.L. (1990). Role of Neural Crest in Congenital Heart-Disease. *Circulation* 82, 332-340.

Knudsen, T.B., Bulleit, R.F., and Zimmerman, E.F. (1985). Histochemical localization of glycosaminoglycans during morphogenesis of the secondary palate in mice. *Anat Embryol (Berl)* 173, 137-142.

Kobrynski, L.J., and Sullivan, K.E. (2007). Velocardiofacial syndrome, DiGeorge syndrome: the chromosome 22q11.2 deletion syndromes. *Lancet* 370, 1443-1452.

- Kulesa, P., Bronner-Fraser, M., and Fraser, S. (2000). In ovo time-lapse analysis after dorsal neural tube ablation shows rerouting of chick hindbrain neural crest. *Development* 127, 2843-2852.
- Kurosaka, S., and Kashina, A. (2008). Cell biology of embryonic migration. *Birth Defects Res C Embryo Today* 84, 102-122.
- Lan, Y., and Jiang, R. (2009). Sonic hedgehog signaling regulates reciprocal epithelial-mesenchymal interactions controlling palatal outgrowth. *Development* 136, 1387-1396.
- Lan, Y., Ovitt, C.E., Cho, E.S., Maltby, K.M., Wang, Q., and Jiang, R. (2004). Odd-skipped related 2 (*Osr2*) encodes a key intrinsic regulator of secondary palate growth and morphogenesis. *Development* 131, 3207-3216.
- Landini, G. (2004). Colour Deconvolution.
- Lania, G., Zhang, Z., Huynh, T., Caprio, C., Moon, A.M., Vitelli, F., and Baldini, A. (2009). Early thyroid development requires a *Tbx1-Fgf8* pathway. *Developmental Biology* 328, 109-117.
- Larsson, K.S. (1962). Studies on the closure of the secondary palate. III. Autoradiographic and histochemical studies in the normal mouse embryo. *Acta Morphol Neerl Scand* 4, 349-367.
- Laufer, E., Nelson, C.E., Johnson, R.L., Morgan, B.A., and Tabin, C. (1994). Sonic Hedgehog and *Fgf-4* Act through a Signaling Cascade and Feedback Loop to Integrate Growth and Patterning of the Developing Limb Bud. *Cell* 79, 993-1003.
- Lazzaro, C. (1940). Sul meccanismo di chiusura del palato secondario. *Monit zool ital* 51, 249-273.
- Lechler, T., and Fuchs, E. (2005). Asymmetric cell divisions promote stratification and differentiation of mammalian skin. *Nature* 437, 275-280.
- Lecuit, T. (2010).  $\alpha$ -catenin mechanosensing for adherens junctions. *Nature Cell Biology* 12, 522-524.
- Lecuit, T., and Lenne, P.F. (2007). Cell surface mechanics and the control of cell shape, tissue patterns and morphogenesis. *Nat Rev Mol Cell Biol* 8, 633-644.
- Lee, J.M., Kim, J.Y., Cho, K.W., Lee, M.J., Cho, S.W., Zhang, Y.D., Byun, S.K., Yi, C.K., and Jung, H.S. (2007). Modulation of cell proliferation during palatogenesis by the interplay between *Tbx3* and *Bmp4*. *Cell Tissue Res* 327, 285-292.
- Lee, J.Y., and Harland, R.M. (2007). Actomyosin contractility and microtubules drive apical constriction in *Xenopus* bottle cells. *Developmental Biology* 311, 40-52.
- Lengyel, J.A., and Iwaki, D.D. (2002). It takes guts: The *Drosophila* hindgut as a model system for organogenesis. *Developmental Biology* 243, 1-19.
- Lessard, J.L., Wee, E.L., and Zimmerma.Ef (1974). Presence of Contractile Proteins in Mouse Fetal Palate Prior to Shelf Elevation. *Teratology* 9, 113-125.
- Levi, G., Mantero, S., Barbieri, O., Cantatore, D., Paleari, L., Beverdam, A., Genova, F., Robert, B., and Merlo, G.R. (2006). *Msx1* and *Dlx5* act independently in development of craniofacial skeleton, but converge on the regulation of *Bmp* signaling in palate formation. *Mechanisms of Development* 123, 3-16.

- Liao, J., Kochilas, L., Nowotschin, S., Arnold, J.S., Aggarwal, V.S., Epstein, J.A., Brown, M.C., Adams, J., and Morrow, B.E. (2004). Full spectrum of malformations in velo-cardio-facial syndrome/DiGeorge syndrome mouse models by altering Tbx1 dosage. *Hum Mol Genet* 13, 1577-1585.
- Lin, C., Fisher, A.V., Yin, Y., Maruyama, T., Veith, G.M., Dhandha, M., Huang, G.J., Hsu, W., and Ma, L. (2011). The inductive role of Wnt-beta-Catenin signaling in the formation of oral apparatus. *Dev Biol*.
- Lindsay, E.A. (2001). Chromosomal microdeletions: Dissecting del22q11 syndrome. *Nature Reviews Genetics* 2, 858-868.
- Liu, W.J., Lan, Y., Pauws, E., Meester-Smoor, M.A., Stanier, P., Zwarthoff, E.C., and Jiang, R.L. (2008). The Mn1 transcription factor acts upstream of Tbx22 and preferentially regulates posterior palate growth in mice. *Development* 135, 3959-3968.
- Liu, X., Yan, S., Zhou, T.H., Terada, Y., and Erikson, R.L. (2004). The MAP kinase pathway is required for entry into mitosis and cell survival. *Oncogene* 23, 763-776.
- Loganathan, R., Potetz, B.R., Rongish, B.J., and Little, C.D. (2012). Spatial Anisotropies and Temporal Fluctuations in Extracellular Matrix Network Texture during Early Embryogenesis. *Plos One* 7.
- Lu, P.F., Minowada, G., and Martin, G.R. (2006). Increasing Fgf4 expression in the mouse limb bud causes polysyndactyly and rescues the skeletal defects that result from loss of Fgf8 function. *Development* 133, 33-42.
- Luke, D.A. (1976). Development of the secondary palate in man. *Acta Anat (Basel)* 94, 596-608.
- Luke, D.A. (1989). Cell proliferation in palatal processes and Meckel's cartilage during development of the secondary palate in the mouse. *J Anat* 165, 151-158.
- Machacek, M., and Danuser, G. (2006). Morphodynamic profiling of protrusion phenotypes. *Biophysical Journal* 90, 1439-1452.
- Mardia, K.V. (1975). Statistics of Directional Data. *Journal of the Royal Statistical Society* 37, 349-393.
- Martin, A.C., Kaschube, M., and Wieschaus, E.F. (2009). Pulsed contractions of an actin-myosin network drive apical constriction. *Nature* 457, 495-U411.
- Martinez-Alvarez, C., O'Kane, S., Taya, Y., and Ferguson, M.W. (1996). Palate development in the TGF-beta 3 knockout mouse. Low vacuum scanning electron microscopy reveals changes in the medial edge epithelium. *Int J Dev Biol Suppl* 1, 115S-116S.
- Martinez-Alvarez, C., Tudela, C., Perez-Miguelsanz, J., O'Kane, S., Puerta, J., and Ferguson, M.W.J. (2000). Medial edge epithelial cell fate during palatal fusion. *Developmental Biology* 220, 343-357.
- Martynoga, B., Morrison, H., Price, D.J., and Mason, J.O. (2005). Foxg1 is required for specification of ventral telencephalon and region-specific regulation of dorsal telencephalic precursor proliferation and apoptosis. *Developmental Biology* 283, 113-127.



Matsumura, K., Taketomi, T., Yoshizaki, K., Arai, S., Sanui, T., Yoshiga, D., Yoshimura, A., and Nakamura, S. (2011). Sprouty2 controls proliferation of palate mesenchymal cells via fibroblast growth factor signaling. *Biochem Biophys Res Commun* 404, 1076-1082.

McBeath, R., Pirone, D.M., Nelson, C.M., Bhadriraju, K., and Chen, C.S. (2004). Cell shape, cytoskeletal tension, and RhoA regulate stem cell lineage commitment. *Dev Cell* 6, 483-495.

McGonnell, I.M., Clarke, J.D.W., and Tickle, C. (1998). Fate map of the developing chick face: Analysis of expansion of facial primordia and establishment of the primary palate. *Developmental Dynamics* 212, 102-118.

Mcmahon, A.P., Joyner, A.L., Bradley, A., and McMahon, J.A. (1992). The Midbrain Hindbrain Phenotype of Wnt-1--Wnt-1- Mice Results from Stepwise Deletion of Engrailed-Expressing Cells by 9.5 Days Postcoitum. *Cell* 69, 581-595.

Mellor, H. (2004). Cell motility: Golgi signalling shapes up to ship out. *Current Biology* 14, R434-R435.

Merscher, S., Funke, B., Epstein, J.A., Heyer, J., Puech, A., Lu, M.M., Xavier, R.J., Demay, M.B., Russell, R.G., Factor, S., *et al.* (2001). TBX1 is responsible for cardiovascular defects in Velo-Cardio-Facial/DiGeorge syndrome. *Cell* 104, 619-629.

Minc, N. and Piel, M., (2012) Predicting division plane position and orientation. *Trends Cell Biol* 22, 193-200.

Minkoff, R., and Kuntz, A.J. (1978). Cell proliferation and cell density of mesenchyme in the maxillary process and adjacent regions during facial development in the chick embryo. *J Embryol Exp Morphol* 46, 65-74.

Mlodzik, M. (2002). Planar cell polarization: do the same mechanisms regulate Drosophila tissue polarity and vertebrate gastrulation? *Trends in Genetics* 18, 564-571.

Morishita, Y., and Iwasa, Y. (2008). Growth based morphogenesis of vertebrate limb bud. *B Math Biol* 70, 1957-1978.

Murray, J.C. (2002). Gene/environment causes of cleft lip and/or palate. *Clin Genet* 61, 248-256.

Muskhelishvili, L., Latendresse, J.R., Kodell, R.L., and Henderson, E.B. (2003). Evaluation of cell proliferation in rat tissues with BrdU, PCNA, Ki-67(MIB-5) immunohistochemistry and in situ hybridization for histone mRNA. *Journal of Histochemistry & Cytochemistry* 51, 1681-1688.

Myat, M.M. (2005). Making tubes in the Drosophila embryo. *Developmental Dynamics* 232, 617-632.

Nanda, R., and Romeo, D. (1975). DIFFERENTIAL CELL-PROLIFERATION OF EMBRYONIC RAT PALATAL PROCESSES AS DETERMINED BY INCORPORATION OF TRITIATED-THYMIDINE. *Cleft Palate Journal* 12, 436-443.

Nelson, W.J. (2009). Remodeling Epithelial Cell Organization: Transitions Between Front-Rear and Apical-Basal Polarity. *Csh Perspect Biol* 1.

Newbern, J., Zhong, J., Wickramasinghe, S.R., Li, X.Y., Wu, Y.H., Samuels, I., Cherosky, N., Karlo, J.C., O'Loughlin, B., Wikenheiser, J., *et al.* (2008). Mouse and human phenotypes

indicate a critical conserved role for ERK2 signaling in neural crest development. *P Natl Acad Sci USA* *105*, 17115-17120.

Nishita, M., Yoo, S.K., Nomachi, A., Kani, S., Sougawa, N., Ohta, Y., Takada, S., Kikuchi, A., and Minami, Y. (2006). Filopodia formation mediated by receptor tyrosine kinase Ror2 is required for Wnt5a-induced cell migration. *Journal of Cell Biology* *175*, 555-562.

Nowakowski, R.S., Lewin, S.B., and Miller, M.W. (1989). Bromodeoxyuridine immunohistochemical determination of the lengths of the cell cycle and the DNA-synthetic phase for an anatomically defined population. *J Neurocytol* *18*, 311-318.

O'Connell, C.B., and Wang, Y.L. (2000). Mammalian spindle orientation and position respond to changes in cell shape in a dynein-dependent fashion. *Mol Biol Cell* *11*, 1765-1774.

Oh, W.J., Westmoreland, J.J., Summers, R., and Condie, B.G. (2010). Cleft Palate Is Caused by CNS Dysfunction in *Gad1* and *Viaat* Knockout Mice. *Plos One* *5*.

Oka, K., Oka, S., Sasaki, T., Ito, Y., Bringas, P., Jr., Nonaka, K., and Chai, Y. (2007). The role of TGF-beta signaling in regulating chondrogenesis and osteogenesis during mandibular development. *Dev Biol* *303*, 391-404.

Osumiyamashita, N., Ninomiya, Y., Doi, H., and Eto, K. (1994). THE CONTRIBUTION OF BOTH FOREBRAIN AND MIDBRAIN CREST CELLS TO THE MESENCHYME IN THE FRONTONASAL MASS OF MOUSE EMBRYOS. *Developmental Biology* *164*, 409-419.

Paluch, E., and Heisenberg, C.P. (2009). Biology and physics of cell shape changes in development. *Curr Biol* *19*, R790-799.

Pantalacci, S., Prochazka, J., Martin, A., Rothova, M., Lambert, A., Bernard, L., Charles, C., Viriot, L., Peterkova, R., and Laudet, V. (2008). Patterning of palatal rugae through sequential addition reveals an anterior/posterior boundary in palatal development. *Bmc Developmental Biology* *8*.

Papangelis, I., and Scambler, P. (2013). The 22q11 deletion: DiGeorge and velocardiofacial syndromes and the role of TBX1. *Wiley Interdiscip Rev Dev Biol* *2*, 393-403.

Parada, C. (2013). Crucial role for ERK2 signaling in palate development. Paper presented at: IADR General Session (Seattle, USA).

Peter, K. (1924). Die Entwicklung des Säugetiergaumens. *Ergebn Anat EntwGesch* *25*, 448-564.

Peterkova, R., Klepacek, I., and Peterka, M. (1987). PRENATAL DEVELOPMENT OF RUGAE PALATINAE IN MICE - SCANNING ELECTRON-MICROSCOPIC AND HISTOLOGIC-STUDIES. *Journal of Craniofacial Genetics and Developmental Biology* *7*, 169-189.

Pons-Tortella, E. (1937). Über die Bildungsweise des sekundären Gaumens. *Anat Anz* *84*, 13-17.

Pratt, R.M., Jr., and King, C.T. (1972). Inhibition of collagen cross-linking associated with beta-aminopropionitrile-induced cleft palate in the rat. *Dev Biol* *27*, 322-328.

Pratt, R.M., and Martin, G.R. (1975). Epithelial-Cell Death and Cyclic-Amp Increase during Palatal Development. *P Natl Acad Sci USA* *72*, 874-877.

Preisinger, C., Short, B., De Corte, V., Bruyneel, E., Haas, A., Kopajtich, R., Gettemans, J., and Barr, F.A. (2004). YSK1 is activated by the Golgi matrix protein GM130 and plays a role in cell migration through its substrate 14-3-3 zeta. *Journal of Cell Biology* 164, 1009-1020.

Prewitt, J.M.S., and Mendelso.MI (1966). Analysis of Cell Images. *Ann Ny Acad Sci* 128, 1035- &.

Prigozhina, N.L., and Waterman-Storer, C.M. (2004). Protein kinase D-mediated anterograde membrane trafficking is required for fibroblast motility. *Current Biology* 14, 88-98.

Reszka, A.A., Seger, R., Diltz, C.D., Krebs, E.G., and Fischer, E.H. (1995). Association of Mitogen-Activated Protein-Kinase with the Microtubule Cytoskeleton. *P Natl Acad Sci USA* 92, 8881-8885.

Rice, R., Connor, E., and Rice, D.P.C. (2006). Expression patterns of Hedgehog signalling pathway members during mouse palate development. *Gene Expr Patterns* 6, 206-212.

Rice, R., Spencer-Dene, B., Connor, E.C., Gritli-Linde, A., McMahon, A.P., Dickson, C., Thesleff, I., and Rice, D.P.C. (2004). Disruption of Fgf10/Fgfr2b-coordinated epithelial-mesenchymal interactions causes cleft palate. *J Clin Invest* 113, 1692-1700.

Richardson, S.H., Starborg, T., Lu, Y.H., Humphries, S.M., Meadows, R.S., and Kadler, K.E. (2007). Tendon development requires regulation of cell condensation and cell shape via cadherin-11-mediated cell-cell junctions. *Mol Cell Biol* 27, 6218-6228.

Ridley, A.J., Schwartz, M.A., Burridge, K., Firtel, R.A., Ginsberg, M.H., Borisy, G., Parsons, J.T., and Horwitz, A.R. (2003). Cell migration: Integrating signals from front to back. *Science* 302, 1704-1709.

Robert, B., Sassoon, D., Jacq, B., Gehring, W., and Buckingham, M. (1989). Hox-7, a Mouse Homeobox Gene with a Novel Pattern of Expression during Embryogenesis. *Embo Journal* 8, 91-100.

Roszko, I., Sawada, A., and Solnica-Krezel, L. (2009). Regulation of convergence and extension movements during vertebrate gastrulation by the Wnt/PCP pathway. *Seminars in Cell & Developmental Biology* 20, 986-997.

Sandham, A. (1985). Embryonic facial vertical dimension and its relationship to palatal shelf elevation. *Early Hum Dev* 12, 241-245.

Sandham, A. (1986). Cervical vertebral anomalies in cleft lip and palate. *Cleft Palate J* 23, 206-214.

Sasaki, Y., Tanaka, S., Hamachi, T., and Taya, Y. (2004). Deficient cell proliferation in palatal shelf mesenchyme of CL/Fr mouse embryos. *J Dent Res* 83, 797-801.

Satokata, I., and Maas, R. (1994). Msx1 Deficient Mice Exhibit Cleft-Palate and Abnormalities of Craniofacial and Tooth Development. *Nature Genetics* 6, 348-356.

Saunders, J.W., Jr. (1948). The proximo-distal sequence of origin of the parts of the chick wing and the role of the ectoderm. *J Exp Zool* 108, 363-403.

Sawyer, J.M., Harrell, J.R., Shemer, G., Sullivan-Brown, J., Roh-Johnson, M., and Goldstein, B. (2010). Apical constriction: A cell shape change that can drive morphogenesis. *Developmental Biology* 341, 5-19.

Schmitt, O., Modersitzki, J., Heldmann, S., Wirtz, S., and Fischer, B. (2007). Image registration of sectioned brains. *Int J Comput Vision* 73, 5-39.

Schnabel, C.A., Selleri, L., Jacobs, Y., Warnke, R., and Cleary, M.L. (2001). Expression of Pbx1b during mammalian organogenesis. *Mech Dev* 100, 131-135.

Schoenwolf, G.C., Folsom, D., and Moe, A. (1988). A REEXAMINATION OF THE ROLE OF MICROFILAMENTS IN NEURULATION IN THE CHICK-EMBRYO. *Anatomical Record* 220, 87-102.

Shah, R.M., Chen, Y.P., and Burdett, D.N. (1989). Growth of the Secondary Palate in the Hamster Following Hydrocortisone Treatment - Shelf Area, Cell Number, and DNA-Synthesis. *Teratology* 40, 173-180.

Shah, R.M., Cheng, K.M., MacKay, R.A., and Wong, A. (1987). Secondary palate development in the domestic duck (Khaki Campbell). An electron microscopic, histochemical, autoradiographic and biochemical study. *J Anat* 154, 245-258.

Shah, R.M., Young, A.V., Song, B.Z., and Wong, D.T.W. (1994). A Novel-Approach to the Growth Analysis of Hamster Secondary Palate by Histone-3 Messenger-Rna in-Situ Hybridization. *Histology and Histopathology* 9, 669-675.

Shibui, S., Hoshino, T., Vanderlaan, M., and Gray, J.W. (1989). Double labeling with iodo- and bromodeoxyuridine for cell kinetics studies. *J Histochem Cytochem* 37, 1007-1011.

Shih, J., and Keller, R. (1992). Cell Motility Driving Mediolateral Intercalation in Explants of *Xenopus-Laevis*. *Development* 116, 901-914.

Simons, M., and Mlodzik, M. (2008). Planar Cell Polarity Signaling: From Fly Development to Human Disease. *Annu Rev Genet* 42, 517-540.

Smith, T.M., Lozanoff, S., Iyyanar, P.P., and Nazarali, A.J. (2012). Molecular signaling along the anterior-posterior axis of early palate development. *Front Physiol* 3, 488.

Smith, T.M., Wang, X., Zhang, W., Kulyk, W., and Nazarali, A.J. (2009). *Hoxa2* Plays a Direct Role in Murine Palate Development. *Developmental Dynamics* 238, 2364-2373.

Snyder-Warwick, A.K., and Perlyn, C.A. (2012). Coordinated Events: FGF Signaling and Other Related Pathways in Palatogenesis. *J Craniofac Surg*.

Snyder-Warwick, A.K., Perlyn, C.A., Pan, J., Yu, K., Zhang, L., and Ornitz, D.M. (2010). Analysis of a gain-of-function FGFR2 Crouzon mutation provides evidence of loss of function activity in the etiology of cleft palate. *Proc Natl Acad Sci U S A* 107, 2515-2520.

Soames, A.R., Lavender, D., Foster, J.R., Williams, S.M., and Wheeldon, E.B. (1994). IMAGE-ANALYSIS OF BROMODEOXYURIDINE (BRDU) STAINING FOR MEASUREMENT OF S-PHASE IN RAT AND MOUSE-LIVER. *Journal of Histochemistry & Cytochemistry* 42, 939-944.

Spokony, R.F., Aoki, Y., Saint-Germain, N., Magner-Fink, E., and Saint-Jeannet, J.P. (2002). The transcription factor Sox9 is required for cranial neural crest development in *Xenopus*. *Development* 129, 421-432.

Stalmans, I., Lambrechts, D., De smet, F., Jansen, S., Wang, J., Maity, S., Kneer, P., von der Ohe, M., Swillen, A., Maes, C., *et al.* (2003). VEGF: A modifier of the del22q11 (DiGeorge) syndrome? *Nat Med* 9, 173-182.

Stanier, P., and Moore, G.E. (2004). Genetics of cleft lip and palate: syndromic genes contribute to the incidence of non-syndromic clefts. *Hum Mol Genet* 13 Spec No 1, R73-81.

Stewart, M.P., Toyoda, Y., Hyman, A.A., and Muller, D.J. (2011). Force probing cell shape changes to molecular resolution. *Trends Biochem Sci* 36, 444-450.

Summerbell, D., and Wolpert, L. (1972). Cell density and cell division in the early morphogenesis of the chick wing. *Nat New Biol* 239, 24-26.

Sutterlin, C., and Colanzi, A. (2010). The Golgi and the centrosome: building a functional partnership. *Journal of Cell Biology* 188, 621-628.

Suzuki, M., Morita, H., and Ueno, N. (2012). Molecular mechanisms of cell shape changes that contribute to vertebrate neural tube closure. *Dev Growth Differ* 54, 266-276.

Sweney, L.R., and Shapiro, B.L. (1970). Histogenesis of Swiss white mouse secondary palate from nine and one-half days to fifteen and one-half days in utero. I. Epithelial-mesenchymal relationships--light and electron microscopy. *J Morphol* 130, 435-449.

Szabo-Rogers, H.L., Smithers, L.E., Yakob, W., and Liu, K.J. (2010). New directions in craniofacial morphogenesis. *Developmental Biology* 341, 84-94.

Takahashi, K., Kuwahara, T., and Nagatsu, M. (1999). Interruption of the aortic arch at the isthmus with DiGeorge syndrome and 22q11.2 deletion. *Cardiol Young* 9, 516-518.

Taya, Y., O'Kane, S., and Ferguson, M.W.J. (1999). Pathogenesis of cleft palate in TGF-beta 3 knockout mice. *Development* 126, 3869-3879.

Team, R.D.C. (2012). R: A language and environment for statistical computing. . In R Foundation for Statistical Computing.

They, M., Racine, V., Pepin, A., Piel, M., Chen, Y., Sibarita, J.B., and Bornens, M. (2005). The extracellular matrix guides the orientation of the cell division axis. *Nat Cell Biol* 7, 947-953.

Torres, M.A., YangSnyder, J.A., Purcell, S.M., DeMarais, A.A., McGrew, L.L., and Moon, R.T. (1996). Activities of the Wnt-1 class of secreted signaling factors are antagonized by the Wnt-5A class and by a dominant negative cadherin in early *Xenopus* development. *Journal of Cell Biology* 133, 1123-1137.

Trainor, A.B.P. Migrating neural crest cells in a mouse embryo.

Turner, N., and Grose, R. (2010). Fibroblast growth factor signalling: from development to cancer. *Nat Rev Cancer* 10, 116-129.

Turner, R. (2007). *deldir*, pp. Calculates the Delaunay triangulation and the Dirichlet or Voronoi tessellation (with respect to the entire plane) of a planar point set.

Vallotton, P., Gupton, S.L., Waterman-Storer, C.M., and Danuser, G. (2004). Simultaneous mapping of filamentous actin flow and turnover in migrating cells by quantitative fluorescent speckle microscopy. *P Natl Acad Sci USA* 101, 9660-9665.

Varju, P., Katarova, Z., Madarasz, E., and Szabo, G. (2001). GABA signalling during development: new data and old questions. *Cell Tissue Res* 305, 239-246.

Vaziri Sani, F., Hallberg, K., Harfe, B.D., McMahon, A.P., Linde, A., and Gritli-Linde, A. (2005). Fate-mapping of the epithelial seam during palatal fusion rules out epithelial-mesenchymal transformation. *Dev Biol* 285, 490-495.

Venza, I., Visalli, M., Parrillo, L., De Felice, M., Teti, D., and Venza, M. (2011). MSX1 and TGF-beta3 are novel target genes functionally regulated by FOXE1. *Hum Mol Genet* 20, 1016-1025.

Verheyden, J.M., Lewandoski, M., Deng, C.X., Harfe, B.D., and Sun, X. (2005). Conditional inactivation of *Fgfr1* in mouse defines its role in limb bud establishment, outgrowth and digit patterning. *Development* 132, 4235-4245.

Vieira, A.R. (2008). Unraveling human cleft lip and palate research. *Journal of Dental Research* 87, 119-125.

Vitelli, F., Taddei, I., Morishima, M., Meyers, E.N., Lindsay, E.A., and Baldini, A. (2002). A genetic link between *Tbx1* and fibroblast growth factor signaling. *Development* 129, 4605-4611.

Walker, B.E. (1971). Palate Morphogenesis in Rabbit. *Archives of Oral Biology* 16, 275-&.

Walker, B.E., and Fraser, F.C. (1956). Closure of the Secondary Palate in 3 Strains of Mice. *Journal of Embryology and Experimental Morphology* 4, 176-189.

Wallingford, J.B., Rowning, B.A., Vogeli, K.M., Rothbacher, U., Fraser, S.E., and Harland, R.M. (2000). Dishevelled controls cell polarity during *Xenopus* gastrulation. *Nature* 405, 81-85.

Webb, D.J., Parsons, J.T., and Horwitz, A.F. (2002). Adhesion assembly, disassembly and turnover in migrating cells - over and over and over again. *Nature Cell Biology* 4, E97-E100.

Wee, E.L., and Zimmerman, E.F. (1983). Involvement of Gaba in Palate Morphogenesis and Its Relation to Diazepam Teratogenesis in 2 Mouse Strains. *Teratology* 28, 15-22.

Wehby, G.L., and Cassell, C.H. (2010). The impact of orofacial clefts on quality of life and healthcare use and costs. *Oral Dis* 16, 3-10.

Wei, Y., and Mikawa, T. (2000). Formation of the avian primitive streak from spatially restricted blastoderm: evidence for polarized cell division in the elongating streak. *Development* 127, 87-96.

Welsh, I.C., Hagge-Greenberg, A., and O'Brien, T.P. (2007). A dosage-dependent role for *Spry2* in growth and patterning during palate development. *Mechanisms of Development* 124, 746-761.

Welsh, I.C., and O'Brien, T.P. (2009). Signaling integration in the rugae growth zone directs sequential SHH signaling center formation during the rostral outgrowth of the palate. *Developmental Biology* 336, 53-67.

Williams-Masson, E.M., Heid, P.J., Lavin, C.A., and Hardin, J. (1998). The cellular mechanism of epithelial rearrangement during morphogenesis of the *Caenorhabditis elegans* dorsal hypodermis. *Developmental Biology* 204, 263-276.

Wilson, V., and Conlon, F.L. (2002). The T-box family. *Genome Biol* 3, REVIEWS3008.

Witze, E.S., Litman, E.S., Argast, G.M., Moon, R.T., and Ahn, N.G. (2008). Wnt5a control of cell polarity and directional movement by polarized redistribution of adhesion receptors. *Science* 320, 365-369.

Wojcik, S.M., Katsurabayashi, S., Guillemin, I., Friauf, E., Rosenmund, C., Brose, N., and Rhee, J.S. (2006). A shared vesicular carrier allows synaptic corelease of GABA and glycine. *Neuron* 50, 575-587.

Wu, M.L., Li, J., Engleka, K.A., Zhou, B., Lu, M.M., Plotkin, J.B., and Epstein, J.A. (2008). Persistent expression of Pax3 in the neural crest causes cleft palate and defective osteogenesis in mice. *J Clin Invest* 118, 2076-2087.

Wurdak, H., Ittner, L.M., Lang, K.S., Leveen, P., Suter, U., Fischer, J.A., Karlsson, S., Born, W., and Sommer, L. (2005). Inactivation of TGF beta signaling in neural crest stem cells leads to multiple defects reminiscent of DiGeorge syndrome. *Gene Dev* 19, 530-535.

Wyngaarden, L.A., Vogeli, K.M., Ciruna, B.G., Wells, M., Hadjantonakis, A.K., and Hopyan, S. (2010). Oriented cell motility and division underlie early limb bud morphogenesis. *Development* 137, 2551-2558.

Xu, H.S., Morishima, M., Wylie, J.N., Schwartz, R.J., Bruneau, B.G., Lindsay, E.A., and Baldini, A. (2004). Tbx1 has a dual role in the morphogenesis of the cardiac outflow tract. *Development* 131, 3217-3227.

Yadav, S., Puri, S., and Linstedt, A.D. (2009). A Primary Role for Golgi Positioning in Directed Secretion, Cell Polarity, and Wound Healing. *Mol Biol Cell* 20, 1728-1736.

Yam, P.T., Wilson, C.A., Ji, L., Hebert, B., Barnhart, E.L., Dye, N.A., Wiseman, P.W., Danuser, G., and Theriot, J.A. (2007). Actin-myosin network reorganization breaks symmetry at the cell rear to spontaneously initiate polarized cell motility. *Journal of Cell Biology* 178, 1207-1221.

Yamagishi, H., Maeda, J., Hu, T.H., McAnally, J., Conway, S.J., Kume, T., Meyers, E.N., Yamagishi, C., and Srivastava, D. (2003). Tbx1 is regulated by tissue-specific forkhead proteins through a common Sonic hedgehog-responsive enhancer. *Gene Dev* 17, 269-281.

Yamamoto, T., Cui, X.M., and Shuler, C.F. (2003). Role of ERK1/2 signaling during EGF-induced inhibition of palatal fusion. *Dev Biol* 260, 512-521.

Yu, H., Smallwood, P.M., Wang, Y., Vidaltamayo, R., Reed, R., and Nathans, J. (2010). Frizzled 1 and frizzled 2 genes function in palate, ventricular septum and neural tube closure: general implications for tissue fusion processes. *Development* 137, 3707-3717.

Yu, K., and Ornitz, D.M. (2011). Histomorphological study of palatal shelf elevation during murine secondary palate formation. *Dev Dyn* 240, 1737-1744.

Zhang, C., Halsey, L.E., and Szymanski, D.B. (2011). The development and geometry of shape change in *Arabidopsis thaliana* cotyledon pavement cells. *BMC Plant Biol* 11, 27.

Zhang, F.P., Mikkonen, L., Toppari, J., Palvimo, J.J., Thesleff, I., and Janne, O.A. (2008). Sumo-1 function is dispensable in normal mouse development. *Mol Cell Biol* 28, 5381-5390.

Zhang, Z., Huynh, T., and Baldini, A. (2006). Mesodermal expression of Tbx1 is necessary and sufficient for pharyngeal arch and cardiac outflow tract development. *Development* 133, 3587-3595.

Zhang, Z.Y., Song, Y.Q., Zhao, X., Zhang, X.Y., Fermin, C., and Chen, Y.P. (2002). Rescue of cleft palate in Msx1-deficient mice by transgenic Bmp4 reveals a network of BMP and Shh signaling in the regulation of mammalian palatogenesis. *Development* 129, 4135-4146.

Zheng, Z., Wan, Q., Liu, J., Zhu, H., Chu, X., and Du, Q. (2013). Evidence for dynein and astral microtubule-mediated cortical release and transport of Galphai/LGN/NuMA complex in mitotic cells. *Mol Biol Cell* 24, 901-913.

Zigman, M., Trinh le, A., Fraser, S.E., and Moens, C.B. (2011). Zebrafish neural tube morphogenesis requires Scribble-dependent oriented cell divisions. *Curr Biol* 21, 79-86.

Zitova, B., and Flusser, J. (2003). Image registration methods: a survey. *Image Vision Comput* 21, 977-1000.

Zoupa, M. (2008). The Role of TBX-1 in Craniofacial Development. In *Craniofacial Development Department* (London, Kings College London), pp. 223.

Zoupa, M., Seppala, M., Mitsiadis, T., and Cobourne, M.T. (2006). Tbx1 is expressed at multiple sites of epithelial-mesenchymal interaction during early development of the facial complex. *International Journal of Developmental Biology* 50, 505-510.

Zuk, P.A. (2008). Tissue engineering craniofacial defects with adult stem cells? Are we ready yet? *Pediatr Res* 63, 478-486.